

Spring 5-8-2021


## Development of Long-Acting Antiviral Drug Nanoformulations

Denise Cobb

*University of Nebraska Medical Center*

Tell us how you used this information in this [short survey](#).

Follow this and additional works at: <https://digitalcommons.unmc.edu/etd>

 Part of the [Infectious Disease Commons](#), [Medical Biotechnology Commons](#), [Nanomedicine Commons](#), [Pharmaceutical Preparations Commons](#), [Pharmacology Commons](#), and the [Virus Diseases Commons](#)

---

### Recommended Citation

Cobb, Denise, "Development of Long-Acting Antiviral Drug Nanoformulations" (2021). *Theses & Dissertations*. 524.

<https://digitalcommons.unmc.edu/etd/524>

This Dissertation is brought to you for free and open access by the Graduate Studies at DigitalCommons@UNMC. It has been accepted for inclusion in Theses & Dissertations by an authorized administrator of DigitalCommons@UNMC. For more information, please contact [digitalcommons@unmc.edu](mailto:digitalcommons@unmc.edu).

# **Development of Long-Acting Antiviral Drug Nanoformulations**

by Denise A. Cobb

A DISSERTATION

Presented to the Faculty of the University of  
Nebraska Graduate College  
in Partial Fulfillment of the Requirements  
for the Degree of Doctor of Philosophy

Pharmacology and Experimental Neuroscience  
Graduate Program

Under the Supervision of Drs. Benson Edagwa and Howard E. Gendelman

University of Nebraska Medical Center  
Omaha, Nebraska  
May, 2021

Supervisory Committee:

Dr. JoEllyn McMillan, Ph.D

Dr. Larisa Poluektova, MD, Ph.D

Dr. Joseph Vetro, Ph.D

Dr. Ram Mahato, Ph.D

Dr. Shilpa Buch, Ph.D

# **Development of Long-Acting Antiviral Drug Nanoformulations**

by Denise A. Cobb, Ph.D.

University of Nebraska, May 2021

Supervisors: Benson Edagwa, Ph.D., and Howard E. Gendelman, M.D.

Antiretroviral therapy (ART) has improved the quality and duration of life for people living with human immunodeficiency virus (HIV) infection. However, opportunities to improve its profile abound. ART is limited by putative viral reservoir penetrance, emergence of viral mutations, inherent toxicities, and regimen non-adherence. These highlight the need improved drug delivery schemes. Previously, our lab has demonstrated that targeting mononuclear phagocytes for antiretroviral drug delivery extends drug half-life and improves penetrance into viral reservoirs, addressing these limitations of ART. Herein, we developed synthetic and biologic antiretroviral (ARV) drug nanocarriers improve the pharmacokinetic (PK) and pharmacodynamic (PD) profiles of ARVs through macrophage-targeted delivery.

We posited that exosomes could be harnessed as biologic nanocarriers of ART, capable of targeting macrophages for drug delivery, building intracellular drug depots, and improving the pharmacokinetic and pharmacodynamic profile of ARVs. In a step towards achieving this goal, we studied the encapsulation of hydrophilic parent ARVs, hydrophobic parent ARVs, and lipophilic prodrug ARVs, using a variety of loading methods. The combination of sonication and lipophilic ARV prodrugs resulted in the highest drug encapsulation into exosomes. The data suggest the method of drug loading and the active pharmaceutical ingredient are important parameters to optimize. Despite these findings, further investigation of optimal cargo and large-scale production of exosome delivery systems are needed.

In tandem, a polymeric nanoparticle delivery system was developed as a means to improve the profile of tenofovir. To this end, we report the synthesis of two lipophilic tenofovir (TFV) ProTides (M1TFV, M2TFV) designed to improve drug stability, half-life, membrane penetrance, and enhance tissue distribution. The lead prodrug candidate M1TFV was nanoformulated to develop a stable LA injectable dosage form (NM1TFV). Specifically, NM1TFV provided PBMC concentrations of the active metabolite, tenofovir diphosphate (TFV-DP) four times above the IC<sub>90</sub> for 2 months, while concurrently generating substantial lymphatic and reticuloendothelial drug depots after a single injection in SD rats. Therefore, these results provide proof-of-concept nanoformulated TFV ProTides can effectively extend the apparent half-life and improve tissue distribution, warranting further investigation and optimization.

## ACKNOWLEDGEMENTS

My time in Nebraska has been accompanied by successes and failures. Outside the lab has been a resounding success, as I met my husband Ian while in Omaha. Ian's support and belief in me have propelled me to personal and professional heights I could not have achieved alone. As a child my parents' constant emphasis on education and unconditional support truly propelled me to where I am today. I hope that I continue to make them proud. I would also like to extend my gratitude to all my amazing and supportive in-laws. Surrounding yourself with people you love has made successes more enjoyable and my failures manageable. Thank you all for your love and support.

On a professional level Dr. Gendelman has been an important in my development as a scientist. Dr. Gendelman's integrity and work ethic has left a lasting impact on me. To witness an accomplished scientist continually innovating and pushing the boundaries has been inspiring. Throughout my time at UNMC, I faced many failures. In these moments Dr. Edagwa was a constant source of support and encouragement, knowing that I would eventually breakthrough scientifically. Dr. Edagwa's mentorship has been instrumental in my development as a scientist. His ideas, patience, and commitment to students has been integral to my own success. Another scientist whose mentorship cannot be underscored is Dr. JoEllyn McMillan. Dr. McMillan has been a steady source of support for me, continually displaying a willingness to listen, discuss ideas, and improve my scientific directions. Additionally, I would like to thank all the members of my advisory committee: Drs. Ram Mahato, Shilpa Buch, JoEllyn McMillan, Larisa Poluektova, and Joseph Vetro. All committee members have provided valuable insight not only towards my research, but also how to think and develop into a better scientist. I'd like to thank Dr. Poluektova for her generous and invaluable support with the HBV project, along with Weimin Wang and Edward Makarov, who helped to generate the HBV data herein. Additionally, I would like to thank Drs. Lee Mosley, Bhavesh Kevadiya, and Aditya Bade for their insightful critiques and

commentary on my research during my numerous laboratory presentations and Nagsen Gautam for analysis of many tenofovir samples. An important aspect of my life as a student at UNMC is the support received from Lana Reinhardt, Myhanh Che, Na Ly, Theresa Grutel, Julie Ditter, Reed Felderman, Johna Belling, Sandy Mahoney, Robin Taylor, and Kim Morrison. They have also made me feel supported and welcome in the PEN department. A special thank you is necessary for all the lab technicians I have worked with. Ted, Diana, Melinda, and Bhagya have been instrumental for sample processing and I greatly appreciate their tireless work.

Something I cherish about my time at UNMC are the moments spent with my lab-mates over the years. They have been instrumental in not only discussing science, but also making the lab a fun space where we can enjoy the day. Therefore, thank you to the numerous past and present members of the Gendelman lab; from summer students and techs to graduate students and postdoctoral fellows to instructors and faculty. Each and every person within the lab has contributed in some way to where I am today.

Denise Cobb

## TABLE OF CONTENTS

<u>LIST OF ABBREVIATIONS .....</u>	<u>ix</u>
<u>LIST OF FIGURES .....</u>	<u>xiii</u>
<u>LIST OF TABLES .....</u>	<u>xv</u>
<u>CHAPTER 1- INTRODUCTION .....</u>	<u>1</u>
1.1 Global Impact of HIV/AIDS .....	1
1.2 HIV-1 Pathobiology .....	1
1.3 Clinical Features of HIV-1 .....	3
1.4 ART   3	
1.4.1 Tenofovir and Related Prodrugs.....	4
1.5 Clinical History of long acting (LA) Therapy.....	5
1.6 Long-Acting Antiretroviral Therapies for HIV Treatment and Prevention.....	6
1.6.1. Long-Acting Oral Delivery .....	7
1.6.2. Long-Acting Transdermal Therapies .....	11
1.6.3. HIV-1 Microbicides.....	13
1.6.4. Broadly Neutralizing Antibodies .....	15
1.6.5. Long-Acting Implants. ....	16
1.6.6. Long-Acting Cabotegravir (CAB) and Rilpivirine (RPV) .....	18
1.6.7. Long-acting HIV-1 capsid inhibitor .....	20
1.6.8. Long-Acting Slow Effective Release (LASER) ART .....	20
1.7 Exosomes .....	22
1.7.1. Exosome Biogenesis .....	23
1.7.2. Exosome Lipid Composition .....	24
1.7.3. Exosome Protein Composition .....	24
1.7.4. Exosome Cargo .....	25
1.8 Exosomes in Nanomedicine .....	26
1.9 Summary .....	27
1.10 Figures and Tables .....	28
<u>CHAPTER 2- EXOSOMES AS AN ANTIVIRAL DRUG DELIVERY PLATFORM .....</u>	<u>39</u>
2.1 Abstract.....	39
2.2 Introduction .....	39
2.3 Materials and Methods .....	40
2.3.1 Materials .....	40
2.3.2 Human MDMs .....	41
2.3.3 Exosome isolation from supernatants.....	41

2.3.4 <i>In vitro</i> exosome ATV loading .....	42
2.3.5 <i>Ex vitro</i> ATV loading.....	42
2.3.6 Exosome purification after drug loading .....	42
2.3.7 Exosome depletion from human serum .....	43
2.3.8 Characterization of exosomes by Nanoparticle tracking analysis .....	43
2.3.9 Characterization of exosomes by Western blotting.....	43
2.3.10 Cytotoxicity.....	44
2.3.11 Exosome uptake and retention in MDM.....	44
2.3.12 Transmission electron microscopy .....	45
2.3.13 Antiretroviral efficacy of ATV exosomes .....	45
2.3.14 Antiretroviral efficacy of SDTG and DDTG exosomes .....	46
2.4 Results.....	46
2.4.1 Isolation and Characterization of <i>in vitro</i> loaded ATV exosomes .....	46
2.4.2 Synthesis and Characterization of <i>ex vitro</i> loaded ATV exosomes .....	47
2.4.3 <i>In vitro</i> characterization of <i>ex vitro</i> loaded ATV exosomes .....	48
2.4.4 MTT of exoATV and exoDTG formulations.....	48
2.4.5 Investigation of cytotoxicity.....	48
2.4.6 Encapsulation of hydrophilic ARVs into exosomes .....	49
2.4.7 Characterization of hydrophilic ARV-loaded exosomes .....	49
2.4.8 Encapsulation of lipophilic prodrug ARVs into exosomes .....	50
2.4.9 <i>In vitro</i> characterization of lipophilic ARV-loaded exosomes.....	50
2.5 Discussion .....	51
2.6 Conclusion .....	52
2.7 Figures and Tables .....	52
<b><u>CHAPTER 3: DEVELOPMENT OF LONG-ACTING TFV PROTIDE</u></b>	
<b><u>NANOFORMULATIONS.....</u></b>	<b>71</b>
3.1 Abstract.....	71
3.2 Introduction .....	72
3.3 Materials and Methods.....	74
3.3.1 Materials .....	74
3.3.2 Synthesis of L-phenylalanine and L-alanine docosyl esters.....	75
3.3.3 Synthesis and characterization of TFV ProTides.....	75
3.3.4 Ultraperformance liquid chromatography–ultraviolet/visible drug and prodrug quantifications.....	77
3.3.5 Solubility .....	77



3.3.6 Nanoparticle synthesis and characterization .....	78
3.3.7 Prodrug chemical stability .....	78
3.3.8 Plasma prodrug stability .....	79
3.3.9 Human monocyte-derived macrophage (MDM) isolation, cultivation and cytotoxicity measurements.....	79
3.3.10 Drug nanoformulation uptake and retention.....	80
3.3.11 Transmission electron microscopy to assess intracellular drug nanoformulations .....	80
3.3.12 TFV-DP measurements in MDM .....	80
3.3.13 Antiretroviral Efficacy of ProTide Nanoformulations.....	81
3.3.14 EC testing in HIV-1 target cells.....	81
3.3.15 PK studies.....	82
3.3.16 TFV-DP extraction from mucosal tissues.....	83
3.3.17 Sample Preparation and LC-MS/MS Analyses .....	83
3.3.18 Pharmacodynamics in a humanized mouse model of HIV-1 infection.....	85
3.3.19 Generation of humanized liver TK-NOG and FRG mouse models.....	85
3.3.20 Dosing of TK-NOG and FRG mice .....	86
3.3.21 Human Serum Albumin .....	86
3.3.22 Measurement of Blood HBV DNA and HBsAg levels.....	87
3.3.23 HBV RNA, DNA isolation, Real-time PCR and digital droplet PCR.....	87
3.3.24 Statistical analyses.....	88
3.3.25 Study approvals .....	88
3.4 Results.....	88
3.4.1 Synthesis and characterization of TFV ProTides.....	88
3.4.2 Nanoformulation of TFV ProTides .....	90
3.4.3 Cellular Drug Uptake and Retention .....	91
3.4.4 PK testing .....	94
3.4.5 TFV-DP measurements.....	95
3.4.6 Toxicology and evaluation of injection site reactions .....	96
3.4.7 Pharmacodynamic evaluations in HIV-infected humanized mice.....	98
3.4.8 Pharmacodynamic evaluations in HBV-infected humanized mice .....	98
3.5 Discussion .....	99
3.6 Conclusion .....	105
3.7 Figures.....	106
<u>CHAPTER 4- Summary, Challenges, Future Directions .....</u>	<u>128</u>

4.1 Summary .....	129
4.2 Exosomes: Summary and Future Directions .....	129
4.2.1 Exosome mediated CRISPR-Cas9 delivery.....	130
4.2.2 Exosome Scalability and Production .....	132
4.3 TFV: Summary and Future Directions .....	133
4.3.1 Pharmacokinetic and dynamic assessments .....	134
4.3.2 Scalability and production .....	136
4.4 Conclusions .....	138
4.5 Figures.....	139
<u>REFERENCES.....</u>	<u>139</u>

## LIST OF ABBREVIATIONS

$^{13}\text{C}$ NMR	carbon nuclear magnetic resonance spectroscopy
$^1\text{H}$ NMR	proton nuclear magnetic resonance spectroscopy
3TC	lamivudine
AAV	adeno-associated virus
ABC	abacavir
ACN	acetonitrile
AIDS	acquired immunodeficiency syndrome
API	active pharmaceutical ingredient
ART	antiretroviral therapy
ARV	antiretroviral drugs
ATV	atazanavir
AUC	area under the curve
BD	biodistribution
bNAbs	broadly neutralizing antibodies
CAB	cabotegravir
$\text{CHCl}_3$	chloroform
D8232	22 carbon modified GSK8232
DCM	dichloromethane
DDTG	22 carbon modified DTG
DLS	dynamic light scattering
DMF	dimethylformamide
DMSO	dimethyl sulfoxide
DRV	darunavir
DTG	dolutegravir

EC50	50% effective concentration
ESI-MS	electrospray ionization mass spectrometry
Et <sub>3</sub> N	triethylamine
exoATV	exosomes loaded with atazanavir
FDA	food and drug administration
FTC	emtricitabine
FTIR	Fourier-transformation infrared spectroscopy
H&E	hematoxylin and eosin
HBV	hepatitis B virus
HCl	hydrochloric acid
HIV-1	human immunodeficiency virus type-one
IC50	50% inhibitory concentration
IC90	90% inhibitory concentration
ILV	intraluminal vesicle
IM	intramuscular
INSTI	integrase strand transfer inhibitor
ISL	islatravir
IP	intraperitoneal
IS	internal standard
LA	long-acting
LASER-ART	long-acting slow effective release antiretroviral therapy
LN	lymph nodes
M1TFV	modified tenofovir 1 (phenylalanine modification)
M2TFV	modified tenofovir 2 (alanine modification)
M8232	Ester prodrug of GSK8232
MDM	monocyte-derived macrophages

MOI	multiplicity of infection
MRT	mean resonance time
MS/MS	tandem mass spectrometry
MTT	3-(4,5-dimethylthiazol-2-yl)-2,5-diphenyl-2H-tetrazolium bromide
MVB	multivesicular body
MVC	maraviroc
NaOH	sodium hydroxide
NM1TFV	nanoformulated modified tenofovir 1 (phenylalanine modification)
NM2TFV	nanoformulated modified tenofovir 2 (alanine modification)
NNRTI	non-nucleoside reverse transcriptase inhibitor
NRTI	nucleoside reverse transcriptase inhibitor
NTA	nanoparticle tracking analysis
NTAF	nanoformulated tenofovir alafenamide
NTZ	nitazoxanide
ORF	open reading frame
P338	poloxomer 338
P407	poloxomer 407
PBS	phosphate buffered saline
PD	pharmacodynamics
Pd/C	palladium on carbon
PDI	polydispersity index
PEG	polyethylene glycol
PI	protease inhibitor
PK	pharmacokinetics
PLWHA	people living with HIV/AIDS
PrEP	pre-exposure prophylaxis

RPV	rilpivirine
RT	reverse transcriptase activity
SQ	subcutaneous
SDTG	18 carbon modified DTG
SEM	standard error of the mean
STR	single tablet regimen
$t_{1/2}$	half-life
TAF	tenofovir alafenamide fumarate
TEM	transmission electron microscopy
TDF	tenofovir disoproxil fumarate
TFV	tenofovir
TFV-DP	tenofovir diphosphate
UPLC	ultra-performance liquid chromatography
UV/Vis	dual-wavelength ultraviolet/visible light detection

## LIST OF FIGURES

Figure 1.10.1	Schematic representation of the HIV-1 genome .....	28
Figure 1.10.2	Structure of wild type HIV-1 .....	29
Figure 1.10.3	HIV-1 life cycle and ART targets.....	30
Figure 1.10.4	Role of CD4 <sup>+</sup> T-cells HIV-1 disease progression .....	31
Figure 1.10.5	FDA approved drugs and drug combinations .....	32
Figure 1.10.6	Intracellular metabolism of TFV .....	33
Figure 1.10.7	Schematic representation of different types of extracellular vesicles .....	34
Figure 1.10.8	Different cargoes of exosome drug delivery systems.....	35
Figure 2.7.1	Different approaches for drug loading into exosomes.....	53
Figure 2.7.2	Characterization of naïve exosomes .....	54
Figure 2.7.3	ATV loading and characterization of exosomes.....	55
Figure 2.7.4	Antiretroviral activity of in vitro loaded exosomes .....	56
Figure 2.7.5	Ex vitro ATV loading.....	57
Figure 2.7.6	TEM imaging of exosome formulations .....	58
Figure 2.7.7	MDM uptake of ATV exosomes.....	59
Figure 2.7.8	Antiretroviral activity of ex vitro loaded exosomes .....	60
Figure 2.7.9	Exosome cytotoxicity studies.....	61
Figure 2.7.10	MDM Cytotoxicity studies .....	62
Figure 2.7.11	Morphology of hydrophilic ARV- loaded exosomes .....	63
Figure 2.7.12	Cytotoxicity and uptake of hydrophilic ARV loaded exosomes.....	64
Figure 2.7.13	Cytotoxicity of lipophilic prodrug loaded exosomes .....	65
Figure 2.7.14	MDM uptake and retention of DDTG exosomes .....	66
Figure 2.7.15	MDM uptake and retention of DDTG exosomes .....	67
Figure 2.7.16	Antiretroviral activity of DTG prodrug exosomes.....	68
Figure 3.7.1	Synthesis of TFV ProTides.....	107
Figure 3.7.2	Characterization of TFV ProTides .....	108
Figure 3.7.3	Physical and chemical characterization of TFV ProTides .....	109
Figure 3.7.4	Stability of ProTides in serum.....	110
Figure 3.7.5	Nanoformulation of TFV ProTides .....	111
Figure 3.7.6	Intracellular drug content.....	112
Figure 3.7.7	In vitro characterizations .....	113
Figure 3.7.8	Intracellular retention of drug.....	114
Figure 3.7.9	Antiretroviral activity .....	115

Figure 3.7.10	Pharmacokinetics .....	116
Figure 3.7.11	Biodistribution.....	117
Figure 3.7.12	In vivo TFV-DP levels.....	118
Figure 3.7.13	Site of injection.....	119
Figure 3.7.14	Drug quantitation at the site of injection.....	120
Figure 3.7.15	Statistical correlations .....	121
Figure 3.7.16	Single-dose acute toxicity testing .....	122
Figure 3.7.17	Serum chemistry .....	123
Figure 3.7.18	Kidney, liver, NTAF muscle histopathology .....	124
Figure 3.7.19	NM1TFV injection site histopathology .....	125
Figure 3.7.20	Design of HIV-1 PD study.....	126
Figure 3.7.21	PD in HIV-1 infected humanized mice .....	127
Figure 3.7.22	PD in HBV infected humanized mice.....	128
Figure 3.7.23	TFV-DP measurements in HBV infected humanized mice.....	129
Figure 4.5.1	Methods of RNA enrichment into exosomes.....	140



## LIST OF TABLES

Table 1.10.1	Advantages and limitations of long-lasting approaches for HIV-1 treatment and prevention.....	36
Table 1.10.2	Long-acting approaches for the treatment and prevention of HIV-1 ....	37
Table 1.10.3	Common exosome markers.....	38
Table 2.6.1	Loading of hydrophilic ARVs.....	69
Table 2.6.2	Loading of hydrophobic and prodrug ARVs .....	



## **CHAPTER 1- INTRODUCTION**

### **1.1 Global Impact of HIV/AIDS**

Antiretroviral therapy (ART) has been one of most significant achievements in modern medicine, providing human immunodeficiency virus type one (HIV-1) infected persons a life span and quality of life comparable to the general population [1, 2]. Between 2000 and 2019, new HIV infections and deaths decreased by 37% and 51% respectively [3]. Though access to ART increases each year, as of 2019 only 67% of infected adults received ART [3]. Furthermore, HIV remains endemic in eastern and southern Africa where an estimated 20.7 million people are currently living with HIV/acquired immunodeficiency syndrome (AIDS) (PLWHA), a disproportionate 55% of the global disease burden [3]. Within this region, young women remain an at-risk population, where five in six new infections were among teenage girls [3]. This coupled with the fact the number of new infections in 2019 was three times greater than UNAIDS targets. Thus, it is evident that reducing HIV transmission remains a challenge [4]. Therefore, future prevention strategies must focus on delivering ART in a more efficient and reliable manner to be effective in reducing new cases of HIV-1 infection [5].

### **1.2 HIV-1 Pathobiology**

Even considering the efficacy of ART there are limitations seen in the control of HIV-1 infection. This parallel the complexity of the viral life cycle, the high viral mutation rates, the existence of virus in a latent proviral DNA state and the ongoing infection and cell to cell spread that occurs despite adequate ART [6]. As per the viral life cycle, HIV is classified as a lentivirus which belongs to a genus of retroviruses characterized by long incubation periods. The size of the viral particle is between 80-120 nm in diameter with a lipid membrane surrounding its core structural components (Figure 1.10.2) [12]. Within each virion there are two viral RNA copies that code for multiple types of viral proteins: structural polypeptides env and gag which form components relating to the core virion and outer envelope; pol which

breaks into three proteins responsible for vital HIV-1 functions; gene regulatory proteins *tat* and *rev*; and accessory proteins *nef*, *vif*, *vpr*, and *vpu* (Figure 1.10.1) [7]. The viral RNA copies are housed within a p24 capsid to maintain core structure (Figure 1.10.2). The virion membrane bilayer has multiple glycoprotein (gp) spikes – a gp160 trimer composed of a heterodimer exterior gp120 and transmembrane gp41 subunit. The entry of HIV-1 into its target CD4+ T-cells, monocytes, dendritic cells and macrophages is facilitated when the viral envelope (env) glycoprotein 120 (gp120) binds to CD4 on the host cell surface (Figure 1.10.3). This interaction induces a conformational change in gp120, exposing and allowing V3 loop to bind its co-receptor target (CCR5 or CXCR4) [8]. Coreceptor binding exposes HIV-1 gp41, leading to membrane fusion and entry of viral RNA to the cytoplasm [9]. Following fusion and entry, the retrovirus converts its single stranded RNA genome into circular DNA through the virus reverse transcriptase (RT) enzyme [10]. The viral DNA is subsequently transported into the nucleus and integrated into the host cell genome by virally encoded integrase enzyme (Figure 1.10.3) [11]. From there, the integrated proviral DNA can remain latent or be expressed using host cell factors that affect viral replication by transcriptional and post-translational mechanisms serving to control the level and activity of HIV-1 growth by a number of host regulatory factors. Expression of HIV-1 DNA produces viral proteins such as trans-activator of transcription (Tat) which drives HIV-1 expression [12]. Another virally encoded protein, HIV-1 gag, facilitates the assembly and budding of infectious virions in conjunction with the HIV-1 protease (Figure 1.10.1) [13].

In addition to the *gag*, *pol*, and *env* genes contained in all retroviruses, and the *tat* and *rev* regulatory genes, HIV-1 contains four additional accessory genes: *nef*, *vif*, *vpr* and *vpu*, referred to as accessory proteins, most of which have multiple functions. Nef is expressed from a multiply spliced mRNA and is therefore Rev independent [14]. Nef is known to perturb T cell activation [15], enhance the infectivity of HIV virions [16], and downregulate CD4 and Class I MHC, promoting virion budding and reducing recognition

by cytotoxic T cells, respectively [17-19]. In contrast to Nef, Vpr, Vpu, and Vif are products of incompletely spliced mRNA, therefore only expressed during the late, Rev-dependent phase of infection[14]. Similarly, Vpu, also plays a role down-modulation of CD4 and the enhancement of virion release. Vpr is a protein incorporated into viral particles which plays a role in facilitating the nuclear localization of the preintegration complex [20]. Finally, Vif is essential for viral replication in cells such as peripheral blood lymphocytes and macrophages [21].

### **1.3 Clinical Features of HIV-1**

HIV-1 infection leads to functional changes in immune function. Infection in the absence of ART follows three phases: (1) acute infection, (2) clinical latency, and (3) acquired immunodeficiency syndrome (AIDS) [22] (Figure 1.10.4). The acute phase lasts from 2-4 weeks heralded by a marked depletion of CD4+ CCR5+ T-cells (Figure 1.10.4), particularly in the gut [23]. Clinical manifestations include flu-like symptoms that such as fever, fatigue, enlarged lymph nodes, swollen tonsils joint and muscle pain, diarrhea and rash [22] (Figure 1.10.4). In the second phase, the virus replicates slowly, and patients may be, in part, asymptomatic for months to years. As viral load increases and CD4+ T cell decline symptoms arise [22] (Figure 1.10.4). Without ART HIV-1 leads to AIDS, leaving individuals who succumb to a variety of cancers, opportunistic viral, parasitic and mycobacterial infections [22] (Figure 1.10.4). Therefore, monitoring of HIV-1 plasma viral load, monitoring of CD4+ T cell counts, and ART are key in preventing morbidity, mortality, and transmission.

### **1.4 ART**

Early clinical studies of HIV demonstrated that combination ART slowed disease progression, preventing drug resistance, and reduced disease morbidity and mortality [24, 25]. As the basic understanding of HIV-1 and its viral life cycle improved, more targets were identified which antiretroviral compounds could inhibit (Figures 1.10.3, 1.10.5). In 1995, protease inhibitors (PIs) reached the clinic (saquinavir), followed by the approval of the first

non-nucleoside reverse transcriptase inhibitors (NNRTIs) in 1996 (nevirapine) [26]. Shortly after, new classes of compounds such as fusion inhibitors (enfuvirtide; 2003), entry inhibitors (maraviroc; 2007), and integrase inhibitors (raltegravir; 2007) gained US Food and Drug Administration (FDA) approvals [26]. Additional novel classes of compounds beyond the more common nucleoside reverse transcriptase inhibitors (NRTI) such as nucleoside reverse transcriptase translocation inhibitors (Islatravir, ISL) [27], capsid inhibitors, and maturation inhibitors (MI) that work by blocking the processing of Gag, the core structural protein responsible for assembling HIV[28] are under clinical development. As ARV regimens became more effective, quality of life has also improved for people living with HIV/AIDS (PLWHA). Though effective in managing HIV, ARV regimens were also burdensome, sometimes requiring complex dosing [29]. Thus, the development of single tablet regimens (STR), tablets containing multiple drug classes, represented an important step in regimen simplification. Though recent ART require strict adherence, they are highly effective in reducing plasma viral loads below the limit of detection. In addition to improving maintenance therapy, combination ART also reduces transmission of HIV-1 in serodiscordant couples [30]. Current guidelines for ART suggest the use of two NRTIs administered in combination with either a integrase strand transfer inhibitor (INSTI) or a PI [31]. Further improvements to ART continue as new potent compounds such as cabotegravir (CAB) and islatravir (ISL) emerge, and existing ARVs are formulated as once monthly formulations [27, 32, 33].

#### **1.4.1 Tenofovir and Related Prodrugs**

Tenofovir (TFV), an analogue of adenosine monophosphate, is an NRTI with activity against HIV-1 and hepatitis B virus (HBV) infections [34, 35]. Once inside the cell, TFV is activated by kinases, resulting in the formation of the mono-, and diphosphorylated metabolites (Figure 1.10.6) [36]. The activated TFV diphosphate (TFV-DP) functions by inhibiting the HIV-1 reverse transcriptase following incorporation into viral DNA chains, where it terminates the elongation process [37]. Several studies have reported low levels of

conversion of nucleoside analogs into their nucleoside monophosphates, creating a rate-limiting step in their activation [38, 39]. Due to polar functional groups that inhibit paracellular transport, NRTIs also demonstrate poor oral bioavailability [40]. TFV overcomes these limitations by delivering the monophosphorylated metabolite directly. However, the use of the monophosphate form also introduces some challenges. For example, the transport of TFV into cells is hindered by the charged phosphate group. To address this, tenofovir disoproxil fumarate (TDF), an acyclic nucleoside phosphonate prodrug of TFV, was developed leading to improved bioavailability compared to TFV [41]. Although TDF addresses issues of bioavailability by masking charged hydroxyl groups, the compound is quickly hydrolyzed into TFV in the plasma, leading to reduced accumulation in target cells of HIV-1 such as CD4<sup>+</sup> T-cells and macrophages [42]. To overcome issues of stability, medicinal chemistry approaches masking either one or two of the oxygens of the monophosphonate group would render TFV more lipophilic and hence inherent membrane permeability, and slow *in vivo* hydrolysis [43-45]. One suitable medicinal chemistry approach is the ProTide prodrug technology developed by Prof. Chris McGuigan [46]. The application of ProTide technology to TFV led to the discovery and FDA approval of tenofovir alafenamide (TAF). In comparison to both TFV and TDF, TAF demonstrated enhanced antiviral activity, higher *in vivo* stability, and reduced side effects such as nephrotoxicity and bone density loss [47, 48]. Importantly, TAF improved biodistribution to lymphatic tissue and the liver [42]. Despite its effectiveness, limitations of TFV and its prodrugs include strict regimen adherence, toxicities, and restricted tissue penetrance, highlighting the need for improved formulation and/or medicinal chemistry strategies [48-50].

### **1.5 Clinical History of long acting (LA) Therapy**

LA dosage forms are available for indications ranging from contraception, to antipsychotics, and for management of symptoms related to metastatic tumors [51-53]. For contraceptives, both LA implants and injectable formulations are available. For example, the

injectable Depo-Provera requires quarterly injections, intrauterine devices (IUDs) such as Kyleena and Mirena are effective for 5 years, while the subdermal implant Nexplanon is effective for 3 years [52]. For management of metastatic carcinoid tumor-related symptoms such as diarrhea and flushing, a once-monthly microsphere formulation of octreotide, a long-acting octapeptide mimetic of the natural hormone somatostatin, is available for intramuscular administration [51]. In the field of LA antipsychotics, formulation approaches such as oil depots, aqueous suspensions, and microparticles are utilized to increase patient compliance and reduce dosing intervals [54]. For second-generation antipsychotics, dosing intervals vary from bimonthly to every three months [55]. The longest-acting antipsychotic formulation on the market, Invega Trinza, a microparticle suspension of paliperidone palmitate is approved for quarterly dosing [55]. Therefore, clinically approved LA dosage forms for birth control, cancer, and schizophrenia provide important clinical examples of extended-release platforms which can also be extended for the treatment and prevention of HIV-1.

### **1.6 Long-Acting Antiretroviral Therapies for HIV Treatment and Prevention**

Antiretroviral therapy (ART) has been effective in the treatment and prevention of human immunodeficiency virus (HIV) infection, reducing disease morbidity, and mortality. Further, oral pre-exposure prophylaxis (PrEP) of uninfected individuals has been shown to effectively reduce the chances of acquiring HIV to near zero when taken correctly and consistently[56, 57]. Therapeutic effectiveness of ART and PrEP, however, is limited by lack of consistent use and adherence to the required strict daily dosing regimens[58-60], leading to development of viral resistance, treatment failure and lack of prevention. To address poor regimen adherence, long-acting formulations offer a promising alternative to traditional regimens and thus could enhance the success rates for prevention and treatment and help lower rates of HIV-1 acquisition and transmission [5, 61, 62]. Longer-acting oral formulations, topical exposure strategies, microbicides and neutralizing antibodies, implantable devices,



as well as long-acting injectable formulations are being developed (Table 1.10.1, 1.10.2). Strategies for improving the pharmacokinetics of oral formulations are focused on enhancing gastric residence and promoting bioavailability in order to reduce dosing frequency. Transdermal delivery approaches can provide sustained drug release that bypasses first-pass metabolism and is quickly reversible if needed. Longer-acting approaches for delivery of HIV microbicides to prevent infection are also being studied. Broadly neutralizing antibodies that can remain in circulation longer than antiretroviral drugs (ARVs) could reduce levels of virus. Implants that provide sustained release of ARVs over months are being developed. Injectable formulations of ARVs currently approved in the US can provide therapeutically effective concentrations of drug for two months for treatment and prevention. Finally, newly developed injectable ARV prodrug formulations have been shown to provide therapeutic plasma and tissue drug levels for up to one year in experimental animals. Strategies fitting the definition of “long-acting” proposed by Owen et al [63] will be included. Specifically, technologies meeting dosing intervals of  $\geq 1$  week for oral and transdermal approaches,  $\geq 1$  month for microbicide and injectable approaches, or  $\geq 6$  months for implantable approaches have been selected for discussion [63].

#### **1.6.1. Long-Acting Oral Delivery**

Oral ART regimens have greatly reduced HIV morbidity and mortality. Since the introduction of ART, the complexity and toxicity of oral regimens has reduced over time. Currently, once-daily single tablet regimens (STRs) have proven successful in both the treatment and prevention of HIV-1 infection when utilized in both post- and pre-exposure prophylaxis (PrEP) regimens [30]. Though these STRs represent a significant advantage over early ART protocols[29] daily dosing still remains a burden to the patient, which may impair the high levels of adherence required for complete, sustained viral suppression and avoidance of drug resistance. Additionally, adolescents, a population at risk for HIV-1 acquisition, often have difficulties adhering to daily oral medication [64]. Thus, the

development of oral sustained release dosage forms is of high interest due to the potential for ease of administration, enhanced pharmacokinetics, reduced dosing frequency, and improved adherence. Although once-daily administration of oral ARVs is the current standard of care, less frequent administration of existing and investigational oral ARV's may be a possibility. TFV, whose intracellular active metabolite tenofovir-diphosphate has a half-life of 60-100 hours, could easily be given less often than once per day while maintaining antiviral effects [65]. With an elimination half-life of ~40 days after oral administration, CAB may also be a candidate for reduced dosing[66]. Efavirenz (EFV), with a plasma half-life of 45-60 hours, is also a good candidate for less frequent dosing. However, regimens involving administration every other or every 3rd day could be difficult to remember, if not more difficult, to adhere to than an every-day regimen[67]. Therefore, one possibility might be to aim for a once-weekly dosing, which offers greater convenience, and possibly adherence compared to daily therapy[68, 69].

ISL is a novel investigational potent nucleoside reverse transcriptase–translocation inhibitor that could potentially enable weekly oral administration. When assessed as a PrEP agent in simian-human immunodeficiency virus (SHIV)-challenged rhesus macaques, once-weekly oral administration of ISL at a dose of either 1.3 mg/kg or 3.9 mg/kg prevented SHIV infection in all treated animals[70]. In humans, single doses of ISL as low as 0.5 mg suppressed HIV-1 RNA plasma levels by more than 1.0 log at day 7 in treatment-naïve adults[27]. The prolonged efficacy observed for ISL distinguishes it from currently approved oral ARV agents. Its 3'-hydroxyl, 4'-ethynyl, and 2-fluoro groups are thought to contribute to its distinct pharmacologic attributes. Specifically, the 4'-ethynyl group binds to a conserved pocket in HIV-1 reverse transcriptase, interfering with extended primer translocation and resulting in chain termination[71, 72]. The 3'-hydroxyl group, a feature shared with natural nucleotides, binds to reverse transcriptase. Finally, the 2-fluoro on the adenine base slows deamination of the drug by adenosine deaminase, contributing to its long intracellular half-

life of over 72 hours [73]. The structure-function relationship of ISL has been thoroughly reviewed by Markowitz, et al[74]. These features, combined with the promising results from macaque and human studies, suggest the potential for once-weekly dosing of ISL. In all, design of potent drug candidates with unique structural features may offer opportunities to extend the half-life of ARV agents, making infrequent oral administration feasible. While modification of compound structural features and enhancement of drug potency may prove an effective approach to extending drug half-life[75, 76] many challenges remain. For instance, while drug monotherapy may be suitable for PrEP regimens, in the context of long-term HIV treatment, drug monotherapy is associated with viral rebound and emergence of viral resistance[77]. Therefore, one of the major challenges with weekly dosing of ISL (or any other long-acting oral agent) for treatment of HIV-1 infection would be finding suitable drug partners with similar pharmacokinetic properties. Given their longer half-lives co-administration with EFV, CAB, or TFV prodrugs are possibilities [13,14] but further work will be required to demonstrate the feasibility of such an approach.

Gastric residence devices could also reduce the dosing frequency of ARVs and improve patient adherence. In recent years there a number of systems have been designed to prolong gastric residence of drugs. Strategies such as high-density sedimentation, low-density flotation, mucoadhesion, and expansion have all prolonged *in vivo* gastric residence to varying degrees[78, 79]. In the case of ARVs, a modular drug delivery system capable of enhancing the gastric residence of up to six different drugs has recently been described. The device, which unfolds after capsule dosing, retains its star-like structure in the stomach, and has demonstrated sustained release of dolutegravir (DTG), CAB, and RPV for a week after a single dose in a swine model[80]. However, device complexity remains a major hurdle for translation; large-scale manufacture of these multi-component, multi-drug devices could prove both difficult and costly.

Nanoparticle formulations have also been employed to enhance oral bioavailability and reduce dosing frequency. In the case of maraviroc (MVC), whose oral bioavailability in humans is estimated to be approximately 33% for a 300 mg dose, solid drug nanoparticle (SDN) formulations produced by emulsion template freeze drying (ETFD) have been employed to overcome MVC's low oral bioavailability[81]. More specifically, a SDN MVC formulation demonstrated a 2.5-fold increase in AUC compared to conventional MVC treatment. Improvements for LPV and EFV formulations were also achieved through ETFD. Similar nanosuspensions have also improved the oral bioavailability of LPV and EFV[82, 83]. Augustine, et al., describe a nanoparticle system capable of enhancing the solubility of darunavir/ritonavir (DRV/r)[84]. The reported Nanoparticle-in-Microparticle Delivery System (NiMDS) contains nanoparticles of DRV/r encapsulated within film-coated microparticles. A series of polymethacrylate copolymers that coat the DRV/r nanoparticles ensure stability at gastric pH. In rats, the DRV/r-loaded NiMDS increased the oral bioavailability of DRV by 2.3-fold. The administration of antiretrovirals formulated as copolymer-stabilized nanoemulsions may also enhance oral ART bioavailability. Self-emulsifying systems are isotropic mixtures that contain an oil phase, the active pharmaceutical ingredient (API), and surfactants which emulsify on contact with the gastrointestinal fluids[85]. Lipid-based nanoemulsions have been reported to enhance drug absorption through a combination of mechanisms including: increasing the aqueous drug solubility, facilitating absorption through bile secretion, and inhibition of enzymes such as P-glycoprotein and cytochrome P450[86, 87]. These nanoemulsifying drug delivery systems have enhanced bioavailability various poorly-water soluble drugs, such as EFV, lopinavir (LPV), and DRV, in a Caco-2 gut epithelium model[87]. Altogether, nanoparticles designed for oral administration may be a strategy that could improve oral bioavailability and reduce the dosing interval of antiretrovirals.

### 1.6.2. Long-Acting Transdermal Therapies

Transdermal systems of current interest include: (1) matrix patches, where the drug is incorporated into an adhesive polymer matrix and continuously released into the skin, (2) reservoir patches, which suspend the drug in a gel or solution and release is controlled by a microporous membrane, and (3) microneedles, which are patches composed of arrayed micron-size needles that are coated or impregnated with drug<sup>31</sup>. Transdermal drug delivery systems offer several benefits that include overcoming hepatic first pass metabolism and gastrointestinal (GI) degradation of drug. Additionally, these approaches are painless, easy to apply without the intervention of a healthcare provider, and could therefore if successful, facilitate patient acceptance and adherence to ART. Moreover, microneedle (MN) patches, which are designed to provide transdermal delivery by bypassing the outer layer of skin, could provide a means of long-acting ARV delivery. Antiretrovirals could benefit from delivery via MN patches. Because MNs deliver drug to the lymphatic system through the skin, they may enhance the efficacy of antiretrovirals by avoiding first pass metabolism and allowing for focused delivery to HIV viral reservoirs[88]. Additionally, lengths and array density of MNs can be tuned to maximize drug loading, possibly increasing plasma concentrations and allowing for weekly dosing intervals. However, unlike reservoir and matrix transdermal patches that can be easily discontinued if adverse reactions arise, microneedle patches are not reversible following microneedle dissolution.

From a transdermal delivery perspective, the choice of antiretroviral agent is important as chemical and physical properties of the drug effect skin permeation. For instance, drugs with low molecular weight (<500 Da), melting point below 250°C, and moderate log P are ideal for transdermal delivery [89]. Fitting within these parameters, tenofovir alafenamide fumarate (TAF) would be a good potential candidate for transdermal patch formulation given its molecular weight of 476.47 g/mol, melting point of 279°C, and a logP = 1.8[90]. A recent study aimed to develop a transdermal patch for sustained release of

TAF for approximately one week. In order to reach clinically relevant concentrations of TAF, it was determined that a 50 cm<sup>2</sup> transdermal patch should release a TAF dose of 8 mg/day, making the target permeation flux 7 µg/cm<sup>2</sup>/h. The authors developed a silicone-based patch composed of 15% (w/w) TAF that achieved the target release and duration profile for TAF suitable for weekly dosing [90].

Microneedles have been employed in transdermal systems to enhance drug delivery. Recently, MN patches comprised of long-acting rilpivirine (RPV LA) nanosuspension were developed as a means to address imperfect ART adherence[91]. The patches were capable of penetrating skin *in vitro* and delivering RPV intradermally<sup>40</sup>. In rats, the mean plasma concentration of RPV at day 7 post-application was found to be 431 ng/ml, a concentration approximately ten-fold greater than the trough concentration observed after a single intramuscular dose of RPV LA in human clinical studies<sup>40</sup>. Therefore, the described MN array patches could potentially be used to deliver translatable human doses of RPV. Of note, the authors also detected RPV in rat lymph nodes, indicating the potential to deliver this ARV agent to a major site of viral replication. Overall, these studies provide proof of principle for the use transdermal patches, specifically MN patches, for HIV-1 treatment and prevention.

Overall, transdermal delivery of ARVs offers several advantages over other routes of administration (Table 1.10.1). Transdermal patches may also address unmet needs for women. For example, women in low- and middle-income countries are at high risk of both HIV infection and unintended pregnancy. There is an unmet need for products that provide long-acting protection against HIV and contraception, and transdermal patches may provide a means of addressing both needs simultaneously[92]. Current transdermal contraceptive patches require a once-weekly application[93]. Thus, if a once-weekly dosing interval could be achieved with ARV patches, a transdermal system that combines ARVs and contraceptive hormones could improve both adherence to PrEP and access to long-acting contraceptives.

However, transdermal systems face multiple challenges. For instance, to maintain consistent drug delivery, transdermal patches must strongly adhere to skin under all conditions such as sweating, bathing, and during physical activities. Host skin characteristics could also affect drug delivery from the patch, therefore comprehensive clinical pharmacokinetic testing should involve patients of different races, sex, ages, and body mass indexes to ensure that patches provide consistent drug exposures under varying conditions[94]. Additionally, due to prolonged physical adherence, transdermal patches are less discreet than other ARV delivery systems. Furthermore, current studies have only demonstrated transdermal delivery of single ARV drugs, however ARV drug combinations are required for treatment of HIV-1 to prevent viral rebound and resistance. Therefore, current transdermal technologies may be better suited for PrEP. However, further work would be required to demonstrate adequate drug biodistribution to rectal and cervicovaginal tissues for successful implementation in HIV-1 PrEP regimens. There are also disadvantages from a regulatory perspective. A combination of a drug and a device, patches could be subject to additional regulatory requirements and/or testing such as human factor and in vivo adhesion studies[95, 96].

### **1.6.3. HIV-1 Microbicides**

HIV microbicides are topical products generally comprised of an ARV drug, that when applied to the vagina or rectum can prevent the sexual acquisition of HIV in women and men. Antiviral agents that women can self-administer to reduce the risk of infection is of great interest. Despite the incidence of new HIV infections declining for many populations, young women in Africa account for a fifth of new HIV infections[97], and are eight times more likely to be infected with HIV than their male peers[98]. Therefore, microbicides, such as gels, films and rings are potentially important female-controlled options for HIV prevention. Tenofovir gels were found to reduce the risk of HIV-1 acquisition in women if the product was used correctly and applied regularly as prescribed[99]. However, these products offer only

short-acting protection from HIV infection. Other alternatives include vaginal rings (VR), which have been successfully used for birth control, and are currently being evaluated for sustained delivery of ART (Table 1.10.2). Compared to gels and films, VRs are longer acting and can provide monthly sustained ARV release. Therefore, by reducing the dosing interval and simplifying the use of antiretroviral medications VRs may enhance HIV-1 protection by facilitating PrEP adherence. Multiple phase 3, randomized, double blind, placebo-controlled trials of a monthly VR containing dapivirine, have demonstrated device safety and reduced risk of HIV-1 acquisition in a cohort of African women[100, 101]. Elsewhere, a VR aimed at preventing both HIV-1 infection and unintended pregnancy has been reported. The VR, which delivers TFV and levonorgestrel (LNG), was evaluated in a randomized, placebo controlled, phase I study (CONRADA13-128)[102]. The study demonstrated the safety of the TFV/ LNG rings, and observed higher anovulation rates in the participants randomized to the TFV/LNG VR compared to controls. Additionally, users of the TFV containing VR exhibited cervicovaginal aspirate TFV concentrations above 100,000 ng/mL 4 hours post insertion and TFV-DP concentrations in vaginal tissue above 1000 fmol/mg even 3 days after removal. However, more clinical evaluations are required to determine the efficacy of the dual contraceptive/ HIV-1 PrEP ring. Despite the potential of VR, not all ARVs are well suited for delivery in this format. For instance, a Phase I study evaluating vaginal rings containing dapivirine and MVC found that only dapivirine, but not MVC, demonstrated concentration-dependent inhibition of HIV-1 infection in cervical tissue [103]. Therefore, selection of ARV drug is important for the clinical translation of VRs for PrEP. In all, VRs offer a longer-acting mode of HIV PrEP. Recently, a yearly contraceptive ring gained FDA approval and these advances in VR technology may translate into VRs for HIV PrEP with even longer duration of action[104].

The rectum is particularly vulnerable to HIV transmission with only a single protective layer of epithelial cells overlying tissue rich in target lymphoid cells. Due these anatomical



features, unprotected anal intercourse high risk of infection. Therefore, attention has been given to the use of rectal microbicides as a PrEP modality, in the absence of effective vaccines. As with vaginal products, the focus has been on the direct application of antiviral agents. In clinical trials microbicide gels[54-58] and films[59] reduce the risk of HIV-1 acquisition in men given correct product use and adherence[98, 99]. However, these products offer only short-acting protection from HIV infection. To date, no rectally- applied microbicide designed for long-acting PrEP has been described.

#### **1.6.4. Broadly Neutralizing Antibodies**

HIV-1 broadly neutralizing antibodies (bNAbs) possess the ability to neutralize HIV-1 strains from diverse genetic and geographic backgrounds through the recognition of highly conserved epitopes. In contrast to current oral ARV regimens which offer highly effective, but short-lasting antiviral activity, bNAbs could remain in circulation longer, reducing the frequency of dosing. Currently, clinical development of bNAbs for the treatment and prevention of HIV-1 is of high interest. Second-generation bNAbs, isolated through cloning of antigen-specific antibodies from B cells of HIV-1 infected patients, target conserved sites of HIV-1 Env such as: N-glycan associated epitopes of V1/V2 (PG9)[105] and V3 regions (PGT121)[106], gp120/gp41 interface (35O22)[107], fusion peptide (VRC34, ACS202)[108, 109], CD4bs (VRC01, 3BNC117)[110], MPER on gp41 (10E8)[111], and silent face center (VRCPG05, SF12)[112]. To date, roughly a dozen second-generation bNABs have reached clinical development[113, 114] for HIV-1 treatment and prevention, demonstrating safety, tolerability, suppression of viremia, and enhanced immune function[115, 116]. Combinations of second-generation bNAbs have demonstrated effective viral suppression and reduced viral escape in individuals with sensitive viruses[117, 118]. Additionally, although clinical studies have demonstrated suppression of viremia following administration of bNAbs in HIV-1 infected individuals, the effect is transient, further emphasizing the need for combinatorial strategies to achieve long-acting treatment of HIV-1[119]. Currently one clinical trial

(NCT03739996) investigating the combination of long-acting CAB plus the bNAb VRC07-523LS in HIV-1 infected adults is underway (Table 1.10.2). bNAbs generally exhibit short half-lives, however, antibody modifications such as Met428Leu and Asn434Ser (LS) substitutions within crystallizable fragment domains and paratope engraftment have resulted in bNAbs with prolonged *in vivo* half-lives, reduced autoreactivity, and increased potency[120, 121]. Altogether, these recent advances provide the framework for implementation of bNAbs in long-acting HIV-1 treatment and PrEP regimens.

#### **1.6.5. Long-Acting Implants.**

Another technology being explored for sustained release of ART to improve patient adherence is implantable ART[61, 122]. In 2005 an implantable version of the non-nucleoside reverse transcriptase inhibitor (NNRTI) nevirapine was developed[123]. Nevirapine was shaped into 2.0 or 4.5 mm granular pellets coated with 5% poly(vinyl alcohol)(PVA) and subcutaneously implanted into rats for three months. However, the amount of active pharmaceutical compound released in blood was lower than the therapeutic drug concentration and a large drug burst release upon implantation was observed. Recent works with biodegradable removable implants have used DTG co-formulated with poly(lactic-co-glycolic acid) (PLGA) and *N*-methyl-2-pyrrolidone (NMP). The formulation solidifies upon administration, allowing removal, and reportedly provides therapeutic drug levels for up to nine months in mice[124]. Long-acting iterations of up to six drugs, based upon solubility with NMP, have been reported using similar technologies[125]. While erodible implants are promising, drug release rates, amounts of organic solvents required to solubilize hydrophobic drugs during scale-up, and implant degradation kinetics need to be optimized for safety and efficacy.

ISL (MK-8591) implants were created that were loaded with 40% weight of drug and coated with biocompatible polymers such as PVA or poly(caprolactone) (PCA). When implanted subcutaneously in rats and monkeys drug release was observed for 6

months[126]. ISL implants using non-erodible poly (ethylene vinyl acetate) were also described. Raman imaging was used to show distribution of drug within the implant prepared by solvent-free hot melt extrusion. The implant was a cylindrical silicone tube with pre-slit pores that determined drug release rate. An initial safety and tolerability study with a removal subdermal implant in humans reported therapeutic drug levels for four weeks and was well-tolerated[127]. Long-term safety concerns with degradation driven diffusion and implant size remain obstacles in these works.

Implantable devices containing TAF are of increased interest due to the drug's potency and long-lasting active metabolite. A PCA membrane incorporating formulated TAF with a polyethylene glycol polymer or castor oil provided controllable *in vitro* release[128, 129]. Tests in beagle dogs demonstrated zero order drug release kinetics (the release rate is based off number of size of pores within PVA membrane) with substantially higher amounts of the active pharmacologically metabolite, tenofovir diphosphate (TFV-DP), detected in peripheral blood mononuclear cells than is required for PrEP for 40 days[130]. This device was non-degradable and constructed by punching 1 mm holes in silicone tubing, coated by a thin heat-annealed PVA membrane, and loaded with TAF free base. Other studies have described the development of refillable implants with the intent to limit the need for surgical removal and implantation. A silicon-coated nanomembrane channel medical grade titanium device was fabricated for both TAF and emtricitabine (FTC). Drug release rates were tuned using an algorithm to predict optimal channel size and physicochemical features of the ARV used. Therapeutic levels of TFV-DP and FTC-triphosphate (FTC-TP) were observed for three months when the devices were implanted in rhesus macaques[131]. A similar positive result was obtained with a 2-hydroxypropyl- $\beta$ -cyclodextrin modified CAB using the same reservoir system[132]. Despite this promise, release rates from the devices were not uniform *in vivo*, and certain animals did not respond well to the implants used. A recent report described the development of an implant prepared by sealing TAF into a pellet with NaCl and magnesium

stearate and inserting the pellets into a medical-grade polyurethane tube. When inserted subcutaneously in rabbits and rhesus macaques therapeutic TFV-DP levels were observed throughout the study, however substantial histological changes were observed in tissues surrounding the implant site[133].

In conclusion, implantable ART technology addresses common adherence issues, with multiple works showing the ability to deliver highly soluble compounds with release profiles that extend to several months in duration[126, 132, 134]. Further, release rates are tailorable according to drug and polymer selection. Implants are also discreet and can remove some of the stigma of taking ART from patients. Depending on polymer and device composition, implantable devices can be surgically removed or be biodegradable. The ability to remove a device can be advantageous in the case of adverse reactions or when a change in therapy is needed due to development of resistance mutations or upon patient request. However, removal requires invasive surgical procedures that may be costly and not practical in rural areas or settings where cost is of importance. The use of placebos to assess the safety of these devices needs further study as initial reports indicate substantial tissue necrosis after 5 and 12 weeks in animals given NRTI-loaded implantable devices[133]. Biodegradable devices require only one insertion, but drawbacks include the inability to remove them in the case of adverse events. The future of implantable ART will need to address long-term drug toxicities and more controlled release rates *in vivo*.

#### **1.6.6. Long-Acting Cabotegravir (CAB) and Rilpivirine (RPV)**

Long-acting RPV and CAB are FDA approved once-every-month injectable formulations for the treatment of HIV infection. Intramuscular administration of CAB and RPV LA creates nanocrystal depots at the injection site that slowly dissociate to provide sustained release of each compound over extended periods of time [135]. Two phase III clinical trials - the Antiretroviral Therapy as Long-Acting Suppression (ATLAS) and First Long-Acting Injectable Regimen (FLAIR) are evaluating CAB and RPV LA in virologically suppressed

patients who were switched from a standard oral three drug regimen. The patients in both studies were started on an oral CAB and RPV lead-in regimen before randomly switching to the monthly regimen. Of significance, the two-drug injectable regimen demonstrated comparable antiretroviral activity to the standard daily oral three-drug regimen for maintenance therapy at 48 weeks[32, 136]. Also, even though the incidence of injection-site reactions was high in both studies, more than 90% of those surveyed preferred the monthly injectable over daily oral therapy. However, limitations of CAB and RPV LA include the requirement for large injection volumes, the risk for emergence of drug resistant virus strains during sub-therapeutic exposure after treatment discontinuation and limited access of native CAB and RPV to cellular and tissue reservoirs of infection [137-139]. To achieve once every two months dosing of CAB and RPV, an ongoing phase III clinical trial, the Antiretroviral Therapy as Long-Acting Suppression every two Months (ATLAS-2M), is evaluating the efficacy and tolerability of the two formulations at higher drug doses in virally suppressed patients. At week 48, the ATLAS-2M study demonstrated comparable efficacy and safety profiles to monthly dosing[140]. The HIV Prevention Trials Network (HPTN) 083 study is a phase 2b/3 double-blind study designed to evaluate the safety and efficacy of CAB LA for HIV prevention administered every eight weeks compared with the daily oral two drug regimen of tenofovir disoproxil fumarate and FTC (TDF/FTC) that is currently indicated for PrEP. A recent announcement from HPTN 083 reported that fewer participants using CAB LA became HIV positive compared to those using the daily oral TDF/FTC regimen[141]. These encouraging findings underscore the potential important role of long-acting single drugs for PrEP. Extended release parenteral dosage forms that would overlap patient dosing schedules with routine once every three to six months CD4+ T cell count and viral load tests could potentially have a major impact on the effectiveness of HIV treatment and prevention efforts.

#### **1.6.7. Long-acting HIV-1 capsid inhibitor**

A novel potent investigational HIV-1 capsid inhibitor GS-6207 is currently being evaluated for treatment of HIV infection[142]. The inherent hydrophobicity and metabolic stability of GS-6207 enabled development of a long-acting surfactant stabilized aqueous suspension of the capsid inhibitor for subcutaneous administration. A single dose of the capsid inhibitor in HIV negative patients demonstrated sustained therapeutic drug concentrations with the potential to be administered once every three months. Importantly, the study recorded no serious adverse events[143]. An ongoing phase 1 clinical trial (NCT03739866) is evaluating the efficacy and safety profiles of injectable suspensions of GS-6207 at doses of 150, 450 and 900 mg in HIV patients. The development of such long-acting formulations with a unique mechanism of action will provide treatment alternatives to existing ART.

#### **1.6.8. Long-Acting Slow Effective Release (LASER) ART**

For LA regimens, the oil-based (haloperidol decanoate) and aqueous drug suspensions (Depo-Provera, paliperidone palmitate, aripiprazole lauroxil, Cabenuva) are two common formulation approaches. Oil based formulations are composed of insoluble active pharmaceutical ingredient (API) and carrier oils such as sesame seed oil. However, this approach can result in accumulation of oil at the injection site and are more painful than water-based formulations [144-146]. In contrast, aqueous drug suspensions produce less pain upon injection and allow for higher drug encapsulation, therefore are the preferred formulation approach. In order to formulate aqueous suspensions using poloxamer and other FDA approved surfactants, APIs must have poor aqueous solubility, precluding all NRTIs and MVC [147]. Additionally, the release of the drug from the depot and clearance from the body must be balanced to achieve sustained therapeutic concentrations while avoiding toxicities. The use of hydrophilic and unstable prodrugs such as TAF or TDF add further complexities; extracellular hydrolysis of these prodrugs into their ionized forms may limit drug

absorption from the muscle depot underscoring the need for stable NRTI prodrugs. Due to above-mentioned challenges, many currently approved ARV drugs are not suitable to be formulated as LA agents.

Attempts to overcome these obstacles led native ARV transformation into long-acting slow effective release antiretroviral therapy (LASER ART). LASER ART is comprised of homogeneous dispersions of solid prodrug nanocrystals stabilized by aqueous surfactants [61, 148, 149]. Chemical modifications of native ARVs into lipophilic and hydrophobic prodrugs facilitate the development of nanocrystal technology to both water insoluble and hydrophilic compounds. These affect the apparent half-life and drug transport across physiological barriers [33, 139, 150-155]. In addition to high drug loading, LASER ART altering drug metabolism and solubility profiles to extend the drug's half life [156-158]. Once inside macrophages, LASER ART is stored in early, late and recycling-endosomes. The extended intracellular storage of the drug nanocrystals affect an extended PK profile [33, 159]. This mechanism is operative in both CD4<sup>+</sup> T cells and macrophages. The latter, principal LASER-ART storage vehicles, are considered early targets for HIV-1 for both transmission and viral dissemination. Macrophages like CD4<sup>+</sup> T cells express CD4 receptors and CCR5 co-receptors [42-44]. Macrophages carry an advantage to T cells as storage vehicles based on their high cytoplasmic to nuclear ratio, their longevity and their insensitivity less to virus-induced cytopathicity. All provide evidence of their abilities to harbor virus for extended periods of time [160, 161]. ART delivery into macrophages can affect the levels of viral suppression (00). Taking advantage of the inherent phagocytic macrophage function, our lab has leveraged the cells as vehicles for ART delivery. Delivering ARVs into macrophages could affect improvements in viral suppression over traditional ART. First, macrophages are highly mobile that they are recruited to the site of viral infection and consequent inflammation [35]. Carried inside macrophages ARV can more easily access tissue viral reservoirs, such as brain and lymphoid tissues that traditional ART do not access

easily. Second, once engulfing drug crystals, macrophages serve as drug depots and slowly release their ARV cargo while protecting drug from systemic metabolism and renal elimination. This supports sustained delivery extend the drug's apparent half-life and reducing toxicities linked to the  $C_{max}$ . Last, macrophages have high drug ARV nanoparticle loading capacity [33, 159]. If the release is controlled this could lead, by itself, to reduced dosing intervals. Recent preclinical evaluations of injectable cabotegravir prodrug nanocrystals demonstrated significantly improved efficacy and PK profiles, offering the feasibility of once-yearly dosing [162]. In addition to enabling less frequent dosing, efficient delivery and sustained release of therapeutic concentrations of ART at intracellular and tissue sites of infection could be combined with viral elimination approaches to potentially leading to a cure as was recently demonstrated in our laboratories in a subset of humanized mice treated with sequential LASER ART and CRISPR-Cas9 therapies [163].

### **1.7 Exosomes**

Nanoformulation of parent and prodrug ARVs using synthetic excipients has improved cellular entry and retention. This can be accelerated by establishing intra- and inter-vesicular drug depots that provide sustained effective drug release and as a consequence long-term protection against HIV challenge in macrophages and by cell to cell transfers between macrophage-CD4<sup>+</sup> T cell interactions [159, 163, 164]. In addition to synthetic nanoparticles, another drug delivery vehicle can take advantage of uptake retention and release of ARV particles in macrophages and could lead to improved drug delivery. These are exosomes. Exosomes are a class of extracellular vesicles with a natural size of 40–200 nm in diameter and serve as important messengers in the interaction between cells, tissues, and organs. Exosomes are constituted by multiple molecules, such as proteins, DNA and RNA, as well as by cholesterol and sphingomyelin [165]. Since exosomes may provide advantages of both synthetic nanotechnologies and cell-based schemes, interest in these carriers continues to grow. These endogenous vesicles travel throughout the body to



facilitate cell to cell communication through the delivery of biologically active cargo. Of note, exosomes possess an innate ability to cross biological barriers, including the blood brain barrier (BBB) [166]. Additionally, exosomes can be manipulated to carry exogenous molecules such as nucleic acids, proteins, and small molecules (Figure 1.10.8). In all, exosomes are emerging as a promising tool for therapeutic delivery due to their biocompatibility, stability, and ability to overcome cellular and anatomical barriers.

#### **1.7.1. Exosome Biogenesis**

The unique properties of exosomes can be attributed to their biogenesis. Exosomes are defined by their specific physical properties as part of greater populations of secreted vesicles. Notably, they differ from other shedding vesicles on their mode of biogenesis. Three main types of vesicles were described and include microvesicles (100 nm–1  $\mu$ m) which directly bud from the plasma membrane; apoptotic blebs (50–500 nm), which are released by cells undergoing apoptosis; and exosomes (30–100 nm) released by exocytosis from multivesicular bodies (MVBs) of late endosomes [167] (Figure 1.10.7). The current dogma of exosome biogenesis involves their generation through endocytic pathways. Here the plasma membrane invaginates to form an intracellular vesicle. The resulting vesicle fuses with endosomal compartments. When the endosomal membrane bubbles inward, the MVB forms, an organelle characterized by multiple internal vesicles enclosed within a single outer membrane[168]. The MVBs generated in the endocytic pathway move along microtubules and fuse with the plasma membrane. Upon fusion of the MVB with the plasma membrane the intraluminal vesicles (ILVs) are released as exosomes into the extracellular environment [168].

The mechanisms underlying exosome biogenesis and trafficking are an area of active investigation (00). Currently, two models have been proposed. One is exosome biogenesis which involves the system related to endosomal-sorting complex required for transport (ESCRT). In this model, MVB formation occurs when membrane proteins are ubiquitinated

and internalized into the early endosome. Here, ubiquitinated to be recognized by ESCRT-0, -I and -II and enter MVBs [169]. Exosomes are also generated through an ESCRT-independent pathway. The concentration of various membrane lipids may allow for raft-based segregation of cargo within the endosomal membrane. Presence of a ceramide microdomain has been shown to trigger budding of the endosomal membrane, and consequently the formation of the MVB [170]. Upon release from cells, exosomes can follow one of these three pathways: (1) they can be captured by nearby cells, (2) they can be internalized by cells within an intermediate distance, or (3) they can enter circulation and travel to distant tissues [171]. Exosomes' mode of action ultimately occurs by affecting intercellular communication. This occurs through transfer of bioactive molecules to their target cells.

#### **1.7.2. Exosome Lipid Composition**

The exosomal membrane is enriched with lipid-rafts including cholesterol, sphingolipids, ceramide and glycerophospholipids containing long and saturated fatty-acyl chains [168]. The concentration of various membrane lipids may allow for raft-based segregation of cargo within the endosomal membrane. Presence of a ceramide microdomain has been shown to trigger budding of the endosomal membrane, and consequently the formation of the MVB [170]. Exosomes contain cell-type specific lipids that reflect host cell identity. Oligodendrocytes release exosomes that include the lipids galactocerebroside, sulfatide, and cholesterol which are also prominent in oligodendroglial lipid rafts and characteristic myelin lipids [172]. Similar to plasma membranes, exosomes are organized in a bilayer. But unlike plasma membranes, the exosomal membrane is relatively rigid at pH 7. This rigidity may protect exosomes from lipolytic or proteolytic degradation in circulation [173].

#### **1.7.3. Exosome Protein Composition**

Exosomes of different cellular origins sequester a common set of molecules involved in biogenesis, fusion, transport, and vesicle structure (Table 1.10.3). They also carry cell-

type specific components, which may reflect the biological function of the parent cell. Proteins incorporated from the plasma membrane retain the same topological orientation as at the cell surface [174]. Because exosomes are generated in the endocytic pathway, neither nuclear, mitochondrial, nor endoplasmic proteins have been observed in exosomes [175]. Also due to their endosomal origin, exosomes contain proteins involved in membrane transport and fusion such as flotillin, Rab-GTPases, and annexin. The presence of such proteins may also be important for fusion of the exosomal membrane with the target cell [176]. Adhesion molecules such as tetraspanins and intercellular adhesion molecules (ICAMS) may also be functionally important for the fusion and trafficking of exosomes [168]. Exosomes contain cell-type specific proteins from the originating cell. For instance, exosomes derived from antigen presenting cells also carry MHC I and II on the surface as well as co-stimulatory molecules. Normal cellular components such as cytoskeletal proteins and metabolic enzymes are also common to the exosomal membrane. Proteome studies have revealed that exosomes contain a conserved set of proteins across species. For example, nearly all exosomes contain cytoplasmic proteins such as tubulin, actin, as well as the signal transduction proteins, kinases, heterotrimeric G-proteins. Proteins most commonly found associated with exosomes include heat shock proteins such as Hsp70 and Hsp 90, and certain members of the tetraspanin superfamily, especially CD9, CD63, CD81, and CD82 [168]. For this reason, the trinity of CD9, CD63, and CD81 is often used as an exosome marker.

#### **1.7.4. Exosome Cargo**

Proteins, messenger RNA (mRNA), micro RNA (miRNA) and DNA have all been identified in exosomal cargoes [177-179]. Cargoes are both cell-type and cell-state specific. Studies have shown that physiological conditions and the cellular microenvironment heavily influence content of exosomes. For example, it was shown that mouse mast cells exposed to oxidative stress released exosomes that differed in their mRNA content compared to their

normal counterparts [180, 181]. The mechanisms underlying the sorting of nucleic acids and proteins into exosomes are far from being unraveled. Recent studies have demonstrated that lipid rafts have the ability to sort proteins into exosomes [182]. Alternatively, the ESCRT complex may also be able to sort exosomal cargoes. Reports have demonstrated that the sorting of trans membrane proteins into the MVB pathway relies on the activity of various ESCRT components [183, 184]. Though ESCRT machinery has not yet been studied specifically in relation to exosomal cargo packaging, this finding encourages further investigation.

A mechanism for exosomal miRNA sorting has also been suggested. Recent studies indicate that the shuttling of miRNAs into exosomes is a selective process where specific miRNA motifs are recognized by the heterogeneous nuclear ribonucleoprotein A2/B1 (hnRNPA2B1), a ubiquitously expressed RNA binding protein [185]. Other reports find that 3'-end uridylated miRNA isoforms are over-represented in exosomes and facilitate selective miRNA sorting into exosomes, while 3'-end adenylation increases the probability for retention within the cell [186]. Consistent with these findings, exosomal miRNAs are composed of a distinct set of miRNAs, different from the miRNA signature of the parent cell [187]. In all, the evidence may imply that certain miRNAs have evolved to be packaged into exosomes to carry out a specific biological function.

### **1.8 Exosomes in Nanomedicine**

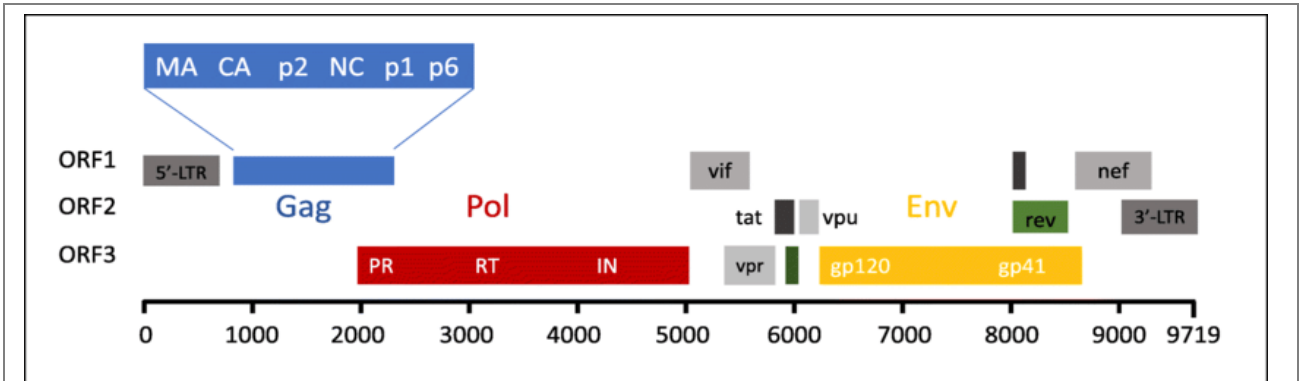
Exosomes have recently come into focus as natural nanoparticles for use as drug delivery vehicles. Their inherent ability to carry metabolically active cargo and travel in the body makes exosomes attractive as therapeutic delivery vehicles. Exosomes may offer several advantages over synthetic nanoscale delivery vectors. One such advantage is that exosomes are able access immunologically restricted tissues. While some exosomes actively participate in immune function, other exosomes can avoid immune-surveillance, perhaps due to the nature of self-tolerance. Several studies have demonstrated the capacity

of exosomes to mediate drug delivery to immune privileged sites. In a report, exosomes were used to encapsulate both curcumin and an activator of Stat3 inhibitor, JSI124. Intranasal administration of these exosome formulations led to rapid delivery of drug to the brain, and protected mice from LPS-induced brain inflammation [188]. In another study, when exosomes loaded with catalase were administered intranasally in a mouse model of Parkinson's, exosomes were readily taken up by neuronal cells, and significant neuroprotective effects were observed in vitro [189]. Exosomes have also been employed for peripheral delivery of small molecules [188, 190-193]. Exosomes loaded with small molecules such as doxorubicin (DOX), paclitaxel (PTX), or the photosensitizer zinc phthalocyanine (ZnPc) were shown to traffic to tumor tissues and reduce tumor growth in mice [191, 192, 194]. Notably in Jang et al., the therapeutic effects of Dox-loaded exosome mimetic nanovesicles were reportedly greater than Doxil, a commercial PEGylated liposomal formulation of Dox [191]. Additionally, PTX-loaded exosomes demonstrated increased cytotoxicity in drug resistant cells, and a potent anticancer effect in a model of murine Lewis lung carcinoma pulmonary metastases [195]. Finally, vesicles loaded with ZnPc, a hydrophobic small molecule that functions as a photosensitizer, exhibited superior phototherapeutic effects compared to polymer-based synthetic nanoparticles [196]. In all, small molecule exosome formulations may more effectively bypass biological membranes and penetrate tissue reservoirs compared to synthetic nanoparticles.

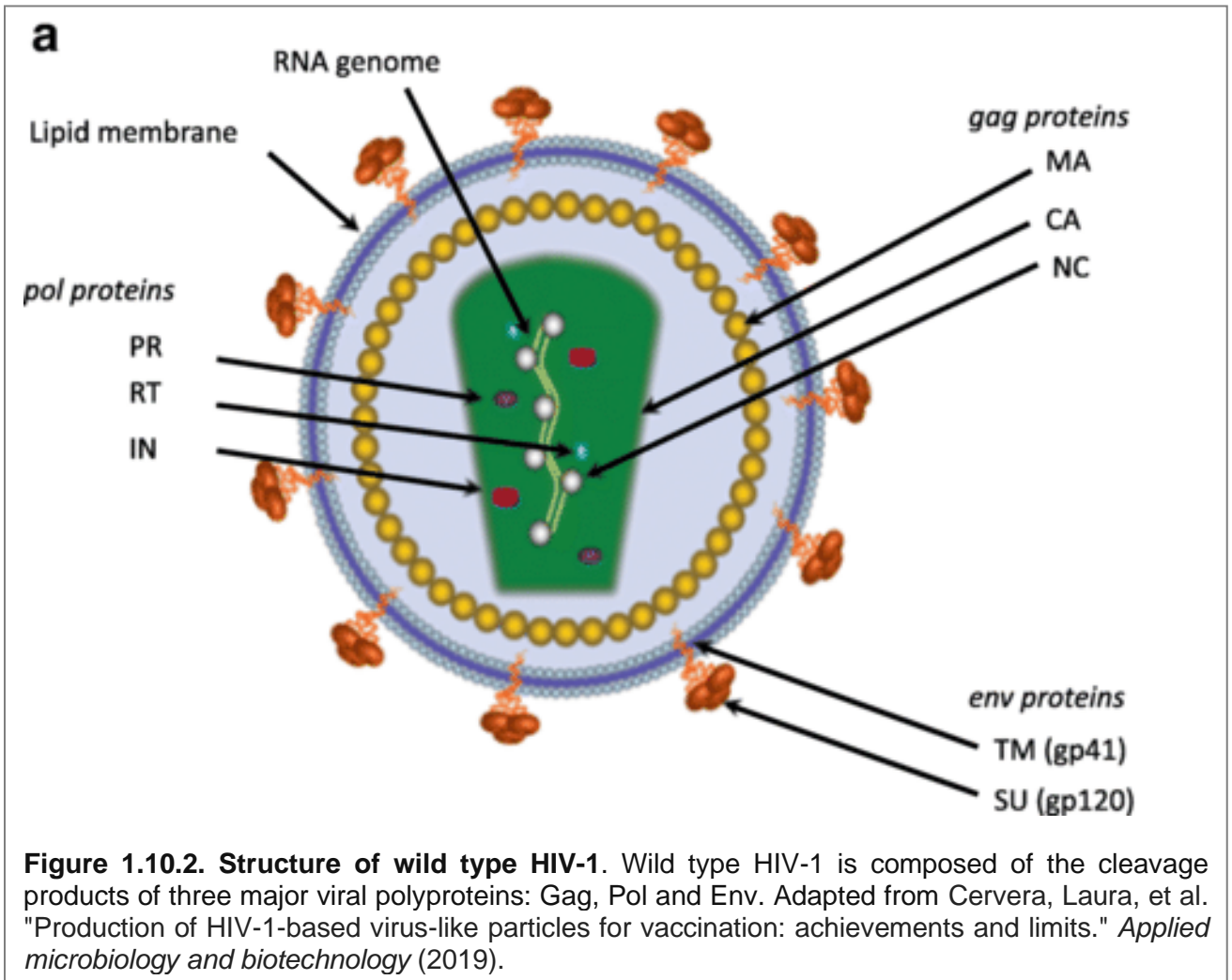
### **1.9 Summary**

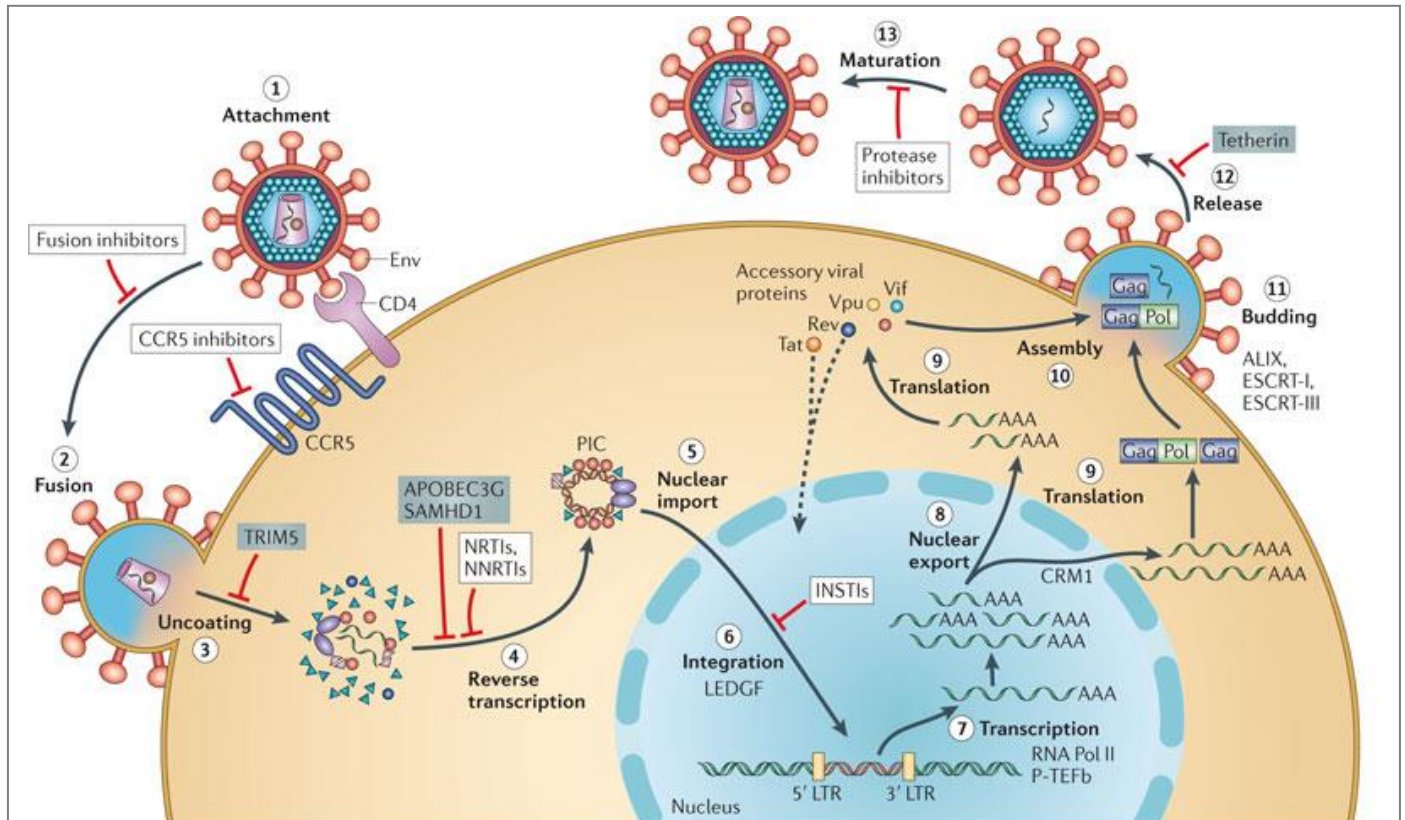
HIV treatment and prevention with a goal of viral eradication is a challenge that needs to be met. Current oral therapies, while effective in preventing disease and reducing disease morbidity and mortality cannot meet this goal alone. Lack of adherence to daily oral dosing regimens leads to viral resistance, reduced treatment effectiveness and lack of prevention. Long-acting synthetic and biologic formulations for ARV delivery provide a potential means of addressing these challenges.

## 1.10 Figures and Tables



**Figure 1.10.1. Schematic representation of HIV-1 genome.** The genome is composed of 3 structural genes (gag, pol and env) 4 accessory genes in grey and 2 regulatory genes in green located throughout the 3 ORFs. Gag is further processed into 6 protein domains known as matrix (MA or p17), capsid (CA or p24), spacer peptide 1 (SP1 or p2), nucleocapsid (NC or p7), spacer peptide 2 (SP2 or p1) and p6. Adapted from Cervera, Laura, et al. "Production of HIV-1-based virus-like particles for vaccination: achievements and limits." *Applied microbiology and biotechnology* (2019).

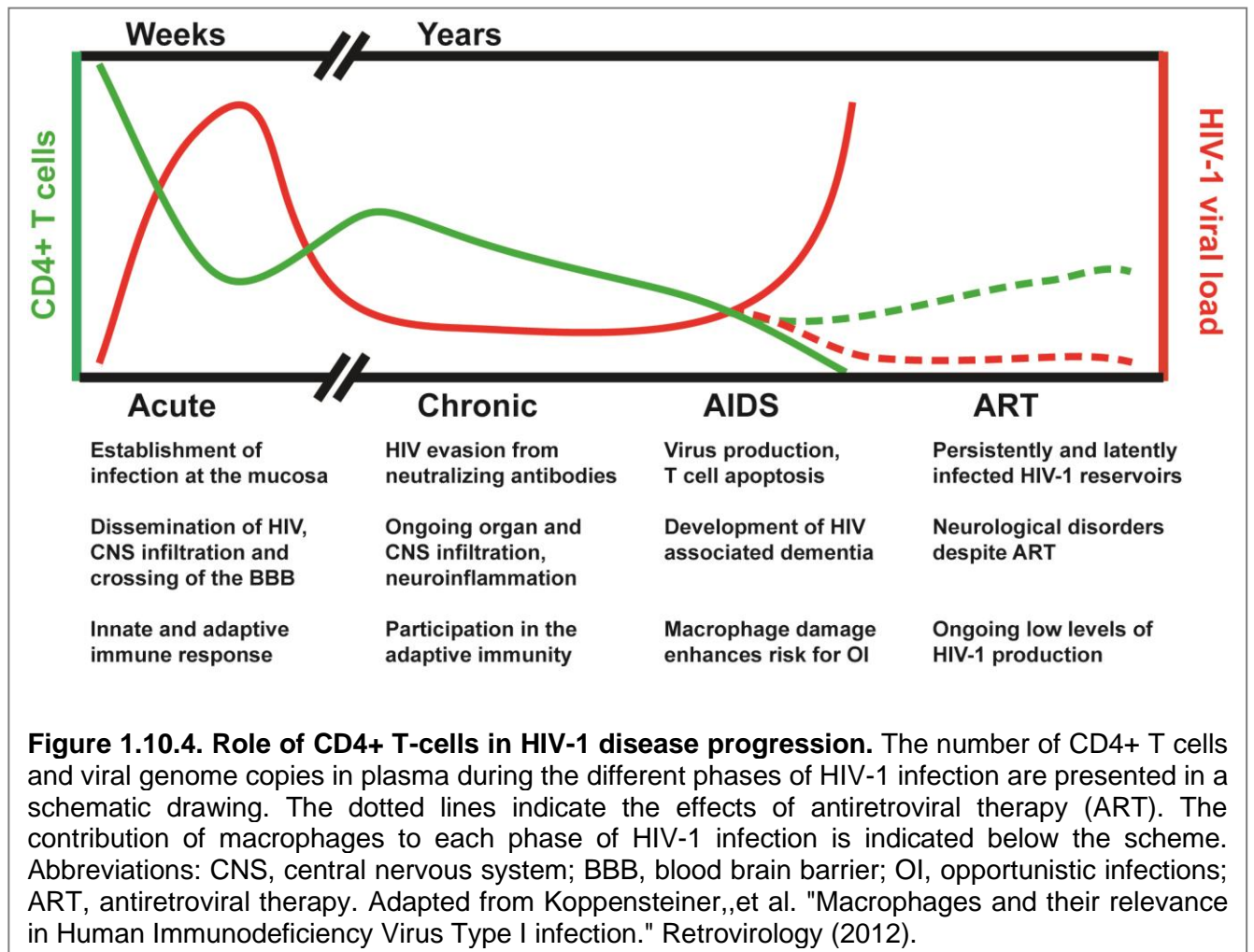


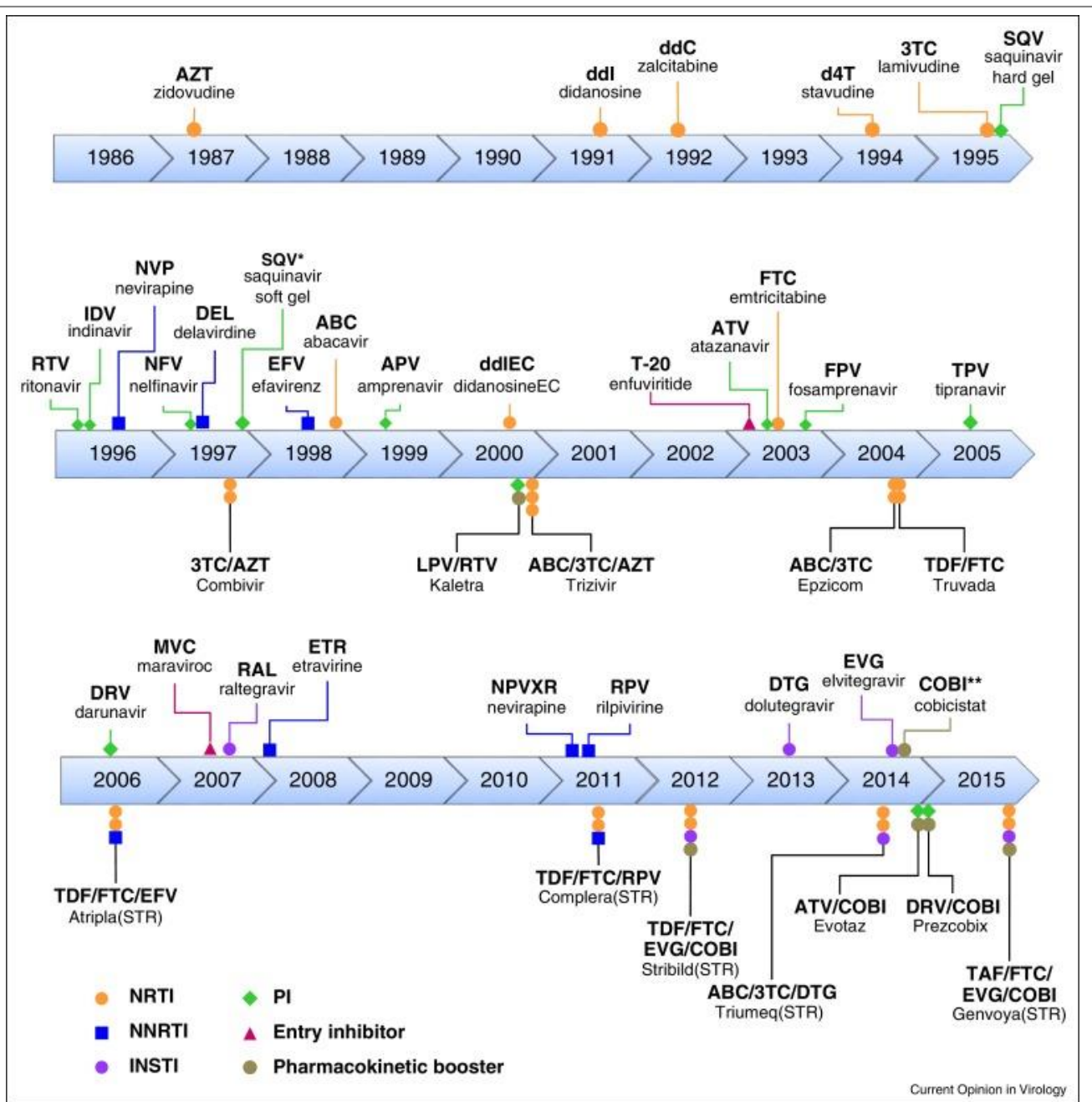


Nature Reviews | Microbiology

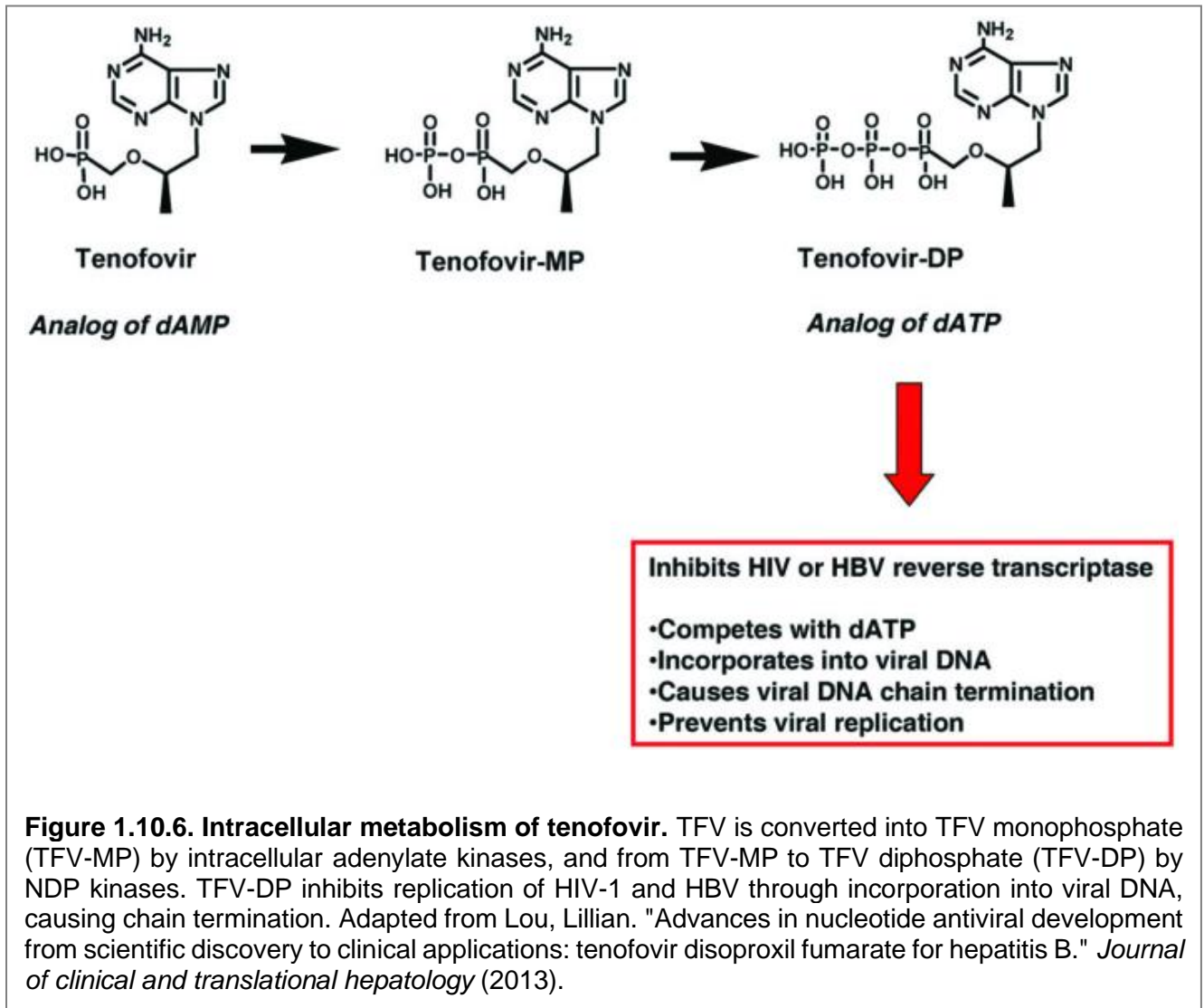
**Figure 1.10.3. HIV-1 Life cycle and ART targets.** HIV-1 must attach to the CD4 receptor and subsequently a coreceptor (CCR5 or CXCR4) to gain cellular entry. Entry inhibitors such as MVC bind to CCR5 and prevent HIV-1 cellular entry. Furthermore, membrane fusion facilitated by HIV-1 gp41 merges the viral and host cell membranes exposing viral RNA into the cytoplasm. Membrane fusion is disrupted by the fusion inhibitor enfuvirtide. Reverse transcriptase converts single stranded RNA into double stranded DNA. This stage of the viral life cycle is inhibited by NRTIs, such as TFV, and NNRTIs, such as RPV. Viral DNA integration into the host cell genome is inhibited by integrase inhibitors (INI, DTG, CAB). Moreover, protease inhibitors prevent new virions from becoming mature and infectious by inhibiting the actions of protease (PI; Darunavir; DRV). Figure adapted from Engelmann, Alan, and Peter Cherepanov. "The structural biology of HIV-1: mechanistic and therapeutic insights." *Nature Reviews Microbiology* (2012).

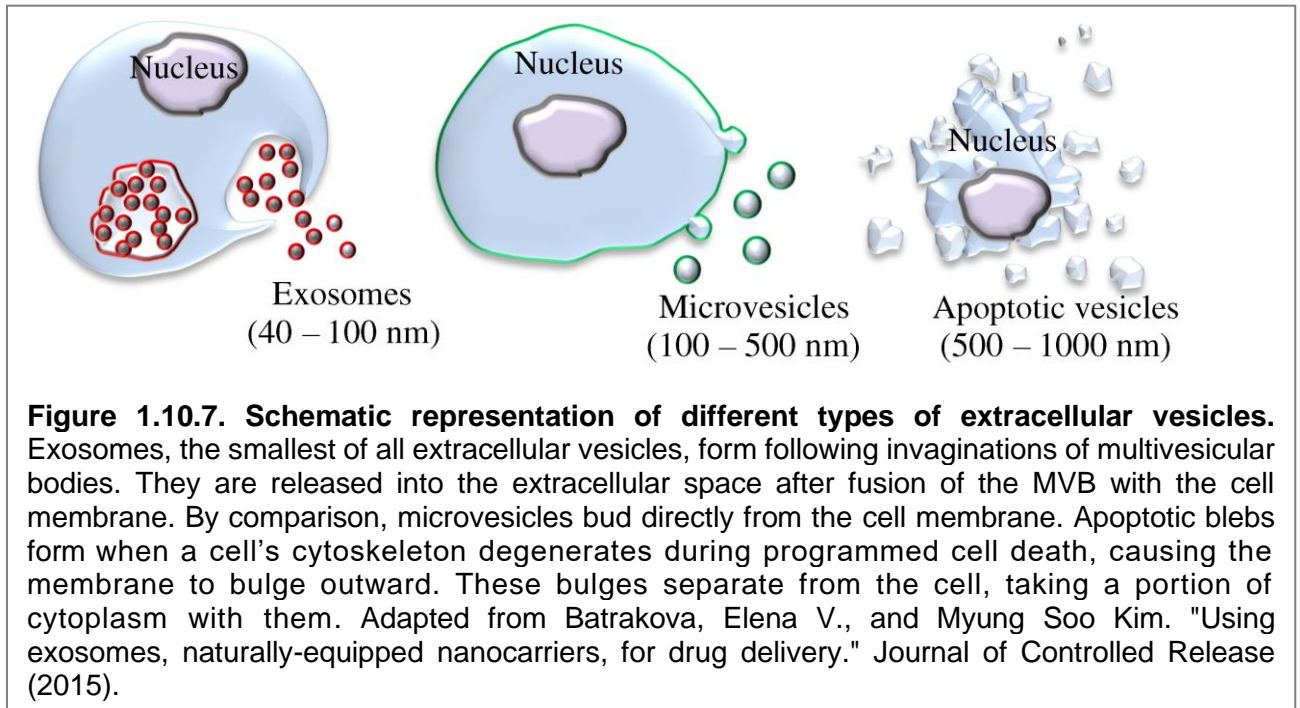


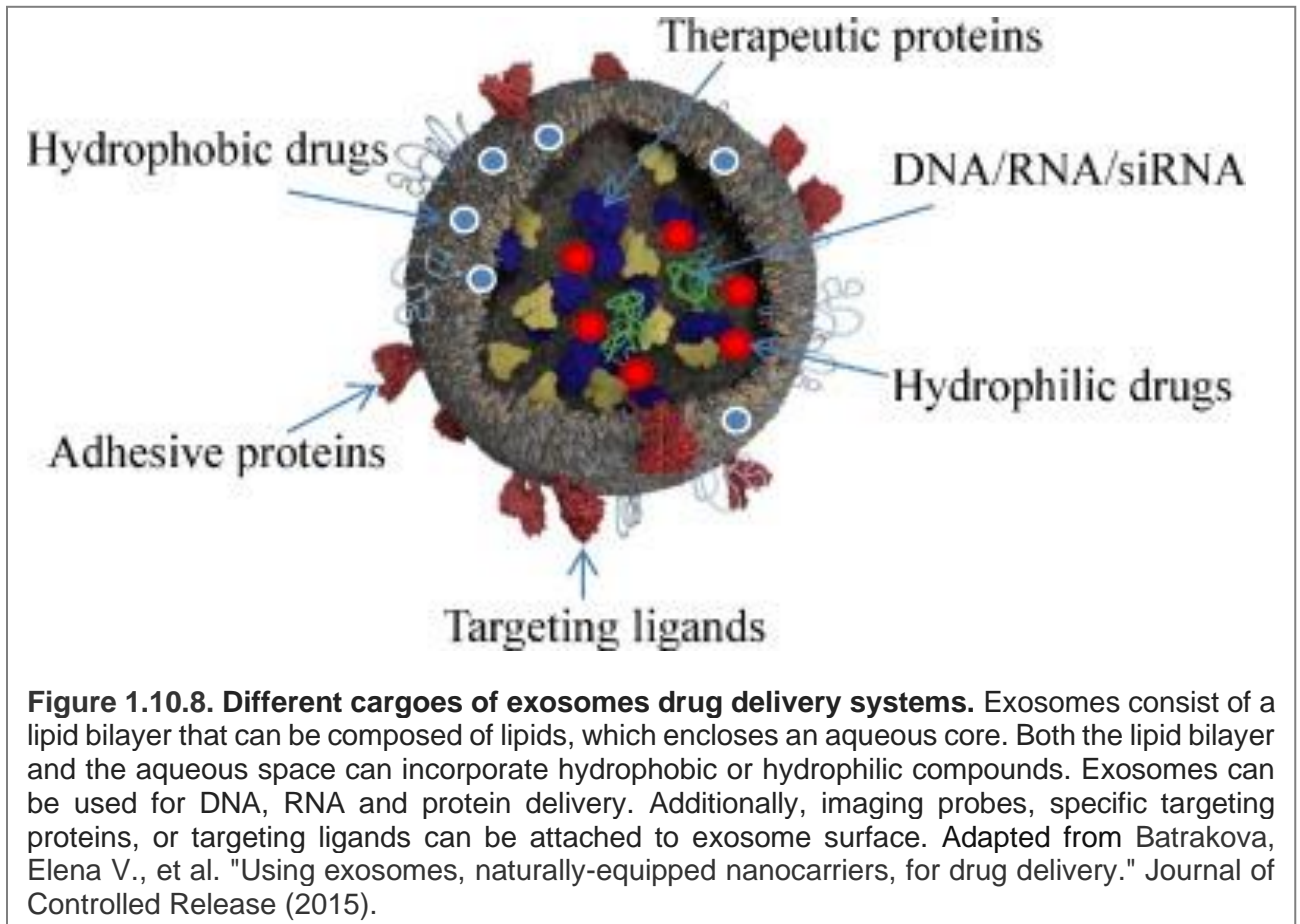




**Figure 1.10.5. FDA-approved individual antiretroviral drugs and drug combinations.** ER, enteric-coated; XR, extended release; STR, single-tablet regimen. Adapted from Cihlar, Tomas, and Marshall Fordyce. "Current status and prospects of HIV treatment." Current opinion in virology (2016).







<b>Table 1.10.1. Advantages and limitations of long-acting approaches to HIV-1 treatment and prevention</b>		
<b>Approach</b>	<b>Advantages</b>	<b>Limitations</b>
Oral delivery (nanoparticle and nano-emulsifying formulations, long acting ARVs)	<ul style="list-style-type: none"> <li>Potential for weekly dosing</li> <li>Convenience of self-administration</li> </ul>	<ul style="list-style-type: none"> <li>Compared to daily dosing, weekly dosing could be more difficult to remember</li> <li>HIV-1 treatment requires drug partners with similar PK properties</li> </ul>
Gastric residence devices	<ul style="list-style-type: none"> <li>Potential for weekly dosing</li> <li>Convenience of self-administration</li> <li>Administration of drug combinations possible</li> </ul>	<ul style="list-style-type: none"> <li>Device failure could result in adverse events such as drug overdose or GI obstruction</li> <li>Compared to daily dosing, weekly dosing could be more difficult to remember</li> <li>Combination product that may be subject to additional testing and/ or regulations</li> </ul>
Suspension and reservoir transdermal patches	<ul style="list-style-type: none"> <li>Potential of weekly dosing for PrEP</li> <li>Avoids first-pass metabolism</li> <li>Convenience of self-administration</li> <li>Easy to discontinue</li> <li>Can combine with contraceptives to prevent unintended pregnancy</li> </ul>	<ul style="list-style-type: none"> <li>Subject to user error</li> <li>Device failure could result in drug overdose</li> <li>May be affected by daily activities such as bathing and swimming</li> <li>Combination product that may be subject to additional testing and/ or regulations</li> </ul>
Transdermal microneedle patch	<ul style="list-style-type: none"> <li>Potential for weekly dosing for PrEP</li> <li>Avoids first-pass metabolism</li> <li>Convenience of self-administration</li> <li>Can combine with contraceptives to prevent unintended pregnancy</li> </ul>	<ul style="list-style-type: none"> <li>Subject to user error</li> <li>Irreversible following microneedle dissolution</li> <li>May be affected by daily activities such as bathing and swimming</li> <li>Combination product that may be subject to additional testing and/ or regulations</li> </ul>
Vaginal rings	<ul style="list-style-type: none"> <li>Once-monthly or greater potential dosing interval for PrEP</li> <li>Avoids first-pass metabolism</li> <li>Convenience of self-administration</li> <li>Can combine with contraceptives</li> </ul>	<ul style="list-style-type: none"> <li>Subject to user error</li> <li>Combination product that may be subject to additional testing and/ or regulations</li> </ul>
Broadly neutralizing antibodies	<ul style="list-style-type: none"> <li>Discreet</li> <li>Unique mechanism of action offers treatment alternative</li> <li>Can be used in both treatment and prevention regimens</li> </ul>	<ul style="list-style-type: none"> <li>Combination approach required to avoid escape mutations</li> <li>Not a user controlled- method, therefore dosing may be less convenient</li> <li>Potentially difficult to administer in regions with limited access to healthcare</li> </ul>
Subcutaneous implants	<ul style="list-style-type: none"> <li>Once every six months or greater dosing interval</li> <li>Avoids first-pass metabolism</li> <li>Discreet</li> <li>Reservoir devices are removable</li> </ul>	<ul style="list-style-type: none"> <li>Device failure could result in drug overdose</li> <li>Biodegradable implants are not fully removable following polymer-dissolution</li> <li>Potentially difficult to administer in regions with limited access to healthcare</li> <li>Combination product that may be subject to additional testing and/ or regulations</li> <li>Use of organic solvents to dissolve hydrophobic drugs maybe challenging during scale up</li> </ul>
Long acting cabotegravir and rilpivirine (cabenuva)	<ul style="list-style-type: none"> <li>Discreet</li> <li>Once every month or two months dosing interval</li> <li>Avoids first-pass metabolism</li> </ul>	<ul style="list-style-type: none"> <li>Not reversible</li> <li>Not a user controlled- method, therefore dosing may be less convenient</li> <li>Monthly injections and clinical visits could be potentially challenging to implement in regions with limited access to healthcare</li> </ul>
Long acting capsid inhibitor (GS-6207)	<ul style="list-style-type: none"> <li>Discreet</li> <li>Once every 3-6 months dosing interval</li> <li>Unique mechanism of action offers treatment alternative</li> <li>Avoids first-pass metabolism</li> </ul>	<ul style="list-style-type: none"> <li>Not reversible</li> <li>Not a user controlled- method, therefore dosing may be less convenient</li> </ul>
LASER ART	<ul style="list-style-type: none"> <li>Offers possibility of once-yearly dosing for PrEP</li> <li>Discreet</li> <li>Avoids first-pass metabolism</li> <li>Drug delivery to sites of infection</li> <li>Potential role in HIV-1 elimination strategies</li> </ul>	<ul style="list-style-type: none"> <li>Not reversible</li> <li>Not a user controlled- method, therefore dosing may be less convenient</li> </ul>

**Table 1.10.2. Long-acting approaches for the treatment and prevention of HIV**

<b>Agent</b>	<b>Route of Administration</b>	<b>Potential Indication</b>	<b>Stage of Development</b>	<b>References</b>
Islatravir	Oral	HIV PrEP	Phase 1b	[27, 74, 126, 127]
Gastric residence device	Oral	HIV treatment and PrEP	Preclinical	[80]
Maraviroc, efavirenz, and lopinavir solid drug nanoparticle formulations	Oral	HIV PrEP	Preclinical	[82]
Darunavir/ ritonavir nanoparticle-in-microparticle delivery system (NIMDS)	Oral	HIV PrEP	Preclinical	[84]
EFV, lopinavir, and darunavir nano-emulsifying systems	Oral	HIV PrEP	Preclinical	[85, 86]
Tenofovir alafenamide fumarate patch	Transdermal	HIV PrEP	Preclinical	[90]
Rilpivirine microneedle patch	Transdermal	HIV PrEP	Preclinical	[91]
Dapivirine ring	Vaginal	HIV PrEP	Phase 3	[100, 101, 103]
Tenofovir and levonorgestrel ring	Vaginal	HIV PrEP	Phase 1	[102]
3BNC117	Intravenous infusion	HIV PrEP	Phase 1	[115]
VRC01LS	Intravenous infusion or subcutaneous injection	HIV PrEP	Phase 1	[116]
3BNC117 + 10-1074	Intravenous infusion	HIV treatment and PrEP	Phase 1b	[106, 118]
Nevirapine implant	Subcutaneous	HIV PrEP	Preclinical	[123]
Dolutegravir implant	Injectable (subcutaneous)	HIV PrEP	Preclinical	[125]
Islatravir implant	Subcutaneous	HIV PrEP	Phase 1	[126, 127]
Tenofovir alafenimide fumarate implant	Subcutaneous	HIV PrEP	Preclinical	[128-131, 133, 197, 198]
Refillable emtricitabine and tenofovir alafenamide fumarate implant	Subcutaneous	HIV PrEP	Preclinical	[131]
Cabotegravir nanofluidic implant	Subcutaneous	HIV PrEP	Preclinical	[132]
Long acting cabotegravir and rilpivirine (cabenuva)	Injectable (intramuscular)	HIV treatment and PrEP	Approved-USA, Europe and Canada	[32, 137, 138, 140, 141, 199, 200]
Long acting capsid inhibitor (GS-6207)	Injectable (subcutaneous)	HIV treatment	Phase 1	[142, 143]
Dolutegravir, lamivudine, emtricitabine, abacavir, rilpivirine, and cabotegravir LASER-ART	Injectable (intramuscular)	HIV PrEP	Preclinical	[33, 139, 148, 150-154, 163, 164, 201]

Table 1.10.3. Common exosome markers
Heat shock proteins <ul style="list-style-type: none"> <li>• Hsp 70, 90</li> </ul>
Adhesion molecules <ul style="list-style-type: none"> <li>• Integrins</li> <li>• Tetraspanins (CD9, CD63, CD81, CD82)</li> <li>• Immunoglobulin family members</li> </ul>
Membrane transport and fusion <ul style="list-style-type: none"> <li>• Rab GTPases</li> <li>• Annexin</li> <li>• Flotillin</li> </ul>
Endosomal sorting proteins <ul style="list-style-type: none"> <li>• Alix</li> <li>• Tsg101</li> </ul>
Lysosomal proteins <ul style="list-style-type: none"> <li>• LAMP</li> </ul>
Antigen presentation <ul style="list-style-type: none"> <li>• MHC class I &amp; II</li> </ul>
Cytoskeletal components <ul style="list-style-type: none"> <li>• Actin</li> <li>• Tubulin</li> <li>• Profilin</li> <li>• Cofilin</li> </ul>
Metabolic enzymes <ul style="list-style-type: none"> <li>• GAPDH</li> <li>• Pyruvate kinase</li> </ul>
Membrane proteins from cell of origin



## CHAPTER 2- EXOSOMES AS AN ANTIVIRAL DRUG DELIVERY PLATFORM

### 2.1 Abstract

Exosomes are 30-150 nm extracellular vesicles that transport RNAs, proteins and small molecules between cells. Exosomes serve as endogenous carriers of biological cargo with natural features for immune cell targeting, and thus have generated immense interest for drug delivery. The physical and biochemical properties of exosomes offer many advantages for drug delivery over alternative synthetic nanoscale systems. With this in mind, we sought to utilize exosomes as a natural vehicle for ARV delivery. We posit that exosomes can be harnessed to carry ARV drugs, target macrophages for drug delivery, build intracellular drug depots, and improve the pharmacokinetic and pharmacodynamic profiles of ARVs. We show through this work that exosomes can carry ARVs, are taken up by macrophages, and display antiviral efficacy. Specifically, we found the combination of lipidic ARV prodrugs, such as 18-carbon modified DTG (SDTG) and 22-carbon modified DTG (DDTG), loaded into exosomes via sonication resulted in highest encapsulation, 898.3  $\mu\text{g}/10^9$  vesicles and 964.9  $\mu\text{g}/10^9$  vesicles, respectively. In monocyte-derived macrophages (MDM), SDTG and DDTG exosome formulations avoided cytotoxicity, an issue observed for exosomes loaded with hydrophobic parent ARVs such as atazanavir (ATV) and DTG. The exosome STDG and DDTG formulations displayed superior uptake and retention in MDM compared to free drug controls, demonstrating the ability of exosomes to target and build drug depots in macrophages. This translated to suppression of viral replication in MDM out to 15 days post-treatment. In all, exosome-based nanoparticle systems hold opportunities for improving ART.

### 2.2 Introduction

Comprised of lipid bilayer membranes expressing a unique set of proteins on their surface, exosomes mediate cell–cell communication through the delivery of bioactive cargo, and are thereby well suited as drug delivery vehicles. Exosomes may offer several advantages

compared to conventional synthetic nanoparticle platforms. For instance, exosomes could increase vesicle trafficking to immune privileged sites and allow for reduced opsonization compared to polymeric PEG formulations. Additionally, bioengineering approaches can be employed to express targeting moieties on the vesicle surface and load RNA or nucleic acid cargo [189, 202, 203]. Due to the advantages conferred by exosome nanocarriers, we herein investigated the production of ARV loaded exosomes. In the current study, combinations of various drug encapsulation methods, as well as ARVs (hydrophobic parent drugs, hydrophilic parent drugs, lipophilic prodrugs) were investigated to identify an optimal exosome ARV formulation. The highest levels of drug encapsulation were achieved when exosomes were loaded with the DTG prodrugs (SDTG and DDTG) using sonication, While exosomes loaded with parent ARVs such as ATV and DTG demonstrated significant concentration-dependent cytotoxicity in MDM, there was no evidence that SDTG and DDTG exosome formulations affected cell vitality. Additionally, the SDTG and DDTG exosomes enhanced uptake and retention in MDM compared to free drug. Such biological outcomes provide evidence that exosome-based nanoparticle systems hold opportunities for improving ART.

## **2.3 Materials and Methods**

### **2.3.1 Materials**

Methanol (MeOH), pluronic F127 (P407), saponin, (3-(4,5-dimethylthiazol-2-yl)-2,5-diphenyl tetrazolium bromide) (MTT), dimethyl sulfoxide, HEPES buffer solution, ciprofloxacin, were purchased from Sigma-Aldrich. Optima MS-grade water, cell-culture-grade water (endotoxin free), and gentamicin, and Pierce 660 nm protein assay kit were purchased from Fisher Scientific. Heat-inactivated pooled human serum was purchased from Innovative Biologics (Herndon, VA). DMEM was purchased from Corning Life Sciences. Plasmotest™ Mycoplasma Detection Kit was obtained from Invivogen. PYROGENT™ 5000 Kinetic Turbidimetric LAL Assay, 100 Test Kit was purchased from Lonza. Human TNF alpha ELISA Kit (ab181421), anti-ALIX antibody (ab117600), and recombinant Anti-CD81

antibody (ab109201) were purchased from Abcam. ExoQuick-TC reagent was purchased from Systems Biosciences. Millex-GV Syringe Filter Unit, 0.22  $\mu\text{m}$ , PVDF, 33 mm, gamma sterilized were purchased from MilliporeSigma. 5 mL, Open-Top Thinwall Polypropylene Tubes, 13 x 51mm (326819) were purchased from Beckman Coulter.

### **2.3.2 Human MDMs**

Human monocytes were obtained by leukapheresis from HIV-1/2 and hepatitis B seronegative donors and purified by counter-current centrifugal elutriation. Monocytes were cultured in DMEM that contained 4.5 g l<sup>-1</sup> glucose, L-glutamine, and sodium pyruvate supplemented with 10% heat-inactivated human serum, 50  $\mu\text{g ml}^{-1}$  gentamicin and 10  $\mu\text{g ml}^{-1}$  ciprofloxacin. Cells were maintained at 37 °C in a 5% CO<sub>2</sub> incubator. Recombinant human macrophage colony stimulating factor (1,000 U ml<sup>-1</sup>) was added to the culture media for the first 7 days to facilitate monocyte differentiation into MDMs. Half-culture media were replaced with fresh media every other day. After differentiation, MDMs were used for the in vitro assays.

### **2.3.3 Exosome isolation from supernatants**

Ultracentrifugation technique: Culture media was removed from the cells and centrifuged twice at 300g for 10 min, once at 2000g for 20 min, and once at 10 000g for 30 min at 4°C. To spin down exosomes, this culture media was centrifuged at 100 000g for 70 min at 4°C. To remove protein contaminants, the pellet was resuspended in PBS and centrifuged at 100 000g for an additional 70 min at 4°C.

Polymer Technique (Figure 2.6.2): One-milliliter aliquots of human monocyte derived macrophages (MDMs) cell-conditioned medium were cleared of cellular debris by centrifugation at 300 × g for 10 min at 4° C, then 2000 × g for 10 min. The fluids were filtered through 0.22  $\mu\text{m}$  filter unit and Exoquick-TC™ added in 1:5 ratio, vortexed gently, and stored at 4°C overnight. After centrifugation at 1500 × g for 30 min the exosome pellet was collected.

### 2.3.4 *In vitro* exosome ATV loading

MDM cultured in exosome-depleted medium were treated for 24 hours with either no treatment, free-ATV (100uM), nano-ATV (100uM), free-ATV (100uM)+URMC-099 (100ng/ml), or free-ATV (100uM)+URMC-099 (400ng/ml). URMC-099, an autophagy potentiator known to enhance drug retention in MDM [204], was employed to determine if it could increase the drug concentration in released exosomes. After the 24-hour period, the drug-containing medium was removed, and cells were washed twice with sterile PBS to remove excess drug. Cells were incubated with exosome-cleared medium. One-milliliter aliquots of cell-conditioned medium were collected everyday for a week. Exosomes were isolated using differential centrifugation and precipitation with Exoquick-TC™. ATV concentration for each sample was measured by UPLC-QDa.

### 2.3.5 *Ex vitro* ATV loading

Four methods of ATV incorporation were tested: sonication, freeze-thaw, incubation at room temp. and incubation with 0.2% saponin. (1) Sonication: 1 mg ARV per  $10^9$  exosomes was sonicated (750 W, 20 kHz, 20% power, 6 cycles by 4 sec pulse / 2 sec pause), cooled down on ice for 30 min. (2) Saponin: A mixture of 1 mg ARV per  $10^9$  was supplemented with 0.2% saponin and placed on shaker for 20 min at room temp. (3) Incubation at room temp: A mixture of 1 mg ARV per  $10^9$  was placed on shaker for 20 min at room temp. (4) Freeze-thaw: 1 mg ATV was added per  $10^9$ , incubated for 30 min, then rapidly frozen at  $-80^{\circ}\text{C}$ , and thawed at room temp. The freeze-thaw cycle was repeated three times.

### 2.3.6 Exosome purification after drug loading

Drug-loaded exosomes were purified from free drug by first centrifuging the mixture at  $200\times g$  at  $4^{\circ}\text{C}$  for three minutes,  $5000\times g$  for 5 minutes, followed by ultracentrifugation at  $100,000\times g$  at  $4^{\circ}\text{C}$  for 70 min in a Beckman SW 55 Ti rotor. ARV content of the exosomes was determined using a Waters UPLC H-Class System coupled to a UV detector, or a Waters UPLC H-Class System coupled to a QDa mass detector as previously described [205].

### **2.3.7 Exosome depletion from human serum**

Experiments were performed with culture media supplemented with exosome depleted human serum. Exosomes were depleted from serum following ultracentrifugation for 18h at 100,000g.

### **2.3.8 Characterization of exosomes by Nanoparticle tracking analysis**

Exosome isolation was performed as described above and the sample was used to analyze exosome size distribution and concentration using Nanosight NS300TM (Malvern Instruments, UK) at the University of Nebraska Medical Center Electron Microscopy Core Facility. Manufacturer's instructions were followed. Briefly, exosomes pellets were resuspended in 100 µl PBS, following which 10 µl of the sample was diluted to 1:100 – 1:1000 in PBS prior to measurements. The machine is equipped with a 488 nm laser and a syringe pump system, with a pump infusion speed of 20. The standard measurement option was selected for the scripted workflow to capture videos. The number and duration of captures was set to 5 and 60s, respectively. The camera level and focus was adjusted. Background measurements were performed with PBS (centrifuged at 100,000g for 70 min). Five video recordings were carried out for each exosome preparation with a duration of 60s with frame rates of 25 frames/sec. Once the videos were recorded, the NTA 3.1 software version analyzed the sample videos. For analysis, the screen gain was set to 1.0, and the detection threshold was adjusted to set the minimum brightness of pixels to be considered. At the end of the analyses, the dilution factor for the samples was accounted for prior to data export.

### **2.3.9 Characterization of exosomes by Western blotting**

Exosome pellets were homogenized in RIPA buffer containing 1% SDS, and protein estimated using the Pierce 660 nm protein assay kit (measured at 660 nm). Briefly, 20-40 µg protein was loaded onto 4–12% Bis-Tris gels and run under reducing conditions followed by transfer to nitrocellulose membranes. Then, membranes were blocked in TBS for 30 min, and immunoblotting carried out overnight at 4°C with Alix primary antibody (1:1000 dilution).

The following day, membranes were incubated with respective HRP conjugated secondary antibody for 1.5 h at room temperature on a rocker. Blots were developed with 1:1 solution of Radiance Chemiluminescent Substrate and Luminol/Enhancer and visualized using x-ray film.

### **2.3.10 Cytotoxicity**

The cell viability after treatment with exosomes was evaluated using the MTT assay. Human MDMs plated in 96-well plates at a density of  $0.08 \times 10^6$  cells per well were treated with MDMs were treated with 50  $\mu$ M exoDTG, free DTG, exoATV, free ATV, or control exosomes for 2h or 8 h. Untreated cells were used as controls. For each group, quadruplicate samples were used. After the 8 h drug treatment, the cells were washed with phosphate buffered saline (PBS) and incubated with 100  $\mu$ l per well of MTT solution (5 mg ml<sup>-1</sup>) for 45 min at 37 °C. After incubation, the MTT solution was removed, and the cells were washed with PBS. Next, dimethyl sulfoxide (200  $\mu$ l) was added to each well, and the absorbance was measured at 490 nm on a Molecular Devices SpectraMax M3 plate reader with SoftMax Pro 6.2 software. Absorbance was compared to that of control cells to determine the cytotoxicity.

### **2.3.11 Exosome uptake and retention in MDM**

Human MDMs were used for in vitro assessments. MDM uptake and retention studies were performed in flat-bottom, 12-well plates at a density of  $1.2 \times 10^6$  cells per well, with n=6 wells for each treatment. For cellular uptake studies, MDMs were treated with 50  $\mu$ M exoDDTG, free DDTG, exoSDTG, free SDTG, exoATV, nanoATV, or free ATV. At 2, 4, and 8 h after treatment, the medium was removed; MDMs were washed twice with PBS then scraped into 1 ml of PBS and counted (Invitrogen Countess Automated Cell Counter). Cells were pelleted by centrifugation at 3000 *rpm* for 8 min at 4 °C. Cell pellets were resuspended in 200  $\mu$ l of HPLC-grade MeOH and sonicated using a probe sonicator, then vortexed for 3 min to extract the intracellular drug. The cell lysates were centrifuged at 17,000 *rpm* for 10 min at 4 °C to separate cell debris from the drug-containing supernatant. Samples were

analyzed for drug content by UPLC–UV/vis spectroscopy. For the retention studies, MDMs were treated with 10  $\mu$ M or 100  $\mu$ M NM1TFV, NM2TFV or NTAF for 8 h, and then washed twice with 1 ml PBS. Then, culture medium (without drug) was added, and a half-media volume was replaced every other day. MDMs were collected at days 1, 5, 10, 15, and 30 post-treatment, and then processed as described to assay the intracellular drug concentrations.

### **2.3.12 Transmission electron microscopy**

After in vitro or ex vitro loading and purification described above, exosomes pellets were resuspended in 1mL PBS. Then the exosome suspension was placed on a formvar/silicon monoxide 200 mesh copper grid and allowed to settle for 2 min. Excess solution was wicked off, and the samples were allowed to dry. NanoVan vanadium negative stain was placed on the grid for 1 min, then wicked away and allowed to dry. Grids were examined on a FEI Tecnai G2 Spirit TWIN TEM operated at 80 kV. Images were acquired digitally with an AMT digital imaging system.

### **2.3.13 Antiretroviral efficacy of ATV exosomes**

HIV-1 reverse transcriptase (RT) activity was determined for MDM treated with nanoATV or exoATV at concentrations of 1  $\mu$ M or 10  $\mu$ M ATV. MDM were treated for 8 hours followed by HIV-1 infection (HIV-1<sub>ADA</sub> at MOI of 0.1), and collection on days 1, 3, 5, 7, 9, 11, and 14. HIV-1 infected cells without treatment served as positive controls while HIV-1 infected cells treated with naïve exosomes acted as vehicle controls. HIV-1 RT assay was used to determine antiretroviral activity of exosome formulations as previously described [205, 206]. Briefly, on days 1, 5, 10, 15, 20, 25 and 30 post- treatment, the cells were infected with HIV-1<sub>ADA</sub> at a multiplicity of infection of 0.1 infectious particles per cell for 8 h. After infection, MDMs were washed twice with PBS and replenished with fresh media without virus or drug. The cells were cultured for an additional 10 days with half-media replacement every other day and full medium replacement on the 8th day. The culture medium was collected on

the 10th day after infection to measure the HIV-1 RT activity. The extent of infection was determined as the percent of RT activity relative to the infected untreated MDM. Results shown are the means of 6 replicates.

#### **2.3.14 Antiretroviral efficacy of SDTG and DDTG exosomes**

MDMs were plated in flat-bottom 12-well plates at a density of  $1.2 \times 10^6$  cells per well. MDMs were treated with 50  $\mu$ M exoSDTG, exoDDTG, free SDTG, or free DDTG for 8 h. After treatment, the cells were washed twice with PBS and cultured in fresh culture medium without drug with half-media replacement every other day. RT assay was performed as described above.

## **2.4 Results**

### **2.4.1 Isolation and Characterization of *in vitro* loaded ATV exosomes**

Exosomes isolated from the media of free-ATV (100 $\mu$ M), nano-ATV (100 $\mu$ M), free-ATV (100 $\mu$ M)+URMC-099 (100ng/ml), or free-ATV (100 $\mu$ M)+URMC-099 (400ng/ml) treated MDM were positive for the exosome-marker Alix, and 54.1 nm in size (Figure 2.6.3). TEM indicated the presence of spherical vesicles ranging from 20-150 nm in size. In all, the isolated extracellular vesicles possessed features of exosomes (Figure 2.6.3).

It is clear ATV is readily packaged into exosomes *in vitro*, though variably according to treatment. MDM showed avid abilities to produce drug-loaded exosomes over a period of 14 days. MDM treated with native ATV secreted  $\sim 1.5 \mu$ g of ATV / $10^9$  exosomes whereas 500 ng of ATV/ $10^9$  exosomes were secreted with nanoATV at day 1 and 3 (Figure 2.6.4). At day 7 nanoATV treated MDM secreted  $\sim 1 \mu$ g of ATV in / $10^9$  exosomes while for native ATV loaded MDM drug levels were at or below limits of detection. The drug concentration was increased 1.5-fold when MDM were treated with URMC-099, a compound known to potentiate macrophage nanoparticle sequestration (Figure 2.6.4). RT assay was employed to determine the antiretroviral efficacy of the ATV-loaded exosomes. HIV-1 RT activity was determined for MDM treated with nanoATV or exoATV at concentrations of 1  $\mu$ M ATV and



10  $\mu\text{M}$  ATV. MDM were treated for 8 hours followed by HIV-1 infection, and collection on days 1, 3, 5, 7, 9, 11, and 14. Exosome ATV formulations suppressed HIV replication for only three days (Figure 2.6.5). In contrast, nanoATV formulations demonstrated enhanced abilities to suppress HIV-1 replication *in vitro*. After observing exoATV's inferior ability to inhibit HIV-1, we reasoned that enhanced drug loading into exosomes may translate into improved antiretroviral efficacy. Therefore, alternative methods of drug incorporation into exosomes were explored.

#### **2.4.2 Synthesis and Characterization of *ex vitro* loaded ATV exosomes**

To improve drug encapsulation into exosomes, exosomes were first isolated from MDM culture media. Then, freeze-thaw, sonication, and detergent-based methods were employed to load ATV into exosomes. The freeze-thaw method resulted in the lowest drug loading, 56.46  $\mu\text{g}/\text{ml}$  of exosomes. Incubation with saponin at RT increased loading to 96.13  $\mu\text{g}/\text{ml}$  (Figure 2.6.6). Sonication allowed for the greatest drug loading, 289.3  $\mu\text{g}/\text{ml}$ . Due to superior drug-loading capacity, sonication was chosen as the exosome-loading method for all following studies. TEM indicated that sonication caused the population of vesicles to become smaller, and more uniform in size (Figure 2.6.7). In tandem, dynamic light scattering (DLS) was used to determine size, PDI, and zeta potential of exosome formulations produced via sonication. Size of exosomes increased from 86 nm to 964 nm after sonication with ATV. Though DLS indicated aggregation, this is not in agreement with the TEM images. PDI increased from 0.29 for control exosomes, to 0.59 for the sonicated. Zeta potential for control exosomes was -4.96 mV, and -7.00 mV for sonicated. Antiretroviral activity of exosomes loaded with ATV via sonication was assessed using RT assay (Figure 2.6.8). At 1  $\mu\text{M}$  and 10  $\mu\text{M}$  concentrations, ATV loaded exosomes produced by sonication show similar RT activity to nanoATV at early time points but were not as effective at later time points. At the 20  $\mu\text{M}$  concentration, the exosome formulation suppressed RT activity to a similar extent as the 20  $\mu\text{M}$  nanoATV treatment.

### **2.4.3 *In vitro* characterization of *ex vitro* loaded ATV exosomes**

When monocyte-derived macrophages (MDM) were treated with 50  $\mu$ M concentrations of exosome-ATV, nanoATV, or free ATV, enhanced cellular uptake of the exosome-ATV was observed (Figure 2.6.8). At 24 hours, 96% drug uptake was observed with the exosome-ATV treatment, while nanoATV and free ATV resulted in 46% and 0.02% respectively. Exosome-ATV formulations showed similar antiretroviral efficacy as nanoATV at a concentration of 20  $\mu$ M (Figure 2.6.8). However, we observed that MDM treated with exosome-ATV began to lift off the cell culture plate between 8-24 hrs (while nanoATV and free ATV treated MDM did not), suggesting potential cytotoxicity of the exosome formulation (Figure 2.6.9).

### **2.4.4 MTT of *exo*ATV and *exo*DTG formulations**

To determine whether or not the cytotoxicity observed in the uptake study was due to the exosomes alone or the combination of exosomes and drug, MTT assay was performed with *exo*ATV and *exo*DTG (a HIV-1 integrase inhibitor with similar solubility properties as ATV), and free ATV & DTG. Marked reduction in MDM viability was observed following 2- and 8-hour incubation with both *exo*ATV and *exo*DTG formulations (Figure 2.6.10). In contrast, free ATV, free DTG, and control exosomes did not induce cell death to the extent of *exo*ATV and *exo*DTG. This suggested that a factor unique to the sonicated exosome-drug formulations induced the cytotoxicity.

### **2.4.5 Investigation of cytotoxicity**

Microbial contamination of the exosome samples was first considered as the source of cytotoxicity. However, exosome samples were negative for both endotoxin and mycoplasma (Figure 2.6.10). TNF- $\alpha$  production was not induced by the exosome formulations, indicating no macrophage activation by the exosome formulations (Figure 2.6.10). This suggested an innate property of the vesicles and/or formulation was responsible for the cytotoxicity. Since DLS indicated significant exosome aggregation following

sonication, we investigated whether this could have a damaging effect on MDMs. Transmission electron microscopy (TEM) was used to probe the structure of sonicated ATV-exosomes. TEM analysis revealed that the exosomes did not aggregate as indicated by DLS. Instead, sonication produced a monodisperse population of vesicles 20-35 nm in diameter. TEM also indicated the presence of large drug crystals within the sample (Figure 2.6.6). We posited that the presence of large crystals may underlie the cytotoxicity associated with exosome-ATV formulations. Crystalline structures may damage cells in a variety of manners. For example, large crystals may damage the plasma membrane, causing cell lysis. Alternatively, if phagocytosed, crystals can rupture endo-lysosomal compartments and activate the inflammasome complex. Therefore, we reasoned that loading exosomes with hydrophilic ARVs instead of hydrophobic ATV, would reduce crystal formation in the exosomes and thus cytotoxicity as well.

#### **2.4.6 Encapsulation of hydrophilic ARVs into exosomes**

Sonication, saponin, and incubation at room temp. were employed to load maraviroc (MVC), MVC-Cl (hydrophilic salt of MVC), lamivudine (3TC), abacavir (ABC), and ATV-sulfate (hydrophilic salt of ATV) into exosomes (Table 2.6.1). Concentration of MVC-Cl, 3TC, ABC, and ATV-sulfate in exosomes after sonication was 46.96, 19.2, 15.6, and 177.46  $\mu\text{g}/10^9$  vesicles, respectively (Table 2.6.1). Though MVC was loaded into exosomes at the highest concentration, the formulation was dropped due to MVC's limited aqueous solubility.

#### **2.4.7 Characterization of hydrophilic ARV-loaded exosomes**

MTT was performed on MDM treated MVC-Cl, 3TC, ABC, and ATV-sulfate exosomes prepared by sonication (Figure 2.6.12). Reduction in cell viability (below 80% of untreated controls) was observed for the exosome ATV-sulfate preparation. However, cytotoxicity was not observed for MVC-Cl, 3TC, ABC exosomes. Therefore, TEM was used to assess morphology of MVC-Cl, 3TC, ABC exosomes manufactured by sonication and saponin methods (Figure 2.6.11). No major morphological changes were observed for any of the

sonicated exosomes. However, exosomes exposed to 0.2% saponin displayed filamentous structures. Due to these morphological changes, sonication was selected as the optimal drug-loading method. Balancing drug loading and cytotoxicity, MVC-Cl exosomes produced by sonication were tested for intracellular uptake in MDM. At a 50  $\mu\text{M}$  concentration, the exosome formulation did enhance cellular uptake compared to free MVC-Cl (Figure 2.6.12). However, the maximal drug concentration did not exceed 1  $\mu\text{g}$  per  $10^6$  cells, suggesting MDM did not avidly phagocytose the exosome formulation.

#### **2.4.8 Encapsulation of lipophilic prodrug ARVs into exosomes**

Though MVC-Cl exosome formulations did not induce cytotoxicity and enhanced cellular uptake compared to free drug, overall uptake of the exosomes was minimal. Therefore, we investigated the encapsulation efficiency of lipophilic ARV prodrugs into exosomes. We posited that the fatty acid chain of ARV prodrugs would increase their concentration in exosomes and facilitate improved cellular uptake and antiviral responses. To these ends, M8232 (18 carbon modified GSK-8232), M8232-LAP (18 carbon modified 8232, Tween solution), T8232 (1-tetradecanol modified GSK-8232), D8232 (22 carbon modified GSK-8232), MCAB (14 carbon modified CAB), MDTG (14 carbon modified DTG), SDTG (18 carbon modified DTG), and DDTG (22 carbon modified DTG) were loaded into exosomes via sonication (Table 2.6.2). Of these prodrugs SDTG and DDTG were incorporated into exosomes at the highest concentrations, 898.3 and 964.9  $\mu\text{g}/10^9$  vesicles, respectively.

#### **2.4.9 *In vitro* characterization of lipophilic ARV-loaded exosomes**

MTT assay demonstrated that SDTG and DDTG exosome formulations did not induce marked reductions in cell viability (below 80% of untreated controls) (Figure 2.6.13). Additionally, both exosome formulations enhanced intracellular uptake and retention of prodrug compared to free prodrug (Figures 2.6.14 and 2.6.15). While exo-SDTG and exo-DDTG suppressed viral replication for 15 days, free drugs controls also performed similarly.

(Figure 2.6.16). Therefore, to elucidate differences in antiretroviral responses, future studies should extend the experiment out to 30 days or reduce the dose.

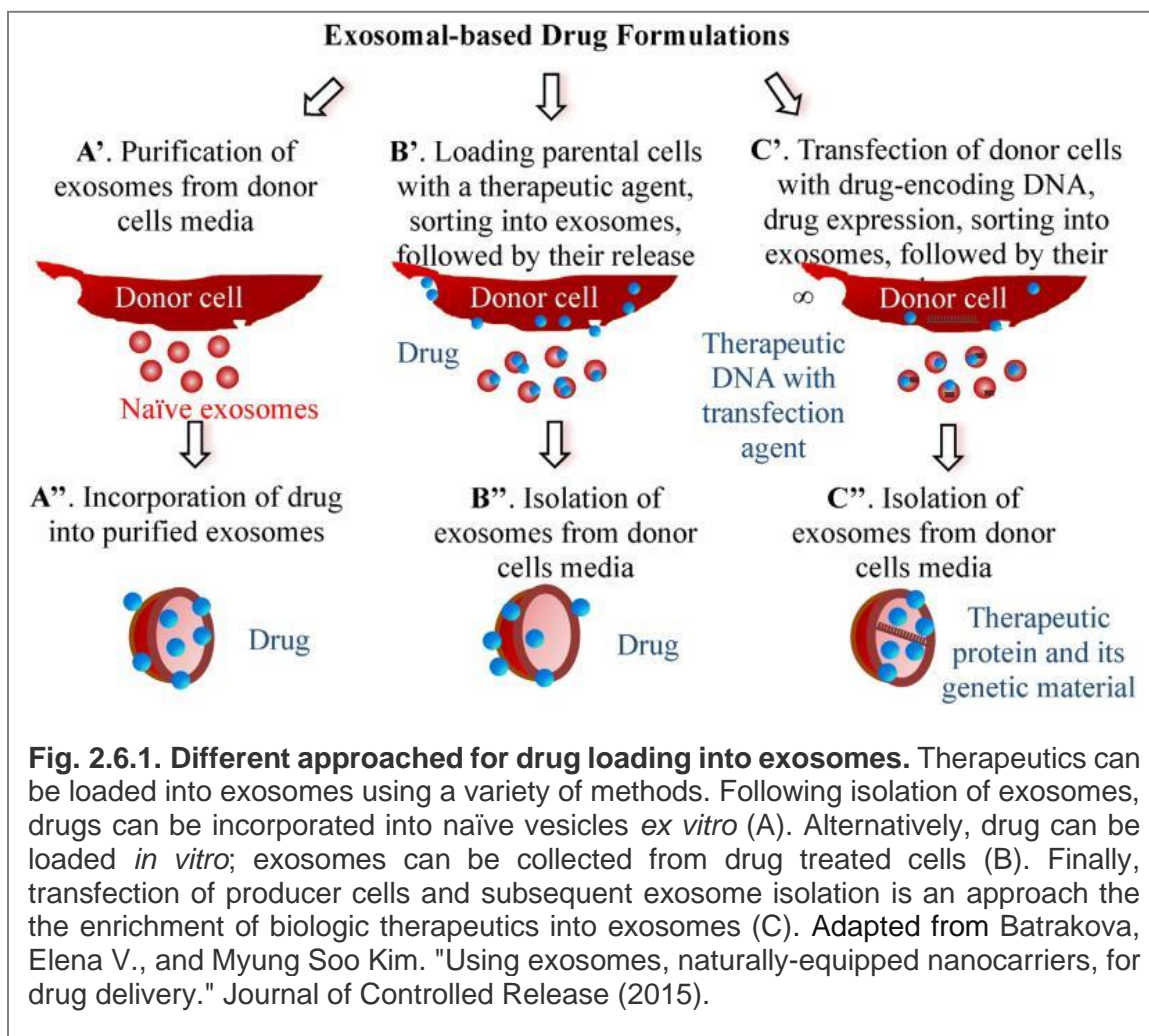
## 2.5 Discussion

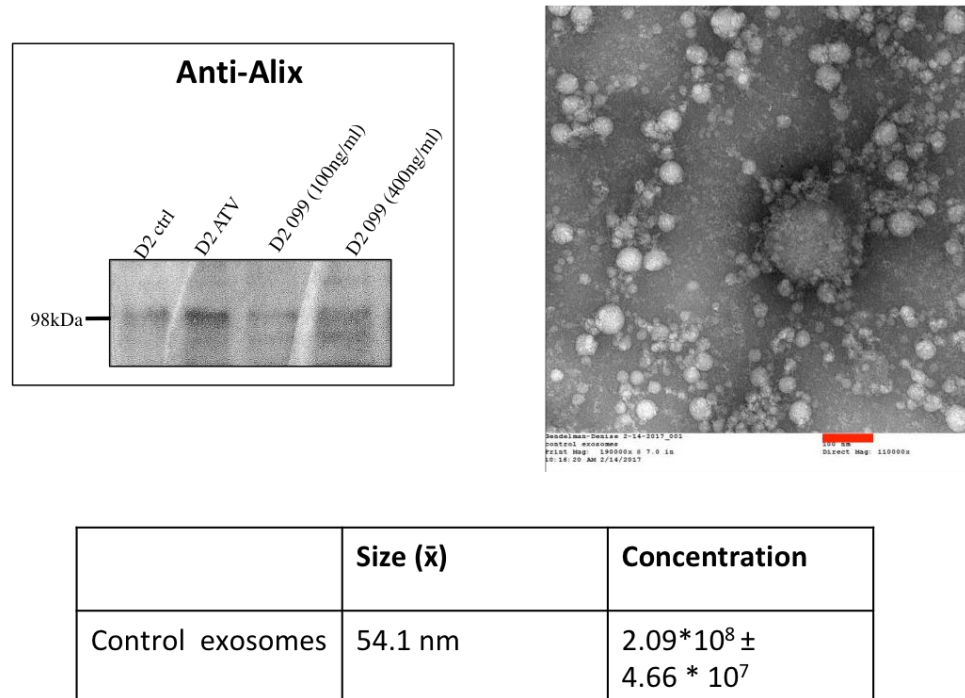
These data demonstrate that *in vitro* methods (Figure 2.6.1 panel B) and *ex vitro* methods (Figure 2.6.1 panel A) can be employed to load ARV agents into exosomes. Herein, two exosome drug-loading approaches were investigated (Fig 2.6.1): (1) loading naïve exosomes isolated from parental cells *ex vitro*; (2) loading cells with drug *in vitro*, which is then released in exosomes. In the case of *in vitro* and *ex vitro* drug loading, the maximum ARV concentration in exosomes is  $\sim 1 \mu\text{g}$  of ATV in  $10^9$  exosomes for both methods. Regarding *in vitro* loading, following incubation of human MDM with nanoformulated ATV, the cells released ATV-loaded exosomes into the culture media for two weeks (Fig 2.6.4). However, the released ATV-loaded exosomes did not demonstrate antiviral efficacy equivalent to poloxamer-formulated nanoATV. Therefore, *ex vitro* loading of exosomes was investigated. Regarding *ex vitro* loading of naïve exosomes different APIs (hydrophobic parent drug, hydrophilic parent drug, lipophilic prodrugs), and different methods of drug incorporation were evaluated (sonication, incubation at room temp., incubation with saponin, freeze-thaw) (Tables 2.6.1, 2.6.2). When drug-loaded exosomes were imaged by TEM, no abnormal morphological changes were detected following sonication. However, the process did appear to make the population of vesicles more uniform in size. Other drug-loading methods such as incubation with 0.2% saponin appeared to cause morphological changes to exosomes; filamentous structures were observed by TEM. The combination of sonication and lipophilic ARV prodrugs resulted in the highest drug encapsulation into exosomes, while avoiding cytotoxicity, and demonstrating viral inhibition for out to 15 days (Fig 2.6.14- 2.6.16, Table 2.6.2). In all, the system developed herein represents a major step forward in the creation of a long-acting ARV exosome system.

## 2.6 Conclusion

The data suggest that (1) the method of drug loading and (2) the selection of API are the two major parameters governing exosome drug loading. Herein we compared the encapsulation of hydrophilic parent ARVs, hydrophobic parent ARVs, and lipophilic prodrug ARVs via sonication, freeze/ thaw, incubation, and detergent based methods. The data clearly demonstrate that sonication and lipophilic prodrug ARVs result in the greatest incorporation of drug into exosomes compared to ARVs possessing different physiochemical characteristics. It is likely the fatty chain of the ARV prodrugs synthesized by our lab enhance the membrane permeability of the molecule and allow for more efficient encapsulation. However, exosome drug encapsulation remained low, especially in comparison to poloxamer –based nanoformulations. For example, prodrug nanoformulations of various DTG prodrugs can surpass concentrations of 200 mg/ mL, while exosomes formulations are limited to approximately 1mg/  $10^9$  vesicles. Given that there are  $10^9$  exosomes per 1mL of MDM culture fluid, it is apparent that the exosome-based ARV delivery system described herein would face challenges in scale-up, even for preclinical studies in small animals. This suggests exosomes may not be the most efficient drug carrier for ARVs. Given their natural function, exosomes may prove more efficient carriers of nucleic acids compared to small molecule drugs. Therefore, future studies should explore the use of exosomes in HIV cure strategies, for example as delivery vehicles for CRISPR-Cas9. Regardless of cargo, further investigation of exosomes' *in vivo* biodistribution and toxicity, and large-scale production are imperative for clinic translation.

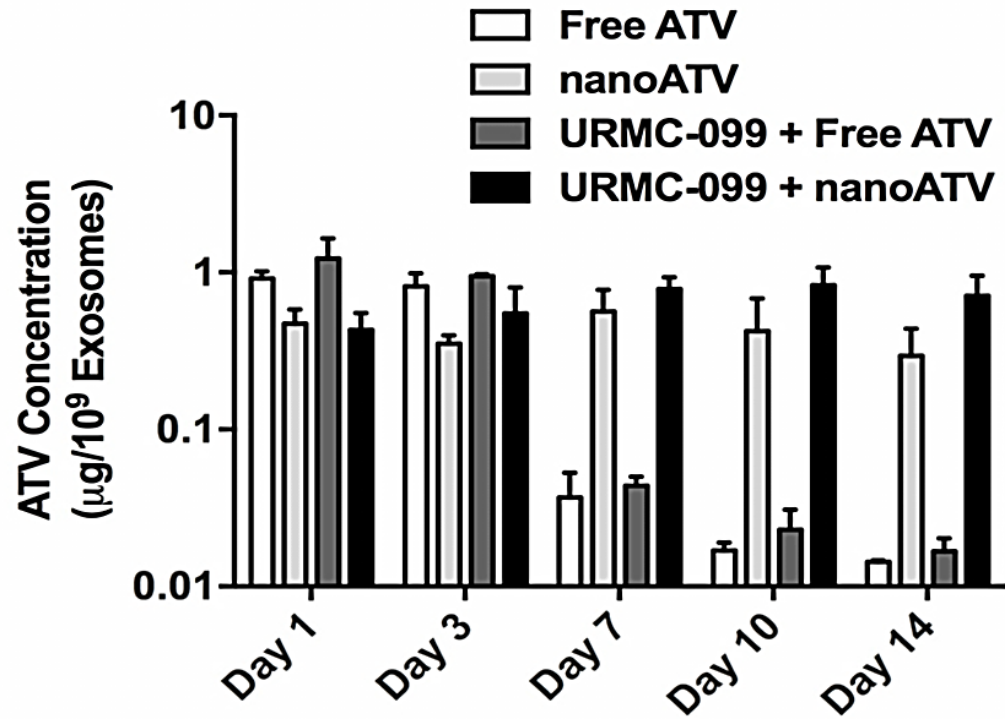
## 2.7 Figures and Tables



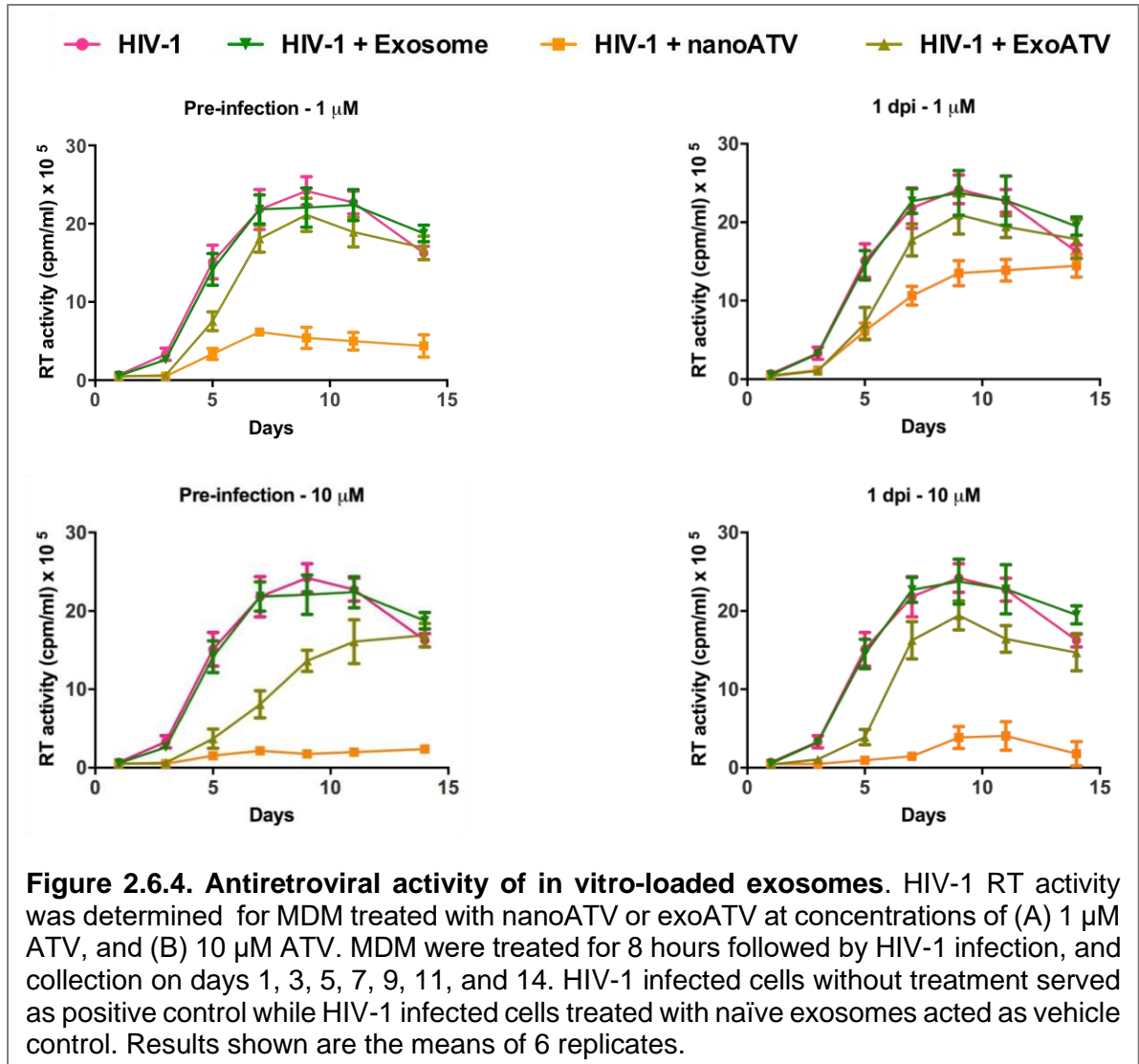


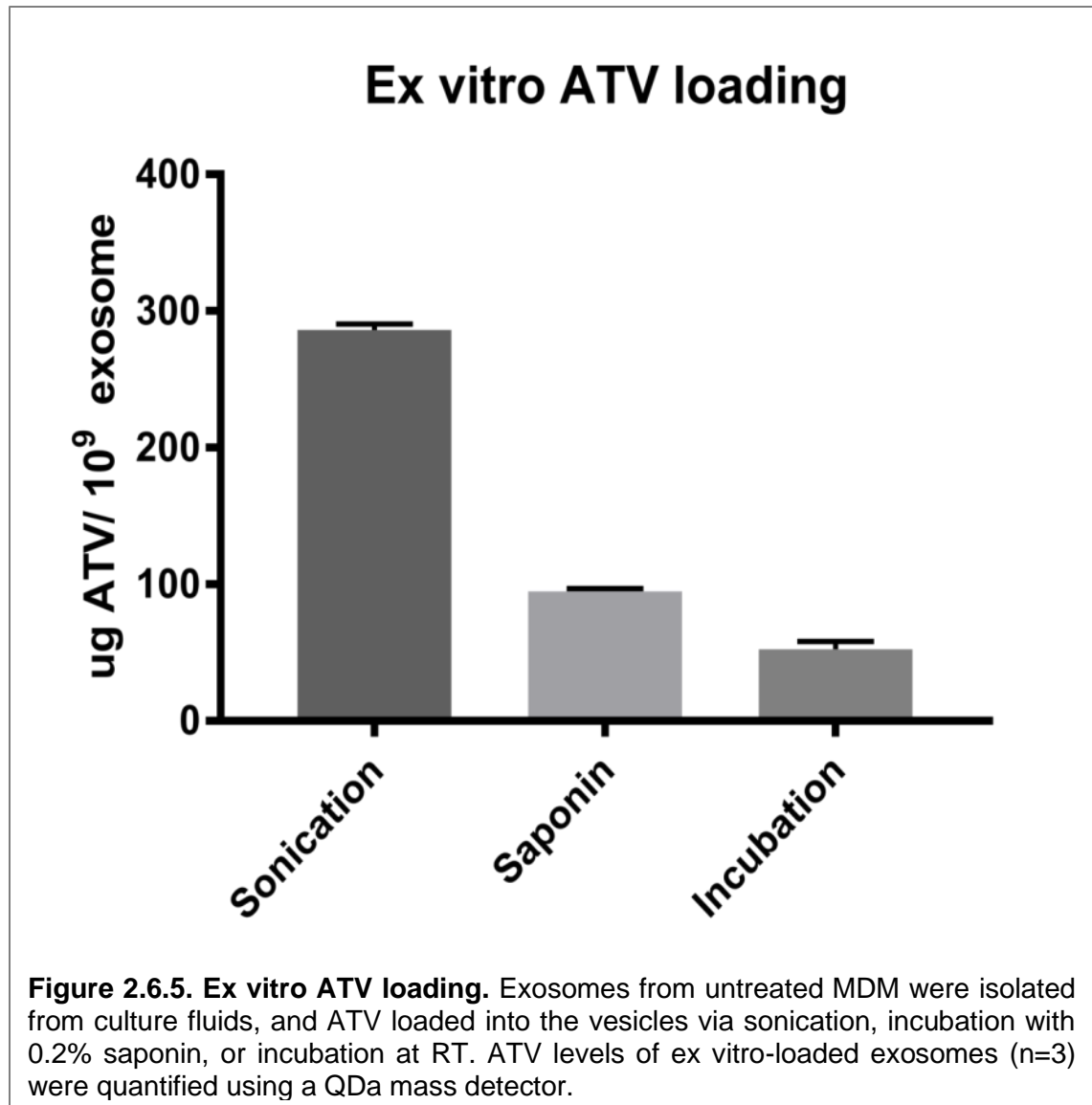
**Fig. 2.6.2. Characterization of naive exosomes.** Following isolation, exosomes from untreated MDM were characterized by western blot, nanoparticle tracking analysis (NTA), and TEM. Isolated exosomes expressed the Exosomal marker Alix. Additionally, the size and shape of the isolated vesicles was characteristic of exosomes.

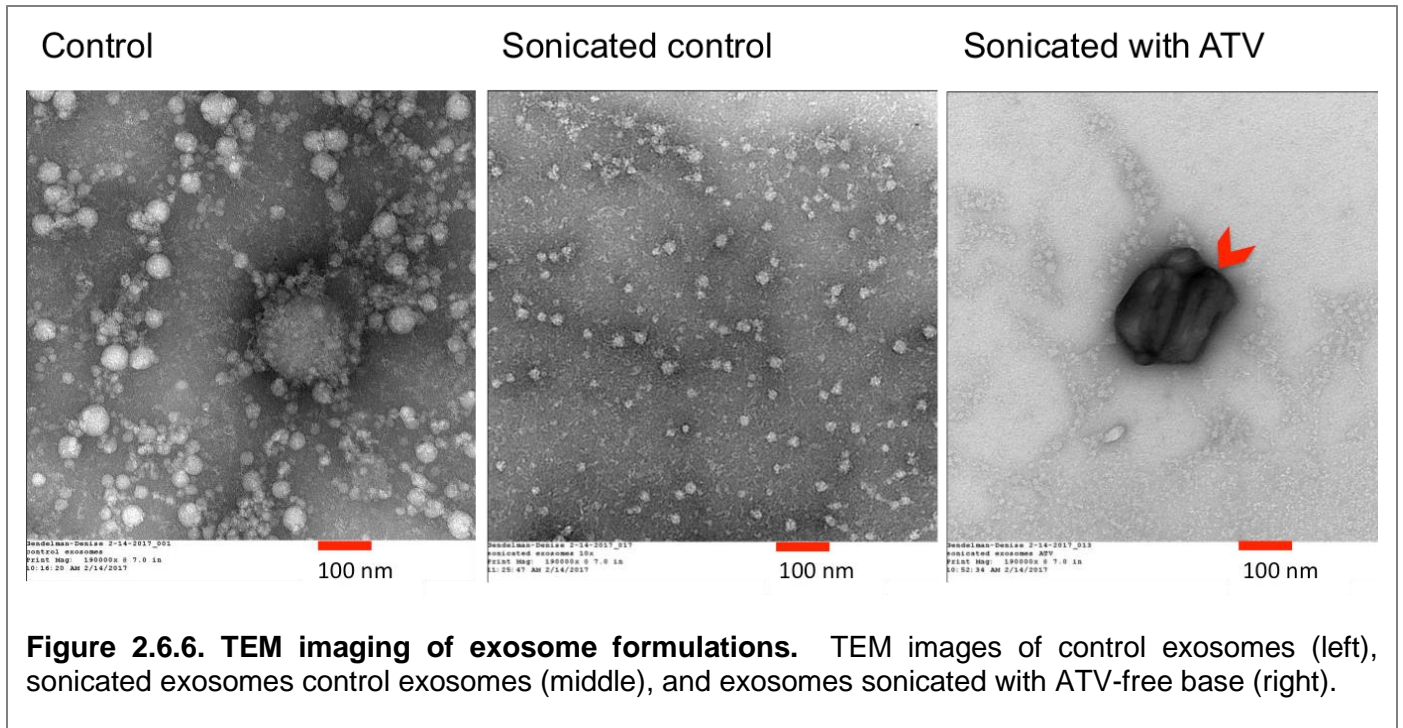


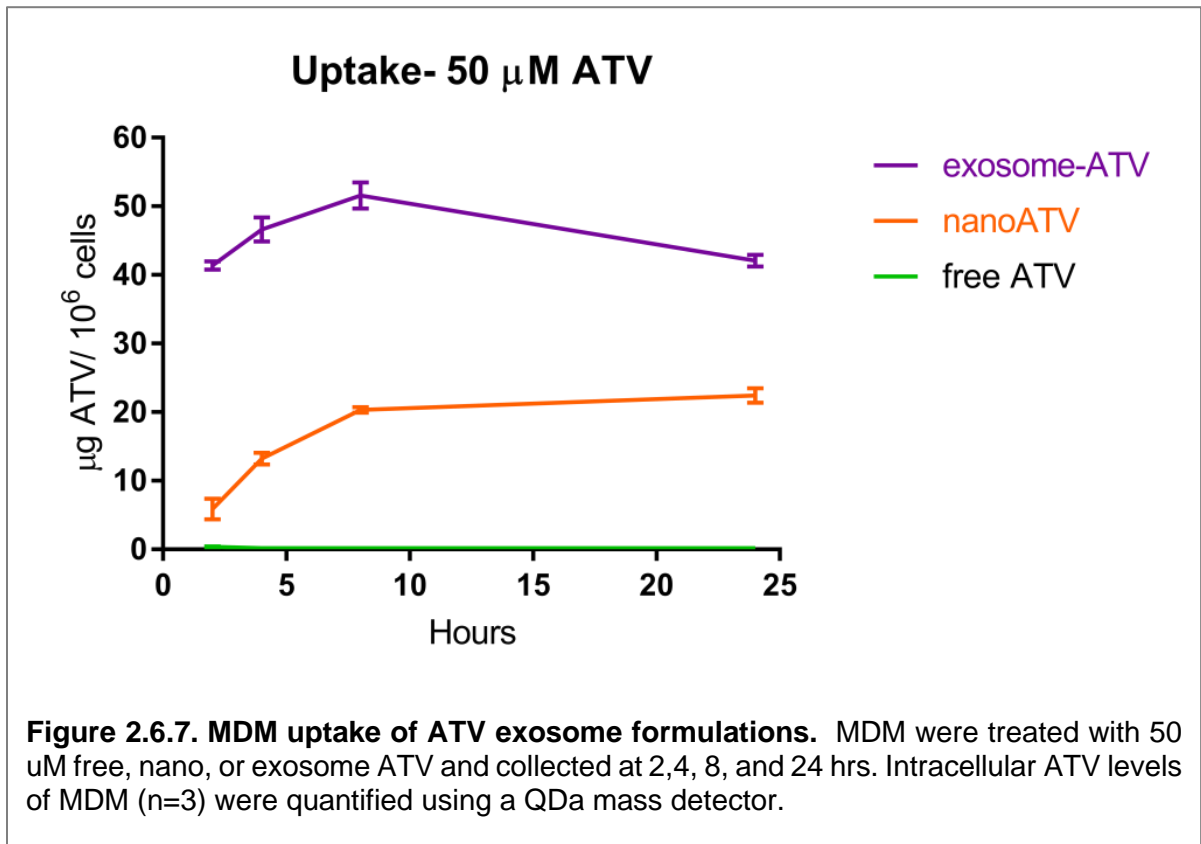


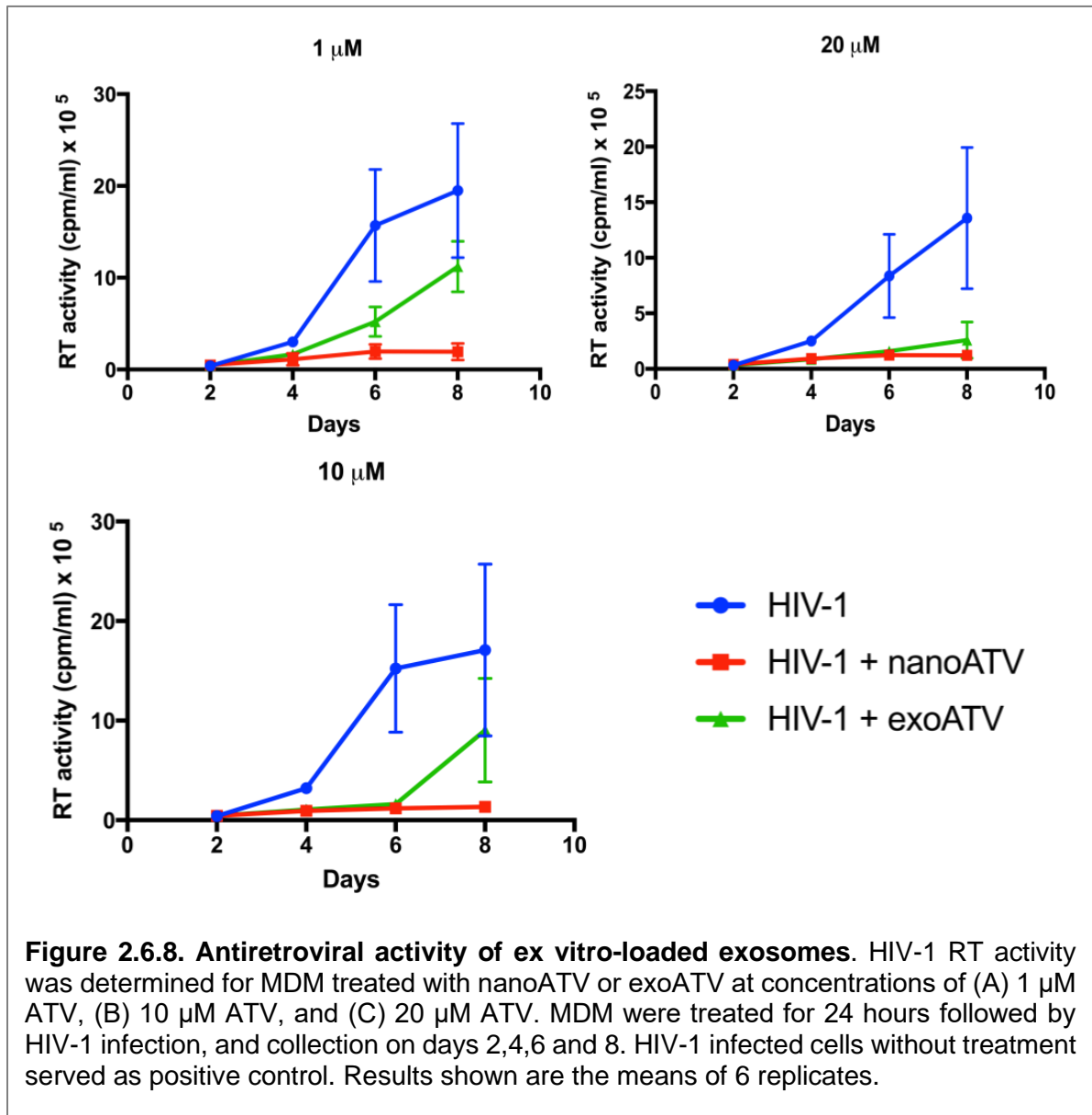
**Figure 2.6.3. Atazanavir loading and characterization of exosomes.** MDM were treated with 100  $\mu\text{M}$  free ATV, or nanoATV with or without the autophagy potentiator URM-099. Exosomes were isolated from cell-conditioned media, and ATV levels of in vitro-loaded exosomes ( $n=3$ ) were quantified using a QDa mass detector.

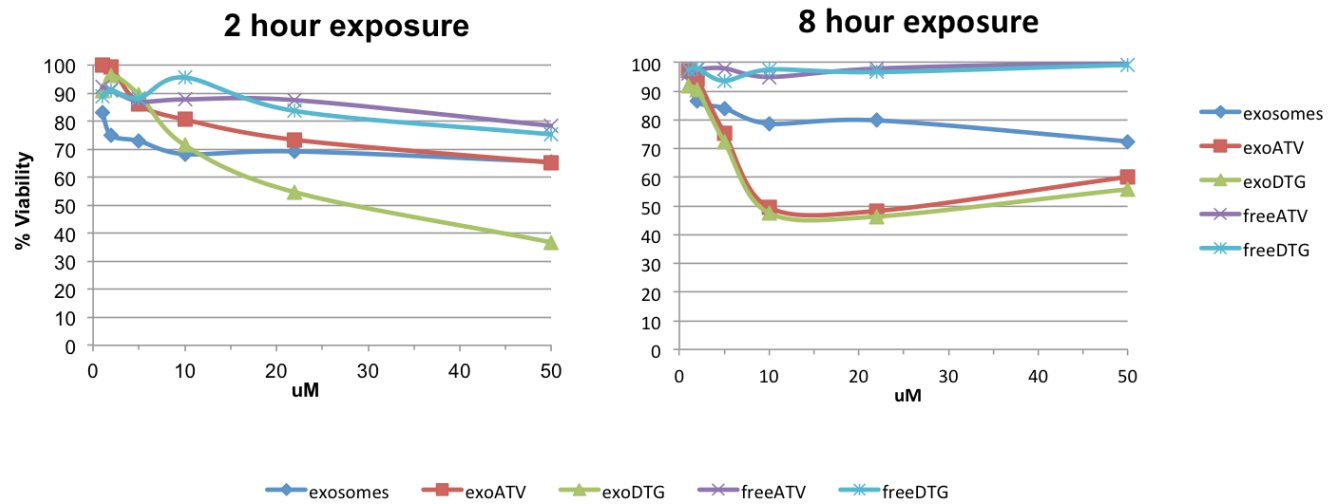




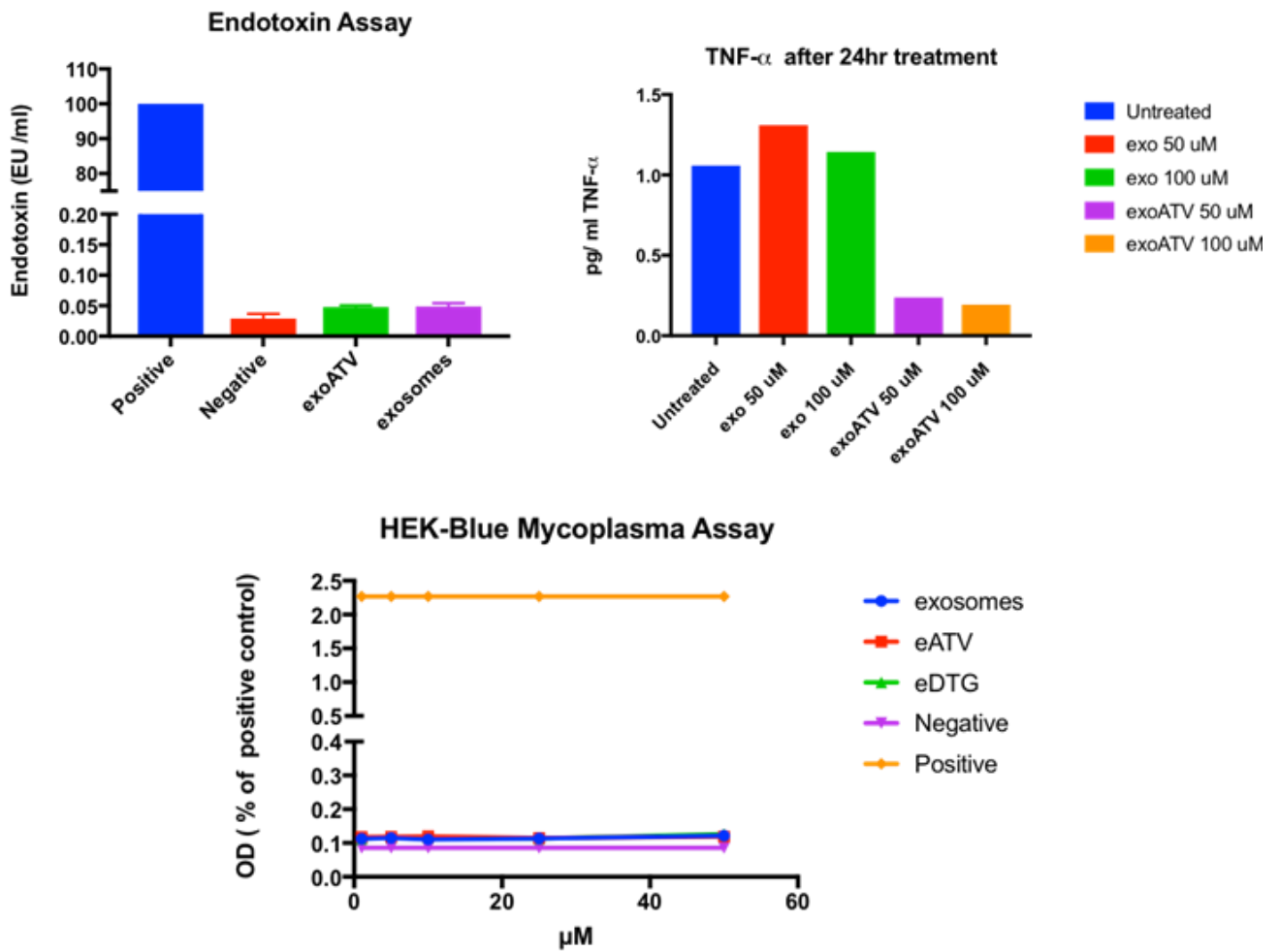






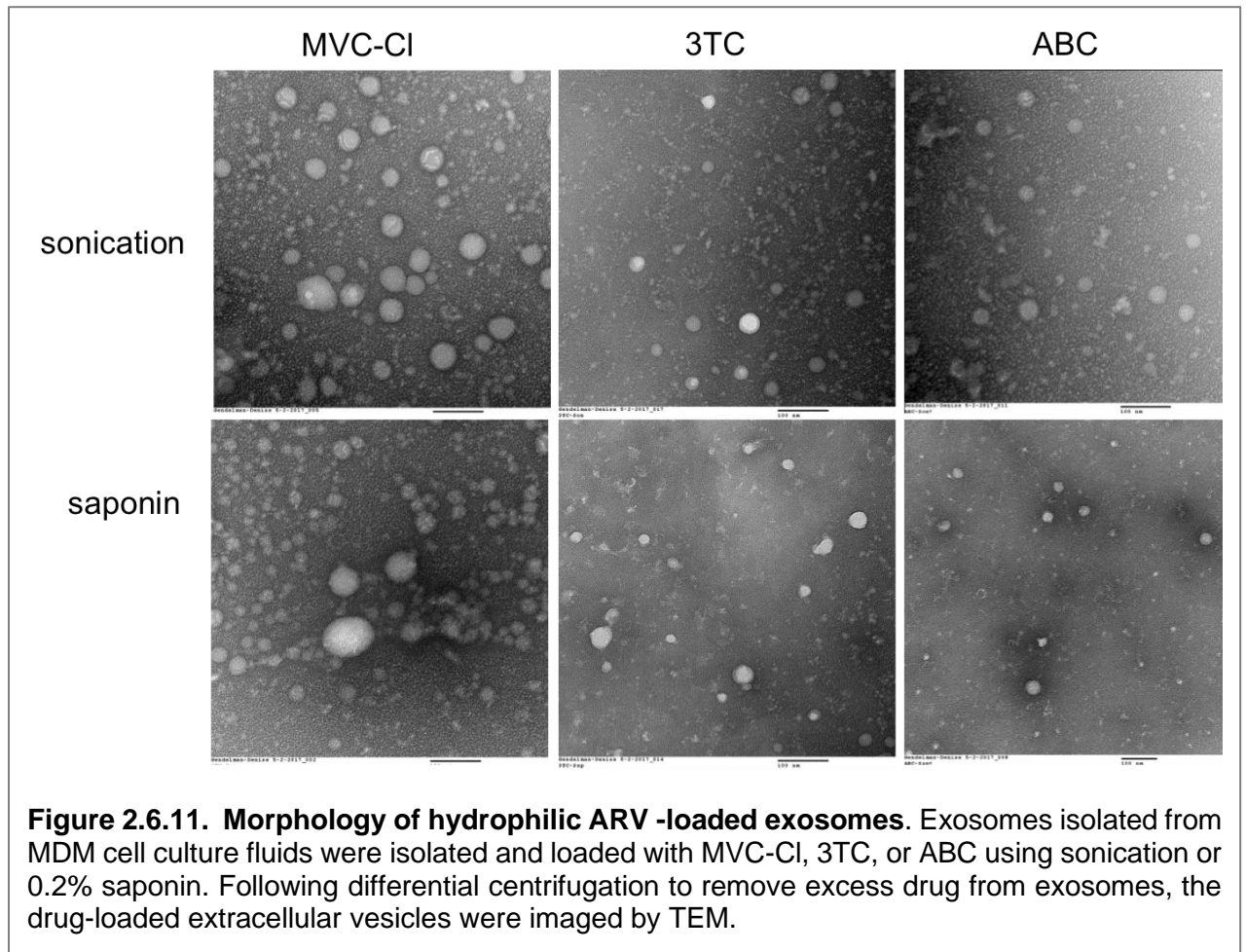


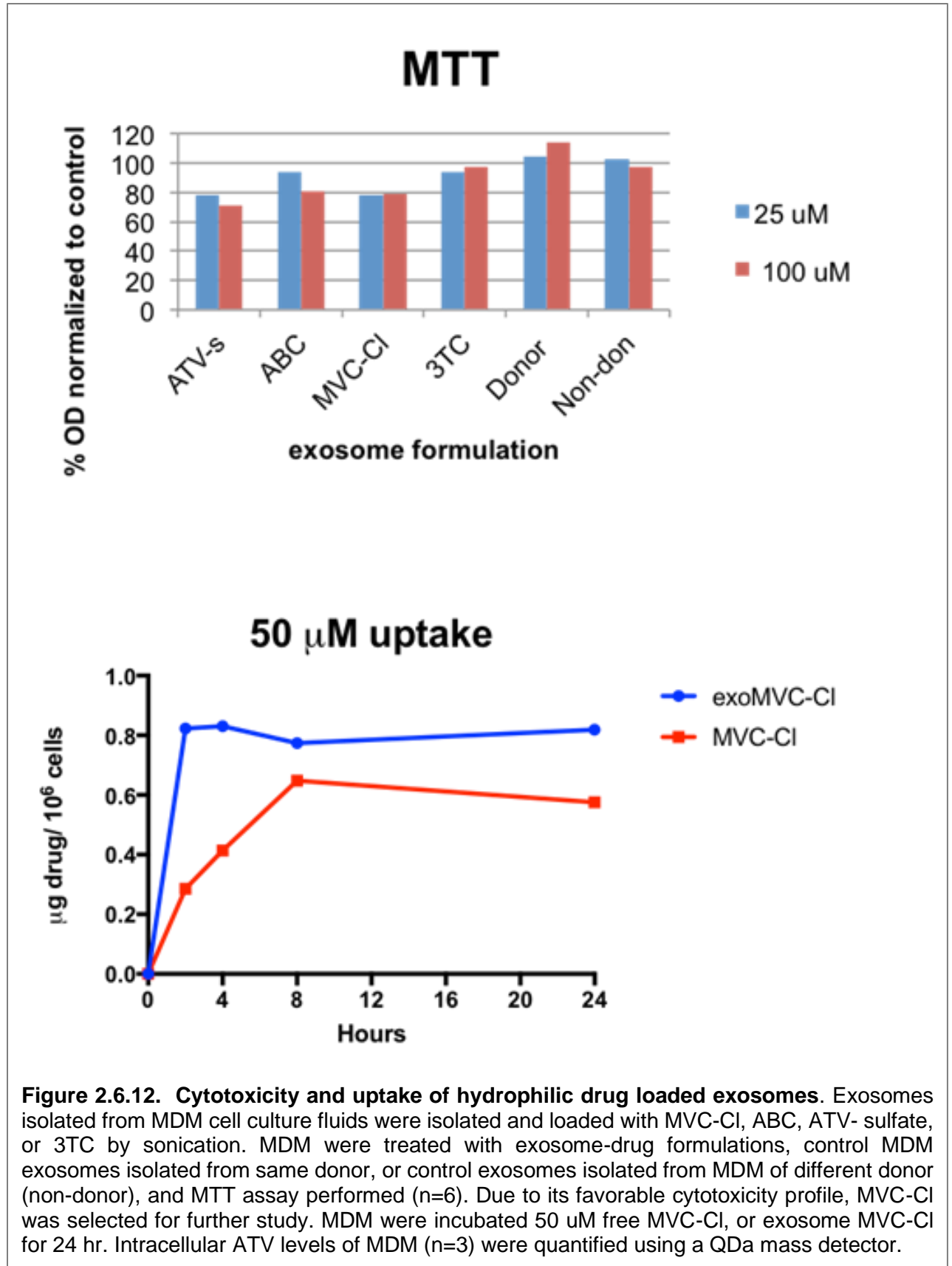
**Figure 2.6.9. Exosome Cytotoxicity studies.** Cell viability as determined by MTT after 2 and 8 hours of treatment. Results shown are the means of 6 replicates.



**Figure 2.6.10. MDM cytotoxicity studies.** Endotoxin levels were measured in control exosome and drug-exosomes formulations (n=3). MDM were treated with drug-exosome formulations or an equal number of control exosomes, then assayed for subsequent TNF-alpha production (n=4). Mycoplasma levels were measured in exosome pellets or MDM treated with exosome-drug formulations (n=3).







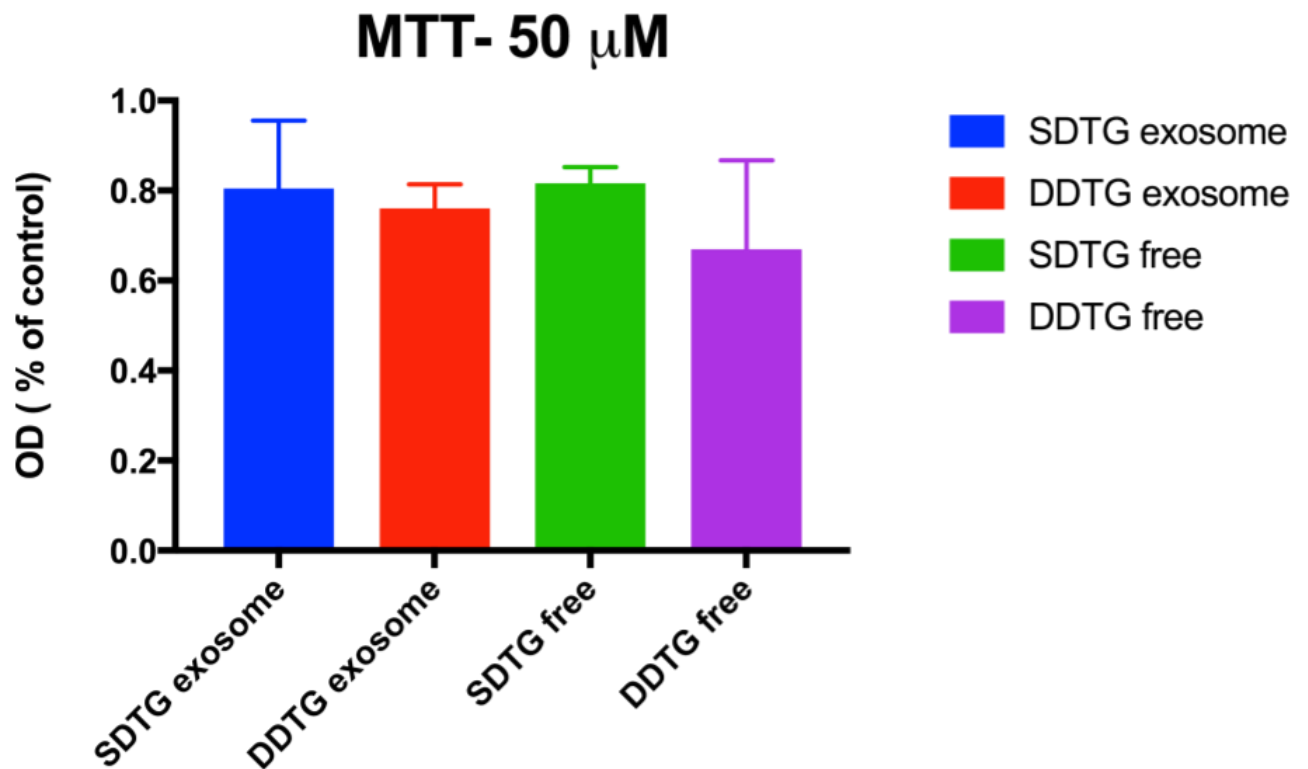


**Figure 2.6.13. Cytotoxicity of lipophilic prodrug loaded exosomes.** Exosomes isolated from MDM cell culture fluids were isolated and loaded with DDTG or SDTG by sonication. MDM were treated with exosome-drug formulations, or free drug controls for 8 hrs, then MTT assay performed (n=6).

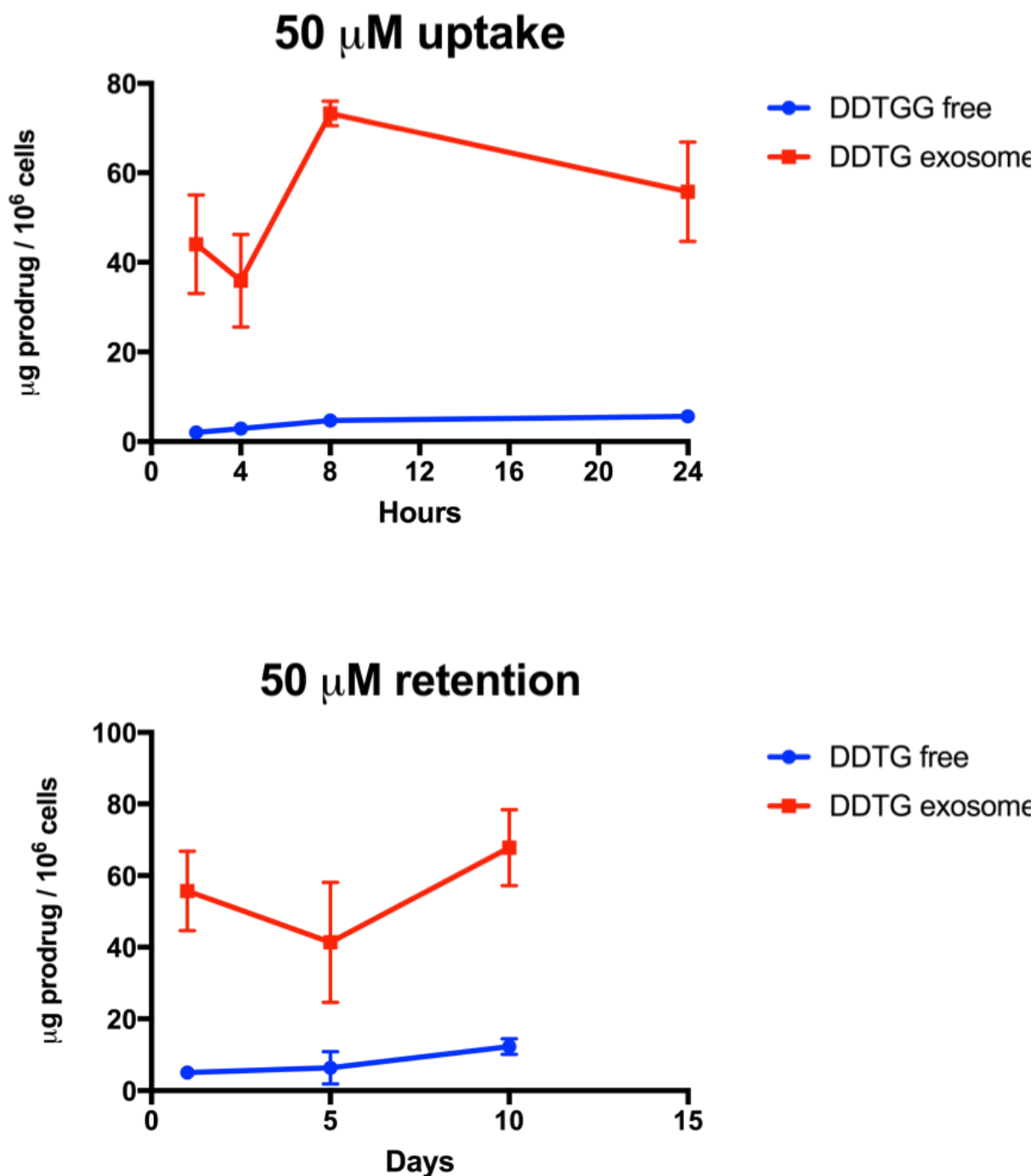


**Figure 2.6.14. MDM Uptake and retention of DDTG loaded exosomes.** Exosomes isolated from MDM cell culture fluids were isolated and loaded with DDTG by sonication. MDM were treated with exosome-drug formulations, or free drug control for 24 hrs (top graph). Intracellular prodrug levels in MDM (n=3) were quantified using a Waters H-Class UPLC coupled to a UV/Vis detector (n=3). Retention of prodrug (bottom) following a 24 hr treatment with exosome DDTG or free drug was determined over two weeks. Intracellular prodrug levels in MDM (n=3) were quantified using a Waters H-Class UPLC coupled to a UV/Vis detector (n=3).

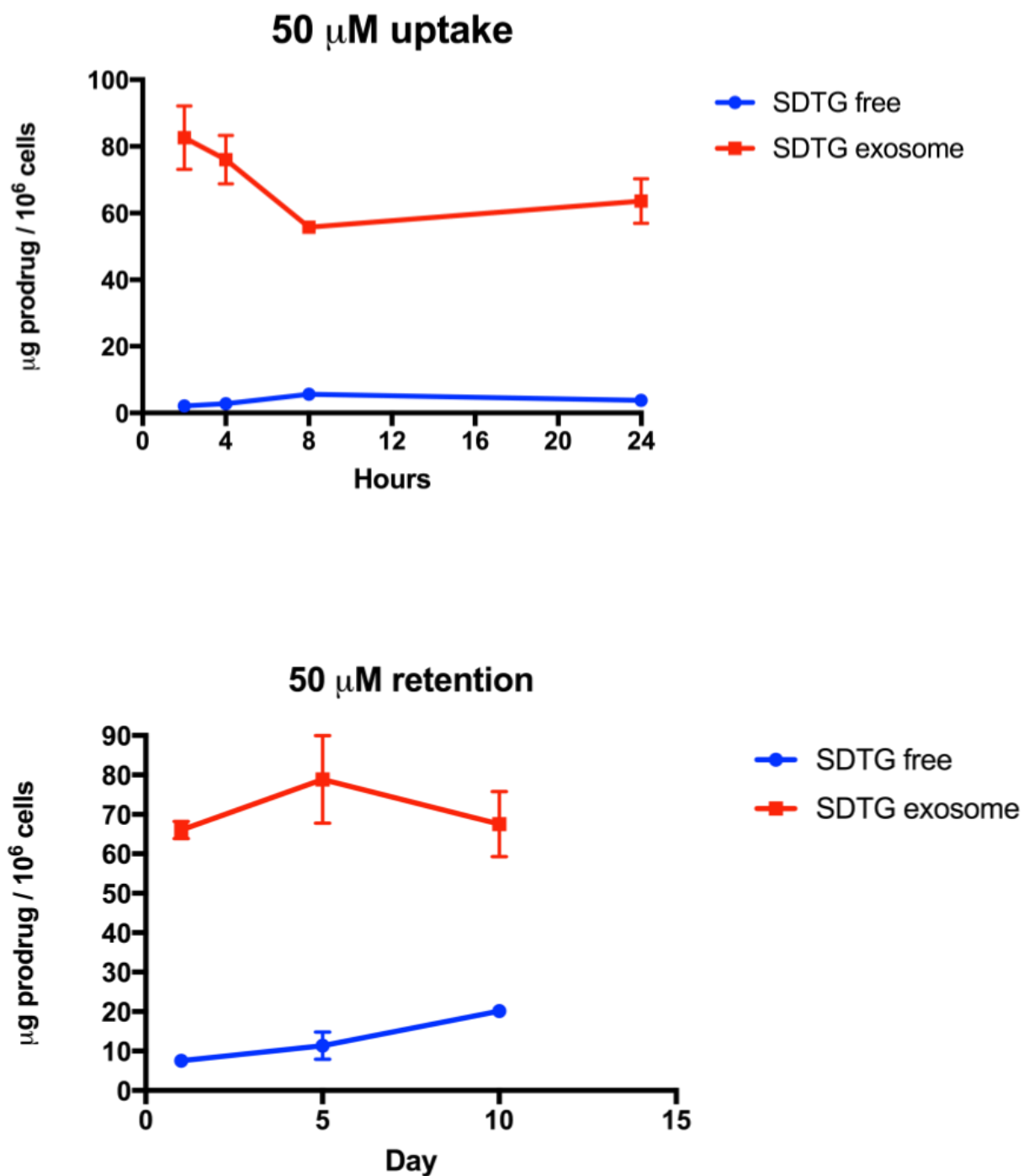


**Figure 2.6.15. MDM Uptake and retention of SDTG loaded exosomes.** Exosomes isolated from MDM cell culture fluids were isolated and loaded with SDTG by sonication. MDM were treated with exosome-drug formulations, or free drug control for 24 hrs (top graph). Intracellular prodrug levels in MDM (n=3) were quantified using a Waters H-Class UPLC coupled to a UV/Vis detector (n=3). Retention of prodrug following a 24 hr treatment with exosome SDTG or free drug was determined over two weeks. Intracellular prodrug levels in MDM (n=3) were quantified using a Waters H-Class UPLC coupled to a UV/Vis detector (n=3).

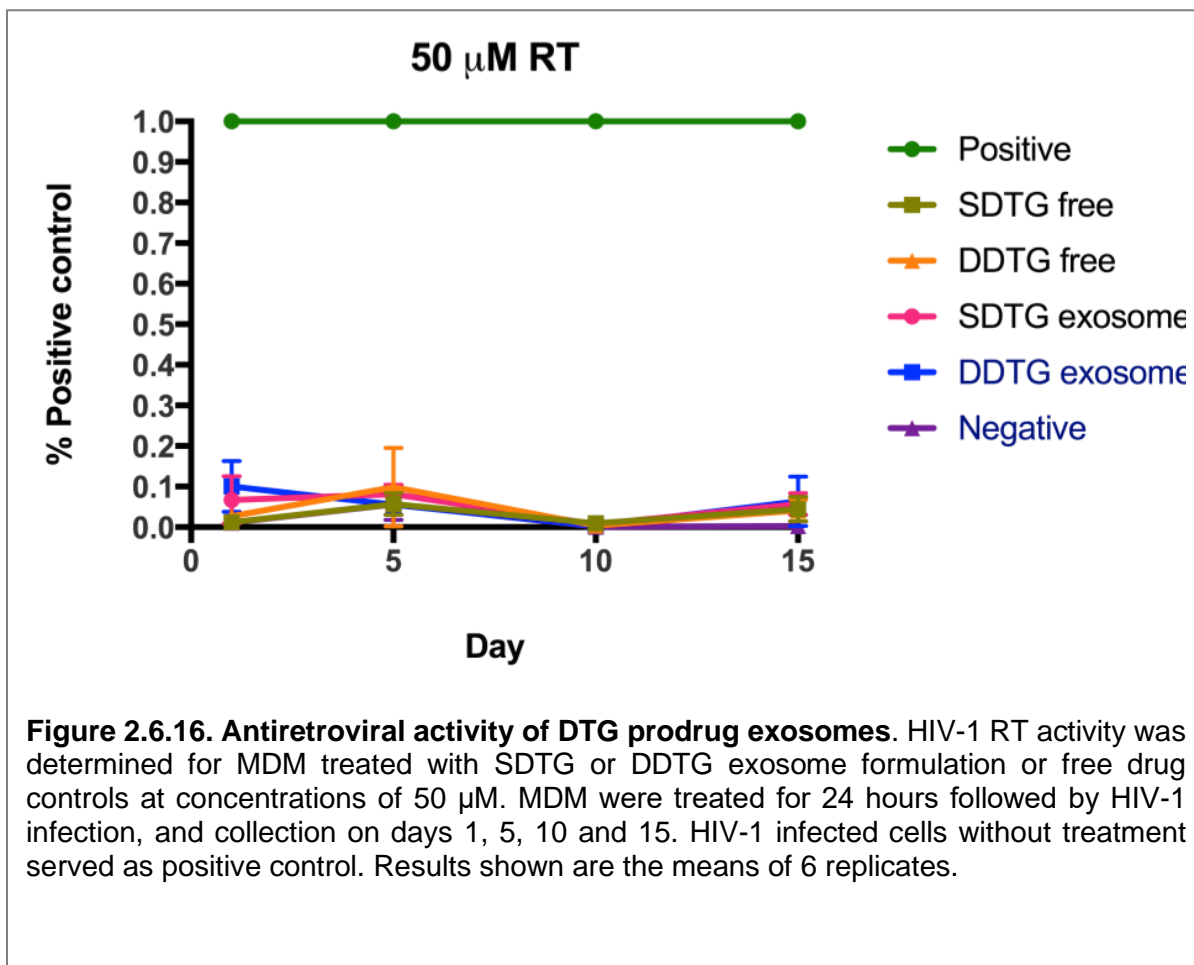


Table 2.6.1. Loading of hydrophilic ARVs			
$\mu\text{g drug/ } 10^9 \text{ vesicles}$			
Drug	Sonication	0.2% saponin	RT incubation
Maraviroc	669.68	445.85	734.46
Maraviroc-Chloride	46.96	46.88	28.06
3TC	19.12	36.04	20.59
ATV-sulfate	177.46	137.29	59.44
Abacavir	15.60	36.55	20.83
ATV- free base	289.35	96.13	56.46
DTG	52.14	43.78	20.9

Table 2.6.2. Loading of hydrophobic and prodrug ARVs			
$\mu\text{g drug/ } 10^9 \text{ vesicles}$			
Drug	Sonication	0.2% saponin	RT incubation
M8232	7.6	--	0.3
M8232-LAP	171.5	--	155.7
T8232	878.1	--	199.21
D8232	100.5	--	130.7
MCAB	59.9	--	22.4
MDTG	20.3	--	--
SDTG	898.3	--	--
DDTG	964.9	--	--



## **CHAPTER 3: DEVELOPMENT OF LONG-ACTING TFV PROTIDE NANOFORMULATIONS**

### **3.1 Abstract**

Numerous biologic and synthetic nanomedicines are being investigated to improve ARV half-life, biodistribution, to mitigate off target toxicity, and improve penetrance into viral reservoirs. Medicinal chemistry and nanotechnology approaches have been employed to produce long-acting slow effective release (LASER-ART) formulations of ARVs. The LASER-ART strategy can facilitate drug depot formation and lymphoid targeting, have the potential to better penetrate HIV reservoirs, provide sustained release of active compound, and reduce systemic toxicities. In this chapter, prodrug and polymeric nanoformulation strategies were employed to improve the PK and PD profile of TFV. To this end, hydrophobic and lipophilic stable ProTides of TFV were created. These were then transformed into long acting scalable aqueous poloxamer stabilized TFV prodrug nanocrystals (called NM1TFV and NM2TFV). Aqueous stability, intracellular uptake into primary human macrophages and CEM-ss CD4<sup>+</sup> T cells, conversion into active metabolite (TFV-diphosphate, TFV-DP) and protection against HIV-1<sub>ADA</sub> challenge were tested at five-day intervals for 30 days. PK evaluations followed a single 75 mg/kg TFV equivalent intramuscular injection of NM1TFV, NM2TFV or a control nanoformulated TAF (NTAF) to Sprague Dawley rats. Here TFV-DP levels were  $\geq$  four times the effective dose 90% concentrations of 16-48 fmol/10<sup>6</sup> cells for two months. NM1TFV and NM2TFV and NTAF showed TFV-DP levels of 11,276.3, 1651.3 and 397.8 fmol/g of rectal tissue, respectively. Prodrug levels at the site of injection at day 56 were 433,475 ng/g for NM1TFV. release, improved tissue drug concentrations after a single intramuscular injection. Furthermore, in humanized mouse models of HIV-1 and HBV infection, LA TFV formulations demonstrated antiviral efficacy. These results are a first step towards producing a LA TFV ProTide to facilitate drug stability and cell and tissue delivery.

### 3.2 Introduction

A first-generation combination of long-acting (LA) antiretroviral drugs (ARVs), cabotegravir and rilpivirine (CAB and RPV), have been approved for treatment of human immunodeficiency virus type one (HIV-1) infection by the US Food and Drug Administration (FDA). The intent is to improve patient regimen adherence and impact a sustained antiretroviral clinical efficacy. Indeed, despite the significant advances seen in treatment and prevention of HIV-1 infection, remembering to take daily ART regimens remain a major obstacle towards achieving sustained viral suppression and in precluding viral transmission [207]. LA formulations have previously found utility as contraceptives and antipsychotics for improved regimen adherence [53, 208]. For HIV-1, LA RPV and CAB developed for viral prevention and treatment [5, 209] have recently been approved for use in Canada, Europe and by the US FDA [199]. These are now used as injectable solid drug nanosuspensions for monthly or every other month administration [32, 140]. Extended-release dosage forms that would facilitate overlap of patient dosing schedules with routine CD4+ T cell count and measures of HIV-1 viral loads could further have a major impact on the effectiveness of treatment efforts. Such LA ARV delivery strategies could also benefit vulnerable populations. These include intravenous drug users, children and adolescents, and pregnant women. However, limitations of CAB and RPV LA are recorded and include requirement for large injection volumes, monthly or bi-monthly dosing in a clinical setting and limited drug access to cellular and tissue reservoirs of infection [137, 138, 164]. Attempts to overcome such limitations have led to transformation of native ARVs into nanoformulated prodrugs designated as slow effective release antiretroviral therapy (LASER ART) comprised of homogeneous dispersions of solid prodrug nanocrystals stabilized by aqueous surfactant solutions [33, 150, 151, 201]. The LASER ART lipophilic prodrug nanocrystals provide slow drug dissolution and transport across biological membranes. This can achieve sustained

delivery of drug concentrations above the effective concentration 90 (EC90) for periods of up to one year in plasma and infectious tissue reservoirs [148].

The target product profile of compounds suitable for LA formulations include high potency to facilitate lower dosage and injection volumes, extended dosage intervals, low aqueous solubility for drug stability, slow dissolution and release profiles and extended elimination times. These can be achieved, in part, through the creation of prodrugs. For instance, the ProTide prodrug technology has enabled efficient intracellular delivery of phosphorylated nucleoside and nucleotide antiretroviral analogs with improved safety profiles [46]. The application of ProTide technology to TFV resulted in the discovery of tenofovir alafenamide (TAF), a *phosphoramidate prodrug*. Compared to another prodrug, tenofovir disoproxil fumarate (TDF), TAF is more potent and its safety profile makes it a better candidate for transformation into an LA formulation [42, 210]. However, TAF is susceptible to hydrolytic degradation. Prior attempts to modify formulation excipients or pH to affect TAF stability are yet to demonstrate successful PK outcomes [87, 198, 211, 212]. We now describe an improved ProTide strategy that masks the phosphate groups in TFV with cleavable hydrophobic amino acid ester lipids found to have synergistic effects on nucleoside analogs [213, 214]. These all affect drug efficacy, prodrug aqueous stability, dissolution, half-life and safety profiles. The masking groups were selected based on established safety and efficacy profiles [213-215]. The two lipophilic aqueous stable TFV ProTide nanocrystals, NM1TFV and NM2TFV, enhanced intracellular drug delivery, retention with sustained protection against HIV-1 challenge compared against nanoformulated TAF controls. Notably, a single intramuscular injection of NM1TFV, NM2TFV or NTAF to Sprague Dawley rats at 75 mg/kg TFV equivalents demonstrated PBMC TFV-DP levels above the EC90 over the entire 2 months study duration with no recorded adverse events. At two months, the lead candidate (NM1TFV), exhibited enhanced tissue TFV-DP levels four times higher than the reported EC90 of 16-48 fmol/10<sup>6</sup> cells for HIV-1 prevention [216]. Long-acting slow effective release

of the two ProTides were strongly supported when tested as an antiviral agent in model for HBV infection in humanized mice. A single intramuscular injection produced sustained antiviral activities for one month. Taken together, the approaches give validation to potential value of the platform of transforming daily medications into nanoformulated prodrugs for long-acting antiviral activities.

### **3.3 Materials and Methods**

#### **3.3.1 Materials**

Monophenyl tenofovir was purchased from BOC Sciences (Shirley, NY). TAF hemifumarate was a generous gift from Gilead Sciences Inc. (Foster City, CA). N-(carbobenzyloxy)- L-phenylalanine, N-(carbobenzyloxy)- L-alanine, dichloromethane (DCM), diethyl ether, methanol (MeOH) chloroform, tetrahydrofuran (THF), N,N-dimethyl formamide (DMF), 1-octanol, imidazole, triethylamine, 1-docosanol, triethyl silane ( $\text{Et}_3\text{Si}$ ), thionyl chloride, pluronic F127 (P407), polyethylene glycol 3350, ciprofloxacin, 3-(4,5-dimethylthiazol-2-yl)-2,5-diphenyltetrazolium bromide (MTT), dimethyl sulfoxide (DMSO) ammonium bicarbonate, HEPES buffer solution, potassium chloride, ciprofloxacin, paraformaldehyde (PFA) and 3,3'-diaminobenzidine were purchased from Sigma-Aldrich (St. Louis, MO). Palladium, 10% on activated carbon, was purchased from STREM Inc. (Newburyport, MA). 1-[Bis(dimethylamino)methylene]-1H-1,2,3-triazolo[4,5-b] pyridinium 3-oxidhexafluorophosphate (HATU) was obtained from Chem Impex Intl Inc. (Wood Dale, IL), optima water, cell-culture-grade water (endotoxin free), and gentamicin reagents were purchased from Fisher Scientific (Hampton, NH). Monoclonal mouse anti-human HIV-1 p24 (clone Kal-1) and polymer-based horseradish-peroxidase-conjugated anti-mouse EnVision+ secondary were purchased from Dako (Carpinteria, CA). Heat-inactivated pooled human serum was purchased from Innovative Biologics (Herndon, VA). Dulbecco's Modified-Eagle's Media (DMEM) was purchased from Corning Life Sciences (Tewksbury, MA). Flash

chromatography was performed using 32-63  $\mu\text{m}$  flash silica gels from SiliCycle Inc. (Quebec, Canada). Reactions were monitored by thin-layered chromatography on precoated silica plates (250  $\mu\text{m}$ , F-254) from SiliCycle Inc. (Quebec, Canada). The compounds were visualized by UV fluorescence. CEM-ss CD4+ T cells were obtained from the HIV Reagent Program.

### 3.3.2 Synthesis of L-phenylalanine and L-alanine docosyl esters

N-(carbobenzyloxy)- L- phenylalanine (2g, 1 equiv.), or N-(carbobenzyloxy)- L- alanine (2g, 1 equiv.), and 1-docosanol (1.1 equiv.) were suspended in anhydrous DMF (20 ml) and  $\text{CHCl}_3$  (20 mL) and cooled to  $-10^\circ\text{C}$  on a regular ice/ NaCl bath. To this mixture, HATU (1.5 equiv), and imidazole (1 equiv) were then added. Next,  $\text{Et}_3\text{N}$  (2 equiv) was added to the pre-cooled mixture ( $-10^\circ\text{C}$ ) dropwise. The resultant solution was stirred and gradually warmed to  $45^\circ\text{C}$  over 24 h under an inert argon atmosphere. The reaction mixture was concentrated on a rotary evaporator to yield a light-yellow solid that was purified by silica column flash chromatography eluting with a 4:1 mixture of hexanes and ethyl acetate. Next, the Cbz-protected amino acid esters were dissolved in 30 ml  $\text{CHCl}_3$  and 30 ml MeOH, and deprotected using palladium on carbon (Pd/C, 40% weight of N-Cbz- amino acid) and  $\text{Et}_3\text{Si}$  (15 equiv). After 24 h, the reaction was filtered through celite, concentrated and precipitated from diethyl ether to yield amorphous white powders of the desired free amino acid ester compounds that were used directly in the subsequent steps.

### 3.3.3 Synthesis and characterization of TFV ProTides

Monophenyl tenofovir (2 g, 5.5 mmol, 1 equiv) was dried from anhydrous benzene (15 mL), resuspended in anhydrous ACN (25 mL) and then cooled at  $-10^\circ\text{C}$  under an argon atmosphere. After the addition of 5 equivalents of  $\text{SOCl}_2$  the reaction was heated at  $65^\circ\text{C}$  for 2 h under protection from light. The mixture was then dried from 15 ml benzene by rotary evaporation. The chlorinated compound was then resuspended in 15 ml of ACN and 15 ml THF, and cooled to  $-10^\circ\text{C}$ . A solution of L-phenylalanine docosyl ester (2g, 4.22 mmol, 1

equiv), or L-alanine docosyl ester (2g, 5.06 mmol, 1 equiv) was then added followed by dropwise addition of Et<sub>3</sub>N (4 equiv) at -10 °C. The reaction mixture was then warmed to room temperature, then heated at 45 °C for 24 h under protection from light. The mixture was then concentrated to remove solvents. The residue was purified by silica column flash chromatography, eluting with 95% then 92.5% DCM in methanol. The desired compound fractions from the columns were dried on a rotary evaporator and freeze dried from a mixture of diethyl ether/ water to obtain white powders, with chemical yields of 50-65%. Successful synthesis of the prodrugs was confirmed by <sup>1</sup>H, <sup>13</sup>C, and <sup>31</sup>P NMR spectroscopy using a Bruker Avance-III HD operating at 500 MHz and a magnetic field strength of 11.7 T. **M1TFV**: <sup>1</sup>H NMR (500 MHz, CDCl<sub>3</sub>): 8.32 (2s, 1H), 7.92 (2s, 1H), 7.04-7.38 (m, 7H), 6.93-7.02 (m, 2H), 5.68 (d, *J* = 12.9 Hz, 1H), 4.25-4.13 (m, 2H), 3.80-4.15 (m, 4H), 3.34-3.65 (m, 2H), 2.86-2.94 (m, 2H), 1.82 (b, 3H), 1.51 (b, 2H), 1.21-1.35 (m, 37H), 1.15 (d, *J* = 6.2 Hz, 3H), 0.87 (t, *J* = 6.9 Hz, 3H). <sup>13</sup>C NMR (125 MHz, CDCl<sub>3</sub>): δ 172.6, 155.6, 152.9, 150.2, 150.1, 149.9, 141.7, 135.9, 129.6, 129.5, 129.4, 128.4, 126.9, 124.9, 120.6, 120.5, 120.4, 119.2, 76.6, 76.1, 65.6, 64.9, 63.8, 63.7, 55.0, 54.9, 54.7, 50.4, 48.3, 48.2, 48.1, 41.2, 41.0, 40.5, 31.9, 30.9, 29.7, 29.6, 29.5, 29.3, 29.2, 28.4, 25.8, 22.6, 16.4, 14.1; <sup>31</sup>P NMR (202 MHz, CDCl<sub>3</sub>): 20.9, 22.1. HRMS (ESI-TOF) *m/z*: [M + H]<sup>+</sup>: calcd. for C<sub>46</sub>H<sub>72</sub>N<sub>6</sub>O<sub>5</sub>P<sup>+</sup>, 819.53 (100%), 820.53 (49.8%), 821.54 (12.1%); found, 819.70. **M2TFV**: <sup>1</sup>H NMR (500 MHz, CDCl<sub>3</sub>): 8.34 (2s, 1H), 7.98 (2s, 1H), 7.31 (t, *J* = 7.9 Hz, 1H), 7.21 (t, *J* = 7.8 Hz, 1H), 7.15 (t, *J* = 7.3 Hz, 1H), 7.10 (t, *J* = 7.3 Hz, 1H), 6.99 (d, *J* = 7.3 Hz, 1H), 5.66 (d, *J* = 8.9 Hz, 1H), 4.34 (dd, *J* = 14.4, 2.9 Hz, 1H), 3.86-4.20 (m, 5H), 3.55-3.73 (m, 1H), 3.49 (t, *J* = 10.4 Hz, 1H), 1.53-1.68 (m, 2H), 1.20-1.38 (m, 42H), 0.87 (t, *J* = 6.9 Hz, 3H). <sup>13</sup>C NMR (125 MHz, CDCl<sub>3</sub>): δ 173.8, 155.6, 152.9, 150.5, 150.1, 150.0, 141.7, 129.7, 129.6, 129.5, 129.2, 124.9, 120.8, 120.4, 119.2, 76.6, 76.2, 65.6, 65.3, 64.9, 63.8, 49.9, 49.6, 48.3, 40.9, 31.9, 30.9, 29.7, 29.6, 29.5, 29.4, 29.2, 28.6, 28.5, 25.8, 22.6, 21.6, 20.9, 16.4, 14.1; <sup>31</sup>P NMR (202 MHz, CDCl<sub>3</sub>): 20.7, 22.2. HRMS (ESI-TOF) *m/z*: [M + H]<sup>+</sup>: calcd. for C<sub>40</sub>H<sub>68</sub>N<sub>6</sub>O<sub>5</sub>P<sup>+</sup>, 743.50 (100%), 744.50 (43.3%),

745.51 (9.1%); found, 743.67. FTIR analysis was performed on a Spectrum Two FT-IR spectrometer (PerkinElmer, Waltham, MA, USA). Differential Scanning Calorimetry was performed on Shimadzu DSC-60 (Kyoto, Japan) with a thermal analysis operating system (Shimadzu TA-60WS, Kyoto, Japan). About 8 mg of sample was weighed in an aluminum pan and crimped which was used as the sample pan. An empty crimped aluminum pan was used as the reference pan. The pans were heated from room temperature to 300°C at the rate of 10°C/min in a nitrogen environment (flow rate 20 mL/min). Molecular mass was determined by direct infusion into a Waters TQD mass spectrometer.

### **3.3.4 Ultrapformance liquid chromatography–ultraviolet/visible drug and prodrug quantifications**

A Waters ACQUITY ultrapformance liquid chromatography (UPLC) H-Class system with a UV detector and Empower 3 software was used to measure the drug concentrations. M1TFV and M2TFV samples were separated on a Waters Acquity UPLC BEH 1.7  $\mu$ m C18 column (50 x 2.1 mm). TAF samples were separated on a Phenomenex Kinetex 5  $\mu$ m C18 column (150 x 4.6 mm). TAF was detected at 260 nm using an isocratic elution with a mobile phase that consisted of 40% 7.5 mM ammonium acetate pH 4 / 60% MeOH with a flow rate of 0.25 ml/ min. M1TFV and M2TFV were detected at 254 nm using an isocratic elution with a mobile phase consisting of 98% MeOH/ 2% 7.5 mM ammonium bicarbonate pH 7.0 at a flow rate of 0.2 ml min. The drug content was determined relative to the peak areas of drug standards (0.05–50  $\mu$ g /ml) in MeOH.

### **3.3.5 Solubility**

The aqueous and 1-octanol solubility of TAF, M1TFV, and M2TFV were determined by adding an excess of drug to water or 1-octanol at room temperature and mixing for 48 h. Samples were centrifuged at 20,000g for 10 min to separate solubilized drug from insoluble pellet. Aqueous supernatants were frozen, lyophilized and then resuspended in MeOH. 1-

octanol supernatants were prepared for analysis by dilution in MeOH and samples analyzed for drug content by UPLC-UV (Waters Acquity H Class).

### **3.3.6 Nanoparticle synthesis and characterization**

Similar to how CAB or RPV LA nanocrystals are produced, NM1TFV, NM2TFV, and NTAF solid drug nanocrystals were manufactured by high-pressure homogenization in aqueous buffers stabilized by non-ionic surfactants. The prodrug to surfactant ratio was maintained at 2:1 (w/w), and the suspension concentration was in the range 0.1–10% w/v for the drug/prodrug and 0.05–5% w/v for P407. Both NM1TFV and NM2TFV nanoformulations were prepared in P407 surfactant solution in 10mM HEPES at pH 7. For NTAF, a mixture of P407 and PEG 3350 were used as stabilizers. Specifically, TAF was dispersed in a P407/PEG 3350 solution in 10mM HEPES pH 5.5 and allowed to form a presuspension. The prodrug to P407 to PEG 3350 ratio was maintained at 2: ½: ½ (w/w), and the suspension concentration was in the range 0.1–10% w/v for the drug/prodrug and 0.025–2.5% w/v for P407/ PEG. The presuspensions were homogenized on an Avestin EmulsiFlex-C3 high-pressure homogenizer at 15,000- 20,000 psi until the desired particle size of 250-350 nm was achieved. Nanoparticles were characterized for particle size, PDI and zeta potential by dynamic light scattering using a Malvern Zetasizer Nano-ZS. The stabilities of the nanoformulations were monitored at room temperature for 1-3 months. The drug/prodrug concentration in each nanoformulation was determined by diluting the nanoformulation in MeOH (1,000–10,000-fold dilution) and analyzed by UPLC–ultraviolet/visible (UV/vis) spectroscopy. The encapsulation efficiency was calculated using the equation: encapsulation efficiency (%) = (weight of drug in formulation/initial weight of drug added) × 100.

### **3.3.7 Prodrug chemical stability**

The pH buffers included 0.1% formic acid (pH 2.0), 7.5mM ammonium acetate buffer (pH 6.0 adjusted with acetic acid), optima water (pH 7.0), 7.5 mM ammonium bicarbonate buffer (pH 8.0 adjusted with acetic acid), and 0.1 % ammonium hydroxide (pH 10.8) and



stored at 4°C until use. NM1TFV or NTAF were incubated at 37 °C in 100 µL of the buffer. The final concentration of methanol in the incubation mixture was 1% (v/v). The reactions stopped by addition of 1 mL of acidified methanol (0.1% formic acid + 2.5 mM ammonium formate) at 0 min, 5 min, 30 min, 1 hr, 2 hr, 6 hr, 12 hr, and 24 hr hour time points. Control samples were incubated using the same method as in the absence of substrates; substrates were added after the addition of acidified methanol. The mixtures were centrifuged at 16,000g for 10 minutes. The supernatants were aspirated and stored at -80°C until LC-MS/MS analysis.

### **3.3.8 Plasma prodrug stability**

The hydrolysis kinetics of M1TFV and M2TFV were determined in rat, mouse, rabbit, monkey and human plasma. Solutions of 10 µM of M1TFV, M2TFV, TAF, and their corresponding nanoformulations (NM1TFV, NM2TFV, and NTAF) were incubated in 100 µL of plasma at 37 °C. At specified time points, 900 µL of acidified methanol (0.1% formic acid in MeOH) was added to each sample and vortexed for 3 min to stop the reaction. For the 0-min time point, 900 µL of ice-cold MeOH was added to 100 µL of plasma and then spiked with 1 µM of each prodrug. After the addition of prodrug, samples were centrifuged at 15,000g for 15 min and the supernatants were analyzed for drug content by a Waters Acquity H-class UPLC system coupled to UV/Vis detector.

### **3.3.9 Human monocyte-derived macrophage (MDM) isolation, cultivation and cytotoxicity measurements**

Human monocytes were obtained, cultured, and differentiated into MDM as previously described [33, 164, 217, 218]. The cell viability after treatment with nanoparticles was evaluated using the MTT assay. Human MDMs plated in 96-well plates at a density of  $0.08 \times 10^6$  cells per well were treated with various concentrations (1.5625- 200 µM) of NM1TFV, NM2TFV, or TAF for 8 h. After drug treatment, cells were washed and incubated with 100 µL/well of MTT solution (5 mg/mL) for 45 min at 37 °C. After incubation MTT was

removed, and 200  $\mu$ L/well of DMSO was added and mixed thoroughly. Absorbance was measured at 490 nm on a Molecular Devices SpectraMax M3 plate reader with SoftMax Pro 6.2 software (Sunnyvale, CA).

### **3.3.10 Drug nanoformulation uptake and retention**

Human MDMs were used for in vitro assessments. MDM uptake and retention studies were performed in flat-bottom, 12-well plates at a density of  $1.2 \times 10^6$  cells per well, with each treatment completed in triplicate. For cellular uptake studies, MDMs were treated with 10  $\mu$ M or 100  $\mu$ M NM1TFV, NM2TFV, and TAF. At 2, 4, and 8 h after treatment, the cells were collected, processed, and analyzed for drug content by UPLC-UV/vis as previously described [33, 139, 150, 154]. For the retention studies, MDMs were treated with 10  $\mu$ M or 100  $\mu$ M NM1TFV, NM2TFV or NTAF for 8 h, and then washed twice with 1 ml PBS. Then, culture medium (without drug) was added, and a half-media volume was replaced every other day. MDMs were collected at days 1, 5, 10, 15, and 30 after treatment, and then analyzed for intracellular drug content by UPC-UV/vis.

### **3.3.11 Transmission electron microscopy to assess intracellular drug nanoformulations**

MDMs were treated with 10  $\mu$ M NM1TFV, NM2TFV, or TAF for 8 h and then washed twice with PBS. MDMs were then collected immediately after the 8-h treatment and analyzed by TEM to image the intracellular nanoparticles as previously described [33, 164, 201].

### **3.3.12 TFV-DP measurements in MDM**

Intracellular TFV-DP was extracted from cells and levels quantified as follows. MDM were treated with 10  $\mu$ M or 100  $\mu$ M NM1TFV, NM2TFV, or TAF. At 2, 4, and 8 hours after treatment, MDM were washed with PBS to remove excess free drug. The cells were then collected in 70% methanol. TFV-DP from MDM was extracted as follows. Sep-Pak QMA cartridges (360 mg, 37-55  $\mu$ m; Waters, Milford, MA) were used to separate TFV-DP from TFV- and mono-phosphate counterparts. The QMA cartridges were conditioned with 10 ml

of 500 mM KCl, followed by 10 ml of 5mM KCl. Sample (200  $\mu$ L) was loaded onto the cartridges and washed with 12 ml of 75 mM KCl. The triphosphate fraction was eluted with 3 ml of 500 mM KCl. The pH of the TP fraction was lowered to 4.25 by adding 45  $\mu$ L ammonium acetate buffer (pH 4, 10 mM) per ml eluate, and dephosphorylated by adding one unit of type XA sweet potato acid phosphatase (Sigma-Aldrich) per ml eluate (3  $\mu$ L per sample) and incubating at 37 °C for 45 min. 150  $\mu$ L of 12% TFA and 10  $\mu$ L of  $^{15}\text{N}_2$   $^{13}\text{C}$ -3TC and d4- ABC internal standard were then added. Samples were then loaded onto Waters OASIS HLB cartridges (60 mg, 30  $\mu$ m; Waters, Milford, MA) pre-conditioned with 3 ml 100% methanol followed by 3 ml 1% TFA to remove salts. Salts were removed from the dephosphorylated samples with 3.5 ml of 1% TFA in water, then eluted with 1.5 ml 100% methanol and evaporated under vacuum. Once dry, the residue was stored at -80°C until UPLC–MS/MS analyses. Samples were reconstituted in 100  $\mu$ L of 10% MeOH, 90% 7.5 mM ammonium bicarbonate pH 7 in LC-MS grade water.

### **3.3.13 Antiretroviral Efficacy of ProTide Nanoformulations**

MDMs were plated in flat-bottom 12-well plates at a density of  $1.2 \times 10^6$  cells per well. MDMs were treated with 10  $\mu$ M or 100  $\mu$ M NM1TFV, NM2TFV, NTAF or TAF for 8 h. After treatment, the cells were washed twice with PBS and cultured in fresh culture medium without drug with half-media replacement every other day. On days 1, 5, 10, 15, 20, 25 and 30 following treatment, the cells were infected with HIV-1<sub>ADA</sub> (a macrophage-tropic viral strain) at a multiplicity of infection of 0.1 infectious particles/cell for 8 h. MDM were cultured, and media samples collected on day 10 for the measurement of RT activity as previously described [205, 206]. Cells were fixed in 2% PFA at each time point, and expression of the HIV-1p24 antigen was determined by immunocytochemistry.

### **3.3.14 EC testing in HIV-1 target cells**

MDMs were plated in flat-bottom 96-well plates ( $0.08 \times 10^6$  cells per well). Cells were treated with a range of drug concentrations, 0.00005–5,000 nM, of TAF, M1TFV, M2TFV,

NTAF, NM1TFV, or NM2TFV for 1 h prior to infection with HIV-1<sub>ADA</sub> (multiplicity of infection of 0.1) for 4 h. After 4 h of viral challenge, the cells were washed with PBS and given fresh media that contained the same concentrations of drug (0.00005–5,000 nM). Cell supernatants were collected 10 days later and assayed for HIV-1 RT activity as described above. Replicate studies were performed in CEM-ss CD4<sup>+</sup> T-cell cultures. Specifically, cells were plated in 96-well plates, centrifuged at 650g for 5 min and resuspended in (0.1–1000 nM) drug-containing media for 1 h. Subsequent challenge with HIV-1<sub>NL4-3-eGFP</sub>, cell culture, sample collection, and determination of HIV-1 RT activity were performed as previously reported[150, 151].

### **3.3.15 PK studies**

Twelve-week-old healthy Sprague Dawley rats (male, 300-350 g; female, 200-230 g; SASCO) were purchased from Charles River Laboratories (Wilmington, MA) and housed in the University of Nebraska Medical Center (UNMC) laboratory animal facility according to the American Animal Association and Laboratory Animal Care guidance. All procedures were approved by the Institutional Animal Care and Use Committee at the University of Nebraska Medical Center (UNMC) as set forth by the National Institutes of Health (NIH). The animals were administered a single intramuscular injection (IM, caudal thigh muscle; 200 µl) of 75 mg/kg TFV equivalents of either NM1TFV, NM2TFV, or NTAF (male) or NM2TFV or NTAF (female). On days 1, 14, 28, 42 and 56 after injection, blood samples were collected into EDTA tubes via the retro-orbital sinus using autoclaved glass capillaries. A 25 µl aliquot of blood was immediately diluted into 1 ml of MeOH (containing 2.5mM ammonium formate and 0.1% formic acid) for drug quantitation. The remaining blood sample was used for PBMC isolation. On either day 28 (female) or days 28 and 56 (male) post drug administration, animals were humanely euthanized, and spleen, lymph node, adipose, testes, liver, lung, gut (duodenum/jejunum), kidney, brain, vaginal and rectal tissue were collected for the quantitation of TFV and prodrugs. Additionally, rat peripheral blood mononuclear cells

(PBMcs), splenocytes, lymphocytes, liver parenchymal and non-parenchymal cells were isolated on sacrifice days for analysis of TFV-DP content. TFV, M1TFV, M2TFV were quantitated in rat blood and tissues by UPLC–MS/MS using a Waters ACQUITY H-class UPLC connected to a Xevo TQ-S micro mass spectrometer. All the solvents for sample processing and UPLC–MS/MS analysis were liquid chromatography–MS grade (Fisher). Toxicity of the formulations in SD rats was assessed by determining serum chemistry profiles, organ to body weight ratios, complete blood counts, and histological examinations. For the histological examination, 5- $\mu$ m sections of paraffin-embedded tissues were stained with hematoxylin and eosin. Images were captured with a 4 and  $\times$ 40 objective using a Nuance EX multispectral imaging system affixed to a Nikon Eclipse E800 microscope (Nikon Instruments). Histopathological assessments were conducted by a certified pathologist in accordance with the guidelines of the Society of Toxicologic Pathology. Serum chemistry profiles were determined using a VetScan comprehensive diagnostic profile disc and a VetScan VS-2 instrument (Abaxis Veterinary Diagnostics). Complete blood counts were determined using an Abaxis Vetscan HM5 Hematology Analyzer. For both, the results for treated animals were compared with those from age-matched untreated control rats.

#### **3.3.16 TFV-DP extraction from mucosal tissues**

On either day 28 (female rats) or days 28 and 56 (male rats) post drug treatment, rats were humanely sacrificed. Rectal and vaginal tissues were collected, flash-frozen, and stored at -80°C until further processing. Vaginal and rectal tissues were homogenized with a Qiagen TissueLyser II, and TFV-DP was extracted from vaginal and rectal tissue using 50% and 70% MeOH, respectively. Individual cell populations were not isolated from the tissues. TFV-DP samples were further processed and analyzed as described previously.

#### **3.3.17 Sample Preparation and LC-MS/MS Analyses**

TFV quantitation in whole blood and tissues was determined by UPLC-MS/MS using a Waters Acquity UPLC- Xevo TQ-S micro mass spectrometry system (Milford, MA) and a

CSH C18 (1.7  $\mu\text{m}$ , 2.1 mm  $\times$  100 mm) column. For blood and tissue analysis, 10  $\mu\text{L}$  of internal standard (IS) solution was added to each sample; 3TC-d3 was used as IS for TFV analysis. Mobile phase A consisted of 7.5 mM ammonium bicarbonate adjusted to pH 7 and mobile phase B consisted of 100% Optima-grade methanol at a flow rate of 0.22 mL/min and run time of 8 mins. Multiple reaction monitoring (MRM) transitions used for TFV, and the IS 3TC-d3, were 288.23 > 159.01, and 233.23 > 114.97 m/z, respectively. The initial mobile phase composition was 5% B for the first 4.25 min at which time it was increased to 30% B over 0.25 min, then increased to 90 % B and held for further 0.6 min before returning to initial conditions. Spectra were analyzed and quantified by MassLynx software version 4.1. Quantitation was based upon drug peak area to internal standard peak area ratios.

Prodrug concentration in whole blood and tissues was determined by UPLC-MS/MS using a Waters Acquity UPLC- Xevo TQ-S micro mass spectrometry system (Milford, MA). For blood and tissue analysis, 10  $\mu\text{L}$  of internal standard (IS) solution was added to each sample. 3TC-d3 was used as IS for TFV and M1TFV/ M2TFV analysis, respectively. Chromatographic separation of 10  $\mu\text{L}$  sample injections of M1TFV/ M2TFV was achieved with an ACQUITY UPLC-BEH Shield RP18 column (1.7  $\mu\text{m}$ , 2.1 mm  $\times$  30 mm) using a gradient of mobile phase A (7.5 mM ammonium formate in Optima-grade water adjusted to pH 3 using formic acid) and mobile phase B (100% Optima-grade methanol) at a flow rate of 0.35 mL/min. The initial mobile phase composition was 88% B for the first 5 min at which time it was increased to 95% B over 0.25 mins and held constant for 1.50 min. For Multiple reaction monitoring (MRM) transitions used for M1TFV, M2TFV, and 3TC-d3, were 819.70 > 206.10, 743.68 > 206.10, and 233.39 > 114.97 m/z, respectively. Spectra were analyzed and quantified by MassLynx software version 4.1. Quantitation was based upon drug peak area to internal standard peak area ratios.

TFV-DP: Parent TFV was generated from TFV-DP during sample preparation and then subjected to UPLC-MS/MS analyses. The UPLC-MS/MS system comprised of a Waters

ACQUITY ultra-performance liquid chromatography (UPLC) system (Waters, Milford, MA) coupled to a triple quadrupole mass spectrometer with electrospray ionization (ESI) source (Waters Xevo TQ-XS). An ACQUITY UPLC using a CSH C18 analytical column (2.1×100 mm, 1.7µm; Waters) equipped with a guard column (Waters, Milford, MA) at 30°C was used for analyte separation. Sample was maintained at 4°C. The transition of 288.10 < 159.04 m/z and 232.97 < 115.00 m/z were used for TFV and 3TC-d3 internal standard (IS) quantification, respectively. Mobile phase A consisted of 7.5mM ammonium bicarbonate in water (MS grade, Fisher), pH was adjusted to 7.0 with glacial acetic acid (ACS grade, Sigma). Mobile phase B was 100% methanol (MS grade, Fisher). The flow rate was 0.22 mL/min. A gradient of 95% A and 5% B was held for 4.25 min, and then B was ramped to 30% for 0.25 min. B was then held at 90% for 0.4 min before returning to initial conditions. Spectra were analyzed and quantified by MassLynx software version 4.1. Quantitation was based upon drug peak area to internal standard peak area ratios.

### **3.3.18 Pharmacodynamics in a humanized mouse model of HIV-1 infection**

NOD/scid-IL-2R $\gamma$ null (NSG) mice were reconstituted with CD34<sup>+</sup> human hematopoietic stem cells (HSC) isolated from umbilical cord blood. Mice were administered NM2TFV and NM4FTC (75 mg/kg parent drug eq. each; IM) and subsequently challenged with HIV-1ADA (1 × 10<sup>4</sup> TCID<sub>50</sub>; Intraperitoneal; IP) two weeks following drug treatment. Two and 4 weeks after viral challenge blood was collected by cheek puncture into EDTA-coated tubes. Blood samples were centrifuged (2,000 g for 5 min) and collected plasma was stored at -80°C until further analyses. Viral load (HIV-1 RNA) was quantified in collected plasma samples using a Roche Amplicor and TaqMan-48 system. Additionally, plasma drug concentrations were determined by UPLC-MS/MS.

### **3.3.19 Generation of humanized liver TK-NOG and FRG mouse models**

To deplete mouse parenchymal cells, mice were injected with ganciclovir (GCV) at a dose of 6 mg/kg, 2x a day, on day -7 and day -5, followed by a treosulfan injection on days

-3, -2 and -1. To screen the mice for the transplantation, alanine aminotransferase (ALT) was assayed one day before human hepatocyte transplantation, and mice with ALT levels of >200 and <600 U/L were selected. TK-NOG mice (NOD/Shi-scid IL-2 R $\gamma$ c null) expressing a herpes simplex virus type 1 thymidine kinase transgene under regulation of the albumin gene promoter, or FRG KO mice (Fah $^{-/-}$ /Rag2 $^{-/-}$ /Il2rg $^{-/-}$  triple knock-out) were intrasplenically infused with 2 million human hepatocytes from Lonza (lot#4145) [214]. After transplantation, the mice were checked for liver reconstitution by assessing their albumin level using ELISA.

### **3.3.20 Dosing of TK-NOG and FRG mice**

NM1NTZ, NM1TFV, NM2TFV, and NTAF were prepared as described. In the case of NTAF, the formulation was used without further processing. For NM1TFV, and NM2TFV, the formulations were concentrated by differential centrifugation. Specifically, the initial formulations were centrifuged at 4°C for 10 minutes at 200 x g to remove excess polymer. The supernatant was transferred and centrifuged again at 15000 x g for 20 minutes at 4°C. The resulting size, PDI, zeta potential and concentration of the formulation were measured. The formulation was prepared immediately before dosing. HBV infected mice were treated four weeks after infection, when peripheral blood levels of HBV DNA had been established. For a 75 mg/kg (TFV eq.) dose of NM1TFV or NM1NTZ, 25 microliters of suspension were injected intramuscularly into the caudal thigh muscle. For a 168 mg/kg (TFV eq.) dose of NM1TFV or NM2TFV, 25 microliters of suspension were injected intramuscularly into each caudal thigh muscle. For a 168 mg/kg (TFV eq.) dose of NTAF, 20 microliters of suspension were injected intramuscularly into each caudal thigh muscle. After injection, formulation integrity was monitored by DLS and drug concentration was again determined.

### **3.3.21 Human Serum Albumin**

Serum human albumin levels [214] were measured in 50 $\mu$ L of serum and analysis performed using the Human Albumin ELISA Quantitation Set (E80-129, Bethyl Laboratories Inc., Montgomery, TX).



### **3.3.22 Measurement of Blood HBV DNA and HBsAg levels**

HBV DNA levels were measured using the COBAS TaqMan HBV Test (Roche Diagnostics, Switzerland). The samples were diluted approximately 20-fold and detection limits were 2240-3360 DNA copies/ml. Plasma HBsAg levels were measured by ELISA using the QuickTiter Hepatitis B Surface Antigen ELISA Kit (Cell Biolabs, Inc, VPK-5004, San Diego, CA) according to assay protocol.

### **3.3.23 HBV RNA, DNA isolation, Real-time PCR and digital droplet PCR**

Reagents for RNA isolation, cDNA synthesis and real time PCR were purchased from Life Technologies and Applied Biosystems by Thermo Fisher Scientific (Carlsbad & Foster city, CA). Primers and Probes were bought from Integrated DNA Technologies, Inc (Coralville, IA). Total RNA was isolated from liver cells by mixing Trizol with liver homogenate in PBS. A 2-step procedure was applied, first reverse-transcribing HBV RNA to cDNA using the high capacity reverse transcription synthesis kit. cDNA then was amplified using TaqMan Universal Master Mix with fluorescent labeled primers (TaqMan gene expression systems) in a Model 7500 qRT-PCR thermal cycler. GAPDH cDNA was used to normalize RNA. Data were expressed as the quantity of transcript (RQ). HBV DNA levels were quantified by ddPCR. Total DNA was prepared using the DNeasy Kit (Qiagen, Germany) according to the manufacturer's protocol. The concentrations of DNA were quantified using the QX200™ Droplet Digital™ PCR System (Bio-Rad, Hercules, CA). HBV sense and antisense primers were 5'- CGACGT GCA GAG GTG AAG-3' and 5'- CAC CTC TCT TTA CGC GGA CT-3' respectively. The HBV probe was 5'/56-FAM/ATC TGC CGG /ZEN/ACC GTGTGC AC-3'. Prepared droplets were transferred to a Bio Rad 96-well PCR plate and underwent thermal cycling. After amplification, the ddPCR data were analyzed using the QuantaSoft analysis software version 1.8 (Bio-Rad). The absolute concentration of each sample was automatically reported by the ddPCR software.

### 3.3.24 Statistical analyses

Statistical analyses were conducted using GraphPad Prism 8.0 software. Data from in vitro studies were expressed as mean  $\pm$  SEM with a minimum of three biological replicates. Results from the in vivo studies were expressed as mean  $\pm$  SEM with a minimum of three biological replicates. For comparison of two groups, Student's t-test (two-tailed, paired and unpaired) was used. A one-way ANOVA followed by Tukey's post hoc test was used to compare three or more groups. Statistical significances were denoted as \* $P$  < 0.05, \*\* $P$  < 0.01, \*\*\* $P$  < 0.001 and \*\*\*\* $P$  < 0.0001. Pearson correlation and linear regression models were used to examine the association between in intramuscular drug concentrations and tissue drug concentrations.

### 3.3.25 Study approvals

All the animal studies were approved by the University of Nebraska Medical Center Institutional Animal Care and Use Committee in accordance with the standards incorporated in the *Guide for the Care and Use of Laboratory Animals* [219]. Human monocytes were isolated by leukapheresis from HIV-1/2 and hepatitis B seronegative donors according to an approved University of Nebraska Medical Center Institutional Review Board exempt protocol.

## 3.4 Results

### 3.4.1 Synthesis and characterization of TFV ProTides

We created novel M1TFV and M2TFV ProTides bearing alanine and phenylalanine amino acid esters by replacing optimal short chain alkyl ester groups in conventional ProTide strategies [215, 220, 221]. Previously unexplored and less preferred bulky residues were used to create the ProTides (Fig. 3.7.1). The docosanol masking ester motif was selected based on inherent lipophilicity and for synergistic effects on the nucleoside analogs [213, 214]. M1TFV and M2TFV were synthesized by coupling a phenylalanyl or alanyl docosyl ester (Fig. 3.7.1) to monophenyl TFV in the presence of Et<sub>3</sub>N to yield the desired compounds with yields of 50-60%. Since the conjugation step is moisture sensitive, further improvements

to the chemical yields could be achieved by either optimizing the coupling reagents or reaction vessels. Infusion of the synthesized compounds into a Waters Xevo TQ-S micro mass spectrometer confirmed a molecular mass ion of 819.2 for M1TFV, and 742.0 for M2TFV (Fig.3.6.3). Conversion of TFV into ProTides altered the physicochemical properties of TFV. TAF, M1TFV and M2TFV exhibited aqueous solubilities of 5.52-, 0.002- and 0.007-mg/mL, respectively. In contrast, the solubility of the prodrugs in 1-octanol were 4.85-, 29.2- and 20.9- mg/mL for TAF, M1TFV and M2TFV. This confirmed substantial increases in prodrug lipophilicity (Fig.3.6.2). To determine the effect of prodrug modifications on chemical stability, 1  $\mu$ M NM1TFV or NTAF solutions were incubated for 24 hrs at varying pH. These included pH of 2 (0.1% formic acid), 6.0 (7.5mM ammonium acetate), 7.0 (PBS), 8 (7.5mM ammonium bicarbonate), and 10.8 (0.1% ammonium hydroxide). No statistical differences in prodrug stability were observed between NM1TFV and NTAF at pH 2 from 0 to 2 hrs, pH 6 from 0-12 hrs, or in pH 7.0 over the 24 hrs (Fig.3.6.3). However, M1TFV demonstrated significantly greater prodrug stability in pH 2 at 6 and 12 hrs, pH 6 at 24 hrs, and in pH 8 and 10.8 at all time points (Fig.3.6.3), suggesting that unlike TAF that is hydrolytically unstable at basic pH, M1TFV confers enhanced prodrug stability over a broader pH range. The two ProTides were further characterized by  $^1\text{H}$  and  $^{31}\text{P}$  NMR. The triplet at 0.87 ppm and multiplets at 1.21-1.35 ppm on the spectrum of M1TFV correspond to the terminal methyl and methylene protons of the docosyl ester, respectively. Chemical shifts at 7.04-7.38 ppm represent the aryl and phenylalanine masking promoieties (Fig.3.6.2). For M2TFV, the triplet at 0.87 ppm and multiplets at 1.20-1.38 ppm correspond to the terminal methyl and methylene protons of the docosyl ester, respectively. The triplets at 7.10, 7.15 and 7.31 ppm represent the aryl and phenol groups (Fig.3.6.2). Peak splitting in the phosphorous NMR spectra indicated a 1:1 mixture of the R and S stereoisomers [222](Fig.3.6.3). Even though phosphorous chirality of ProTides has been shown to affect potency, our studies used the mixture of isomers since the chirality would be lost following intracellular cleavage of the

masking groups. Further chemical characterization of the ProTides by FTIR showed absorption bands at  $2844\text{cm}^{-1}$  and  $2912\text{cm}^{-1}$  corresponding to asymmetric and symmetric C-H stretches from the long chain fatty alcohol (Fig. 3.6.2). Since ideal ProTides should exhibit greater stability in plasma to facilitate intracellular and tissue drug delivery, we assessed metabolic stability of the M1TFV and M2TFV in rat and human plasma. Notably, species-specific differences in prodrug stability were observed. In the case of M2TFV, mouse and rabbit plasma exhibited more rapid prodrug hydrolysis (38.4% and 46.8% respectively) while rat, monkey and human plasma exhibited slower prodrug breakdown (0%, 8.3%, and 7.3%) over a 24-hour period (Fig. 3.6.4). Species-specific differences in M1TFV hydrolysis was less apparent over the 24-hour period and resulted in prodrug hydrolysis of 19.9% in mouse plasma, 14.7% in rat, 12.6% in monkey, 25.7% in rabbit, and 9.981% in human (Fig.3.6.4).

### 3.4.2 Nanoformulation of TFV ProTides

Nanocrystal formulation strategy has so far resulted in the successful development of several monthly IM injectable products that include CAB and RPV LA. Nanocrystals provide enhanced drug dissolution, high loading while obviating organic solvent usage and associated toxicities [130]. Aqueous surfactant stabilized M1TFV, M2TFV and TAF nanocrystals (NM1TFV, NM2TFV, NTAF) were therefore produced by high-pressure homogenization. Drug encapsulation efficiencies for NM1TFV, NM2TFV and NTAF nanocrystals were 94.6%, 92.2%, and 78.8%, respectively. The size, polydispersity index (PDI), and zeta potential for NM1TFV, were  $215 \pm 10.3$  nm,  $0.30 \pm 0.03$ , and  $-16.4 \pm 0.6$  mV, respectively, and remained stable at 25 °C for at least 90 days (Fig. 3.6.5A). The size, polydispersity index (PDI), and zeta potential for NM2TFV, were  $261.6 \pm 12.9$  nm,  $0.38 \pm 0.08$ , and  $-22.7 \pm 0.7$  mV, respectively, and remained stable at 25 °C for at least 10 days (Fig. 3.6.5A). The size, polydispersity index (PDI), and zeta potential for NTAF, was  $284.3 \pm 14$  nm,  $0.3 \pm 0.005$ , and  $6.55 \pm 0.15$  mV, respectively, and remained stable at 25 °C for at

least 30 days (Fig. 3.6.5A). We then determined the effect of the prodrugs on mitochondrial function by MTT in MDM. No adverse effects on mitochondrial activity or cell viability were observed at 200  $\mu\text{M}$  in MDM for NM1TFV and NM2TFV (Fig. 3.6.5B). In contrast, a decrease in cell viability was observed for TAF at concentrations above 12.5  $\mu\text{M}$  (Fig. 3.6.5B). We next evaluated the ProTides for antiretroviral activity. The  $\text{EC}_{50}$  values for unformulated M1TFV and M2TFV in human monocyte-derived macrophages (MDMs) were 109 nM and 45.75 nM, respectively (Fig. 3.6.5C). The observed potency is likely linked to poor prodrug solubility upon dilution and precipitation in aqueous culture media. Notably, nanoformulation of the prodrugs significantly improved drug potency, with  $\text{EC}_{50}$  values of 0.71 nM and 2.08 nM for NM1TFV and NM2TFV, respectively (Fig. 3.6.5C). The antiretroviral activity of TAF (0.22 nM) was not improved following nanoformulation into NTAF (0.44 nM, Fig. 3.6.7A). In CEM-ss T-cells the  $\text{EC}_{50}$  of NM1TFV, NM2TFV, and TAF were 28.8 nM, 30.0 nM, and 0.33 nM respectively (Fig. 3.6.7C).

### 3.4.3 Cellular Drug Uptake and Retention

Macrophage-drug interactions have been shown to improve ART pharmacokinetics and pharmacodynamics by facilitating cell and tissue drug depots in the reticuloendothelial system [33, 164]. Macrophages are ideal carriers for LASER ART due to their natural function as phagocytic cells, large intracellular storage capacity, high mobility that allows entry to sites of infection and inflammation, and their role as viral reservoirs [148]. We therefore evaluated NM1TFV, NM2TFV and TAF in MDMs at concentrations of 10  $\mu\text{M}$  and 100  $\mu\text{M}$ . It is worth noting that evaluation of TAF in MDMs was performed at 10  $\mu\text{M}$  since 100  $\mu\text{M}$  was found to be highly toxic to cells. Intracellular prodrug concentrations were evaluated over 8 h. As shown in Fig. 3.6.6A, the highest drug uptake was observed with NM1TFV. Intracellular prodrug concentration for NM1TFV at 8h after treatment with 10  $\mu\text{M}$  of drug was 8.62  $\mu\text{g}$  per  $10^6$  cells, a 4.2- and 22.7-fold higher concentration than that observed for NM2TFV (2.04  $\mu\text{g}$  per  $10^6$  cells) or TAF (0.38  $\mu\text{g}$  per  $10^6$  cells), respectively. For 100  $\mu\text{M}$  drug treatment after 8

h (Fig.3.6.6B), intracellular prodrug concentration for NM1TFV was 42.36  $\mu\text{g}$  per  $10^6$  cells, a 2.2-fold higher concentration than that observed for NM2TFV (19.4  $\mu\text{g}$  per  $10^6$  cells). Visualization of MDMs treated with equimolar drug nanoparticles by TEM revealed greater accumulation of NM1TFV and NM2TFV drug reservoirs in the cytoplasm compared to TAF (Fig. 3.6.6C). In CEM-ss T-cells, significantly improved prodrug uptake was observed for NM1TFV compared to NM2TFV and NTAF (Fig. 3.6.7B). To further confirm the release of ProTides from the nanoparticles and their conversion to active metabolites, we quantified the intracellular TFV-DP levels in the MDMs after a single exposure to NM1TFV, NM2TFV or TAF. As shown in Fig. 3.6.6A, the 10  $\mu\text{M}$  TAF treatment produced the highest TFV-DP concentration, peaking at 8h (690,949 fmol per  $10^6$  cells). For NM1TFV at 10  $\mu\text{M}$ , the maximum TFV-DP levels were observed at 8 h (7,056.7 fmol per  $10^6$  cells), and of 57,113 fmol per  $10^6$  cells at 8h for NM2TFV. Even though lower concentrations of TFV-DP were measured for NM1TFV compared to NM2TFV or TAF, the active metabolite levels were sustained over 8hrs, well above the human EC90 of 40 fmol per  $10^6$  cells. At the 100  $\mu\text{M}$  dose (Fig. 3.6.6B), the TFV-DP concentrations for NM1TFV and NM12TFV peaked after 8 h and the difference was not found to be statistically significant (160,867 fmol per  $10^6$  cells, and 239,422 fmol per  $10^6$  cells, respectively).

Prior data from our laboratories demonstrate sustained and enhanced storage of nanoformulations in MDM [159]. Thus, retention of TFV nanoformulations in MDM was determined. Following a 10  $\mu\text{M}$  dose, NM1TFV facilitated retention of the prodrug in MDM for up to 30 days (0.13  $\mu\text{g}$  / $10^6$  cells), while NM2TFV and native TAF treatments showed no detectable drug within 15 days, and 24 h respectively (Fig. 3.6.8A). At a higher dose of 100  $\mu\text{M}$  (Fig. 3.6.8C) both NM1TFV and NM2TFV facilitated prodrug retention for up to 30 days (19.53  $\mu\text{g}$  / $10^6$  cells and 0.64  $\mu\text{g}$  / $10^6$  cells respectively). To assess the extent of active metabolite retention, intracellular TFV-DP was measured over a 30-day time period after a single exposure of drug for 8h. Notably, a single treatment of MDMs with NM1TFV or

NM2TFV provided steady and sustained TFV-DP levels over the entire 30-day period (Fig. 3.6.8B, C). As shown in Fig. 3.6.8B, the amount of TFV-DP retained by 10  $\mu$ M NM1TFV-treated MDM was 48,232.4 fmol per  $10^6$  cells on day 1, and 10,507.7 fmol per  $10^6$  cells on day 30. Similarly, 10  $\mu$ M of NM2TFV provided sustained TFV-DP concentrations of 349,162 and 64,057.4 fmol per  $10^6$  cells at days 1 and 30, respectively (Fig.3.6.8B). TAF demonstrated a rapid decline of the active metabolite concentration compared to NM1TFV or NM2TFV; levels of TFV-DP fell from 59,239.4 fmol per  $10^6$  cells at day 1 to 1013.4 fmol per  $10^6$  cells on day 30. Sustained intracellular TFV-DP concentrations were also observed at the 100  $\mu$ M of NM1TFV or NM2TFV treatments. For NM1TFV, intracellular active metabolite TFV-DP was retained at levels of 47,622.4 fmol/ $10^6$  cells at day 1 then 41,219.4 fmol per  $10^6$  cells by day 30. Similarly, NM2TFV provided sustained TFV-DP concentrations of 348,132 and 45,144.8 fmol per  $10^6$  cells at days 1 and 30, respectively (Fig.3.6.8D). Such sustained release formulations could maintain effective drug concentrations at cellular and tissue reservoirs of infection. To assess whether enhanced intracellular TFV-DP levels would translate into improved efficacy, MDM were challenged every five days with HIV-1<sub>ADA</sub> to an end point of 30 days following an 8-hour drug loading and assayed quantitatively for HIV-1 RT activity (Fig. 3.6.9CA, B), as well as qualitatively for HIV-1 p24 antigen expression (Fig. 3.6.9C, D). At the 100  $\mu$ M dose, no statistically significant differences in RT activity were detected in media from NM1TFV and NM2TFV-treated cells. At 10  $\mu$ M, significantly lower RT activity was detected in media from NM1TFV and NM2TFV-treated cells compared to TAF and NTAF treatment beginning on day 10 post treatment and continuing out to 30 days. NM1TFV treatment also resulted in significantly lower RT activity compared to NM2TFV at day 30 (Fig. (Fig. 3.6.9B). Both 10 and 100  $\mu$ M NM1TFV suppressed HIV-1 RT activity by >92% and >96% at all time points, respectively (Fig. 3.6.9A, B). While 100 $\mu$ M NM2TFV also suppressed HIV-1 RT activity by >92% at all the time points, treatment with 10  $\mu$ M of NM2TFV provided incomplete viral inhibition of 62.57% at day 30. Similarly, 10  $\mu$ M NTAF

and TAF provided reduced viral inhibition of 81.1% and 84.5% respectively at day 10, with complete viral breakthrough occurring at day 30 (Fig. 3.6.9B, D). In all, these findings demonstrate that NM1TFV improves intracellular delivery of TFV-DP with enhanced drug potency and sustained antiretroviral efficacy.

#### **3.4.4 PK testing**

To assess the PK and drug biodistribution (BD) profiles, male and female Sprague-Dawley rats were injected intramuscularly (IM) with a single dose of 75 mg per kg body weight TFV-equivalents of NM1TFV, NM2TFV or NTAF. Area under the curve (AUC) for whole blood prodrug (6427 ng/mL) in NM1TFV treated animals was found to be statistically greater than whole blood prodrug (2792 ng/mL) in NM2TFV animals (one-way ANOVA,  $p=0.0340$ ) (Fig. 3.6.10A). However, no statistically significant differences in whole blood TFV levels were recorded among animals treated with NM1TFV, NM2TFV, and NTAF except at day 14 (Fig. 3.6.10A). NM1TFV significantly improved tissue drug delivery compared to NM2TFV and NTAF. Specifically, compared to NTAF and NM2TFV, NM1TFV exhibited significantly higher TFV concentration in the spleen, lymph node, liver, gut, kidney, and site of injection 28 and 56 days-post drug administration (Fig. 3.6.10B–F, Fig. 3.6.11B). For NM1TFV at day 56, the TFV levels were 102.4, 26, 12.5, 12.5, 1258.1, and 8883.2 ng per g tissue in the liver, spleen, lymph nodes, gut, kidney, and site of injection, respectively. By comparison, TFV levels 56 days after NTAF treatment were 0.1, 1.8, 1.03, 5.58, and 18.8 ng per g tissue in the liver, lymph nodes, gut, kidney, and site of injection, respectively. Similarly, TFV levels at day 56 after NM2TFV treatment were 4.87, 1.58, 0.1, 20.28, and 193.975 ng per g tissue in the liver, spleen, gut, kidney, and site of injection, respectively. Also, NM1TFV displayed substantially higher prodrug levels compared to other treatments (Fig. 3.6.10B–F, Fig. 3.6.11). For NM1TFV at day 56, the prodrug levels were 65.6, spleen, 27.8, 18.3, 5.3 and 433,475 ng per g tissue in the liver, spleen, lymph nodes, gut, kidney, and site of injection respectively (Fig. 3.6.10B–F, Fig. 3.6.11B). These data suggest NM1TFV undergoes slower in vivo hydrolysis



and/or dissolution from the intramuscular depot compared to NM2TFV and NTAF. At the time of sacrifice, 100% of animals treated with NM1TFV had visible intramuscular drug depots, while only ¼ of animals treated with NM2TFV did, and none animals treated with NTAF (Fig. 3.6.13). At the site of injection, significantly greater levels of prodrug were observed for NM1TFV at day 28 (1253500 ng per g tissue) and 56 (433,475 ng per g tissue) (Fig. 3.6.10F). Based on the initial dose, the total amount of drug at the site of injection after NM1TFV treatment was ~10% at day 28 and declined to 5% at day 56 (Fig. 3.6.14A). For NM2TFV, the muscle drug depot was 0.1% and 0.05% of the initial dose at days 28 and 56, respectively (Fig. 3.6.14A). The molar ratios of prodrug to TFV levels in the muscle demonstrated that a significant proportion of drug after NM1TFV treatment remained in prodrug form when compared against NM2TFV (Fig. 3.6.14B). Additionally, statistical analysis determined that prodrug concentration at the site of injection directly correlated with prodrug and parent drug concentration in most of the tissues, supporting a linear relationship between the magnitude of the prodrug intramuscular depot and tissue drug concentrations (Fig. 3.6.15). In all, the data suggests that NM1TFV is more stable at the site of injection and is released more slowly than NM2TFV from the intramuscular depot. Given the enhanced stability of M1TFV prodrug in the muscle at day 56, NM1TFV offers the potential for sustained drug delivery beyond two months.

#### **3.4.5 TFV-DP measurements**

We next determined the concentration of the active metabolite in key HIV and HBV target cells and tissues. In PBMCs, a single treatment with either NM1TFV, NM2TFV or NTAF demonstrated TFV-DP concentrations above the human EC90 (40 fmol/10<sup>6</sup> cells) during the entire study duration. Specifically, TFV-DP levels for NM1TFV, NM2TFV, and NTAF at 8 weeks were 156.28, 291.75, and 305.33 fmol per 10<sup>6</sup> cells, respectively (Fig. 3.6.12A). Similarly, no significant differences in diphosphate levels were recorded in splenocytes, non-parenchymal liver cells, and in vaginal tissue among the three treatments (Fig. 3.6.12).

However, NM2TFV resulted in significantly higher TFV-DP levels in lymphocytes at D28 (239.319 fmol per  $10^6$  cells), compared to NM1TFV (156.26 fmol per  $10^6$  cells) and NTAF (71.94 fmol per  $10^6$  cells) (Fig. 3.6.12B). Compared to NM2TFV and NTAF, NM1TFV exhibited significantly higher TFV-DP levels in parenchymal liver cells at D56 (328.02 fmol per  $10^6$  cells) and in rectal tissue at all time points (36575.61 fmol per  $10^6$  cells on D28, and 11276.31 fmol per  $10^6$  cells on D56) (Fig. 3.6.12D, F). Importantly, NM1TFV exhibited sustained PBMC and tissue TFV-DP concentrations higher than those associated with effective pre-exposure prophylaxis in humans at the end of the study. Given the high muscle M1TFV levels at 2 months, it is feasible to achieve sustained therapeutic TFV-DP levels beyond 56 days.

#### **3.4.6 Toxicology and evaluation of injection site reactions**

To assess toxicity in SD rats after NM1TFV, NM2TFV, or NTAF treatments, animal weights were recorded weekly, organ to body weight ratios were determined on the days of sacrifice (days 28 and 56); plasma and tissues were collected for CBC, metabolic profiles, and histopathology (Fig. 3.6.16-19). Controls were age-matched untreated rats. Erythema and edema were not observed at the site of injection in any of the treatment groups. No statistically significant differences in body weights were observed between the treatment groups (Fig. 3.6.16B). Transient differences in lung and spleen to body weight ratios were observed between NM1TFV and NTAF groups at day 28. However, no statistically significant differences in organ to body weight ratios were detected on day 56 (Fig. 3.6.16A). No hematological abnormalities were detected by CBC (Fig. 3.6.16C). Comprehensive serum chemistry profiles were quantified with no notable differences between treatment groups (Fig. 3.6.17), suggesting that NM1TFV, NM2TFV, and NTAF did not adversely affect the functions of systemic organs. Hematoxylin and eosin-stained tissue sections, examined by a certified pathologist in a blinded fashion, revealed no abnormal pathology in the kidneys and livers of NM1TFV and NTAF treated animals (Fig. 3.6.18B). Histopathological evaluation of injection

site reactions following NM1TFV and NTAF injections demonstrated limited granulomatous reactions (Fig. 3.6.19, Fig. 3.6.18A). Specifically, one week after NM1TFV administration, a central area containing foamy macrophages, cellular debris and amorphous material were present, typical of necrosis and reaction detected at the injection site [223]. Spindle-shaped fibroblasts and vascular proliferation surrounded the necrotic region, indicating wound healing and granulation tissue formation. Histiocytic infiltration of the intramuscular depot was also observed, including minimal infiltration of the adjacent skeletal muscle. Regions of extracellular amorphous eosinophilic material were also noted. Interspersed within the nuclear debris and foamy histiocytes were small, spherical basophilic granules, mostly extracellular. Given that NM1TFV carries a negative surface charge (Fig. 3.6.5A) and is readily stained by hematoxylin (Fig. 3.6.19A), the observed basophilic granules are likely NM1TFV aggregates. Clusters of these basophilic granules were noted 7 days following the intramuscular injection of the prodrug nanoformulation, suggesting aggregation of NM1TFV particles (Fig. 3.6.19). By day 28, there were small basophilic intracellular granules present in the histiocytes along with large extracellular basophilic staining globules along indicating further extracellular aggregation of NM1TFV (Fig. 3.6.19). This was accompanied by a foreign body granulomatous reaction, including foreign body giant cells (Fig. 3.6.19). When sections were imaged by TEM, the basophilic granules observed by light microscopy appeared as non-cellular electron dense aggregates, further suggesting that this foreign material was the NM1TFV formulation and corresponding to the presence of the drug by chemical analysis (Fig. 3.6.19B, Fig. 3.6.10F). These electron dense aggregates of NM1TFV appeared extracellularly and intracellularly within the histiocytes (Fig. 3.6.19B). At 56 days, the foreign material appeared mostly amorphous, with a foreign body giant cell granulomatous reaction. Extracellular basophilic globules and finer granular intracellular basophilic material were present, indicating sustained phagocytosis of NM1TFV by histiocytes (Fig. 3.6.19A). One rat at 56 days showed a small focus of fibrosis. TEM

observations supported the light microscopic findings, showing extracellular electron-dense aggregates of NM1TFV along with intracellular aggregates within the histiocytes (Fig. 3.6.19A). The injection sites in rats treated with NTAF showed small areas of histiocytic infiltrate at 28 days, mostly in the interstitium (Fig. 3.6.18A). Amorphous foreign material was present, and this persisted in one of the three rats at 56 days, including a foreign body giant cell granulomatous reaction (Fig. 3.6.18A). There was no evidence of muscle degeneration, eosinophilic or basophilic infiltration, cellulitis, or abscesses in any of the treatment groups at any time point.

### **3.4.7 Pharmacodynamic evaluations in HIV-infected humanized mice**

In PrEP regimens, TFV is paired with FTC in the form of Truvada (FTC and TDF), or Descovy (FTC & TAF). Thus, to determine the efficacy of NM2TFV and NM4FTC (22-carbon and alanine modified FTC) against HIV-1 challenge, we employed a CD34+ humanized mouse model for PrEP studies. Specifically, animals were given a single injection of NM2TFV and NM4FTC (75 mg/kg parent drug eq. each) and subsequently challenged with HIV-1<sub>ADA</sub> (IP) 2 weeks after treatment (Fig. 3.6.20). Plasma viral loads 4 and 8 weeks after challenge revealed plasma viral RNA levels below the limit of detection in 3 of 4 animals treated with the combination of NM2TFV+ NM4FTC (Fig. 3.6.21). Furthermore, PBMCs and splenocytes were collected to assay TFV-DP and FTC-TP concentrations at the time of viral challenge. Specifically, TFV-DP concentrations in PBMCs and splenocytes were above the IC<sub>90</sub> at time of viral challenge. While FTC-TP concentration in PBMCs was above the IC<sub>90</sub> at time of challenge, FTC-TP levels in splenocytes were not (Figure 3.6.21).

### **3.4.8 Pharmacodynamic evaluations in HBV-infected humanized mice**

TFV is widely prescribed for the treatment of not only HIV-1 but also for HBV. HBV virus etiology is substantially different than HIV; however daily treatment is required, and current regimens include similar limitations such as short plasma drug elimination half-life, a weak barrier to resistance, and limited drug penetration into viral sanctuaries. To eliminate

HBV infection, complete suppression of progeny virus and elimination of infected cells must be concurrently achieved. These events can be facilitated by enhancing innate and adaptive immune responses alongside antiviral therapy. To these ends, the combination of nitazoxanide (NTZ), a broad-spectrum antiviral and immune stimulating agent, and TFV were transformed into hydrophobic prodrug nanocrystals, then stabilized into aqueous nanosuspensions. TK-NOG and FRG mice with chimeric humanized liver infected with HBV were used to evaluate the efficacy of long-acting formulations. A single intramuscular administration of NM1TFV and NM1NTZ (nanoformulated 18-carbon modified NTZ) (75 mg/kg parent drug equiv. each) suppressed HBV replication and viral load in peripheral blood for up to 4 weeks[224]. In this set of experimental animals, the levels of human albumin remained stable, indicating decrease in viral load was due to treatment, and not loss of human hepatocytes [224]. In similar studies investigating the efficacy of NM1TFV, NM2TFV, and NTAF monotherapy in HBV-infected FRG mice, higher doses of 168 mg/ kg were employed. Single intramuscular doses of NM1TFV and NM2TFV were able to reduce HBV viral load for 4 weeks, while NTAF treatment did not (Fig. 3.6.22). When parenchymal and non-parenchymal liver cells were isolated from NM1TFV, NM2TFV, and NTAF dosed animals and TFV-DP concentration analyzed, we observed low TFV-DP levels in hepatocytes of treatment non-responders (animals D196, D184) (Fig. 3.6.23). Of note, TFV-DP concentrations were generally higher in liver non-parenchymal cells compared to parenchymal cells, with similar findings reported in rats (Fig. 3.6.12D, E).

### 3.5 Discussion

Although LA ARV formulations could potentially have a major impact on HIV treatment and prevention, most oral ARV drugs are not compatible with existing sustained release formulation approaches. Thus, improvements in ARV regimens are needed emergently for use in pre-exposure prophylaxis (PrEP) and maintenance therapy. While current HIV treatment consists of three-drug regimens, and current PrEP consists of a two-

drug regimen; both require once-daily dosing. Change in these paradigms is now possible. This resides in harnessing the potential role of TAF in LA delivery systems. Indeed TAF and TDF prodrugs clearly demonstrate potent activity against HIV and HBV infections and making the agent the most commonly used antiretroviral [34, 35]. The combination of TFV and FTC is effective at preventing HIV-1 transmission when taken daily [30, 56]. Additionally, the current recommended first line antiretroviral regimen for HIV treatment consists of combinations of TAF/TDF and FTC together with an integrase, protease, or non-nucleoside reverse transcriptase inhibitor [31]. Despite its effectiveness the needs for strict regimen adherence, noted toxicities, and restricted tissue penetrance all highlight immediate needs for improved formulation strategies [48-50]. Thus, LASER ART and delivery devices for ARVs are being developed to extend dosing intervals, reduce systemic toxicity, and improve PK profiles [5, 128-131, 148]. Herein, we report on the development of novel TFV ProTides with improved prodrug stability. In this approach, the ionizable phosphate groups in the drug are masked by aromatic and amino acid ester moieties, which upon delivery undergo intracellular enzymatic or chemical hydrolysis to release the free form of the phosphorylated compounds for subsequent activation and competitive inhibition of the viral reverse transcriptase. The lead TFV ProTide candidate (M1TFV) facilitated production of stable aqueous nanocrystals that exhibited enhanced drug and active metabolite delivery into macrophages and CD4<sup>+</sup> T cells. PK and efficacy evaluations showed significant improvements in drug apparent half-life, biodistribution, and antiretroviral activities over TAF. These data, taken together, support the idea that NM1TFV could enable sustained release of TFV-DP to enable dosing intervals for TFV beyond every two months.

TAF is a ProTide of the acyclic nucleoside phosphonate drug tenofovir. The application of ProTide technology to TFV led to the discovery of TAF that is characterized by enhanced potency, improved lymphoid tissue drug delivery, and has also limited the risk for nephrotoxicity and loss of bone mineral density associated with another prodrug of tenofovir,

tenofovir disoproxil fumarate (TDF) [42, 210]. Despite the advantages conferred by TAF, its application in LA systems remains limited by inherent hydrolytic instability of the prodrug. The enhanced potency and chemical composition of TAF further limit the possibility of making direct chemical modifications to the prodrug to improve compound stability without affecting efficacy and safety profiles. Moreover, prior attempts to improve prolonged TAF stability by either using excipients, formulation approaches or pH modulation have yet to demonstrate successful *in vivo* outcomes [128, 198]. To these ends, we explored TFV ProTides bearing safe but bulky hydrophobic lipids not explored by conventional ProTide designs due to their presumed undesired effect on compound dissolution properties in physiological fluids to affect efficacy. Two hydrophobic and lipophilic stable docosyl phenylalanyl and alanyl ester TFV ProTides (M1TFV, M2TFV) were created and nanoformulated by high pressure homogenization as aqueous suspensions of crystalline drugs stabilized by P407 surfactant. Even though solubility and dissolution rates are inherent properties of organic compounds, the actual dissolution rate is dependent on the surface area and degree of saturation. The reduced particle size was expected to enhance prodrug dissolution to produce rapid absorption and therapeutic onset upon administration. Since solubilized form of TAF is pH and water sensitive, saturated aqueous solid drug nanoparticles were prepared at a pH of 5.5 to maintain prodrug stability within the formulation. The recorded uniform particle sizes, narrow polydispersity indices and negative zeta potentials for NM1TFV and NM2TFV formulations are suggestive of nanoparticle stability and homogeneity. Importantly, the high drug loading capacity for the TFV ProTide nanocrystals could facilitate reduced injection volumes.

After producing and characterizing the stable TFV ProTide formulations, we then evaluated their abilities to enter and slowly release the drug within HIV-1 target cells. Nanocrystal delivery to phagocytic and highly mobile macrophages facilitates drug transfer to CD4<sup>+</sup> T cells and other restricted tissue reservoirs of infection [33]. We have previously

demonstrated that once inside macrophages, drug nanocrystals are stored in the late- and recycling-endosomes [159]. This intracellular particle storage protects drugs from systemic metabolism and prolongs half-life, ultimately leading to improved PK and drug biodistribution (BD) profiles [33, 164]. Also, transformation of ProTides into active nucleotide metabolites to competitively inhibit the activity of HIV reverse transcriptase is mediated by intracellular kinases, underscoring the importance of cellular NRTI delivery. Compared to NTAF and NM2TFV, treatment of human MDM with NM1TFV resulted in enhanced cellular uptake and intracytoplasmic retention of the prodrug and TFV-DP over 30 days. The observed intracellular TFV-DP levels for NTAF and NM2TFV were expected given their rapid hydrolysis rates when compared against NM1TFV. Prior studies have also shown that TFV-DP exhibits an intracellular half-life of 60-100 hours [5] and likely to be extended when delivered in form of solid drug nanoparticles that readily undergo dissolution prior to prodrug release, hydrolysis and activation. Consequently, NM1TFV exhibited sustained antiretroviral activity as determined by HIV-1 p24 antigen expression and RT activity. Together, these characterization data sets demonstrate that NM1TFV improves prodrug stability, cell uptake, retention and efficacy.

Optimal approaches for effective treatment and prevention of HIV-1 infection should deliver and sustain therapeutic drug concentrations at cellular and tissue sites of infection [225]. We therefore investigated the abilities of NTAF, NM1TFV and NM2TFV to improve drug PK and biodistribution. Pharmacokinetic tests in SD rats demonstrated TFV-DP levels in PBMCs at or above 100 fmol/ million cells for 56 days for all treatments. Notably, NM1TFV exhibited sustained intramuscular and enhanced lymphatic tissue drug levels compared to NM2TFV and NTAF. Toxicological assessments (CBC, comprehensive serum chemistry profiles, organ to body weight ratios, kidney and liver histopathology) demonstrated that neither NM1TFV, NM2TFV nor NTAF induced systemic or organ adverse effects. Following intramuscular administration of nanoformulations, the injection site serves as a primary depot



from where the drug is slowly absorbed and eventually released into circulation. Though, the precise mechanisms of distribution of the intramuscular drug nanosuspensions represents a current knowledge gap, prior studies have shown that absorption of solid drug nanocrystals following IM administration is dependent on the rate of particle size and dissolution, host protein adsorption on the particle surface, and type of primary depot formed (particle agglomerates or dispersion)[226]. In these prior studies, the local inflammatory response was found to affect nanoparticle phagocytosis efficiency, prodrug stability, and uptake of lipophilic compounds by the lymphatic system[135, 226-229]. For TFV prodrugs, minimizing extracellular prodrug hydrolysis at the site of injection would limit accumulation of polar and ionic TFV or ProTide degradation products in the muscle. Compared to TAF prodrug, earlier studies have demonstrated direct links between extracellular TFV and delayed wound healing, marked alterations in epidermal cell proteomics and ulcerations[230, 231], underscoring the importance of prodrug stability in extracellular compartments. Of particular note, NM1TFV demonstrated sustained prodrug stability at the site of injection.

Intramuscular injection of NM1TFV nanocrystals induced subclinical granulomatous foreign body reactions. The observed granuloma formation and subsequent intracellular sequestration of NM1TFV by infiltrating histiocytes and giant cells facilitates drug uptake and accumulation within reticuloendothelial and lymphoid tissues to create secondary drug depots. Inflammatory granulomatous tissue reactions have previously been observed for similar FDA approved long-acting injectable aqueous drug nanosuspensions[135, 226-229] where macrophage infiltration and subsequent phagocytosis of nanocrystals is known to modulate biphasic flip-flop pharmacokinetics by promoting both prodrug dissolution and activation[226, 228]. Similarly, injection site analysis by TEM demonstrated that the reticuloendothelial system and immune cell infiltration play important roles in lipophilic drug nanocrystal distribution into tissues[139]. Therefore, in addition to inherent physicochemical properties of the active pharmaceutical ingredient and nanoparticle, local tissue responses

likely play a considerable role in the enhanced drug biodistribution to the reticuloendothelial system and the sustained release profile of NM1TFV. Importantly, intramuscularly delivered NM1TFV did not exhibit severe injection site reactions such as allergic reactions, cellulitis, abscesses, or chronic necrosis, the latter of which has been associated with subcutaneous TAF implants[133]. In addition to improved PK and safety profiles, NM1TFV and NM2TFV demonstrated antiviral efficacy in HBV infected humanized mice proof-of-concept PD studies [224]. These results are a first step towards producing a long-acting TFV for human use by affecting cell and tissue drug penetration, and antiretroviral activity, and drug apparent half-life.

Long-acting NM1TFV potentially extends antiretroviral drug administration from daily to beyond bimonthly. The TFV ProTides reported in this work confer therapeutic and safety benefits over conventional ProTides or other previously published long-acting TFV formulations. For instance, a previous report demonstrated that TFV-DP levels in PBMCs of humanized mice declined below 100 fmol/million cells less than a week after subcutaneous administration of 200 mg/ kg TAF loaded nanoparticles [212]. In contrast, our novel ProTide formulations sustained TFV-DP levels above this level in PBMCs for out to 2 months using a dose 2.7 times lower than reported by the previous study [212]. Therefore, the formulations reported herein may facilitate reduction of injection volumes without compromising therapeutic efficacy. Another technology being explored for sustained release of TFV are implants [128-131]. Implantable devices containing TAF are of increased interest due to the drug's potency and long half-life of the active metabolite [197, 198]. However, a recent report on subcutaneous TAF implants inserted in rabbits and rhesus macaques demonstrated substantial histological changes in tissues surrounding the implant site [133]. Significant tissue necrosis was noted after 5 weeks and worsened by 12 weeks in animals implanted with the TAF devices [133]. Though a necrotic focus was observed one week after prodrug formulation injection, in contrast to what had been reported for TAF implants, no adverse

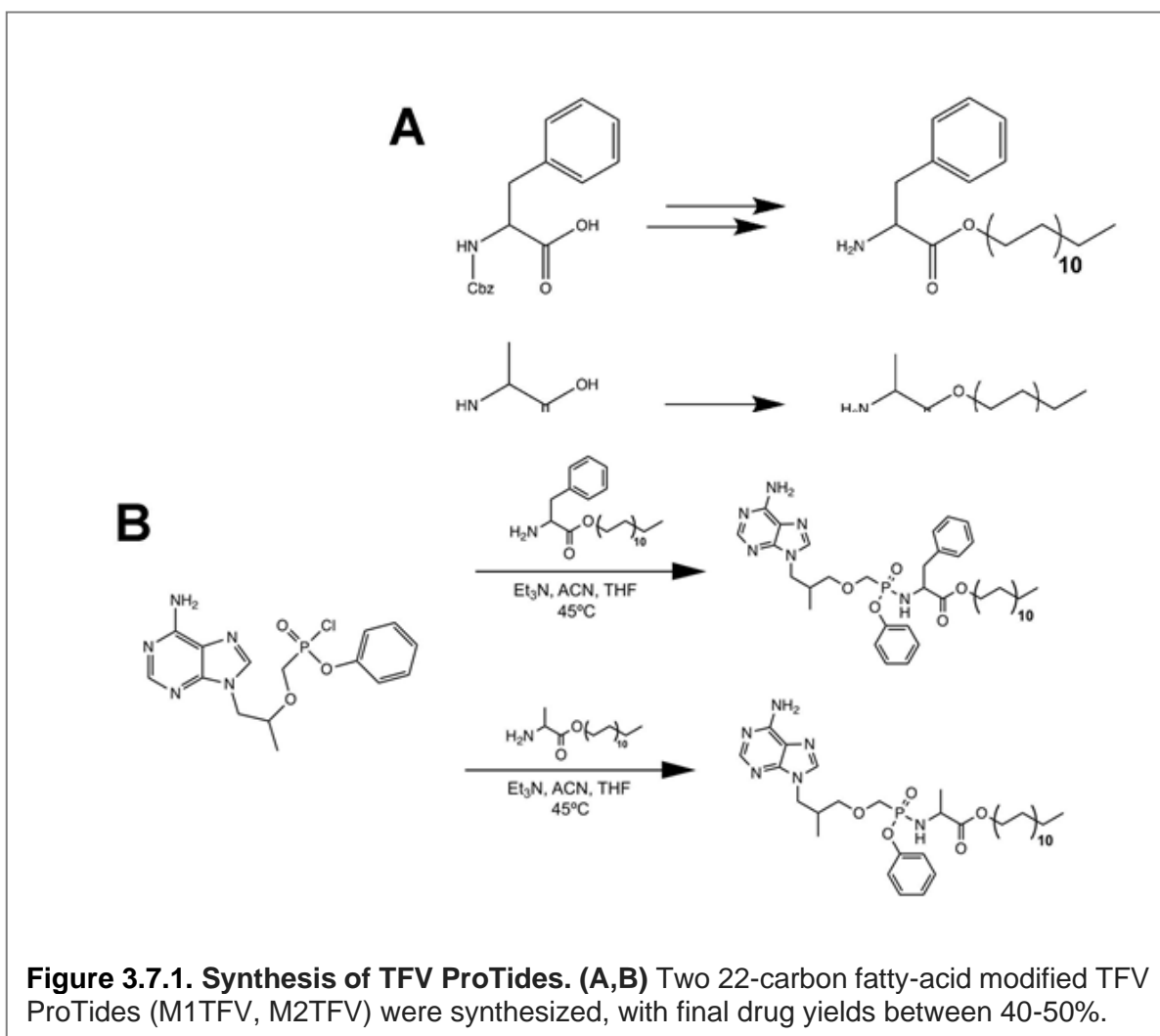
histological changes were observed at the site of injection for time periods up to 2 months. This observation is linked, in part, to the sustained prodrug and formulation stability within the muscle. With injectables, one potential drawback includes the inability to remove in the case of adverse events. Utilizing an oral lead in to preemptively identify adverse drug reactions can minimize the risk of such events. Additionally, in the case of NM1TFV, the predominantly drug depot at the site of injection could offer the possibility of surgical removal in emergent cases. Thus, NM1TFV could potentially overcome major obstacles associated with transformation of TFV into long-acting products.

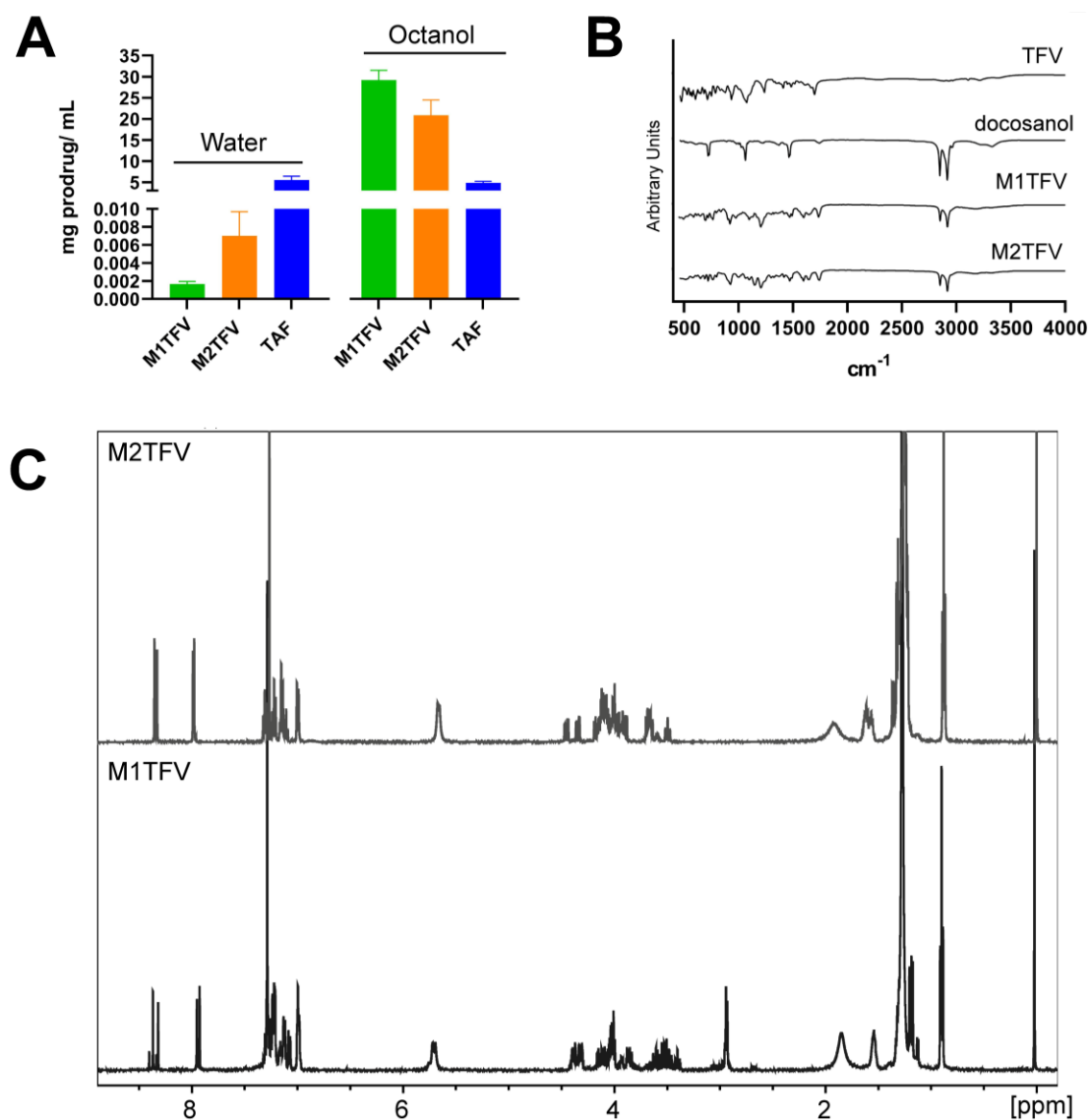
### **3.6 Conclusion**

In the present study, NM1TFV significantly improved drug and TFV-DP BD compared to NM2TFV and NTAF. These results underscore the importance of extended PK evaluations beyond two months to further elucidate the potential future dosing intervals in humans. To this end, future studies will focus on extended-period PK studies of NM1TFV in rats and rhesus macaques. Given recent reports from HPTN 083 and HPTN 084 studies demonstrating that long-acting injectable cabotegravir administered every two months is more effective than daily pills in preventing HIV acquisition [200], it is clear that long-acting formulations may represent an important tool in controlling the HIV epidemic. Given the important role of TFV prodrugs in combination therapies, the lead candidate NM1TFV could potentially have a major impact on HIV treatment and prevention. TFV also inhibits major co-infections, such as HBV [232]. In vivo proof of concept studies to assess the efficacy of NM1TFV have demonstrated the ability of the formulation to suppress HBV replication in humanized mice over 4 weeks following a single intramuscular dose [224]. Future studies will examine the use of NM1TFV for both monotherapy in HBV, and for the treatment of HIV-HBV coinfections. Overall, NM1TFV provides an attractive candidate for beyond every two months dosing of TFV to improve treatment outcomes. There is clearly a need for LA TFV. This is especially noteworthy for PrEP. Recent findings from the HIV Prevention Trials

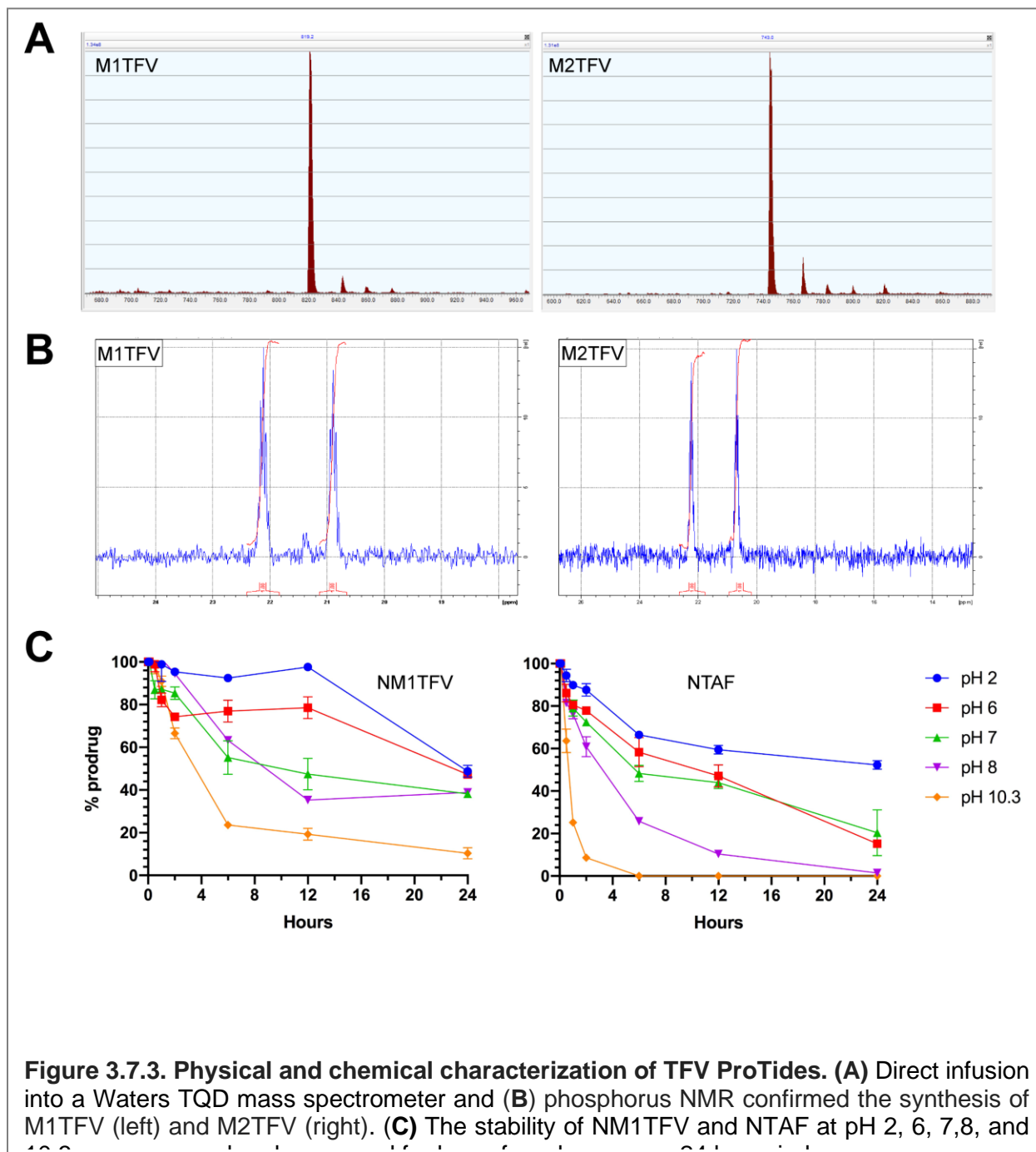
Network (HPTN) 083 study recorded fewer HIV infections in healthy participants using bimonthly CAB LA injectable compared to the group that received daily oral Truvada (TDF/FTC) [200]. Nonetheless, reports by the Centers for Disease Control and Prevention have shown that consistent use of Truvada reduces the risk of getting HIV from sex by 99%, underscoring the need for strict compliance to therapy and the potential future important role of long-acting formulations for PrEP. Thus, bypassing oral dosing could potentially protect drugs from gastrointestinal degradation at acidic pH and improve drug absorption and make these created LA formulations of significant impact in preventing HIV-1 transmission.

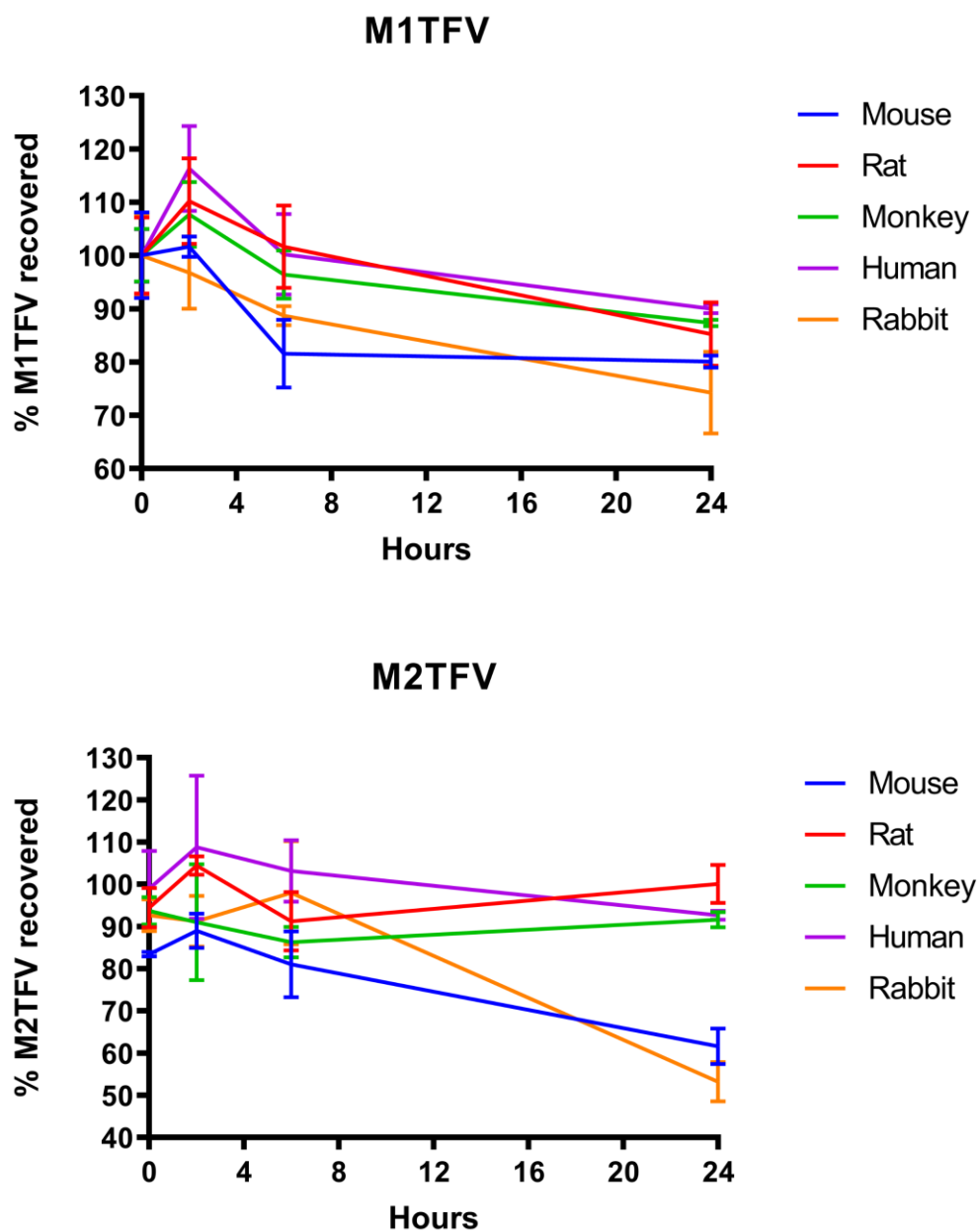
### 3.7 Figures



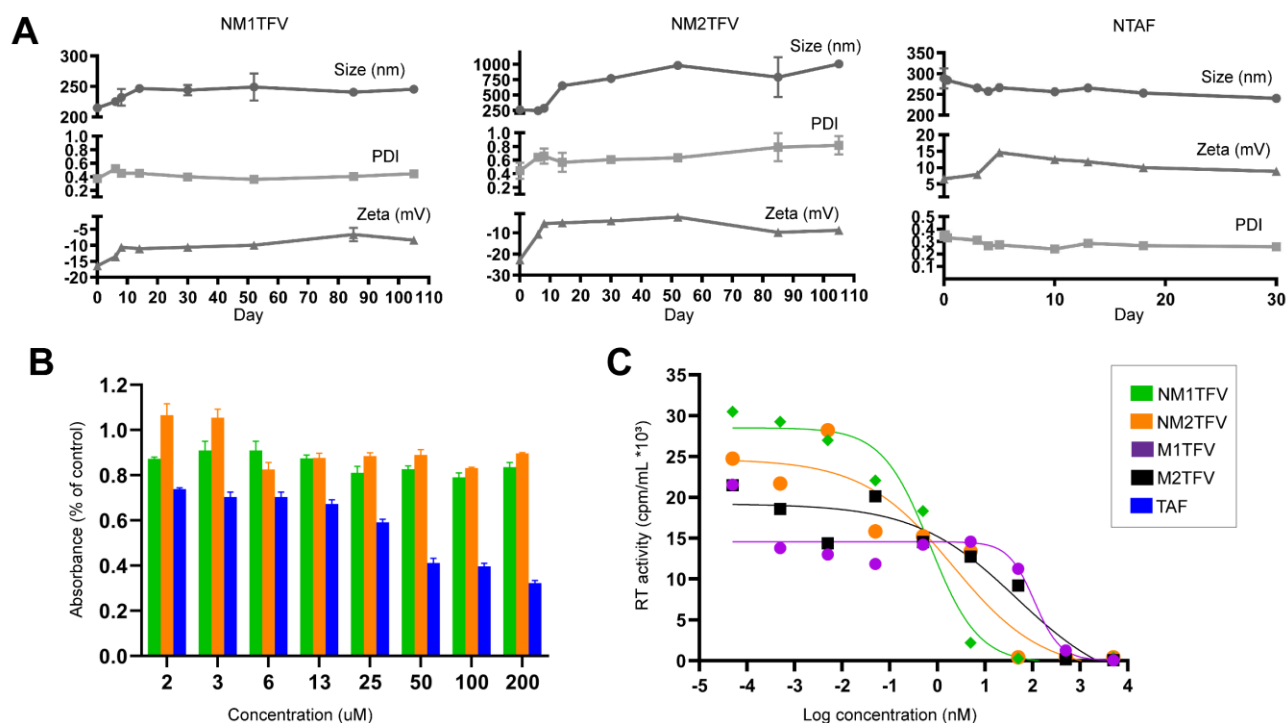


**Figure 3.7.2. Characterization of TFF ProTides.** (A) Aqueous and octanol solubility of M1TFV and M2TFV demonstrate the decreased aqueous solubility of M1TFV and M2TFV, and increased octanol solubility. (B) FT-IR Absorption bands at 2844  $\text{cm}^{-1}$  and 2912  $\text{cm}^{-1}$  illustrate the asymmetric and symmetric C-H stretches from the long chain fatty acid. (C) Proton NMR spectra confirmed the synthesis of M1TFV (below) and M2TFV (above). Specifically, the triplet peak at 0.87 ppm and multiplets at 1.21-1.35 ppm correspond to the terminal methyl and methylene protons of the docosyl ester on M1TFV, respectively. Chemical shifts at 7.04-7.38 ppm represent the aryl and phenylalanine masking promoieties. In the case of M2TFV, the triplet at 0.87 ppm and multiplets at 1.20-1.38 ppm correspond to the terminal methyl and methylene protons of the docosyl ester, respectively. Chemical shifts at 7.10, 7.15 and 7.31 ppm represent the aryl and alanine masking promoieties.



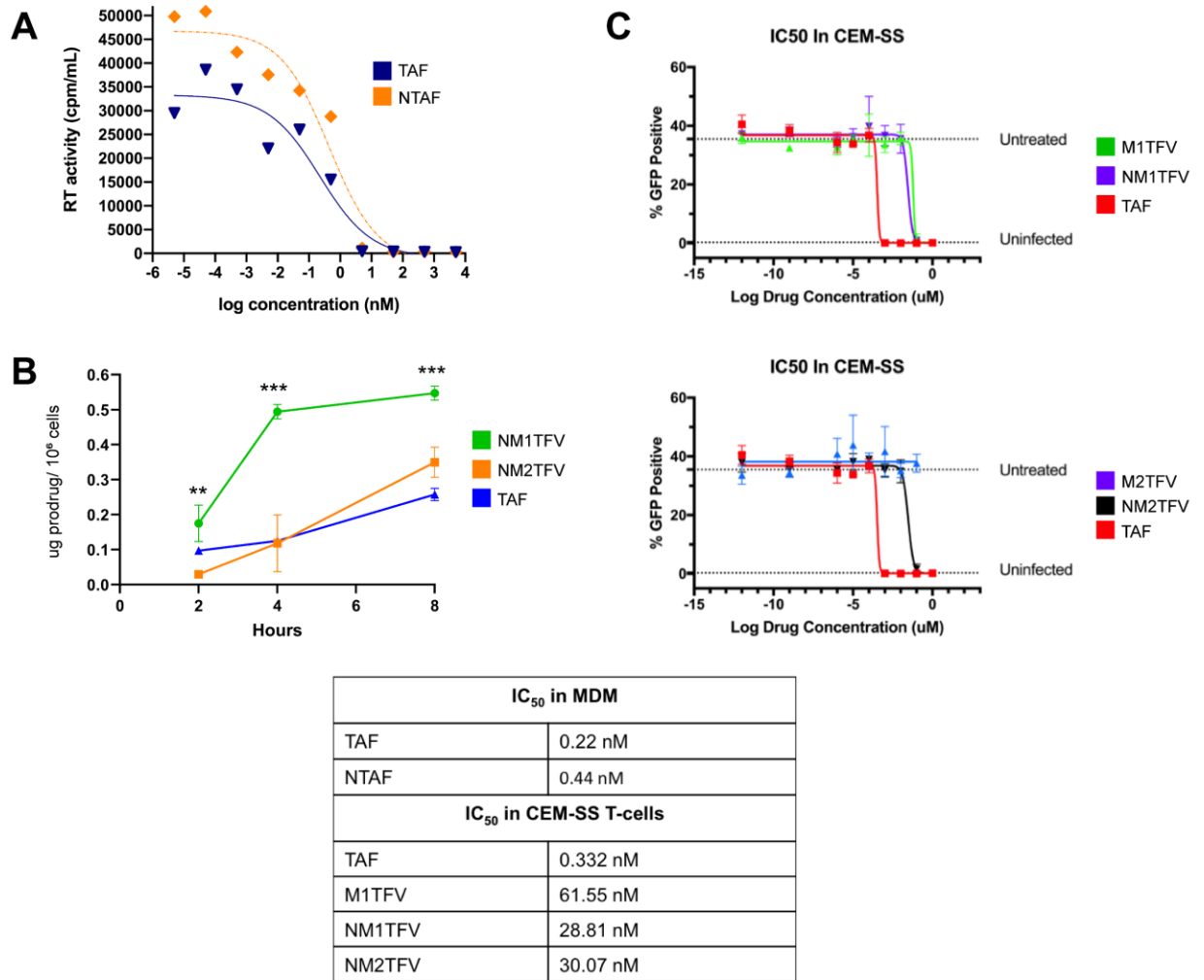


**Figure 3.7.4. Stability of ProTides in serum.** 10  $\mu$ M M1TFV or M2TFV was incubated in mouse, rat, monkey, human, and rabbit plasma, then assayed for loss of prodrug over a 24 hr period via UPLC-UV/Vis.

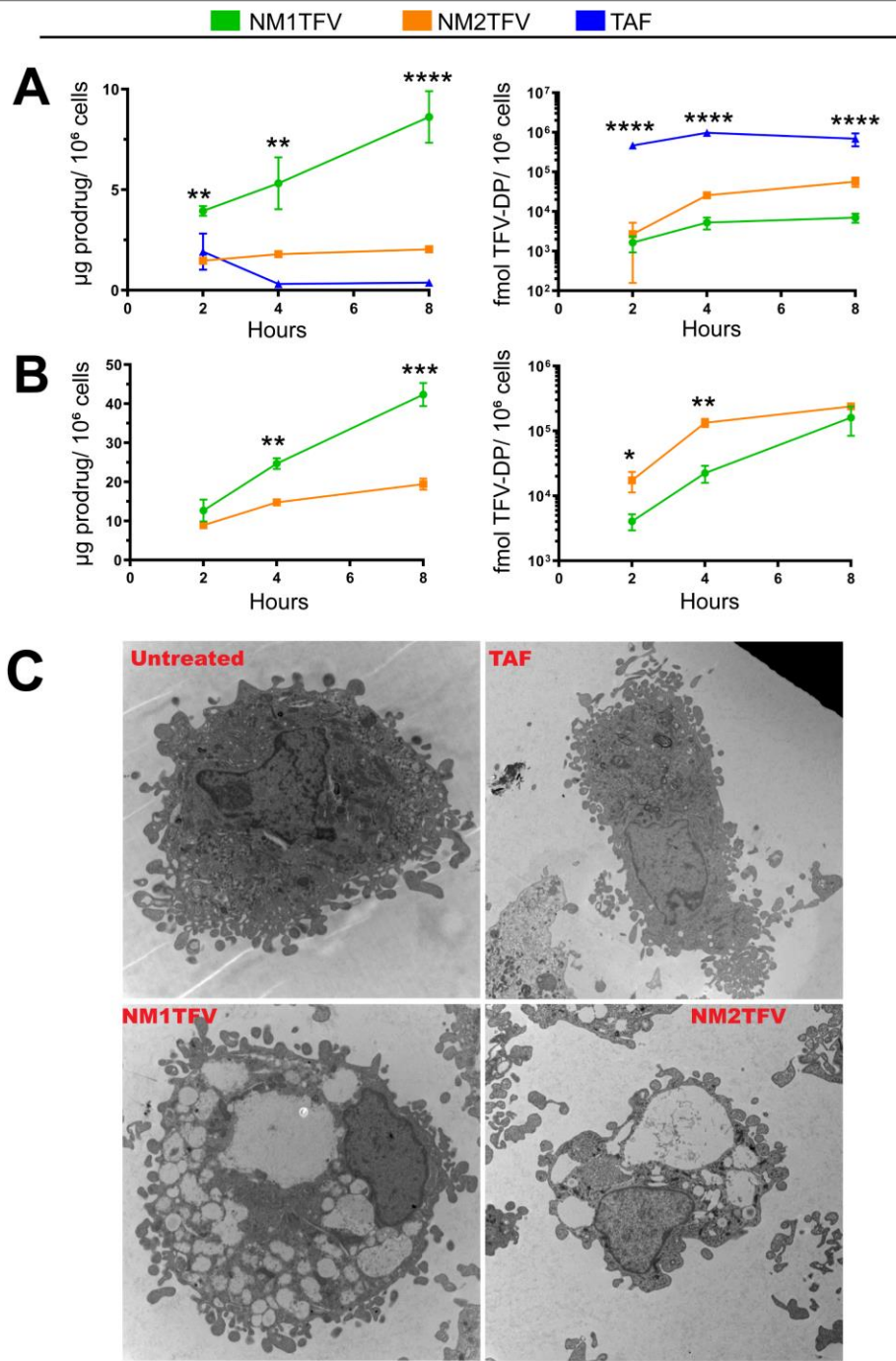


**Figure 3.7.5. Nanoformulation of TFV ProTides.** Nanoformulations were synthesized by high-pressure homogenization using poloxamer 407 (P407) as the excipient for NM1TFV/ NM2TFV, or P407 and PEG 3350 as excipients for NTAF. **A–C** Formulation stability at 25 °C (up to 110 days) was measured by particle hydrodynamic diameter (size), polydispersity index (PDI), and zeta potential as determined by dynamic light scattering (DLS). **F** Cell viability was assessed in MDM by MTT assay 24 h after NM1TFV, NM2TFV, or TAF treatment over a range of concentrations (1–200  $\mu$ M). Results were normalized to untreated control cells. All results are shown as the mean  $\pm$  SEM of at least three replicates. **(D)** IC<sub>50</sub> of M1TFV, M2TFV, and their nanoformulations in MDM was investigated at a range of concentrations (0.0001–1000 nM) and determined by HIV-1 reverse transcriptase (RT) activity after viral challenge with HIV-1<sub>ADA</sub> at an MOI of 0.1. Data was normalized and expressed as percentage of HIV-1 control  $\pm$  SEM; N = 4.

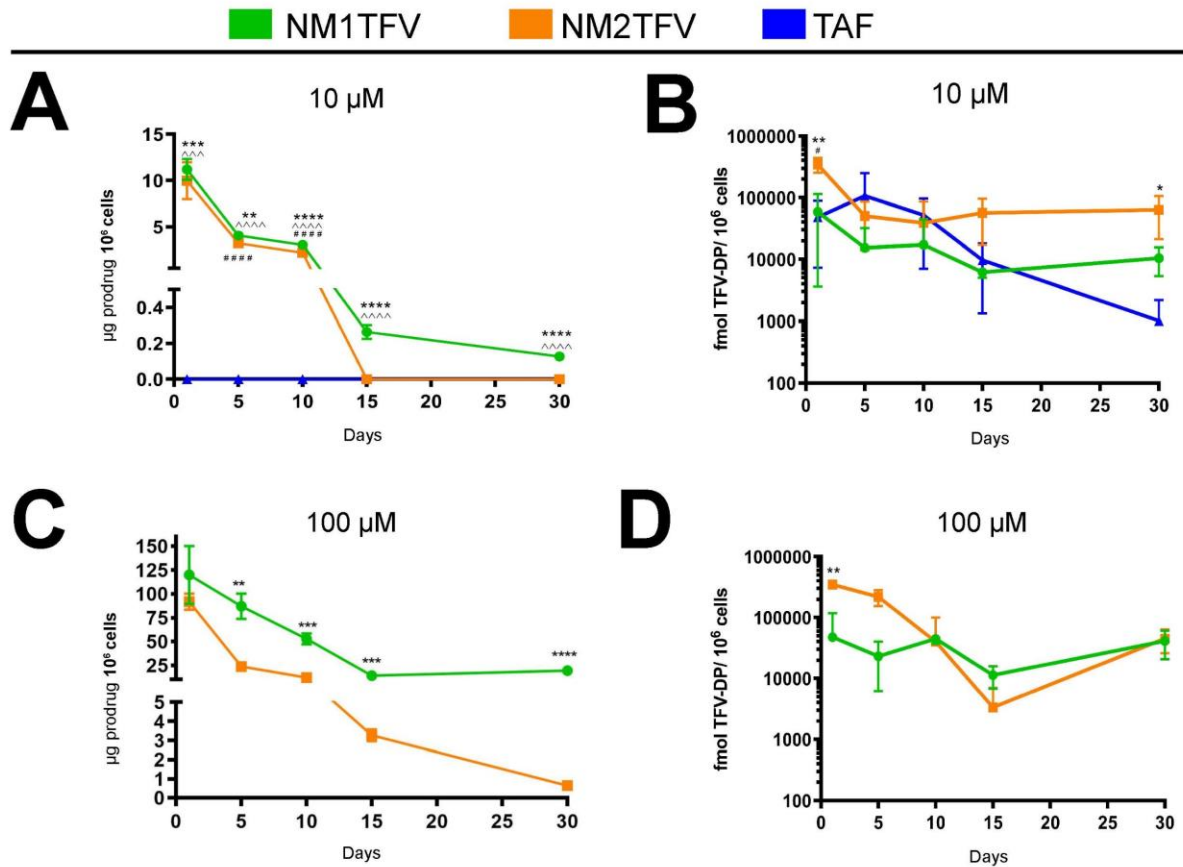




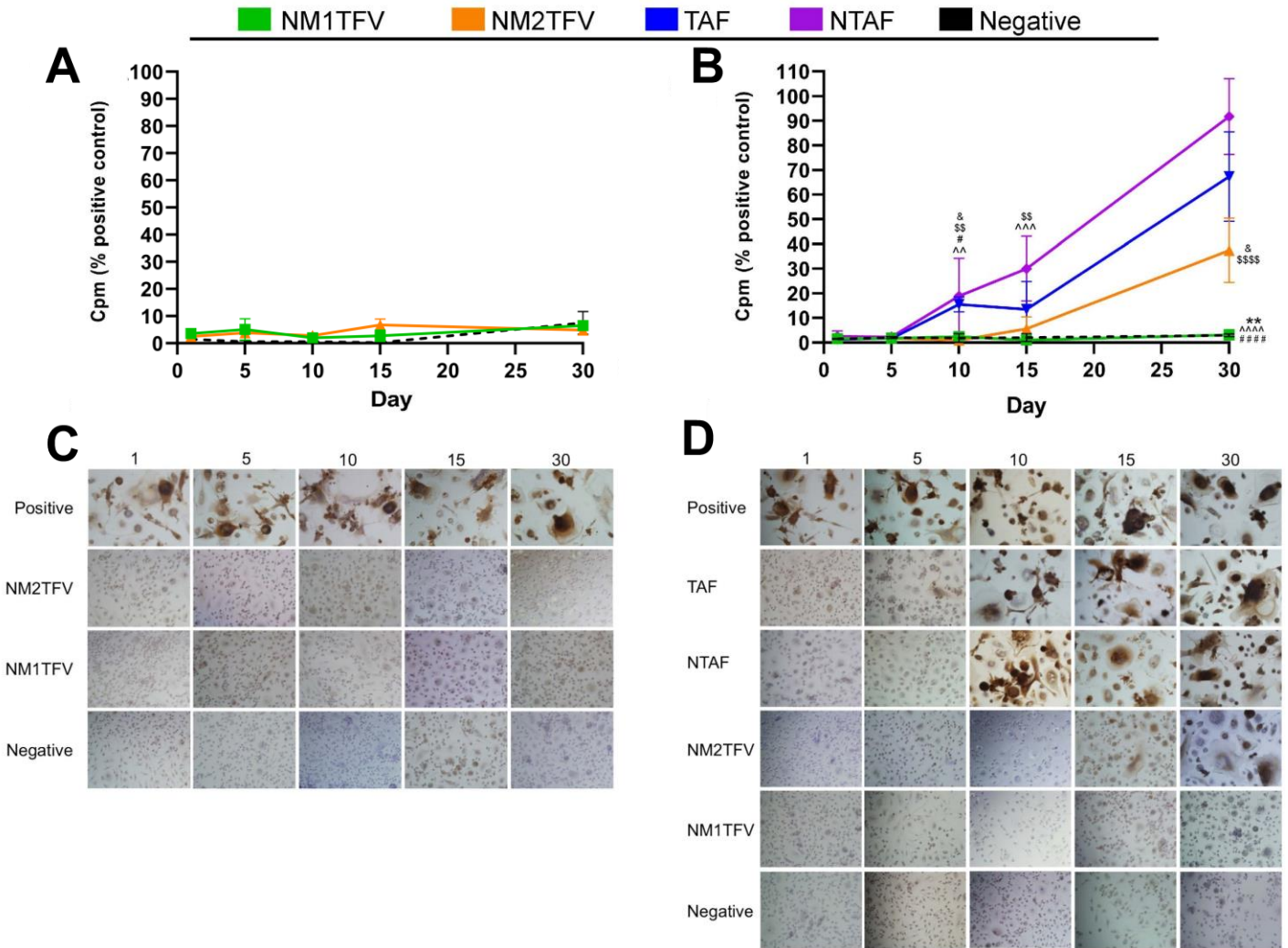
**Figure 3.6.7. In vitro characterizations.** (A) IC<sub>50</sub> of, TAF and NTAF in MDM and (B) Uptake of NM1TFV, NM2TFV, and TAF was determined in CEM-SS T-cells. (C) IC<sub>50</sub> of M1TFV, M2TFV, NM1TFV, NM2TFV, and TAF were investigated in CEM-SS T-cells at a range of concentrations (0.0001–1000 nM) and determined by HIV-1 reverse transcriptase (RT) activity after viral challenge with HIV-1<sub>ADA</sub> at an MOI of 0.1. Data was normalized and expressed as percentage of HIV-1 control  $\pm$  SEM; N = 4.



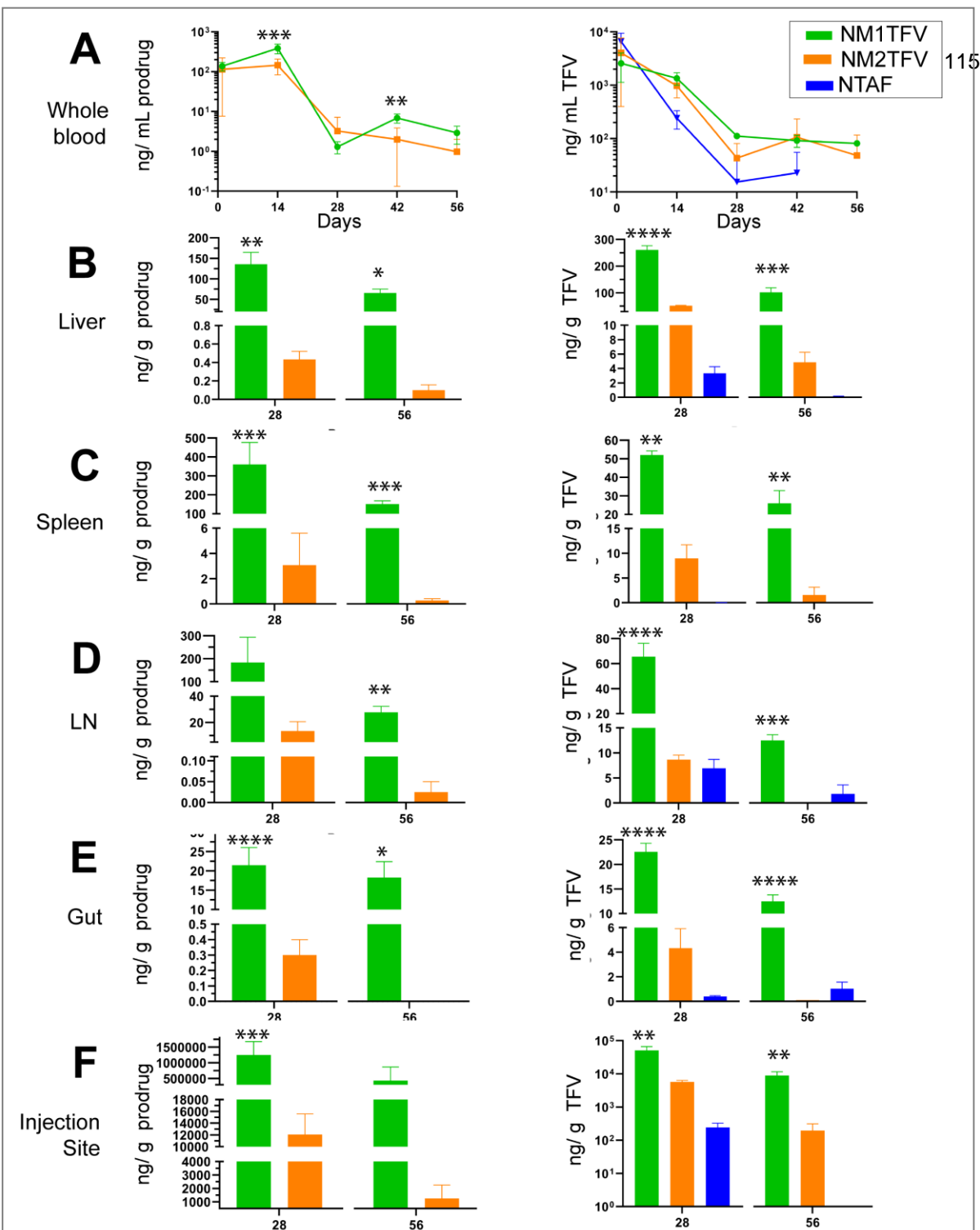
**Figure 3.7.6. Intracellular drug content.** Drug uptake in MDM was measured over a 24-h period at 10 μM and 100 μM drug concentrations. **A,C** Prodrug uptake of NM1TFV significantly greater than NM2TFV and NTAf. **B,D** TAF treatment resulted in the most rapid prodrug conversion to TFV-DP, followed by NM2TFV, and NM1TFV. **E** Transmission electron microscopy (TEM) of control, TAF, NM1TFV, and NM2TFV loaded MDM after 8-h drug incubation with 10 μM drug. For comparison of two groups (**c,d**), Student's t-test (two-tailed, unpaired) was used (\* $P \leq 0.05$ , \*\* $P < 0.01$ , \*\*\* $P < 0.001$ , \*\*\*\* $P < 0.0001$  NM1TFV compared with NM2TFV). A one-way analysis of variance (ANOVA) followed by Tukey's post hoc test was used to compare the prodrug and TFV-DP (**a,b**) levels among three treatment groups (\* $P \leq 0.05$ , \*\* $P < 0.01$ , \*\*\* $P < 0.001$ , \*\*\*\* $P < 0.0001$  NM1TFV compared with NM2TFV), (^ $P \leq 0.05$ , ^^ $P < 0.01$ , ^^ $P < 0.001$ , ^^ $P < 0.0001$  NM1TFV compared with NTAf).



**Figure 3.6.8. Intracellular retention of drug.** For all assays (A-D), data are expressed as mean  $\pm$  SEM,  $N=3$  biological replicates. Cellular retention of the (A,C) prodrug and (B,D) TFV-DP in MDM was assessed. For comparison of two groups (c,d), Student's t-test (two-tailed, unpaired) was used ( $*P \leq 0.05$ ,  $**P < 0.01$ ,  $***P < 0.001$ ,  $****P < 0.0001$  NM1TFV compared with NM2TFV). A one-way analysis of variance (ANOVA) followed by Tukey's post hoc test was used to compare the prodrug and TFV-DP (A,B) levels among three treatment groups ( $*P \leq 0.05$ ,  $**P < 0.01$ ,  $***P < 0.001$ ,  $****P < 0.0001$  NM1TFV compared with NM2TFV), ( $^{\wedge}P \leq 0.05$ ,  $^{\wedge\wedge}P < 0.01$ ,  $^{\wedge\wedge\wedge}P < 0.001$ ,  $^{\wedge\wedge\wedge\wedge}P < 0.0001$  NM1TFV compared with NTAF), ( $^{\#}P \leq 0.05$ ,  $^{\#\#}P < 0.01$ ,  $^{\#\#\#}P < 0.001$ ,  $^{\#\#\#\#}P < 0.0001$  NM2TFV compared with NTAF).

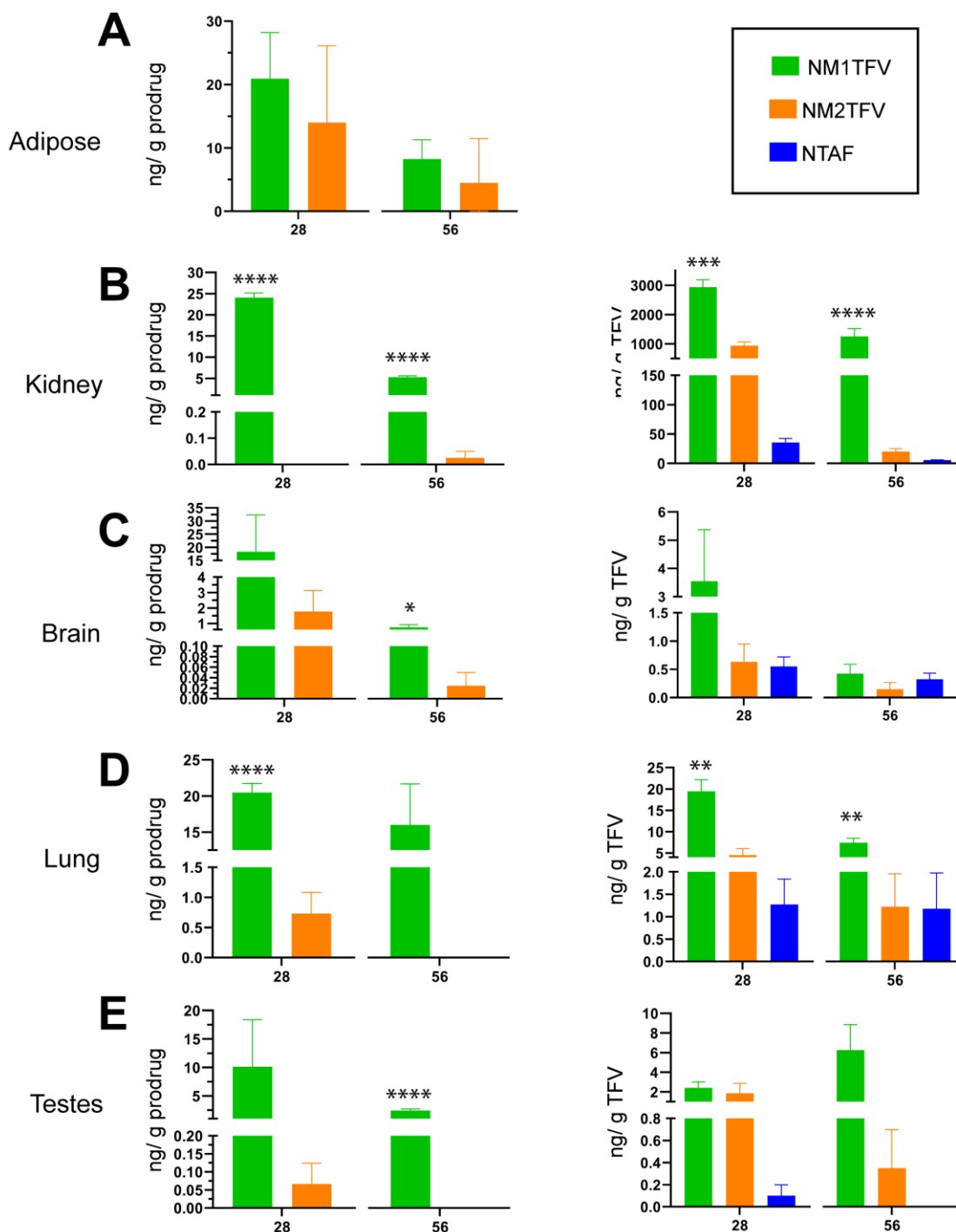


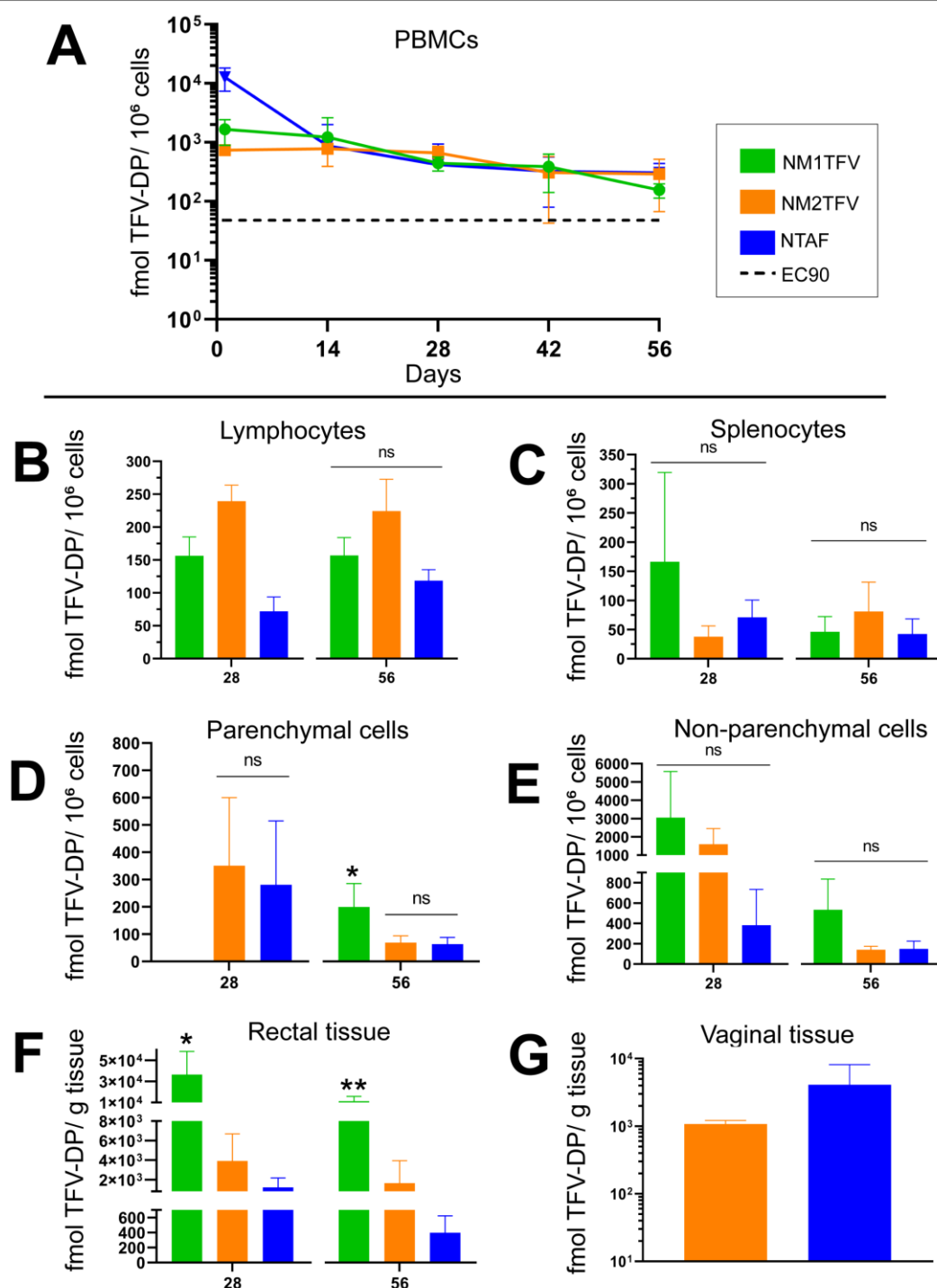
**Figure 3.7.9. Antiretroviral activity.** A-D, Infection was determined by measuring the HIV-1 RT activity in culture medium and HIV-1 p24 antigen immunocytochemistry following a single 10μM (A,C) and 100μM (B,D) dose. The antiretroviral activities of NM1TFV and NM2TFV were determined by measures of HIV-1 RT activity in culture supernatants (A,B) and by cell-associated HIV-1p24 antigens by immunocytochemistry (C,D). HIV-1 RT activity is expressed as mean ± SEM,  $N=4$  biological replicates. Each experiment was repeated independently three times with equivalent results. Student's t-test (two-tailed, unpaired) was used ( $*P \leq 0.05$ ,  $**P < 0.01$ ,  $***P < 0.001$ ,  $****P < 0.0001$  NM1TFV compared with NM2TFV). A one-way analysis of variance (ANOVA) followed by Tukey's post hoc test was used to compare antiretroviral activity between three or more groups. ( $*P \leq 0.05$ ,  $**P < 0.01$ ,  $***P < 0.001$ ,  $****P < 0.0001$  NM1TFV compared with NM2TFV), ( $^{\wedge}P \leq 0.05$ ,  $^{\wedge\wedge}P < 0.01$ ,  $^{\wedge\wedge\wedge}P < 0.001$ ,  $^{\wedge\wedge\wedge\wedge}P < 0.0001$  NM1TFV compared with NTAF), ( $^{\#}P \leq 0.05$ ,  $^{\#\#}P < 0.01$ ,  $^{\#\#\#}P < 0.001$ ,  $^{\#\#\#\#}P < 0.0001$  NM1TFV compared with TAF), ( $^{\&}P \leq 0.05$ ,  $^{\&\&}P < 0.01$ ,  $^{\&\&\&}P < 0.001$ ,  $^{\&\&\&\&}P < 0.0001$  NM2TFV compared with NM2TFV), ( $^{\$}P \leq 0.05$ ,  $^{\$\$}P < 0.01$ ,  $^{\$$$}P < 0.001$ ,  $^{\$$$$}P < 0.0001$  NM2TFV compared with NTAF).



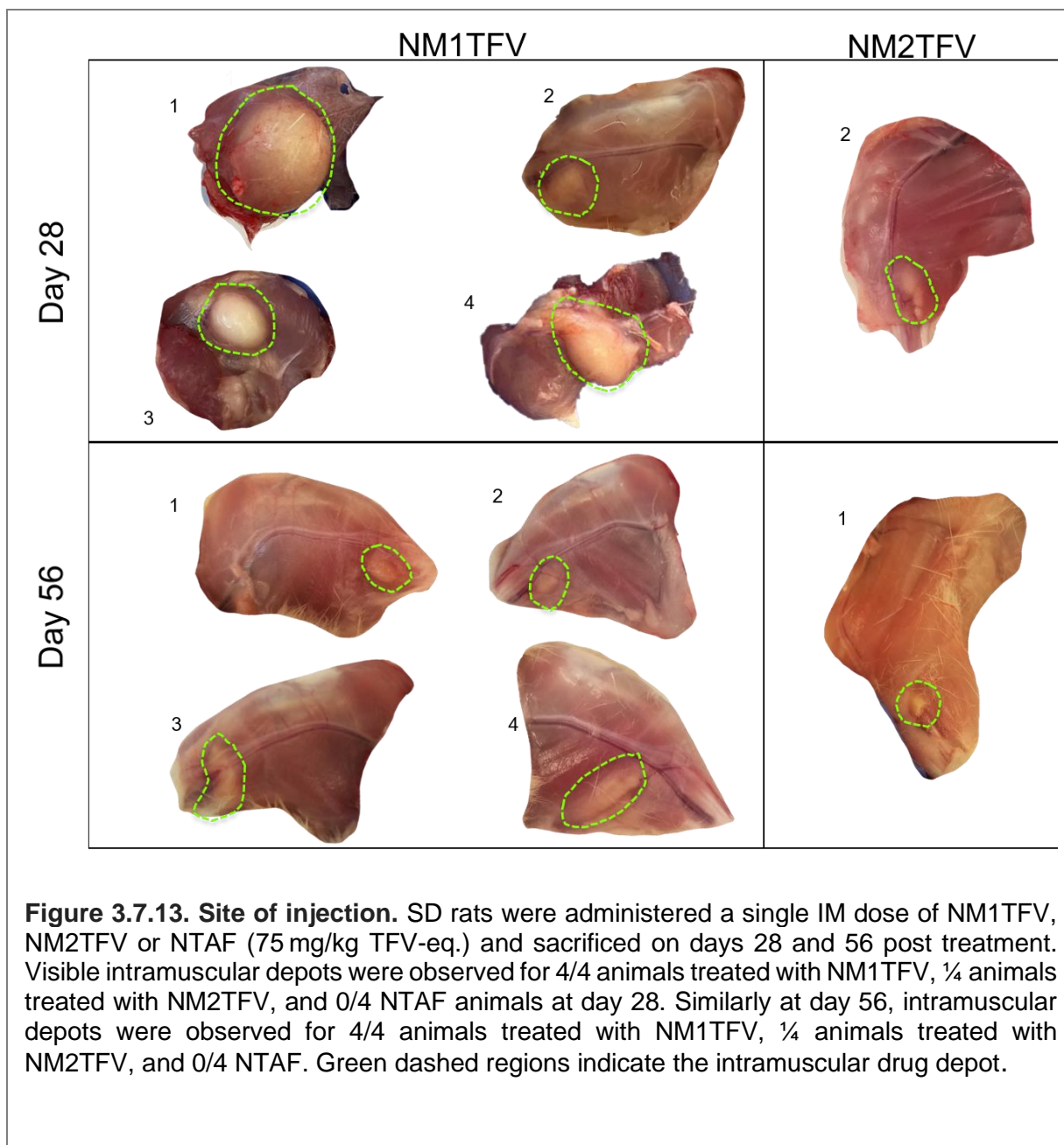
**Figure 3.7.10. Pharmacokinetics.** SD rats were administered a single IM dose of NM1TFV, NM2TFV or NTAF (75 mg/kg TFV-eq.) to determine pharmacokinetic (PK) profiles. (A) Prodrug and TFV concentrations in blood were determined at days 1 and 14 then every two weeks for 8 weeks. Tissue biodistribution of M1TFV/ M2TFV and TFV was assessed at 28 and 56 days after injection in the (B) liver, (C) spleen, (D) lymph node, (E) gut and (F) site of injection. Data is expressed as mean  $\pm$  SEM where  $N=4$  biological replicates. Prodrug concentrations were compared using Student's  $t$ -test (\*\*\*\* $P<.0001$ , \*\*\* $P<.001$ , \*\* $P<.01$ , \* $P<.05$  NM1TFV compared with NM2TFV). To compare TFV levels between three or more groups, ANOVA followed by Tukey's post hoc test was used (\*\*\*\* $P<.0001$ , \*\*\* $P<.001$ , \*\* $P<.01$ , \* $P<.05$  NM1TFV compared with NM2TFV), ( $^{\wedge}P\leq 0.05$ ,  $^{\wedge\wedge}P<0.01$ ,  $^{\wedge\wedge\wedge}P<0.001$ ,  $^{\wedge\wedge\wedge\wedge}P<0.0001$  NM1TFV compared with NTAF), ( $^{\#}P\leq 0.05$ ,  $^{\#\#}P<0.01$ ,  $^{\#\#\#}P<0.001$ ,  $^{\#\#\#\#}P<0.0001$  NM2TFV compared with NTAF).



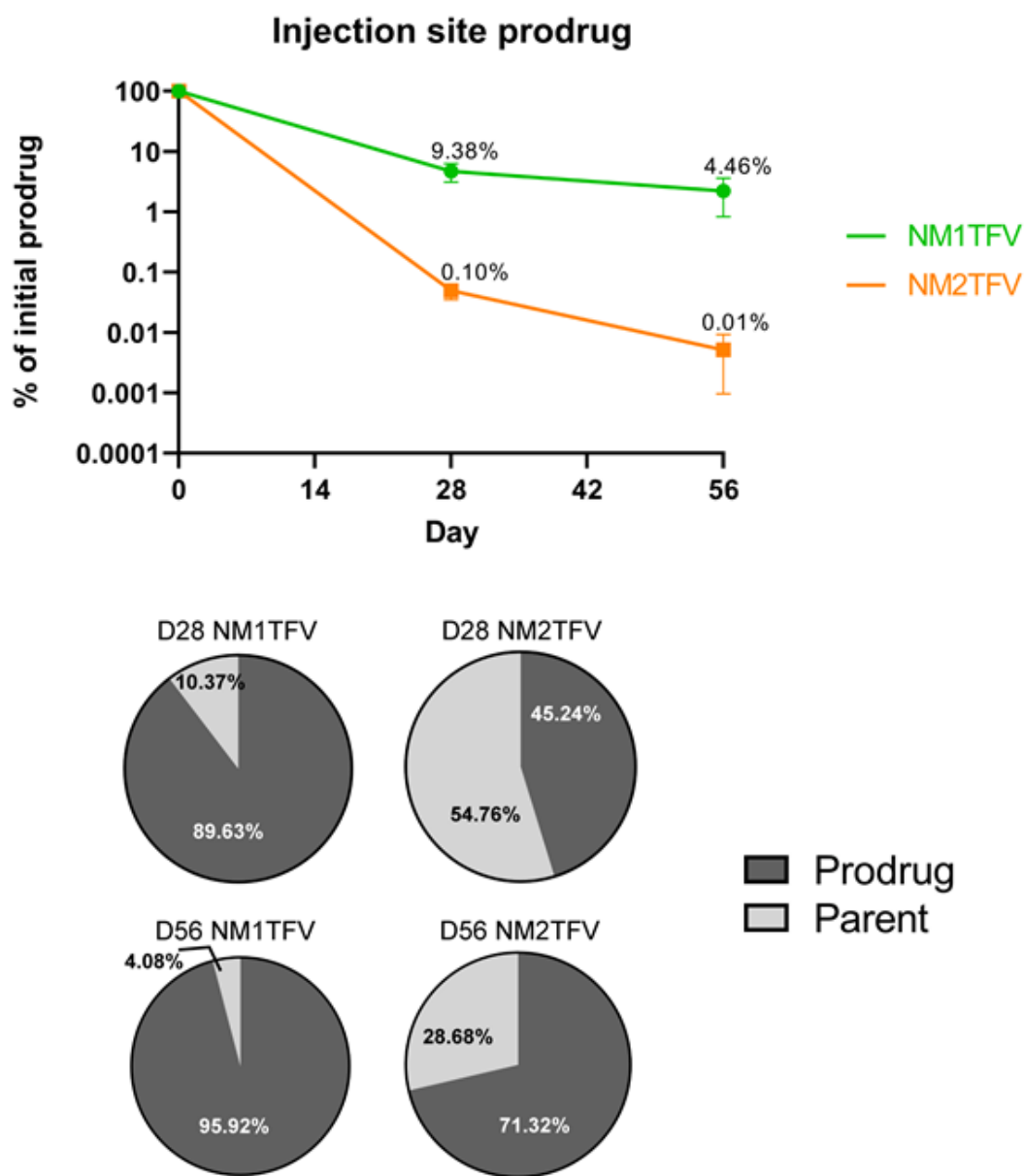




**Figure 3.7.12. *In vivo* TFV-DP levels.** SD rats were administered a single IM dose of NM1TFV, NM2TFV or NTAF (75 mg/kg TFV-eq.) to determine pharmacokinetic (PK) profiles. **(A)** TFV-DP concentrations in PBMCs were determined at days 1 and 14 then every two weeks for 8 weeks. Tissue biodistribution of TFV-DP was assessed at 28 and 56 days after injection in the **(B)** lymphocytes, **(C)** splenocytes, **(D)** parenchymal liver cells, **(E)** non-parenchymal liver cells, **(F)** rectal tissue, and **(G)** vaginal tissue. Data is expressed as mean  $\pm$  SEM where  $N = 4$  biological replicates. Vaginal TFV-DP concentrations were compared using Student's *t*-test (\*\*\*\* $P < .0001$ , \*\*\* $P < .001$ , \*\* $P < .01$ , \* $P < .05$  NM1TFV compared with NM2TFV). To compare TFV-DP levels between three or more groups, ANOVA followed by Tukey's post hoc test was used (\*\*\*\* $P < .0001$ , \*\*\* $P < .001$ , \*\* $P < .01$ , \* $P < .05$  NM1TFV compared with NM2TFV).



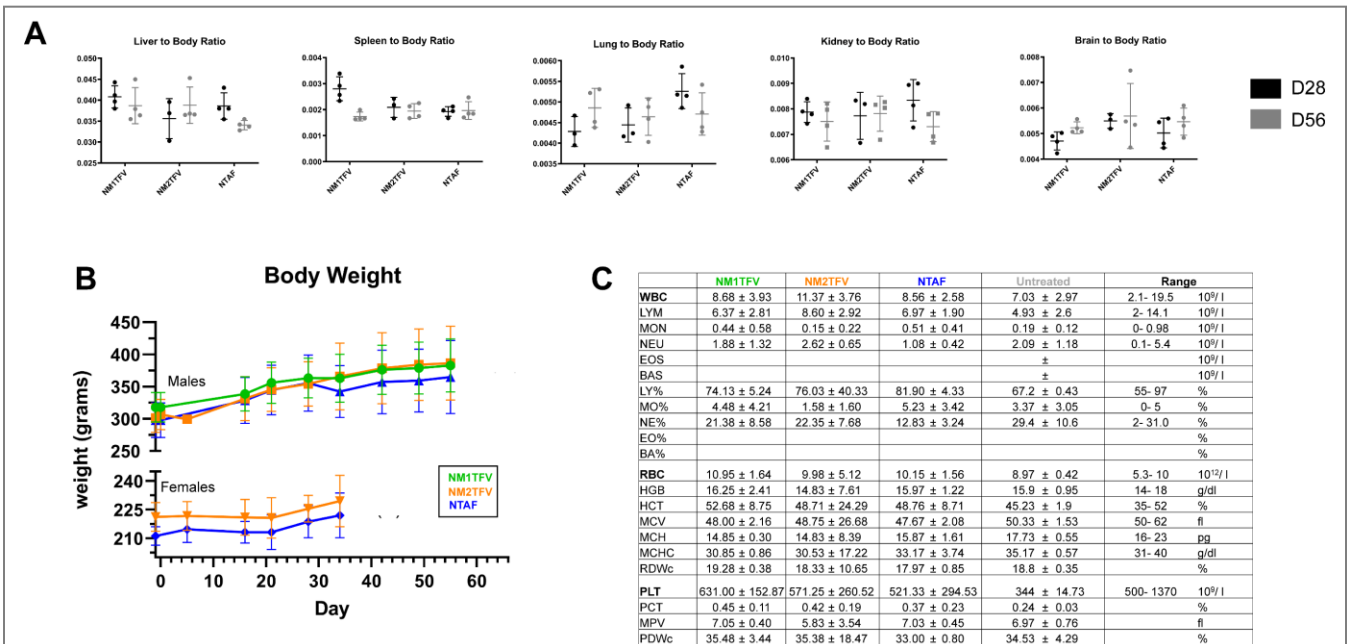




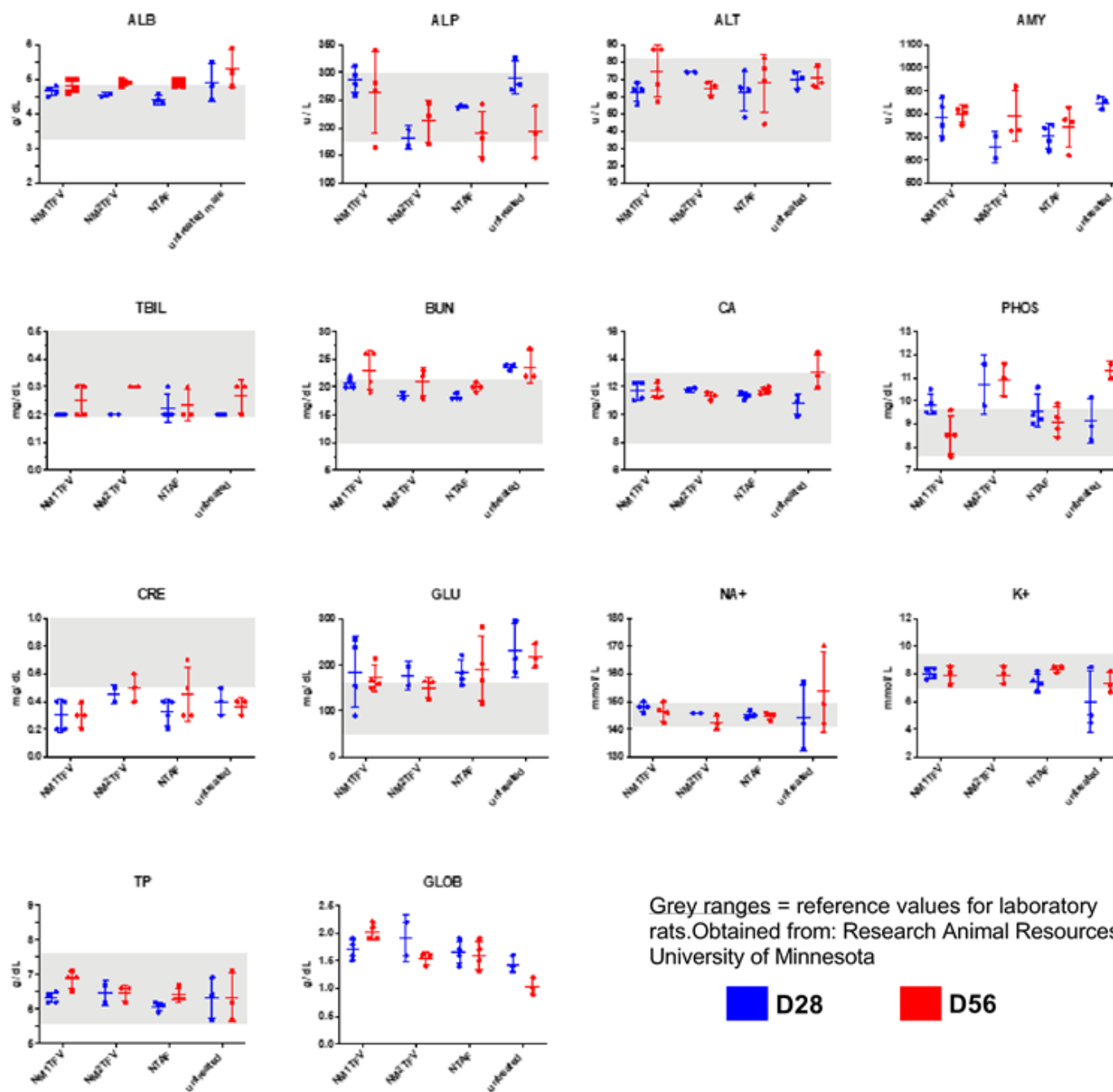
**Figure 3.7.14. Drug quantification at the site of injection.** SD rats were administered a single IM dose of NM1TFV, NM2TFV or NTAF (75 mg/kg TFV-eq.), and sacrificed on days 28 and 56 post treatment. (A) Concentration of prodrug at the site of injection over the course of the study was measured. Percent of initial dose is indicated at each time point. (B) Prodrug to parent drug ratios were determined on days 28 and 56.

Statistically-significant correlations between muscle prodrug and tissue <b>prodrug</b> levels				
X	Y	r	r <sup>2</sup>	P value
Liver prodrug	Muscle prodrug	0.7601	0.5778	0.0016
Spleen prodrug	Muscle prodrug	0.8158	0.6656	0.0002
Lung prodrug	Muscle prodrug	0.6306	0.3977	0.0156
Whole blood prodrug	Muscle prodrug	0.6208	0.3854	0.0135
Gut prodrug	Muscle prodrug	0.7520	0.5655	0.0012
Adipose prodrug	Muscle prodrug	0.5430	0.2948	0.0448
Testes prodrug	Muscle prodrug	0.5977	0.3572	0.0240
Statistically-significant correlations between muscle prodrug and tissue <b>TFV</b> levels				
X	Y	r	r <sup>2</sup>	P value
Liver TFV	Muscle prodrug	0.8503	0.7230	0.0001
Spleen TFV	Muscle prodrug	0.9228	0.8516	<0.0001
Lung TFV	Muscle prodrug	0.8847	0.7827	<0.0001
Whole blood TFV	Muscle prodrug	0.6981	0.4873	0.0055
LN TFV	Muscle prodrug	0.9018	0.8132	<0.0001
Kidney TFV	Muscle prodrug	0.8109	0.6576	0.0002
Gut TFV	Muscle prodrug	0.8242	0.6793	0.0002

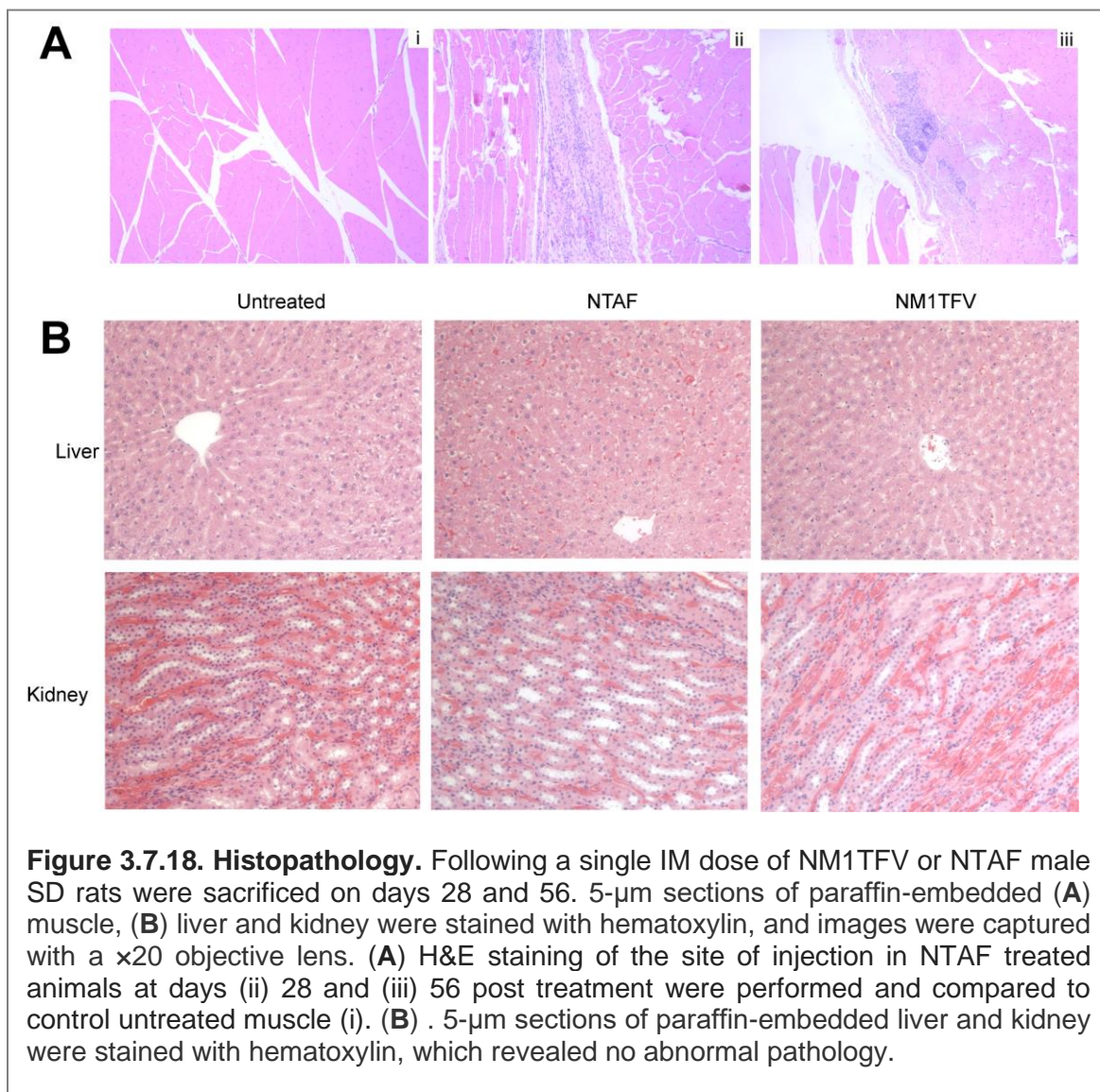
**Figure 3.7.15. Statistical correlations.** SD rats were administered a single IM dose of NM1TFV, NM2TFV or NTAF (75 mg/kg TFV-eq.), and sacrificed on days 28 and 56 post treatment. Muscle prodrug concentrations of individual NM1TFV and NM2TFV treated animals (X) was plotted against the corresponding tissue drug concentration (Y) for individual animals (NM1TFV and NM2TFV), and Pearson correlation used to assess the relationship between the two variables. ( $\alpha = 0.05$ , \*\*\*\* $P < .0001$ , \*\*\* $P < .001$ , \*\* $P < .01$ , \* $P < .05$ ).



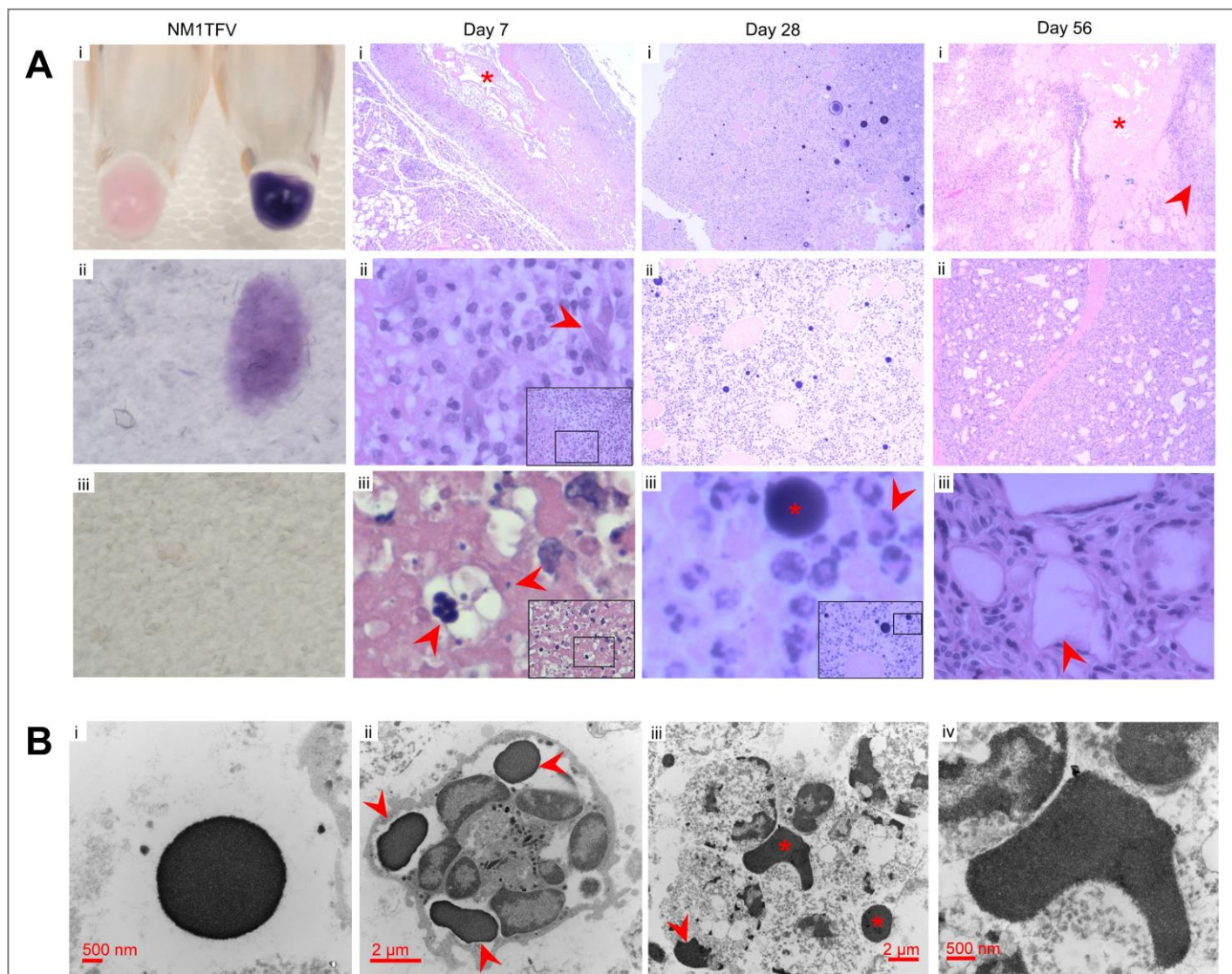
**Figure 3.7.16. Single dose acute toxicity testing.** Toxicity was assessed in SD rats after NM1TFV, NM2TFV, and NTAF treatment. (A) Organ to body weight ratios were determined on the days of sacrifice (days 28 and 56), and (B) animal weights were recorded weekly. (C) Plasma was collected for CBCs, controls were age-matched untreated mice. Values reported are the SEM of 4 replicates.



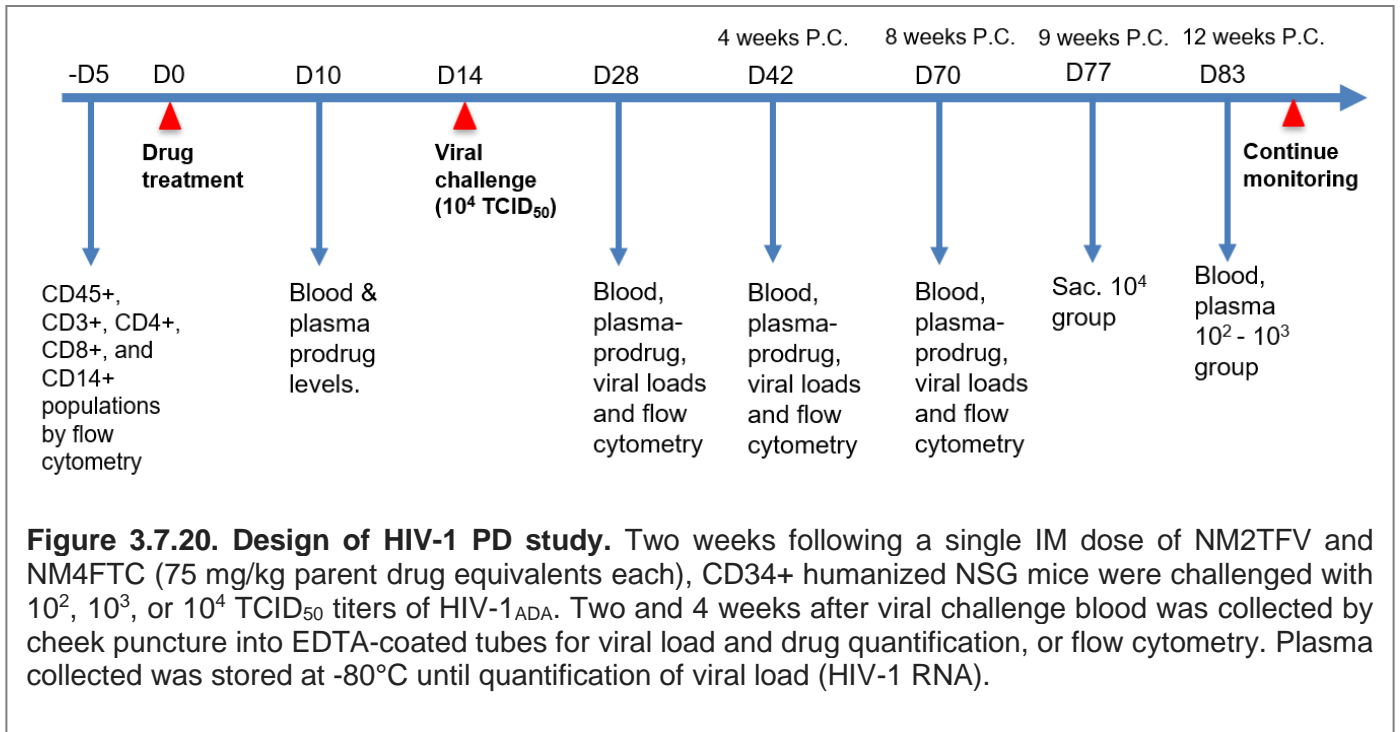
**Figure 3.7.17. Serum chemistry.** Toxicity was assessed in SD rats after NM1TFV, NM2TFV, and NTAF treatment. Comprehensive serum chemistry profiles determined on the days of sacrifice (days 28 and 56), values reported are the SEM of at least 3 replicates. Grey rectangles indicate reference laboratory values for rats, obtained via University of Minnesota, Research animal resources.







**Figure 3.7.19. Injection site histopathology.** Following a single IM dose of NM1TFV or NTAF male SD rats were sacrificed on days 7, 28, and 56. **(A)** H&E staining of NM1TFV (i) revealed the formulation was readily stained by hematoxylin (ii), but not eosin (iii). Images were captured with a  $\times 60$  objective lens. For the histological examination of the site of injection, 5- $\mu\text{m}$  sections of paraffin-embedded tissues were stained with hematoxylin and eosin. Images were captured with a  $\times 4$  and  $\times 40$  objective using a Nuance EX multispectral imaging system affixed to a Nikon Eclipse E800 microscope (Nikon Instruments). At day 7, a necrotic focus was observed (i, indicated by \*), surrounded by histiocytes, and fibroblasts (ii, arrow). Clusters of basophilic foreign material, likely NM1TFV were also observed interspersed in nuclear debris (iii, arrows). By day 28, larger extracellular basophilic staining globules (iii, indicated by \*) along with small basophilic intracellular granules present in the histiocytes (iii, indicated by arrow), along with foreign body granulomatous reaction. At 56 days, the foreign material appeared mostly amorphous (i, indicated by \*), with a foreign body giant cell granulomatous reaction (ii, iii). **(B)** TEM images of the NM1TFV site of injection at day 28 (i & ii), and 56 (iii & iv) confirmed the light microscopic findings.



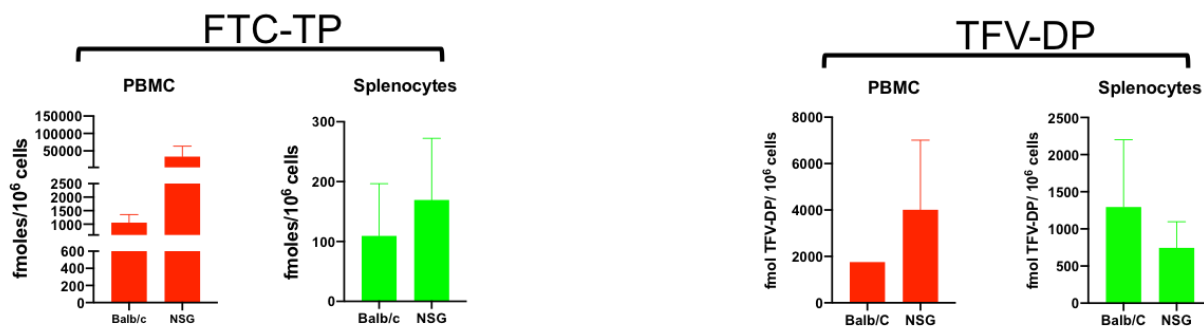
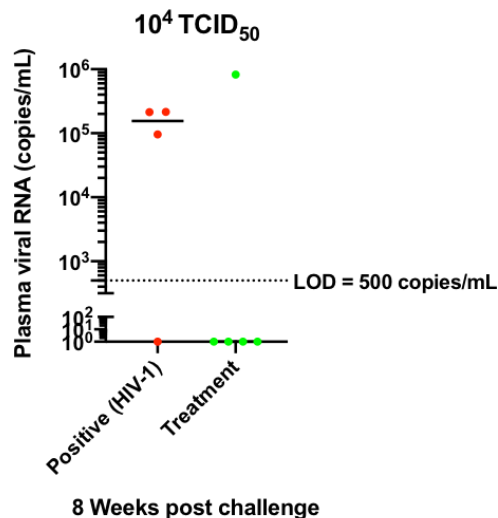


**Figure 3.7.21. PD in HIV-1 infected humanized mice.** Two weeks following a single IM dose of NM2TFV and NM4FTC (75 mg/kg parent drug equivalents each), CD34<sup>+</sup> humanized NSG mice were challenged with 10<sup>2</sup>, 10<sup>3</sup>, or 10<sup>4</sup> TCID<sub>50</sub> titers of HIV-1<sub>ADA</sub>. After viral challenge, blood was collected by cheek puncture into EDTA-coated tubes for viral load and drug quantification, or flow cytometry. (A) Plasma collected at 8 weeks post viral challenge was assayed for viral load (HIV-1 RNA). (B) The concentration of active metabolites, FTC-TP (left) and TFV-DP (right), were determined in PBMCs and splenocytes at the time of viral challenge in NSG (not humanized) and Balb/C mice.



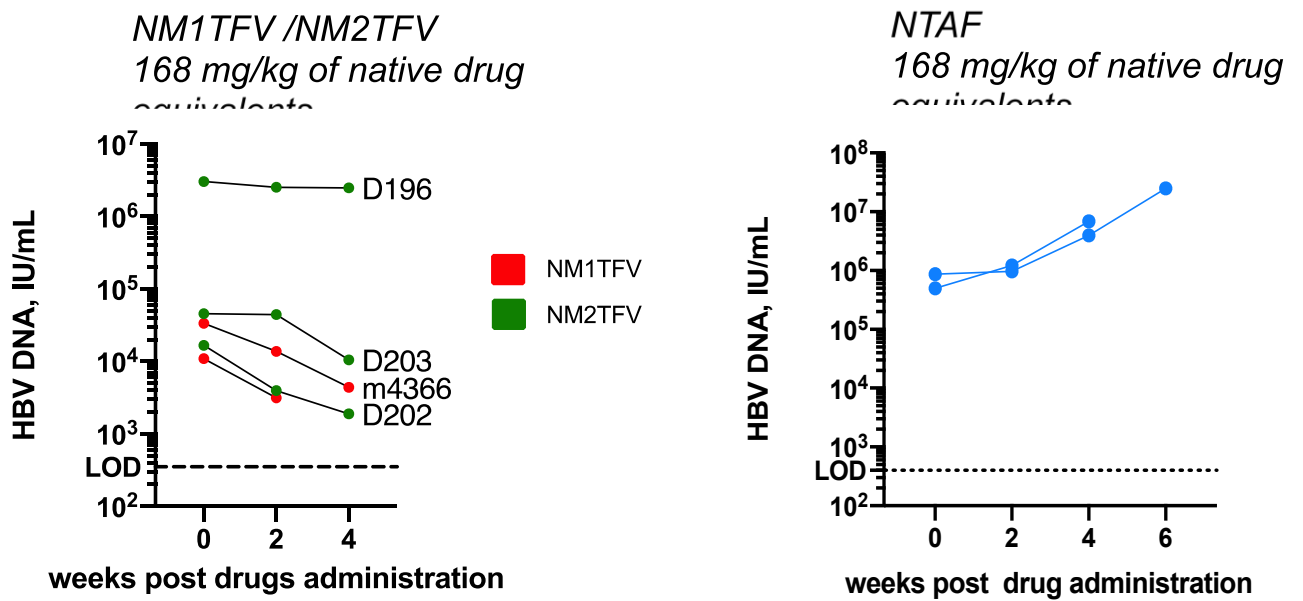
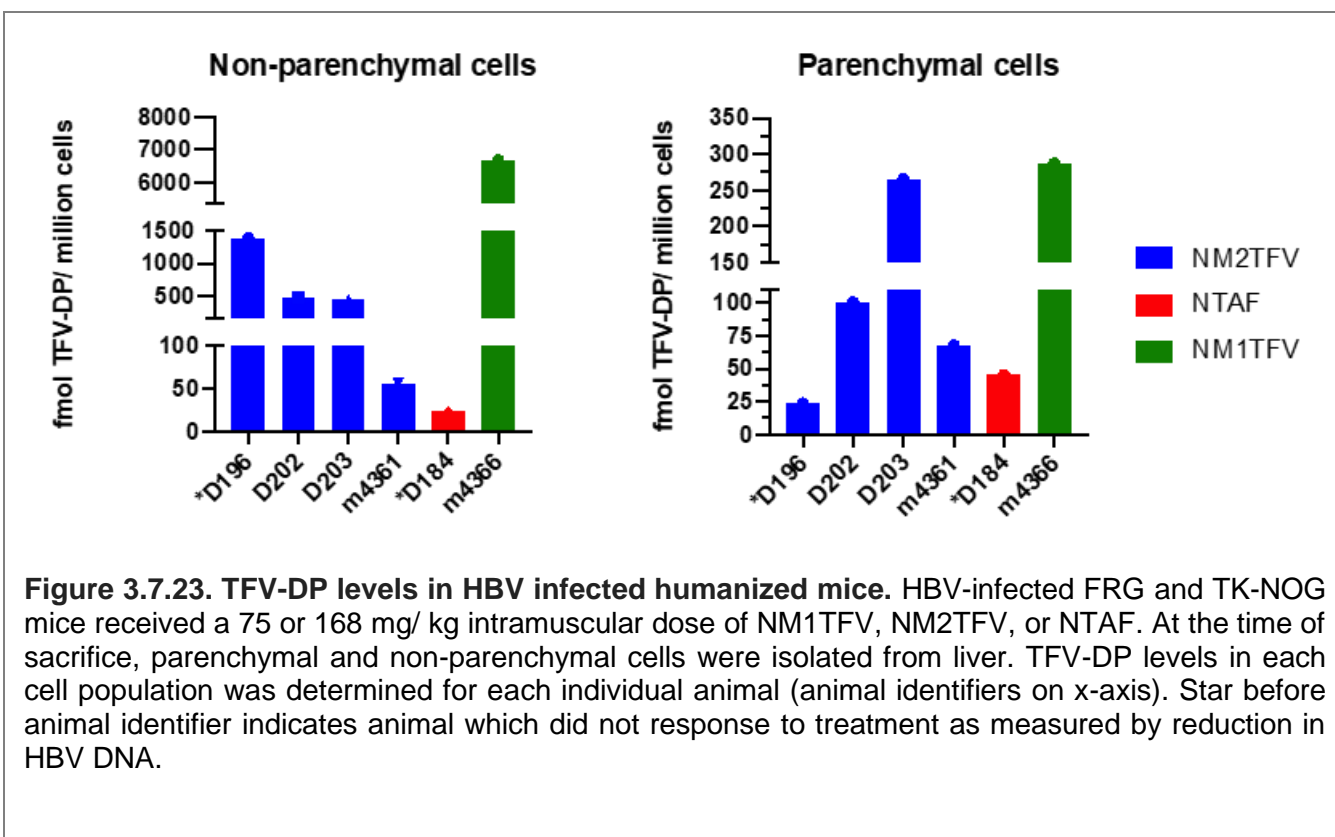


**Figure 3.7.22. PD in HBV infected humanized mice.** HBV-infected FRG mice received a 168 mg/kg intramuscular dose of NM1TFV (red), NM2TFV (green), or NTAF (blue). HBV DNA levels were determined every week out to 6 weeks. Limit of detection indicated by dashed line.



## **CHAPTER 4- Summary, Challenges, Future Directions**

### **4.1 Summary**

HIV treatment and prevention with a goal of viral eradication is a challenge that needs to be met. Current oral therapies, while effective in preventing disease and reducing disease morbidity and mortality cannot meet this goal alone. Lack of adherence to daily oral dosing regimens leads to viral resistance, reduced treatment effectiveness and lack of prevention. Long-acting synthetic and biologic formulations for sustained ART delivery provide a potential means of addressing these challenges. Previous studies indicate that combinations of LASER ART and CRISPR-Cas9 may be effective as an HIV cure strategy [163]. Repurposing of the exosome vector described herein to deliver CRISPR-Cas9 could result in effective gene editing. Additionally, the nanoformulated TFFV ProTides developed represent a major step forward in the creation of a long-acting NRTI and could be paired with other LA drug formulations in such a HIV cure strategy. However, further investigation of pharmacokinetics, pharmacodynamics, and large-scale production are imperative for bringing these exciting developments closer to the clinic.

### **4.2 Exosomes: Summary and Future Directions**

To determine the feasibility and utility of a long-acting exosome ARV delivery system, two exosome drug-loading approaches were employed herein: (1) loading naïve exosomes isolated from parental cells *ex vitro* (Fig. 2.6.1A): (2) loading cells with drug *in vitro*, which is then released in exosomes (Fig. 2.6.1B). Regarding *in vitro* loading, following incubation of human MDM with nanoformulated ATV, the cells released ATV-loaded exosomes into the culture media for two weeks (Fig. 2.10.4). However, the released ATV-loaded exosomes did not demonstrate antiviral efficacy equivalent to poloxamer-formulated nanoATV. Therefore, *ex vitro* loading of exosomes was investigated. Regarding *ex vitro* loading of naïve exosomes different APIs (hydrophobic parent drug, hydrophilic parent drug, lipophilic prodrugs), and different methods of drug incorporation were evaluated (sonication, incubation at room temp.,

incubation with saponin, freeze-thaw) (Tables 2.6.1, 2.6.2). The combination of sonication with lipophilic ARV prodrugs resulted in the highest drug encapsulation into exosomes, while avoiding cytotoxicity, and demonstrating antiviral activity (Fig 2.6.14-17, Table 2.6.1). However, drug encapsulation remained low, especially compared to poloxamer –based nanoformulations. This suggests exosomes may not be the most efficient drug carrier for ART. However, they may hold potential in other areas of HIV therapy, for example as delivery vehicles for CRISPR-Cas9 system. Recently our laboratory demonstrated that LASER ART combined with CRISPR-Cas9 technology facilitated HIV elimination in a subset of humanized mice [163], however, the safety and efficacy of the adeno-associated virus (AAV) vector in humans remains a concern. Exosomes, natural delivery vehicles of nucleic acids and proteins [177, 179, 233, 234] would likely function as efficient carriers of the CRISPR-Cas9 system. Further investigation of exosomes' *in vivo* efficacy and toxicity, and large-scale production are imperative for bringing this exciting development closer to the clinic.

In contrast to poloxamer formulation which demonstrate encapsulation of 70-90%, the loading of small molecules into exosomes is less efficient than synthetic nanoparticle approaches. Of note, the percent encapsulation of DDTG into exosomes was 19.3%, and 17.9% for SDTG. Other small molecule antineoplastic drugs have also demonstrated low encapsulation into exosomes. For example, the loading of paclitaxel and doxorubicin into exosomes via passive incubation, was found to be 7.2% paclitaxel, and 11.7% for doxorubicin in previous reports [192, 235]. This suggests exosomes may not be the most efficient carrier for ART.

#### **4.2.1 Exosome mediated CRISPR-Cas9 delivery**

It is worth noting that exosomes by nature are designed to carry proteins and nucleic acids. Their natural function may explain the relatively low drug loading capacity achieved with these carriers. Based on drug concentrations achieved herein, exosomes do not appear to be ideal delivery vehicles for ARVs. However, they may hold potential in other areas of

HIV therapy, for examples as delivery vehicles for CRISPR-Cas9 system. Recently our laboratory demonstrated that LASER ART combined with CRISPR-Cas9 technology facilitated HIV elimination in a subset of humanized mice[163]. Though this study represents a major step forward for an HIV cure, significant concerns over safety of AAV vectors in humans remain. Evidence supports that high doses of AAV gene therapies, can result in abnormal immune response, cytokine storm, and death [236-238]. Therefore, translation of the CRISPR/ LASER ART dual approach for HIV cure likely requires alternative delivery vector for CRISPR-Cas9.

Exosomes are natural delivery vehicles of nucleic acids such mRNA, miRNA, various noncoding RNA, mitochondrial DNA, and genomic DNA [177, 179, 233]. Therefore, they would likely function as efficient carriers of guide RNA (gRNA) and Cas9 mRNA. Noting their natural function as carriers of nucleic acids, several groups have investigated the use of exosomes as RNA delivery vehicles. For instance, in Alvarez-Erviti et al., electroporation was utilized to incorporate siRNA into dendritic cell-derived exosomes, resulting in knockdown of BACE1, a therapeutic target in Alzheimer's disease, in wild-type mice.[202]. The same method was also employed to incorporate miRNA into exosomes for delivery to breast cancer cells [239], and for incorporation of siRNA for gene silencing of mitogen-activated protein kinase [240]. These studies suggest that exosomes may be efficient gene delivery vectors, providing cells with therapeutic RNAs.

In addition to these exogenous approaches, loading of RNA cargo for transfer via exosomes can be achieved endogenously, by modulating producer cells to package selected RNAs within exosomes. Numerous approaches using a variety of RNA species have been investigated for incorporation of therapeutic RNAs into extracellular vesicles. RNAs can be released in microvesicles. or they can be incorporated into intraluminal vesicles (ILVs) of the multivesicular body (MVB), which are released as exosomes. Several approaches of RNA incorporation into extracellular vesicles have been described including: (1) passive loading

due to an abundance of the RNA in the cytosol [239, 241], (2) through recognition via a number of RNA-binding proteins (RBPs) that bind particular sequence motifs in the RNA or recognize specific secondary structures of RNA [242-244], and (3) through specific modifications, such as uridylation [245] (Fig. 4.5.1). Packaging of RNA into extracellular vesicles can also be promoted by its recognition by retroviral coat proteins such as Gag which efficiently target RNAs they recognize to the plasma or MVB membrane resulting in virus-like particle release (Fig. 4.5.1).

As with nucleic acids, exosomes are also nature's solution to targeted protein delivery [246]. This mechanism could also be harnessed for the delivery Cas9 in protein form. In the literature, a variety of procedures have been employed to load the protein catalase into exosomes including electroporation, incubation at room temp., freeze/thaw cycles, sonication, extrusion, and permeabilization with saponin [189, 247]. Another method of protein incorporation involves the isolation of biologic-loaded exosomes secreted from genetically-modified parental cells (Fig. 2.6.1C) [203, 248, 249]. A third potential approach for the delivery of CRISPR-Cas9 involves the incorporation of AAV capsids into extracellular vesicles to reduce immunogenicity and improve gene delivery compared to conventional AAV vectors [250].

#### **4.2.2 Exosome Scalability and Production**

In addition to cargo loading, another challenge exosome-based therapeutics face is large scale production. Generally, obtaining large amounts of pure extracellular vesicles, such as exosomes, necessitates copious starting material, thus methods of enhanced extracellular vesicle production are under investigation. One possibility is to overexpress regulatory proteins involved in extracellular vesicle biogenesis [243, 251]. Another possible approach to increase production of exosomes in cell culture is treatment of producer cells with compounds that increase exosome biogenesis and/or release, such as bafilomycin

A1, heparanase, or monesin [252-254]. Finally, bioreactors such as hollow fiber bioreactors can also be employed to increase production of exosomes [255, 256].

In addition to the production method, the cell source of exosomes is also an important consideration for scale-up. Though allogenic exosomes produced from patients' tissues or blood (for example, bone marrow, monocytes or macrophages), may have an immune privileged status, personalized-medicine approaches are generally not compatible with large-scale production. Immortal cell-lines are attractive as producer cells, however increasing evidence illustrates that the exosomes derived from tumor cells might trigger tumor initiation, tumor cell growth and progression, metastasis, and drug resistance [257]. Because exosomes can be derived from almost any cell, these issues can be avoided. For large-scale production and isolation of exosomes, the source could potentially be mesenchymal stem cells [258], group O red blood cells [247], or immune cells [259]. Additionally, large-scale methods for exosome isolation and purification under controlled conditions also remains a challenge.

#### **4.3 TFV: Summary and Future Directions**

In addition to biological nanocarriers, polymeric drug nanoparticles represent a new treatment and prevention strategy offering infrequent dosing, with sustained drug release at sites of action and could potentially improve adherence and reduce transmission of infection. Herein, two TFV ProTides chemically modified with 22 carbon chain esters encased into surfactant-coated nanoformulations were created. Single treatment of MDM with NM1TFV demonstrated sustained intracellular prodrug and TFV-DP levels, as well as antiretroviral activity. PK evaluations in Sprague Dawley rats demonstrated that NM1TFV resulted in sustained levels of TFV-DP at or above the  $IC_{90}$  for 2 months in PBMCs, and improved tissue BD compared to NM2TFV and NTAF.

In the present study, although NM1TFV significantly improved drug BD compared to NM2TFV and NTAF, and significant levels of prodrug, TFV, and TFV-DP were detected at

two months. These results underscore the importance of prolonged PK evaluations to further elucidate the potential dosing interval in humans. To this end, future studies will focus on extended-period PK studies of NM1TFV in rats and rhesus macaques. Evaluations of drug biodistribution within vaginal and rectal tissues following NM1TFV treatment will also be conducted in future studies to determine the concentration of active metabolite at sites of viral challenge. While our studies demonstrate that NM2TFV confers high TFV-DP concentrations in vaginal tissue of SD rats, biodistribution of NM1TFV was not investigated at these sites of viral challenge. Given recent reports from HPTN 083 and HPTN 084 studies demonstrating that long-acting injectable CAB administered every two months is more effective than daily pills in preventing HIV acquisition [140], it is clear long-acting formulations may represent an important tool in controlling the HIV epidemic. The lead candidate NM1TFV may provide an attractive alternative by delivering ARV drug to sites of viral exposure and simplify the use of antiretroviral medications, thereby enhancing HIV-1 protection by facilitating PrEP adherence. Therefore future studies should investigate the biodistribution of NM1TFV to the female reproductive tract. TFV also inhibits major co-infections, such as hepatitis B virus [232]. Preliminary studies of NM1TFV have demonstrated the ability of the formulation to suppress HBV replication in humanized mice for 4 weeks following a single intramuscular dose [224]. Therefore, future studies will examine the use of NM1TFV for both monotherapy of HBV, and for the treatment HIV-HBV coinfections.

#### **4.3.1 Pharmacokinetic and dynamic assessments**

In the rat PK study presented herein, high levels of prodrug, parent drug, and active metabolite were observed following NM1TFV treatment at the end of the study. At two months, an estimated 5% of the initial NM1TFV dose remains within the site of injection, indicating drug release from the intramuscular depot could sustain drug levels for a longer period. Of note, NM1TFV also resulted in TFV-DP concentration in PBMCs above the human



IC<sub>90</sub> for the duration of the study. In order to determine how long this formulation may be effective *in vivo*, a 6-month PK assessment will be performed.

An additional observation from the rat PK study was foreign body granulomatous reaction at the site of injection. Though this type of inflammatory response has previously been observed for intramuscular lipidic prodrug formulations, the long-term tissue effects should be further investigated to ensure resolution of these granulomas. Therefore, future studies will investigate the evolution of the inflammatory response at the site of injection over time. We hypothesize that such granulomas will subside once the foreign material (NM1TFV) dissipates. However, when considered under a backdrop of clinical translation, it is important to ensure NM1TFV avoids muscle degeneration, severe fibrosis, or abscesses over time.

Pilot PD studies of NM2TFV in combination with NM4FTC demonstrated protection of HIV-1 infection in a PrEP experimental paradigm. Though these results are promising, further investigation is needed. For instance, FTC-TP levels in the spleen were not at or above the human IC<sub>90</sub> at the time of viral challenge. Additionally, rat recent PK assessments have demonstrated NM1TFV is longer-lived than NM2TFV. Therefore, it would be useful to test NM1TFV alone, NM4FTC alone, and a combination of the two to determine whether the NM1TFV is efficacious alone or requires combination. In the pilot PD study intraperitoneal viral challenge was employed. Future studies should investigate modes of viral challenge that better replicate natural infection such as vaginal and rectal challenge. These studies would further affirm future use of NM1TFV for PrEP in populations at high risk for sexual HIV-1 exposure.

TFV is widely prescribed for the treatment of not only HIV-1 but HBV. HBV virus etiology is substantially different than HIV, however daily treatment is required, and includes similar limitations such as short plasma drug elimination half-life, a weak barrier to resistance, and limited drug penetration into viral sanctuaries. Thus, TK-NOG and FRG mice with

chimeric humanized liver infected with HBV were used to evaluate the efficacy of long-acting TFV formulations. Both NM1TFV and NM2TFV demonstrated the ability to suppress HBV replication for weeks in humanized-liver mice. When TFV-DP concentrations were analyzed in treated animals, it was clear that TFV-DP levels were higher in non-parenchymal liver cells compared to parenchymal cells. In fact, animals that failed to attain viral suppression were found to have the low TFV-DP levels in hepatocytes. Therefore, future studies should strive to determine what TFV-DP levels in hepatocytes are required with viral suppression. Additionally, future studies should investigate whether non-parenchymal population functions as a depot, and is able to transfer prodrug, parent drug, or TFV-DP to hepatocytes over time. In addition to elucidation of the mechanism of action in HBV-infected mice, future works might address HIV-HBV coinfection [260].

#### **4.3.2 Scalability and production**

With laboratory scale, pilot scale, and production scale high pressure homogenizers on the market, the manufacture of nanoformulations such as NM1TFV by high-pressure homogenization is a scalable process. However, the lead formulation NM1TFV may face challenges in clinical translation due to colloidal instability. Current highly concentrated formulations of NM1TFV (above 150 mg/ mL) are prone to particle aggregation. When large-scale production and global distribution are considered, any unstable product would face significant challenges in terms of cost and implementation. While the formulations described herein have enabled a vast array of preclinical evaluations and identification of a lead candidate, further formulation optimization would likely be required for successful translation into the clinic. To develop a stable formulation (of at least 300 mg/mL concentration, similar to Cabenuva), inclusion of different polymers, as well as altered API to polymer ratios may lead to a more stable product. Specifically, inclusion of PEG may lead to a more stable emulsion, an effect we observed during optimization of the NTAF formulation. Alternatively, freezing and lyophilization are the most used methods for long-term storage of many types

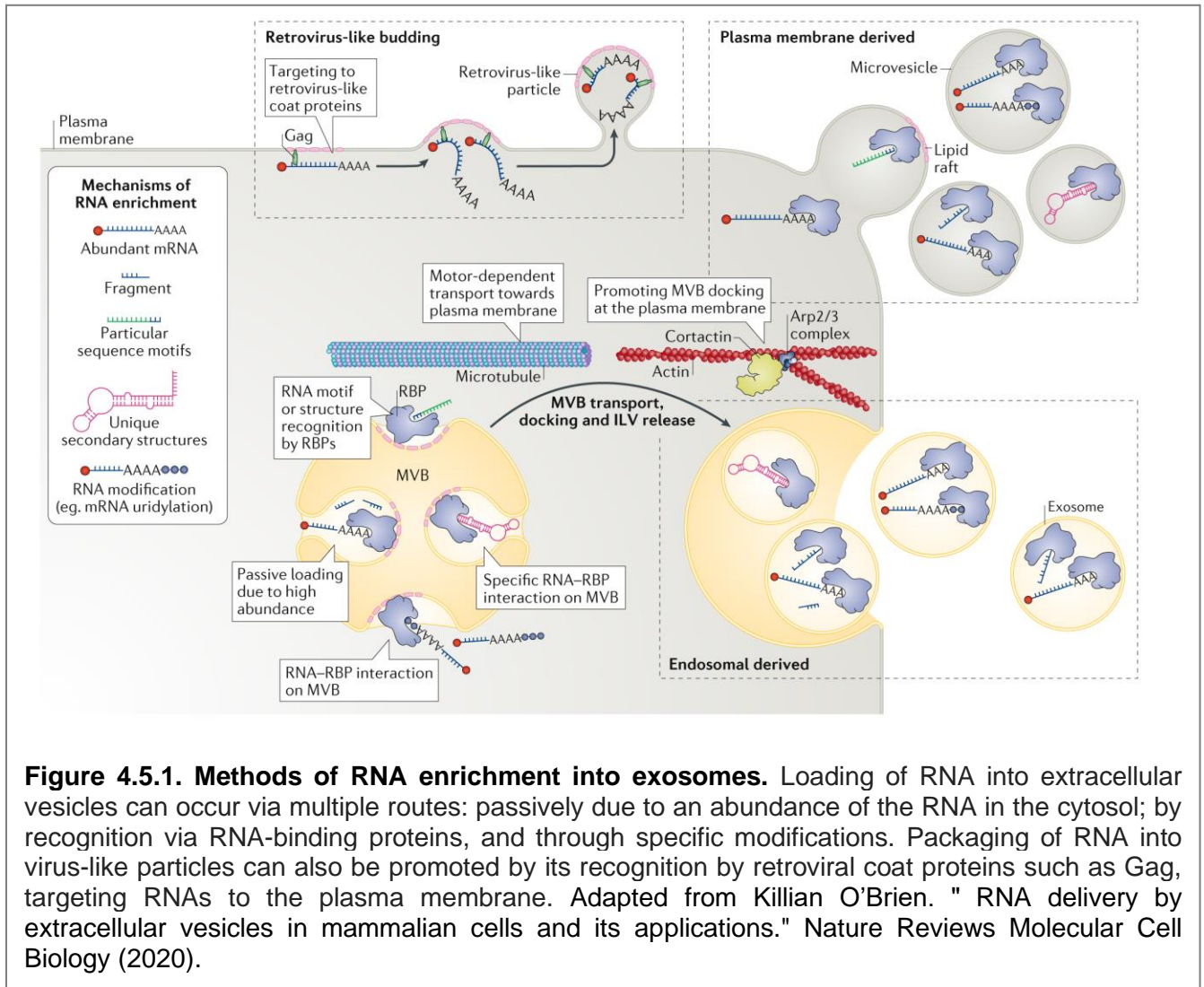
of nanoparticles [261-263]. Therefore, freeze-drying of NM1TFV may also provide enhanced long-term stability and enhanced product shelf-life. However, in order to maintain the physical and chemical properties of NM1TFV nanoparticles, optimization of the lyophilization process and stability assessments under varying conditions (temperature, humidity) are key.

In addition to addressing issues of colloidal instability at higher concentrations, parameters such as tonicity, oxidation, and sterility should also be considered when creating an optimized NM1TFV formulation for market. To avoid damage to the tissues and minimize hypertonicity-induced pain upon product administration, intramuscular formulations should ideally be isotonic with human plasma (300 mOsm/kg) [264]. Tonicity can be adjusted with a variety of additives such as sodium chloride, dextrose, mannitol, glucose, or trehalose[264, 265]. We have not examined whether oxidation of NM1TFV leads to degradation of the API or polymer excipients. However, should the formulation prove prone to oxidative degradation, additives can reduce the rate of product degradation and improve the shelf-life. For instance, vitamin C (ascorbic acid), butylated hydroxyanisole (BHA), and butylated hydroxytoluene (BHT) are used in aqueous parenteral products for this purpose[265]. Should a single vial of the product contain multiple doses, antimicrobial agents would be required to inhibit growth of microorganisms that may be inadvertently introduced into the product during repeated use by a healthcare professional. If not terminally sterilized, single- dose products, may also require addition of antimicrobials such as phenoxyethanol, phenol, benzyl alcohol, or parabens[265, 266]. The addition of excipients may prove important for optimization of NM1TFV formulation by assuring safety (antimicrobial agents), minimizing pain and irritation upon injection (tonicity adjusters), and prolonging drug delivery (polymers). However, excipients may also produce negative effects such as reduced drug stability[267]. Therefore, the interactions between excipients and drug in the optimized NM1TFV formulation must be studied to ensure product stability and efficacy.

#### 4.4 Conclusions

HIV treatment and prevention with a goal of viral eradication is a challenge that needs to be met. Current oral therapies, while effective in preventing disease and reducing disease morbidity and mortality cannot meet this goal alone. Lack of adherence to daily oral dosing regimens leads to viral resistance, reduced treatment effectiveness and lack of prevention. Long-acting formulations and biologic vehicles for ART delivery provide a means of meeting these challenges. Recent success in eliminating viral infection in a murine model of HIV using a combination of long-acting ART and CRISPR-Cas9 highlights the benefits of long-acting intracellular and tissue targeted drug delivery approaches [163]. However, to be impactful therapies must be safe, bioavailable, have non-inferior efficacy compared to existing daily oral medicines, provide sustained therapeutic drug concentrations at sites of action, reach reservoirs of HIV replication, and be accessible and be affordable. For these goals to be met and for these strategies to have a positive impact on HIV treatment and prevention, several challenges need to be realized and overcome. Long-acting drug delivery systems can address these concerns, but their production will require careful evaluation of the resources and equipment needed for cost-effective production under good manufacturing practices guidelines[268]. Development of simple, scalable, efficient and cost-effective synthesis and production processes would enable the use of these technologies in resource-limited areas where PrEP can have an immediate impact [62, 268, 269]. Generic companies could be engaged during early stages of development to facilitate cost-effective production and distribution in countries where the medications are utilized[97]. Also, ARV and delivery system stability would need to be optimized for shipment and long-term storage at ambient temperature in low and middle income and tropical and subtropical regions [62, 97]. Finally, and importantly, the at-risk and patient populations that can most benefit from these formulations should be identified and access for those who are willing to accept such formulation regimens will need to be facilitated.

## 4.5 Figures



## REFERENCES

1. May, M.T., et al., *Impact on life expectancy of HIV-1 positive individuals of CD4+ cell count and viral load response to antiretroviral therapy*. AIDS, 2014. **28**(8): p. 1193-202.
2. Antiretroviral Therapy Cohort, C., *Survival of HIV-positive patients starting antiretroviral therapy between 1996 and 2013: a collaborative analysis of cohort studies*. Lancet HIV, 2017. **4**(8): p. e349-e356.
3. UNAIDS, *Global HIV & AIDS Statistics- 2019 Fact Sheet*. 2019.
4. HIV.gov *Global Statistics*. 2020.
5. Gulick, R.M. and C. Flexner, *Long-Acting HIV Drugs for Treatment and Prevention*. Annu Rev Med, 2019. **70**: p. 137-150.
6. Sigal, A., et al., *Cell-to-cell spread of HIV permits ongoing replication despite antiretroviral therapy*. Nature, 2011. **477**(7362): p. 95-8.
7. Subbramanian, R.A. and E.A. Cohen, *Molecular biology of the human immunodeficiency virus accessory proteins*. J Virol, 1994. **68**(11): p. 6831-5.
8. Dragic, T., et al., *HIV-1 entry into CD4+ cells is mediated by the chemokine receptor CC-CKR-5*. Nature, 1996. **381**(6584): p. 667-73.
9. Melikyan, G.B., *Common principles and intermediates of viral protein-mediated fusion: the HIV-1 paradigm*. Retrovirology, 2008. **5**: p. 111.
10. Hu, W.S. and S.H. Hughes, *HIV-1 reverse transcription*. Cold Spring Harb Perspect Med, 2012. **2**(10).
11. Craigie, R., *The molecular biology of HIV integrase*. Future Virol, 2012. **7**(7): p. 679-686.
12. Das, A.T., A. Harwig, and B. Berkhout, *The HIV-1 Tat protein has a versatile role in activating viral transcription*. J Virol, 2011. **85**(18): p. 9506-16.
13. Sundquist, W.I. and H.G. Krausslich, *HIV-1 assembly, budding, and maturation*. Cold Spring Harb Perspect Med, 2012. **2**(7): p. a006924.
14. Felber, B.K., C.M. Drysdale, and G.N. Pavlakis, *Feedback regulation of human immunodeficiency virus type 1 expression by the Rev protein*. J Virol, 1990. **64**(8): p. 3734-41.
15. Luria, S., I. Chambers, and P. Berg, *Expression of the type 1 human immunodeficiency virus Nef protein in T cells prevents antigen receptor-mediated induction of interleukin 2 mRNA*. Proc Natl Acad Sci U S A, 1991. **88**(12): p. 5326-30.
16. Miller, M.D., et al., *The human immunodeficiency virus-1 nef gene product: a positive factor for viral infection and replication in primary lymphocytes and macrophages*. J Exp Med, 1994. **179**(1): p. 101-13.
17. Lama, J., A. Mangasarian, and D. Trono, *Cell-surface expression of CD4 reduces HIV-1 infectivity by blocking Env incorporation in a Nef- and Vpu-inhibitable manner*. Curr Biol, 1999. **9**(12): p. 622-31.
18. Ross, T.M., A.E. Oran, and B.R. Cullen, *Inhibition of HIV-1 progeny virion release by cell-surface CD4 is relieved by expression of the viral Nef protein*. Curr Biol, 1999. **9**(12): p. 613-21.
19. Garcia, J.V. and A.D. Miller, *Downregulation of cell surface CD4 by nef*. Res Virol, 1992. **143**(1): p. 52-5.
20. Heinzinger, N.K., et al., *The Vpr protein of human immunodeficiency virus type 1 influences nuclear localization of viral nucleic acids in nondividing host cells*. Proc Natl Acad Sci U S A, 1994. **91**(15): p. 7311-5.

21. Strebel, K., et al., *The HIV 'A' (sor) gene product is essential for virus infectivity*. Nature, 1987. **328**(6132): p. 728-30.
22. HIV.gov *Symptoms of HIV*. 2020.
23. Brenchley, J.M., et al., *CD4+ T cell depletion during all stages of HIV disease occurs predominantly in the gastrointestinal tract*. J Exp Med, 2004. **200**(6): p. 749-59.
24. Hammer, S.M., et al., *A controlled trial of two nucleoside analogues plus indinavir in persons with human immunodeficiency virus infection and CD4 cell counts of 200 per cubic millimeter or less*. AIDS Clinical Trials Group 320 Study Team. N Engl J Med, 1997. **337**(11): p. 725-33.
25. Palella, F.J., Jr., et al., *Declining morbidity and mortality among patients with advanced human immunodeficiency virus infection*. HIV Outpatient Study Investigators. N Engl J Med, 1998. **338**(13): p. 853-60.
26. Cihlar, T. and M. Fordyce, *Current status and prospects of HIV treatment*. Curr Opin Virol, 2016. **18**: p. 50-6.
27. Schurmann, D., et al., *Safety, pharmacokinetics, and antiretroviral activity of islatravir (ISL, MK-8591), a novel nucleoside reverse transcriptase translocation inhibitor, following single-dose administration to treatment-naïve adults infected with HIV-1: an open-label, phase 1b, consecutive-panel trial*. Lancet HIV, 2020.
28. DeJesus, E., et al., *A Phase IIa Study Evaluating Safety, Pharmacokinetics, and Antiviral Activity of GSK2838232, a Novel, Second-generation Maturation Inhibitor, in Participants With Human Immunodeficiency Virus Type 1 Infection*. Clin Infect Dis, 2020. **71**(5): p. 1255-1262.
29. Nachega, J.B., et al., *Lower pill burden and once-daily antiretroviral treatment regimens for HIV infection: A meta-analysis of randomized controlled trials*. Clin Infect Dis, 2014. **58**(9): p. 1297-307.
30. Cohen, M.S., *Successful treatment of HIV eliminates sexual transmission*. Lancet, 2019. **393**(10189): p. 2366-2367.
31. Eggleton, J.S. and S. Nagalli, *Highly Active Antiretroviral Therapy (HAART)*, in *StatPearls*. 2020: Treasure Island (FL).
32. Swindells, S., et al., *Long-Acting Cabotegravir and Rilpivirine for Maintenance of HIV-1 Suppression*. N Engl J Med, 2020. **382**(12): p. 1112-1123.
33. Sillman, B., et al., *Creation of a long-acting nanoformulated dolutegravir*. Nat Commun, 2018. **9**(1): p. 443.
34. *Panel on Antiretroviral Guidelines for Adults and Adolescents. Guidelines for the use of antiretroviral agents in adults and adolescents living with HIV* 2020, US Department of Health and Human Services.
35. Terrault, N.A., et al., *Update on Prevention, Diagnosis, and Treatment of Chronic Hepatitis B: AASLD 2018 Hepatitis B Guidance*. Clin Liver Dis (Hoboken), 2018. **12**(1): p. 33-34.
36. Jordheim, L.P., et al., *Advances in the development of nucleoside and nucleotide analogues for cancer and viral diseases*. Nat Rev Drug Discov, 2013. **12**(6): p. 447-64.
37. Shelton, J., et al., *Metabolism, Biochemical Actions, and Chemical Synthesis of Anticancer Nucleosides, Nucleotides, and Base Analogs*. Chem Rev, 2016. **116**(23): p. 14379-14455.
38. Balzarini, J., P. Herdewijn, and E. De Clercq, *Differential patterns of intracellular metabolism of 2',3'-didehydro-2',3'-dideoxythymidine and 3'-azido-2',3'-dideoxythymidine, two potent anti-human immunodeficiency virus compounds*. J Biol Chem, 1989. **264**(11): p. 6127-33.

39. Hao, Z., et al., *Potent DNA chain termination activity and selective inhibition of human immunodeficiency virus reverse transcriptase by 2',3'-dideoxyuridine-5'-triphosphate*. Mol Pharmacol, 1990. **37**(2): p. 157-63.
40. Li, F., H. Maag, and T. Alfredson, *Prodrugs of nucleoside analogues for improved oral absorption and tissue targeting*. J Pharm Sci, 2008. **97**(3): p. 1109-34.
41. De Clercq, E. and A. Holy, *Acyclic nucleoside phosphonates: a key class of antiviral drugs*. Nat Rev Drug Discov, 2005. **4**(11): p. 928-40.
42. De Clercq, E., *Tenofovir alafenamide (TAF) as the successor of tenofovir disoproxil fumarate (TDF)*. Biochem Pharmacol, 2016. **119**: p. 1-7.
43. Thornton, P.J., et al., *Nucleoside Phosphate and Phosphonate Prodrug Clinical Candidates*. J Med Chem, 2016. **59**(23): p. 10400-10410.
44. Hecker, S.J. and M.D. Erion, *Prodrugs of phosphates and phosphonates*. J Med Chem, 2008. **51**(8): p. 2328-45.
45. Wagner, C.R., V.V. Iyer, and E.J. McIntee, *Pronucleotides: toward the in vivo delivery of antiviral and anticancer nucleotides*. Med Res Rev, 2000. **20**(6): p. 417-51.
46. McGuigan, C., et al., *Aryl phosphate derivatives of AZT retain activity against HIV1 in cell lines which are resistant to the action of AZT*. Antiviral Res, 1992. **17**(4): p. 311-21.
47. Grant, P.M. and A.G. Cotter, *Tenofovir and bone health*. Curr Opin HIV AIDS, 2016. **11**(3): p. 326-32.
48. Chan, L., et al., *Potential kidney toxicity from the antiviral drug tenofovir: new indications, new formulations, and a new prodrug*. Curr Opin Nephrol Hypertens, 2018. **27**(2): p. 102-112.
49. Patterson, K.B., et al., *Penetration of tenofovir and emtricitabine in mucosal tissues: implications for prevention of HIV-1 transmission*. Sci Transl Med, 2011. **3**(112): p. 112re4.
50. Cottrell, M.L., et al., *Single-dose pharmacokinetics of tenofovir alafenamide and its active metabolite in the mucosal tissues*. J Antimicrob Chemother, 2017. **72**(6): p. 1731-1740.
51. [https://www.accessdata.fda.gov/drugsatfda\\_docs/label/1998/21008lbl.pdf](https://www.accessdata.fda.gov/drugsatfda_docs/label/1998/21008lbl.pdf), S.L.D.o.a.f.i.s.P.I.
52. Curtis, K.M. and J.F. Peipert, *Long-Acting Reversible Contraception*. N Engl J Med, 2017. **376**(5): p. 461-468.
53. Adams, C.E., et al., *Systematic meta-review of depot antipsychotic drugs for people with schizophrenia*. Br J Psychiatry, 2001. **179**: p. 290-9.
54. Park, E.J., et al., *Long-acting injectable formulations of antipsychotic drugs for the treatment of schizophrenia*. Arch Pharm Res, 2013. **36**(6): p. 651-9.
55. Guzman, F. *Long-Acting Injectable Antipsychotics: A Practical Guide for Prescribers*. 2019.
56. Fonner, V.A., et al., *Effectiveness and safety of oral HIV preexposure prophylaxis for all populations*. AIDS, 2016. **30**(12): p. 1973-83.
57. Grant, R.M., et al., *Preexposure chemoprophylaxis for HIV prevention in men who have sex with men*. N Engl J Med, 2010. **363**(27): p. 2587-99.
58. Karim, S.S. and Q.A. Karim, *Antiretroviral prophylaxis: a defining moment in HIV control*. Lancet, 2011. **378**(9809): p. e23-5.
59. Koenig, L.J., C. Lyles, and D.K. Smith, *Adherence to antiretroviral medications for HIV pre-exposure prophylaxis: lessons learned from trials and treatment studies*. Am J Prev Med, 2013. **44**(1 Suppl 2): p. S91-8.



60. McMahon, J.M., et al., *Oral pre-exposure prophylaxis (PrEP) for prevention of HIV in serodiscordant heterosexual couples in the United States: opportunities and challenges*. AIDS Patient Care STDS, 2014. **28**(9): p. 462-74.
61. Gendelman, H.E., et al., *The Promise of Long-Acting Antiretroviral Therapies: From Need to Manufacture*. Trends Microbiol, 2019. **27**(7): p. 593-606.
62. Nachman, S., et al., *Long-acting or extended-release antiretroviral products for HIV treatment and prevention in infants, children, adolescents, and pregnant and breastfeeding women: knowledge gaps and research priorities*. Lancet HIV, 2019. **6**(8): p. e552-e558.
63. Owen, A. and S. Rannard, *Strengths, weaknesses, opportunities and challenges for long acting injectable therapies: Insights for applications in HIV therapy*. Adv Drug Deliv Rev, 2016. **103**: p. 144-56.
64. Taddeo, D., M. Egedy, and J.Y. Frappier, *Adherence to treatment in adolescents*. Paediatr Child Health, 2008. **13**(1): p. 19-24.
65. Chen, J., et al., *Biphasic elimination of tenofovir diphosphate and nonlinear pharmacokinetics of zidovudine triphosphate in a microdosing study*. J Acquir Immune Defic Syndr, 2012. **61**(5): p. 593-9.
66. Trezza, C., et al., *Formulation and pharmacology of long-acting cabotegravir*. Curr Opin HIV AIDS, 2015. **10**(4): p. 239-45.
67. Jacobson, J.M. and C.W. Flexner, *Universal antiretroviral regimens: thinking beyond one-pill-once-a-day*. Curr Opin HIV AIDS, 2017. **12**(4): p. 343-350.
68. Iglay, K., et al., *Systematic Literature Review and Meta-analysis of Medication Adherence With Once-weekly Versus Once-daily Therapy*. Clin Ther, 2015. **37**(8): p. 1813-21 e1.
69. Kruk, M.E. and N. Schwalbe, *The relation between intermittent dosing and adherence: preliminary insights*. Clin Ther, 2006. **28**(12): p. 1989-95.
70. Stoddart, C.A., et al., *Oral administration of the nucleoside EFdA (4'-ethynyl-2-fluoro-2'-deoxyadenosine) provides rapid suppression of HIV viremia in humanized mice and favorable pharmacokinetic properties in mice and the rhesus macaque*. Antimicrob Agents Chemother, 2015. **59**(7): p. 4190-8.
71. Michailidis, E., et al., *4'-Ethynyl-2-fluoro-2'-deoxyadenosine (EFdA) inhibits HIV-1 reverse transcriptase with multiple mechanisms*. J Biol Chem, 2014. **289**(35): p. 24533-48.
72. Salie, Z.L., et al., *Structural basis of HIV inhibition by translocation-defective RT inhibitor 4'-ethynyl-2-fluoro-2'-deoxyadenosine (EFdA)*. Proc Natl Acad Sci U S A, 2016. **113**(33): p. 9274-9.
73. Kirby, K.A., et al., *Effects of substitutions at the 4' and 2 positions on the bioactivity of 4'-ethynyl-2-fluoro-2'-deoxyadenosine*. Antimicrob Agents Chemother, 2013. **57**(12): p. 6254-64.
74. Markowitz, M. and S.G. Sarafianos, *4'-Ethynyl-2-fluoro-2'-deoxyadenosine, MK-8591: a novel HIV-1 reverse transcriptase translocation inhibitor*. Curr Opin HIV AIDS, 2018. **13**(4): p. 294-299.
75. Gunaydin, H., et al., *Strategy for Extending Half-life in Drug Design and Its Significance*. ACS Med Chem Lett, 2018. **9**(6): p. 528-533.
76. Smith, D.A., et al., *Relevance of Half-Life in Drug Design*. J Med Chem, 2018. **61**(10): p. 4273-4282.
77. Hocqueloux, L., et al., *Dolutegravir Monotherapy Versus Dolutegravir/Abacavir/Lamivudine for Virologically Suppressed People Living With Chronic Human Immunodeficiency Virus Infection: The Randomized Noninferiority MONotherapy of TiviCAY Trial*. Clin Infect Dis, 2019. **69**(9): p. 1498-1505.

78. Pawar, V.K., et al., *Gastroretentive dosage forms: a review with special emphasis on floating drug delivery systems*. Drug Deliv, 2011. **18**(2): p. 97-110.
79. Prinderre, P., C. Sauzet, and C. Fuxen, *Advances in gastro retentive drug-delivery systems*. Expert Opin Drug Deliv, 2011. **8**(9): p. 1189-203.
80. Kirtane, A.R., et al., *Development of an oral once-weekly drug delivery system for HIV antiretroviral therapy*. Nat Commun, 2018. **9**(1): p. 2.
81. Savage, A.C., et al., *Improving maraviroc oral bioavailability by formation of solid drug nanoparticles*. Eur J Pharm Biopharm, 2019. **138**: p. 30-36.
82. Giardiello, M., et al., *Accelerated oral nanomedicine discovery from miniaturized screening to clinical production exemplified by paediatric HIV nanotherapies*. Nat Commun, 2016. **7**: p. 13184.
83. McDonald, T.O., et al., *Antiretroviral solid drug nanoparticles with enhanced oral bioavailability: production, characterization, and in vitro-in vivo correlation*. Adv Healthc Mater, 2014. **3**(3): p. 400-11.
84. Augustine, R., et al., *Nanoparticle-in-microparticle oral drug delivery system of a clinically relevant darunavir/ritonavir antiretroviral combination*. Acta Biomater, 2018. **74**: p. 344-359.
85. Garg, B., et al., *Long-chain triglycerides-based self-nanoemulsifying oily formulations (SNEOFs) of darunavir with improved lymphatic targeting potential*. J Drug Target, 2018. **26**(3): p. 252-266.
86. Negi, L.M., M. Tariq, and S. Talegaonkar, *Nano scale self-emulsifying oil based carrier system for improved oral bioavailability of camptothecin derivative by P-Glycoprotein modulation*. Colloids Surf B Biointerfaces, 2013. **111**: p. 346-53.
87. Hobson, J.J., et al., *Branched copolymer-stabilised nanoemulsions as new candidate oral drug delivery systems*. RSC Advances, 2018. **In Press**(23).
88. Kennedy, J., et al., *In vivo studies investigating biodistribution of nanoparticle-encapsulated rhodamine B delivered via dissolving microneedles*. J Control Release, 2017. **265**: p. 57-65.
89. Pastore, M.N., et al., *Transdermal patches: history, development and pharmacology*. Br J Pharmacol, 2015. **172**(9): p. 2179-209.
90. Puri, A., et al., *Development of a Transdermal Delivery System for Tenofovir Alafenamide, a Prodrug of Tenofovir with Potent Antiviral Activity Against HIV and HBV*. Pharmaceutics, 2019. **11**(4).
91. McCrudden, M.T.C., et al., *Design, formulation and evaluation of novel dissolving microarray patches containing a long-acting rilpivirine nanosuspension*. J Control Release, 2018. **292**: p. 119-129.
92. Rein-Weston, A., I. Tekko, and D. Zehring, *LB8. Microarray Patch Delivery of Long-Acting HIV PrEP and Contraception*. Open Forum Infect Dis, 2019. **6**: p. S996.
93. *RTHO EVRA®(norelgestromin / ethinyl estradiol TRANSDERMAL SYSTEM) 2010* [cited 2020 June]; Available from: [https://www.accessdata.fda.gov/drugsatfda\\_docs/label/2010/021180s035lbl.pdf](https://www.accessdata.fda.gov/drugsatfda_docs/label/2010/021180s035lbl.pdf).
94. Sharma, S., et al., *Recent advances in microneedle composites for biomedical applications: Advanced drug delivery technologies*. Mater Sci Eng C Mater Biol Appl, 2019. **103**: p. 109717.
95. *Human Factors Studies and Related Clinical Study Considerations in Combination Product Design and Development: Draft guidance for industry and FDA staff*. US Department of Health and Human Services FDA, Editor. 2016.
96. *Draft guidance on principles of premarket pathways for combination products: guidance for industry and FDA staff.*, C.f.D.E.a.R.C. US Department of Health and Human Services FDA, Editor. 2019.

97. UNAIDS, *Update on the Access Components of the UNAIDS 2016-2021 Strategy: Removing Access Barriers to Health Technologies for HIV and its Co-Infections and Co-Morbidities in Low- and Middle-Income Countries*. 2018. p. 1-34.
98. Shisana, O., et al., *Does marital status matter in an HIV hyperendemic country? Findings from the 2012 South African National HIV Prevalence, Incidence and Behaviour Survey*. *AIDS Care*, 2016. **28**(2): p. 234-41.
99. Kashuba, A.D., et al., *Genital Tenofovir Concentrations Correlate With Protection Against HIV Infection in the CAPRISA 004 Trial: Importance of Adherence for Microbicide Effectiveness*. *J Acquir Immune Defic Syndr*, 2015. **69**(3): p. 264-9.
100. Baeten, J.M., et al., *Use of a Vaginal Ring Containing Dapivirine for HIV-1 Prevention in Women*. *N Engl J Med*, 2016. **375**(22): p. 2121-2132.
101. Nel, A., et al., *Safety and Efficacy of a Dapivirine Vaginal Ring for HIV Prevention in Women*. *N Engl J Med*, 2016. **375**(22): p. 2133-2143.
102. Thurman, A.R., et al., *Randomized, placebo controlled phase I trial of safety, pharmacokinetics, pharmacodynamics and acceptability of tenofovir and tenofovir plus levonorgestrel vaginal rings in women*. *PLoS One*, 2018. **13**(6): p. e0199778.
103. Chen, B.A., et al., *Phase 1 Safety, Pharmacokinetics, and Pharmacodynamics of Dapivirine and Maraviroc Vaginal Rings: A Double-Blind Randomized Trial*. *J Acquir Immune Defic Syndr*, 2015. **70**(3): p. 242-9.
104. *HIGHLIGHTS OF PRESCRIBING INFORMATION. These highlights do not include all the information needed to use ANNOVERA™ safely and effectively. See Full Prescribing Information for ANNOVERA™. ANNOVERA™ (segesterone acetate and ethinyl estradiol vaginal system)*. 2018 [cited 2020 June]; Available from: [https://www.accessdata.fda.gov/drugsatfda\\_docs/label/2018/209627s000lbl.pdf](https://www.accessdata.fda.gov/drugsatfda_docs/label/2018/209627s000lbl.pdf).
105. McLellan, J.S., et al., *Structure of HIV-1 gp120 V1/V2 domain with broadly neutralizing antibody PG9*. *Nature*, 2011. **480**(7377): p. 336-43.
106. Walker, L.M., et al., *Broad neutralization coverage of HIV by multiple highly potent antibodies*. *Nature*, 2011. **477**(7365): p. 466-70.
107. Huang, J., et al., *Broad and potent HIV-1 neutralization by a human antibody that binds the gp41-gp120 interface*. *Nature*, 2014. **515**(7525): p. 138-42.
108. Kong, R., et al., *Fusion peptide of HIV-1 as a site of vulnerability to neutralizing antibody*. *Science*, 2016. **352**(6287): p. 828-33.
109. van Gils, M.J., et al., *An HIV-1 antibody from an elite neutralizer implicates the fusion peptide as a site of vulnerability*. *Nat Microbiol*, 2016. **2**: p. 16199.
110. Scheid, J.F., et al., *Sequence and structural convergence of broad and potent HIV antibodies that mimic CD4 binding*. *Science*, 2011. **333**(6049): p. 1633-7.
111. Zhou, T., et al., *A Neutralizing Antibody Recognizing Primarily N-Linked Glycan Targets the Silent Face of the HIV Envelope*. *Immunity*, 2018. **48**(3): p. 500-513 e6.
112. Schoofs, T., et al., *Broad and Potent Neutralizing Antibodies Recognize the Silent Face of the HIV Envelope*. *Immunity*, 2019. **50**(6): p. 1513-1529 e9.
113. Gruell, H. and F. Klein, *Antibody-mediated prevention and treatment of HIV-1 infection*. *Retrovirology*, 2018. **15**(1): p. 73.
114. Wang, Q. and L. Zhang, *Broadly neutralizing antibodies and vaccine design against HIV-1 infection*. *Front Med*, 2020. **14**(1): p. 30-42.
115. Caskey, M., et al., *Viraemia suppressed in HIV-1-infected humans by broadly neutralizing antibody 3BNC117*. *Nature*, 2015. **522**(7557): p. 487-91.
116. Gaudinski, M.R., et al., *Safety and pharmacokinetics of the Fc-modified HIV-1 human monoclonal antibody VRC01LS: A Phase 1 open-label clinical trial in healthy adults*. *PLoS Med*, 2018. **15**(1): p. e1002493.
117. Bar-On, Y., et al., *Safety and antiviral activity of combination HIV-1 broadly neutralizing antibodies in viremic individuals*. *Nat Med*, 2018. **24**(11): p. 1701-1707.

118. Mendoza, P., et al., *Combination therapy with anti-HIV-1 antibodies maintains viral suppression*. *Nature*, 2018. **561**(7724): p. 479-484.
119. Lynch, R.M., et al., *Virologic effects of broadly neutralizing antibody VRC01 administration during chronic HIV-1 infection*. *Sci Transl Med*, 2015. **7**(319): p. 319ra206.
120. Gautam, R., et al., *A single injection of crystallizable fragment domain-modified antibodies elicits durable protection from SHIV infection*. *Nat Med*, 2018. **24**(5): p. 610-616.
121. Liu, Q., et al., *Improvement of antibody functionality by structure-guided paratope engraftment*. *Nat Commun*, 2019. **10**(1): p. 721.
122. Nyaku, A.N., S.G. Kelly, and B.O. Taiwo, *Long-Acting Antiretrovirals: Where Are We now?* *Curr HIV/AIDS Rep*, 2017. **14**(2): p. 63-71.
123. Chen, J., K. Walters, and P. Ashton, *Correlation of in vitro-in vivo release rates for sustained release nevirapine implants in rats*. *J Control Release*, 2005. **101**(1-3): p. 357-8.
124. Kovarova, M., et al., *Ultra-long-acting removable drug delivery system for HIV treatment and prevention*. *Nat Commun*, 2018. **9**(1): p. 4156.
125. Benhabbour, S.R., et al., *Ultra-long-acting tunable biodegradable and removable controlled release implants for drug delivery*. *Nat Commun*, 2019. **10**(1): p. 4324.
126. Barrett, S.E., et al., *Extended-Duration MK-8591-Eluting Implant as a Candidate for HIV Treatment and Prevention*. *Antimicrob Agents Chemother*, 2018. **62**(10).
127. Matthews, R.P., et al., *First-in-human trial of MK-8591-eluting implants demonstrates concentrations suitable for HIV prophylaxis for at least one year.*, in *10th IAS Conference on HIV Science*. 2019: Mexico City, Mexico.
128. Johnson, L.M., et al., *Characterization of a Reservoir-Style Implant for Sustained Release of Tenofovir Alafenamide (TAF) for HIV Pre-Exposure Prophylaxis (PrEP)*. *Pharmaceutics*, 2019. **11**(7).
129. Schlesinger, E., et al., *A Tunable, Biodegradable, Thin-Film Polymer Device as a Long-Acting Implant Delivering Tenofovir Alafenamide Fumarate for HIV Pre-exposure Prophylaxis*. *Pharm Res*, 2016. **33**(7): p. 1649-56.
130. Gunawardana, M., et al., *Pharmacokinetics of long-acting tenofovir alafenamide (GS-7340) subdermal implant for HIV prophylaxis*. *Antimicrob Agents Chemother*, 2015. **59**(7): p. 3913-9.
131. Chua, C.Y.X., et al., *Transcutaneously refillable nanofluidic implant achieves sustained level of tenofovir diphosphate for HIV pre-exposure prophylaxis*. *J Control Release*, 2018. **286**: p. 315-325.
132. Pons-Faudoa, F.P., et al., *2-Hydroxypropyl-beta-cyclodextrin-enhanced pharmacokinetics of cabotegravir from a nanofluidic implant for HIV pre-exposure prophylaxis*. *J Control Release*, 2019. **306**: p. 89-96.
133. Su, J.T., et al., *A Subcutaneous Implant of Tenofovir Alafenamide Fumarate Causes Local Inflammation and Tissue Necrosis in Rabbits and Macaques*. *Antimicrob Agents Chemother*, 2020. **64**(3).
134. Pons-Faudoa, F.P., et al., *Advanced implantable drug delivery technologies: transforming the clinical landscape of therapeutics for chronic diseases*. *Biomed Microdevices*, 2019. **21**(2): p. 47.
135. van 't Klooster, G., et al., *Pharmacokinetics and disposition of rilpivirine (TMC278) nanosuspension as a long-acting injectable antiretroviral formulation*. *Antimicrob Agents Chemother*, 2010. **54**(5): p. 2042-50.
136. Orkin, C., et al., *Long-Acting Cabotegravir and Rilpivirine after Oral Induction for HIV-1 Infection*. *N Engl J Med*, 2020. **382**(12): p. 1124-1135.

137. Margolis, D.A., et al., *Long-acting intramuscular cabotegravir and rilpivirine in adults with HIV-1 infection (LATTE-2): 96-week results of a randomised, open-label, phase 2b, non-inferiority trial*. Lancet, 2017. **390**(10101): p. 1499-1510.
138. Markowitz, M., et al., *Safety and tolerability of long-acting cabotegravir injections in HIV-uninfected men (ECLAIR): a multicentre, double-blind, randomised, placebo-controlled, phase 2a trial*. Lancet HIV, 2017. **4**(8): p. e331-e340.
139. Zhou, T., et al., *Creation of a nanoformulated cabotegravir prodrug with improved antiretroviral profiles*. Biomaterials, 2018. **151**: p. 53-65.
140. ViiV Healthcare presents positive 48-week data from phase III study showing every-two-month regimen of investigational long-acting, injectable cabotegravir and rilpivirine has similar efficacy to once-monthly dosing. 2020 [cited 2020 June]; Available from: <https://viivhealthcare.com/en-gb/media/press-releases/2020/march/viiv-healthcare-presents-positive-48-week-data-from-phase-iii-s/>.
141. *Global HIV prevention study to stop early after ViiV Healthcare's long-acting injectable formulation of cabotegravir dosed every two months shows higher efficacy than daily oral PrEP*. 2020 [cited 2020 June]; Available from: <https://viivhealthcare.com/en-gb/media/press-releases/2020/may/global-hiv-prevention-study-to-stop-early-after-viiv-healthcares/>.
142. Singh, K., et al., *GS-CA Compounds: First-In-Class HIV-1 Capsid Inhibitors Covering Multiple Grounds*. Front Microbiol, 2019. **10**: p. 1227.
143. Sager, J.E., et al., *Safety and PK of subcutaneous GS-6207, a novel HIV-1 capsid inhibitor*. , in *Conference on Retroviruses and Opportunistic Infections*. . 2019: Seattle, WA.
144. Hay, J., *Complications at site of injection of depot neuroleptics*. BMJ, 1995. **311**(7002): p. 421.
145. Cleton, A., et al., *A single-dose, open-label, parallel, randomized, dose-proportionality study of paliperidone after intramuscular injections of paliperidone palmitate in the deltoid or gluteal muscle in patients with schizophrenia*. J Clin Pharmacol, 2014. **54**(9): p. 1048-57.
146. Adviser, S. *What should clinicians know about haloperidol decanoate ("Haldol Dec")?* July 17, 2020.
147. Hickey, M.B., et al., *Delivery of long-acting injectable antivirals: best approaches and recent advances*. Curr Opin Infect Dis, 2015. **28**(6): p. 603-10.
148. Edagwa, B., et al., *Long-acting slow effective release antiretroviral therapy*. Expert Opin Drug Deliv, 2017. **14**(11): p. 1281-1291.
149. Zhou, T., et al., *Optimizing the preparation and stability of decorated antiretroviral drug nanocrystals*. Nanomedicine (Lond), 2018. **13**(8): p. 871-885.
150. Hilaire, J.R., et al., *Creation of a long-acting rilpivirine prodrug nanoformulation*. J Control Release, 2019. **311-312**: p. 201-211.
151. Smith, N., et al., *A long acting nanoformulated lamivudine ProTide*. Biomaterials, 2019. **223**: p. 119476.
152. Soni, D., et al., *Synthesis of a long acting nanoformulated emtricitabine ProTide*. Biomaterials, 2019. **222**: p. 119441.
153. Ibrahim, I.M., et al., *Synthesis and characterization of a long-acting emtricitabine prodrug nanoformulation*. Int J Nanomedicine, 2019. **14**: p. 6231-6247.
154. Lin, Z., et al., *ProTide generated long-acting abacavir nanoformulations*. Chem Commun (Camb), 2018. **54**(60): p. 8371-8374.
155. McMillan, J., et al., *Pharmacokinetic testing of a first-generation cabotegravir prodrug in rhesus macaques*. AIDS, 2019. **33**(3): p. 585-588.



156. Rautio, J., et al., *The expanding role of prodrugs in contemporary drug design and development*. Nat Rev Drug Discov, 2018. **17**(8): p. 559-587.
157. Huttunen, K.M., H. Raunio, and J. Rautio, *Prodrugs--from serendipity to rational design*. Pharmacol Rev, 2011. **63**(3): p. 750-71.
158. Rautio, J., et al., *Prodrugs: design and clinical applications*. Nat Rev Drug Discov, 2008. **7**(3): p. 255-70.
159. Guo, D., et al., *Endosomal trafficking of nanoformulated antiretroviral therapy facilitates drug particle carriage and HIV clearance*. J Virol, 2014. **88**(17): p. 9504-13.
160. Zhu, T., et al., *Evidence for human immunodeficiency virus type 1 replication in vivo in CD14(+) monocytes and its potential role as a source of virus in patients on highly active antiretroviral therapy*. J Virol, 2002. **76**(2): p. 707-16.
161. Le Douce, V., et al., *Molecular mechanisms of HIV-1 persistence in the monocyte-macrophage lineage*. Retrovirology, 2010. **7**: p. 32.
162. Kulkarni, T.A., et al., *A year-long extended release nanoformulated cabotegravir prodrug*. Nat Mater, 2020.
163. Dash, P.K., et al., *Sequential LASER ART and CRISPR Treatments Eliminate HIV-1 in a Subset of Infected Humanized Mice*. Nat Commun, 2019. **10**(1): p. 2753.
164. Kulkarni, T.A., et al., *A year-long extended release nanoformulated cabotegravir prodrug*. Nat Mater, 2020. **19**(8): p. 910-920.
165. Thery, C., *Exosomes: secreted vesicles and intercellular communications*. F1000 Biol Rep, 2011. **3**: p. 15.
166. Banks, W.A., et al., *Transport of Extracellular Vesicles across the Blood-Brain Barrier: Brain Pharmacokinetics and Effects of Inflammation*. Int J Mol Sci, 2020. **21**(12).
167. Urbanelli, L., et al., *Signaling pathways in exosomes biogenesis, secretion and fate*. Genes (Basel), 2013. **4**(2): p. 152-70.
168. Thery, C., L. Zitvogel, and S. Amigorena, *Exosomes: composition, biogenesis and function*. Nat Rev Immunol, 2002. **2**(8): p. 569-79.
169. MacDonald, C., et al., *Cargo ubiquitination is essential for multivesicular body intraluminal vesicle formation*. EMBO Rep, 2012. **13**(4): p. 331-8.
170. Trajkovic, K., et al., *Ceramide triggers budding of exosome vesicles into multivesicular endosomes*. Science, 2008. **319**(5867): p. 1244-7.
171. Pant, S., H. Hilton, and M.E. Burczynski, *The multifaceted exosome: biogenesis, role in normal and aberrant cellular function, and frontiers for pharmacological and biomarker opportunities*. Biochem Pharmacol, 2012. **83**(11): p. 1484-94.
172. Kramer-Albers, E.M., et al., *Oligodendrocytes secrete exosomes containing major myelin and stress-protective proteins: Trophic support for axons?* Proteomics Clin Appl, 2007. **1**(11): p. 1446-61.
173. Sampey, G.C., et al., *Exosomes and their role in CNS viral infections*. J Neurovirol, 2014. **20**(3): p. 199-208.
174. Simpson, R.J., S.S. Jensen, and J.W. Lim, *Proteomic profiling of exosomes: current perspectives*. Proteomics, 2008. **8**(19): p. 4083-99.
175. Keller, S., et al., *Exosomes: from biogenesis and secretion to biological function*. Immunol Lett, 2006. **107**(2): p. 102-8.
176. van Niel, G., et al., *Exosomes: a common pathway for a specialized function*. J Biochem, 2006. **140**(1): p. 13-21.
177. Valadi, H., et al., *Exosome-mediated transfer of mRNAs and microRNAs is a novel mechanism of genetic exchange between cells*. Nat Cell Biol, 2007. **9**(6): p. 654-9.

178. Kadiu, I., et al., *Biochemical and biologic characterization of exosomes and microvesicles as facilitators of HIV-1 infection in macrophages*. J Immunol, 2012. **189**(2): p. 744-54.
179. Kahlert, C., et al., *Identification of double-stranded genomic DNA spanning all chromosomes with mutated KRAS and p53 DNA in the serum exosomes of patients with pancreatic cancer*. J Biol Chem, 2014. **289**(7): p. 3869-75.
180. Eldh, M., et al., *Exosomes communicate protective messages during oxidative stress; possible role of exosomal shuttle RNA*. PLoS One, 2010. **5**(12): p. e15353.
181. Biasutto, L., et al., *Retinal pigment epithelium (RPE) exosomes contain signaling phosphoproteins affected by oxidative stress*. Exp Cell Res, 2013. **319**(13): p. 2113-2123.
182. de Gassart, A., et al., *Lipid raft-associated protein sorting in exosomes*. Blood, 2003. **102**(13): p. 4336-44.
183. Katzmann, D.J., M. Babst, and S.D. Emr, *Ubiquitin-dependent sorting into the multivesicular body pathway requires the function of a conserved endosomal protein sorting complex, ESCRT-I*. Cell, 2001. **106**(2): p. 145-55.
184. Babst, M., et al., *Endosome-associated complex, ESCRT-II, recruits transport machinery for protein sorting at the multivesicular body*. Dev Cell, 2002. **3**(2): p. 283-9.
185. Villarroya-Beltri, C., et al., *Sumoylated hnRNPA2B1 controls the sorting of miRNAs into exosomes through binding to specific motifs*. Nat Commun, 2013. **4**: p. 2980.
186. Koppers-Lalic, D., et al., *Nontemplated nucleotide additions distinguish the small RNA composition in cells from exosomes*. Cell Rep, 2014. **8**(6): p. 1649-1658.
187. Squadrito, M.L., et al., *Endogenous RNAs modulate microRNA sorting to exosomes and transfer to acceptor cells*. Cell Rep, 2014. **8**(5): p. 1432-46.
188. Zhuang, X., et al., *Treatment of brain inflammatory diseases by delivering exosome encapsulated anti-inflammatory drugs from the nasal region to the brain*. Mol Ther, 2011. **19**(10): p. 1769-79.
189. Haney, M.J., et al., *Exosomes as drug delivery vehicles for Parkinson's disease therapy*. J Control Release, 2015. **207**: p. 18-30.
190. Sun, D., et al., *A novel nanoparticle drug delivery system: the anti-inflammatory activity of curcumin is enhanced when encapsulated in exosomes*. Mol Ther, 2010. **18**(9): p. 1606-14.
191. Jang, S.C., et al., *Bioinspired exosome-mimetic nanovesicles for targeted delivery of chemotherapeutics to malignant tumors*. ACS Nano, 2013. **7**(9): p. 7698-710.
192. Tian, Y., et al., *A doxorubicin delivery platform using engineered natural membrane vesicle exosomes for targeted tumor therapy*. Biomaterials, 2014. **35**(7): p. 2383-90.
193. Pascucci, L., et al., *Paclitaxel is incorporated by mesenchymal stromal cells and released in exosomes that inhibit in vitro tumor growth: a new approach for drug delivery*. J Control Release, 2014. **192**: p. 262-70.
194. Rani, S., et al., *Mesenchymal Stem Cell-derived Extracellular Vesicles: Toward Cell-free Therapeutic Applications*. Mol Ther, 2015. **23**(5): p. 812-823.
195. Kim, M.S., et al., *Development of exosome-encapsulated paclitaxel to overcome MDR in cancer cells*. Nanomedicine, 2016. **12**(3): p. 655-664.
196. Lee, J., et al., *Liposome-based engineering of cells to package hydrophobic compounds in membrane vesicles for tumor penetration*. Nano Lett, 2015. **15**(5): p. 2938-44.
197. Simpson, S.M., et al., *Design of a Drug-Eluting Subcutaneous Implant of the Antiretroviral Tenofovir Alafenamide Fumarate*. Pharm Res, 2020. **37**(4): p. 83.
198. Sizovs, A., et al., *Trans-urocanic acid enhances tenofovir alafenamide stability for long-acting HIV applications*. Int J Pharm, 2020. **587**: p. 119623.

199. CABENUVA offers adults living with HIV a new once-monthly injectable option for maintaining viral suppression. 2021, Janssen Therapeutics.
200. Healthcare, V., *ViiV Healthcare announces investigational injectable cabotegravir is superior to oral standard of care for HIV prevention in women* 2020.
201. Banoub, M.G., et al., *Synthesis and Characterization of Long-Acting Darunavir Prodrugs*. Mol Pharm, 2020. **17**(1): p. 155-166.
202. Alvarez-Erviti, L., et al., *Delivery of siRNA to the mouse brain by systemic injection of targeted exosomes*. Nat Biotechnol, 2011. **29**(4): p. 341-5.
203. Luo, W., et al., *Spatial and temporal tracking of cardiac exosomes in mouse using a nano-luciferase-CD63 fusion protein*. Commun Biol, 2020. **3**(1): p. 114.
204. Gnanadhas, D.P., et al., *Autophagy facilitates macrophage depots of sustained-release nanoformulated antiretroviral drugs*. J Clin Invest, 2017. **127**(3): p. 857-873.
205. Nowacek, A.S., et al., *Nanoformulated antiretroviral drug combinations extend drug release and antiretroviral responses in HIV-1-infected macrophages: implications for neuroAIDS therapeutics*. J Neuroimmune Pharmacol, 2010. **5**(4): p. 592-601.
206. Balkundi, S., et al., *Comparative manufacture and cell-based delivery of antiretroviral nanoformulations*. Int J Nanomedicine, 2011. **6**: p. 3393-404.
207. Fauci, A.S., et al., *Ending the HIV Epidemic: A Plan for the United States*. JAMA, 2019. **321**(9): p. 844-845.
208. Winner, B., et al., *Effectiveness of long-acting reversible contraception*. N Engl J Med, 2012. **366**(21): p. 1998-2007.
209. Spreen, W., et al., *GSK1265744 pharmacokinetics in plasma and tissue after single-dose long-acting injectable administration in healthy subjects*. J Acquir Immune Defic Syndr, 2014. **67**(5): p. 481-6.
210. Gibson, A.K., et al., *Tenofovir Alafenamide*. Ann Pharmacother, 2016. **50**(11): p. 942-952.
211. Prathipati, P.K., et al., *Pharmacokinetic and Tissue Distribution Profile of Long Acting Tenofovir Alafenamide and Elvitegravir Loaded Nanoparticles in Humanized Mice Model*. Pharm Res, 2017. **34**(12): p. 2749-2755.
212. Mandal, S., et al., *Nanoencapsulation introduces long-acting phenomenon to tenofovir alafenamide and emtricitabine drug combination: A comparative pre-exposure prophylaxis efficacy study against HIV-1 vaginal transmission*. J Control Release, 2019. **294**: p. 216-225.
213. Katz, D.H., et al., *n-docosanol: broad spectrum anti-viral activity against lipid-enveloped viruses*. Ann N Y Acad Sci, 1994. **724**: p. 472-88.
214. Marcelletti, J.F., *Synergistic inhibition of herpesvirus replication by docosanol and antiviral nucleoside analogs*. Antiviral Res, 2002. **56**(2): p. 153-66.
215. McGuigan, C., et al., *Application of phosphoramidate pronucleotide technology to abacavir leads to a significant enhancement of antiviral potency*. J Med Chem, 2005. **48**(10): p. 3504-15.
216. Anderson, P.L., et al., *Emtricitabine-tenofovir concentrations and pre-exposure prophylaxis efficacy in men who have sex with men*. Sci Transl Med, 2012. **4**(151): p. 151ra125.
217. Gendelman, H.E., et al., *Efficient isolation and propagation of human immunodeficiency virus on recombinant colony-stimulating factor 1-treated monocytes*. J Exp Med, 1988. **167**(4): p. 1428-41.
218. Nowacek, A.S., et al., *NanoART synthesis, characterization, uptake, release and toxicology for human monocyte-macrophage drug delivery*. Nanomedicine (Lond), 2009. **4**(8): p. 903-17.
219. Academies, N., *Guide for the Care and Use of Laboratory Animals* N.R.C.U. Committee, Editor. 2011, National Academies Press (US).



220. McGuigan, C., et al., *Synthesis, anti-human immunodeficiency virus activity and esterase lability of some novel carboxylic ester-modified phosphoramidate derivatives of stavudine (d4T)*. *Antivir Chem Chemother*, 1998. **9**(6): p. 473-9.
221. McGuigan, C., et al., *Synthesis and anti-HIV activity of some novel chain-extended phosphoramidate derivatives of d4T (stavudine): esterase hydrolysis as a rapid predictive test for antiviral potency*. *Antivir Chem Chemother*, 1998. **9**(2): p. 109-15.
222. Kandil, S., et al., *ProTides of BVdU as potential anticancer agents upon efficient intracellular delivery of their activated metabolites*. *Bioorg Med Chem Lett*, 2016. **26**(23): p. 5618-5623.
223. Weber, K., et al., *Pathology in Continuous Infusion Studies in Rodents and Non-Rodents and ITO (Infusion Technology Organisation)-Recommended Protocol for Tissue Sampling and Terminology for Procedure-Related Lesions*. *J Toxicol Pathol*, 2011. **24**(2): p. 113-24.
224. Denise A. Cobb, D.S., Weimin Wang, Murali Ganesan, Raghubendra S. Dagur, Edward Makarov, Yimin Sun, JoEllyn McMillan, Howard E. Gendelman, Natalia A. Osna, Larisa Y. Poluektova and Benson Edagwa *LONG-ACTING TENOFOVIR AND NITAZOXANIDE FORMULATIONS SUPPRESS HBV REPLICATION in Conference on Retroviruses and Opportunistic Infections*. 2020: Boston, MA.
225. Alexaki, A., Y. Liu, and B. Wigdahl, *Cellular reservoirs of HIV-1 and their role in viral persistence*. *Curr HIV Res*, 2008. **6**(5): p. 388-400.
226. Darville, N., et al., *Intramuscular administration of paliperidone palmitate extended-release injectable microsuspension induces a subclinical inflammatory reaction modulating the pharmacokinetics in rats*. *J Pharm Sci*, 2014. **103**(7): p. 2072-2087.
227. Darville, N., et al., *Modeling the Time Course of the Tissue Responses to Intramuscular Long-acting Paliperidone Palmitate Nano-/Microcrystals and Polystyrene Microspheres in the Rat*. *Toxicol Pathol*, 2016. **44**(2): p. 189-210.
228. Darville, N., et al., *The effect of macrophage and angiogenesis inhibition on the drug release and absorption from an intramuscular sustained-release paliperidone palmitate suspension*. *J Control Release*, 2016. **230**: p. 95-108.
229. Jucker, B.M., et al., *Multimodal imaging approach to examine biodistribution kinetics of Cabotegravir (GSK1265744) long acting parenteral formulation in rat*. *J Control Release*, 2017. **268**: p. 102-112.
230. Keller, M.J., et al., *Tenofovir disoproxil fumarate intravaginal ring for HIV pre-exposure prophylaxis in sexually active women: a phase 1, single-blind, randomised, controlled trial*. *Lancet HIV*, 2019. **6**(8): p. e498-e508.
231. Rodriguez-Garcia, M., et al., *Tenofovir Inhibits Wound Healing of Epithelial Cells and Fibroblasts from the Upper and Lower Human Female Reproductive Tract*. *Sci Rep*, 2017. **8**: p. 45725.
232. Bollinger, R.C., et al., *Addressing the global burden of hepatitis B virus while developing long-acting injectables for the prevention and treatment of HIV*. *Lancet HIV*, 2020. **7**(6): p. e443-e448.
233. Waldenstrom, A., et al., *Cardiomyocyte microvesicles contain DNA/RNA and convey biological messages to target cells*. *PLoS One*, 2012. **7**(4): p. e34653.
234. Thery, C., M. Ostrowski, and E. Segura, *Membrane vesicles as conveyors of immune responses*. *Nat Rev Immunol*, 2009. **9**(8): p. 581-93.
235. Yang, T., et al., *Exosome delivered anticancer drugs across the blood-brain barrier for brain cancer therapy in Danio rerio*. *Pharm Res*, 2015. **32**(6): p. 2003-14.
236. *High-dose AAV gene therapy deaths*. *Nat Biotechnol*, 2020. **38**(8): p. 910.
237. Stolberg, S.G., *The biotech death of Jesse Gelsinger*. *N Y Times Mag*, 1999: p. 136-140, 149-150.

238. Philippidis, A., *After Third Death, Audentes' AT132 Remains on Clinical Hold*. Hum Gene Ther, 2020. **31**(17-18): p. 908-910.
239. Ohno, S., et al., *Systemically injected exosomes targeted to EGFR deliver antitumor microRNA to breast cancer cells*. Mol Ther, 2013. **21**(1): p. 185-91.
240. Wahlgren, J., et al., *Plasma exosomes can deliver exogenous short interfering RNA to monocytes and lymphocytes*. Nucleic Acids Res, 2012. **40**(17): p. e130.
241. Ridder, K., et al., *Extracellular vesicle-mediated transfer of functional RNA in the tumor microenvironment*. Oncoimmunology, 2015. **4**(6): p. e1008371.
242. Bolukbasi, M.F., et al., *miR-1289 and "Zipcode"-like Sequence Enrich mRNAs in Microvesicles*. Mol Ther Nucleic Acids, 2012. **1**: p. e10.
243. Kojima, R., et al., *Designer exosomes produced by implanted cells intracerebrally deliver therapeutic cargo for Parkinson's disease treatment*. Nat Commun, 2018. **9**(1): p. 1305.
244. Hung, M.E. and J.N. Leonard, *A platform for actively loading cargo RNA to elucidate limiting steps in EV-mediated delivery*. J Extracell Vesicles, 2016. **5**: p. 31027.
245. Abels, E.R. and X.O. Breakefield, *Introduction to Extracellular Vesicles: Biogenesis, RNA Cargo Selection, Content, Release, and Uptake*. Cell Mol Neurobiol, 2016. **36**(3): p. 301-12.
246. Raposo, G. and W. Stoorvogel, *Extracellular vesicles: exosomes, microvesicles, and friends*. J Cell Biol, 2013. **200**(4): p. 373-83.
247. Usman, W.M., et al., *Efficient RNA drug delivery using red blood cell extracellular vesicles*. Nat Commun, 2018. **9**(1): p. 2359.
248. Zhao, Y., et al., *GDNF-transfected macrophages produce potent neuroprotective effects in Parkinson's disease mouse model*. PLoS One, 2014. **9**(9): p. e106867.
249. Shen, B., et al., *Protein targeting to exosomes/microvesicles by plasma membrane anchors*. J Biol Chem, 2011. **286**(16): p. 14383-95.
250. Maguire, C.A., et al., *Microvesicle-associated AAV vector as a novel gene delivery system*. Mol Ther, 2012. **20**(5): p. 960-71.
251. Sinha, S., et al., *Cortactin promotes exosome secretion by controlling branched actin dynamics*. J Cell Biol, 2016. **214**(2): p. 197-213.
252. Savina, A., et al., *Exosome release is regulated by a calcium-dependent mechanism in K562 cells*. J Biol Chem, 2003. **278**(22): p. 20083-90.
253. Thompson, C.A., et al., *Heparanase regulates secretion, composition, and function of tumor cell-derived exosomes*. J Biol Chem, 2013. **288**(14): p. 10093-9.
254. Edgar, J.R., et al., *Tetherin is an exosomal tether*. Elife, 2016. **5**.
255. Mendt, M., et al., *Generation and testing of clinical-grade exosomes for pancreatic cancer*. JCI Insight, 2018. **3**(8).
256. Watson, D.C., et al., *Efficient production and enhanced tumor delivery of engineered extracellular vesicles*. Biomaterials, 2016. **105**: p. 195-205.
257. Abak, A., A. Abhari, and S. Rahimzadeh, *Exosomes in cancer: small vesicular transporters for cancer progression and metastasis, biomarkers in cancer therapeutics*. PeerJ, 2018. **6**: p. e4763.
258. Vakhshiteh, F., F. Atyabi, and S.N. Ostad, *Mesenchymal stem cell exosomes: a two-edged sword in cancer therapy*. Int J Nanomedicine, 2019. **14**: p. 2847-2859.
259. Lamparski, H.G., et al., *Production and characterization of clinical grade exosomes derived from dendritic cells*. J Immunol Methods, 2002. **270**(2): p. 211-26.
260. Tsai, W.C., et al., *Impact of antiretroviral therapy containing tenofovir disoproxil fumarate on the survival of patients with HBV and HIV coinfection*. Liver Int, 2019. **39**(8): p. 1408-1417.
261. Aso, Y. and S. Yoshioka, *Effect of freezing rate on physical stability of lyophilized cationic liposomes*. Chem Pharm Bull (Tokyo), 2005. **53**(3): p. 301-4.

- 262. del Pozo-Rodriguez, A., et al., *Short- and long-term stability study of lyophilized solid lipid nanoparticles for gene therapy*. Eur J Pharm Biopharm, 2009. **71**(2): p. 181-9.
- 263. Ball, R.L., P. Bajaj, and K.A. Whitehead, *Achieving long-term stability of lipid nanoparticles: examining the effect of pH, temperature, and lyophilization*. Int J Nanomedicine, 2017. **12**: p. 305-315.
- 264. Wang, W., *Tolerability of hypertonic injectables*. Int J Pharm, 2015. **490**(1-2): p. 308-15.
- 265. Whelan, J.S., *Encyclopedia of Pharmaceutical Technology (Book)*. Choice: Current Reviews for Academic Libraries, 2003. **40**(11/12): p. 1889.
- 266. Meyer, B.K., et al., *Antimicrobial preservative use in parenteral products: past and present*. J Pharm Sci, 2007. **96**(12): p. 3155-67.
- 267. Akers, M.J., *Excipient-drug interactions in parenteral formulations*. J Pharm Sci, 2002. **91**(11): p. 2283-300.
- 268. Cauchon, N.S., et al., *Innovation in Chemistry, Manufacturing, and Controls-A Regulatory Perspective From Industry*. J Pharm Sci, 2019. **108**(7): p. 2207-2237.
- 269. Moore, G.L., et al., *Practical Synthesis of the Bicyclic Darunavir Side Chain: (3R,3aS,6aR)-Hexahydrofuro[2,3-b]furan-3-ol from Monopotassium Isocitrate*. Org Process Res Dev, 2017. **21**(1): p. 98-106.